CO_2-expanded solvents, promising green solvents for preparing effective formulations of poorly soluble actives

Paula Elena Rojas Labanda

Tesi doctoral

Programa de Doctorat de Química

Directora

Nora Ventosa Rull

Departament de Química
Facultat de Ciències

2015

La present memòria es presenta per aspirar al Grau de Doctor per:

Paula Elena Rojas Labanda ,

Vist i plau:

Dr. Nora Ventosa Rull
(Directora)

Prof. Rosa María Ortuño
(Tutora)

Bellaterra, 18 de Febrer de 2015

Agradecimientos

El desarrollo de la presente tesis doctoral ha sido únicamente posible gracias al esfuerzo, la dedicación, el entusiasmo y el apoyo de muchas personas. Por esta razón, me gustaría expresar mi máxima gratitud a todas las personas que han colaborado en este trabajo.

Me gustaría agradecer al Prof. Jaume Veciana y a la Prof. Concepció Rovira la oportunidad que me han dado para realizar la Tesis Doctoral en su grupo y por haber transmitido la importancia del rigor científico y la excelencia. A continuación, quiero expresar toda mi gratitud a mi directora de Tesis, Nora Ventosa, por todo el tiempo y el esfuerzo que ha dedicado, por haber compartido conmigo tan humanamente las alegrías y los momentos más duros, por su entusiasmo por la ciencia bien hecha. También quiero dar las gracias al Consejo Superior de Investigaciones Científicas por la financiación económica a través de la beca predoctoral JAE-DOC.

Gracias a Noscira por la productiva colaboración y el suministro del fármaco. Este trabajo no habría sido possible sin la fructífera colaboración con el grupo del Dr.Ing. Andreas Brauer, de la Universidad Friedrich-Alexander University Erlangen- Nürnberg. Thank you very much Andreas for all the scientific discussion, for all the support and for having considered my opinion so much. I also would like to express my gratitude for your warm welcome in your group. In addition, I will like to expand my gratitude to Robert and Julian, for teaching me so patiently all the Raman fundamentals and for all the fun moments in the lab and the shared beers. Thank you very much for making my research stays so great! Quiero agradecer al Dr. Jordi Faraudo por habernos ayudado a entender mucho más nuestros sistemas con sus simulaciones. Gracias por tener siempre la puerta abierta y ganas de aclarar todas las dudas posibles. Quiero recalcar también todo el valioso trabajo realizado por Josep Merlo, y en especial de Silvia Illa.

Muchas gracias a todo el personal técnico y al de administración del ICMAB, así como al "Servei D'Anàlisi Química" de la UAB. Quiero agradecer todo el apoyo que he recibido

de Raúl Solanas y Emili de la Serna, vosotros sabéis lo imprescindibles que habéis sido!

Quien sabe si estaría ahora escribiendo estos agradecimientos si no hubiera sido por Joan. Gracias a ti y a todo tu entorno por haberme acogido tan bien en Barcelona, gracias por hacerme querer tanto esta cuidad, GRACIAS por haberme exigido siempre desde el cariño y por haber sido ejemplo.

Estos años no hubieran sido tan especiales si no los hubiera compartido con todos y cada uno de los miembros que han pasado por Nanomol, gracias por las risas en las comidas y vuestra paciencia cuando entraba al laboratorio de la segunda planta. Especialmente, quiero expresar mi más sincera y enorme gratitud a l@s Supercritic@s, sabéis que sin vosotr@s esto no hubiera sido posible. Gracias a vosotras por haber sido AMIGAS con mayúsculas, ejemplo de grandes científicas y mejores personas. Ha sido un placer haber crecido personal y científicamente a lado de gente tan valiosa, no es fácil encontrar personas con las que trabajar sea tan fácil. Mil millones de gracias por todo!

Si hay algo que también ha sido único, ha sido *labirradeldijous*, gracias por todas las conversaciones científicas, políticas, los planes tan chulos y las risas que han hecho todo tan fácil. Gracias a las grandes personas que forman este grupo tan valioso, habéis hecho que crezca mucho!

Quiero agradecer a todos mis amigos, los más nuevos de Barcelona por haber entrado tan de lleno en mi vida, y a mis amigas de toda la vida de Madrid. A estas últimas, gracias por haber hecho que 600km no sea distancia, gracias por hacerme sentir tan querida y por el orgullo y la felicidad que siento por tener a las amigas que tengo. Es un auténtico placer teneos en mi vida y seguir creciendo con vosotras.

Gracias a mi enorme, única y especial familia, por el orgullo que siento de ser Rojas Labanda, soy lo que soy gracias todos vosotros. Quiero agradecer poder compartir tantas cosas valiosas para mi con vosotros. Familia, sois muy grandes!

Definitivamente, todo este proceso no hubiera sido posible sin toda la confianza, el apoyo y el amor de mis padres y mis hermanas. Gracias por la educación que me habéis dado, por hacerme siempre tan feliz y tan querida, gracias por el orgullo que siento de familia.

Por último, quiero agradecer con todo mi corazón a mi compañero de vida, gracias Abel por hacerme dar lo mejor de mi, gracias por exigirme tanto y por hacerme ser mejor persona cada día. Mil millones de gracias por todo lo que me das, por soñar conmigo y por hacerme increíblemente feliz a tu lado.

Abstract

The pharmaceutical industry nowadays is facing several challenges, as more than 40% of compounds identified through combinatorial screening programs are poorly soluble in water. These molecules are difficult to formulate using conventional approaches and are associated with innumerable formulation-related performance issues. Formulating these compounds as pure drug micro particles is one of the newer drug-delivery strategies applied to this class of molecules. The bioperformance of drugs depends on specific characteristics of particles such as size, surface, crystal structure and morphology. Concretely, the control of particle size and shape is of vital relevance as they influence a large variety of important physical properties, manufacturing processability and quality attributes. Moreover, pharmaceutical companies are more and more urged to develop production processes with very low environmental impact in particular for reducing the use of volatile organic compounds in medicine manufacturing as well as the residues in the finished product. In the case of pharmaceutical industry, requirements for high-quality products and society concerns about health and environments, makes the implementation of new efficient and environmentally respectful technologies for the preparation of drugs with tailored properties an urgent necessity.

Compressed fluids (CF), which emerge in the early 90's, present unique properties for the eco-efficient production of Active Pharmaceutical Ingredients (APIs) with an exceptional control of the operational variables that allow tuning the final properties of the active compounds, as detailed in Chapter 1 of this Thesis. Among the most successful applications of CFs, particle engineering of pharmaceutical actives seems to be at the moment, the area with the highest blooming. In contrast to conventional particle formation methods, where a larger particle is originally formed and then milled to the desired size, CF technology involves growing particles in a tailored manner to reach the desired final physical properties. This means that the solid particle, once formed, does not have

to undergo any thermal nor mechanical stresses, as happens in conventional techniques. This feature makes supercritical and compressed fluid technology amenable to produce biomolecules and other sensitive compounds in their native pure state. In addition, CF-based technologies also present an enormous potential for large scale processing.

In light of the need of implementing environmentally friendly process for the production of APIs with controlled size and shape, this Thesis has been devoted to expand the goodness of CF-based methodologies. Concretely, Chapter 2 focuses on the use of DELOS, a CF-based precipitation process, to prepare micronized crystalline particles of poorly soluble actives with low bioavailability and problematic processing by conventional techniques.

Another promising approach to increase the bioavailability of poor soluble drugs is their formulation as micro particles suspended in an aqueous media forming aqueous suspensions. In this context, Chapter 3 explores the application of DELOS-susp as a new one-step method for preparing aqueous suspensions of micronized actives.

Finally, with the objective of expanding the use of CF-based process, the last part of this Thesis endeavors to investigate and characterize the organization, at the molecular level, of surfactant-free microemulsion-like systems formed in "water/organic solvent/CO_2" pressurized systems. These nanostructured liquids can be regarded as a universal green solvents and could be used as nano templates.

Resumen

La industria farmacéutica hoy en día tiene que afrontar varios retos ya que el 40% de los compuestos resultantes de los programas de selección combinatorios son insolubles en agua. Como consecuencia, estas moléculas presentan dificultades a la hora de ser procesadas. Una de las estrategias más implementadas para aumentar la velocidad de disolución de estos nuevos fármacos es su formulación como microparticulas. Las propiedades de los ingredientes activos están directamente relacionadas con propiedades físicas de las partículas tales como el tamaño, la forma, la estructura cristalina y la morfología. Concretamente, el control del tamaño y la forma de un fármaco son de vital importancia ya que estos dos parámetros influencian gran cantidad de propiedades físicas, sus posibilidades de procesado y calidad. Además, las compañías farmacéuticas tienen la necesidad urgente de desarrollar procesos de bajo impacto medioambiental, en particular, para reducir el empleo de disolventes orgánicos volátiles en los procesos de producción de fármacos así como el nivel de residuos en el producto acabado. Las estrictas limitaciones que sufre hoy en día la industria farmacéutica para obtener productos de alta calidad junto con la creciente preocupación de la sociedad por la seguridad y el medioambiente hacen que la implementación de técnicas más eficientes y más respetuosas con el medioambiente se convierta en una necesidad urgente.

Los fluidos comprimidos (CF, en sus siglas en inglés) surgieron en los años 90s y presentan unas propiedades únicas para la preparación de principios activos con un control excepcional de las variables de operación que permiten modelar las propiedades finales de los fármacos de una manera sostenible, como se detalla en el Capitulo 1 de esta Tesis. Una de las aplicaciones más exitosa de los fluidos comprimidos es en la producción de fármacos. En las cristalizaciones con disolventes convencionales, los tamaños de partícula deseados se obtienen sometiendo los fármacos a procesos de molienda. En los procesos a partir de fluidos comprimidos la formación de partículas se hace de manera

controlada para obtener las propiedades finales deseadas en una sola etapa. Esto significa, que una vez que la partícula se forma, no tiene que someterse a tensiones térmicas ni mecánicas. Esta característica hace que las técnicas basadas en el uso de fluidos comprimidos sean adecuadas para producir biomoléculas y compuestos sensibles. Además, los procesos con fluidos comprimidos presentan un gran potencial para la aplicación a grande escala.

En base a la necesidad de implementar procesos sostenibles para la producción de principios activos con un tamaño y forma definidos, el objetivo de esta Tesis es expandir la bondad de los procesos de precipitación basados en fluidos comprimidos. Concretamente, el Capitulo 2 está centrado el uso del DELOS, un proceso basado en CFs, para preparar microparticulas cristalinas de activos con poca solubilidad en agua y que presentan problemas a la hora de ser procesados por técnicas convencionales.

Otra prometedora estrategia para formular compuestos insolubles en agua es su formulación como suspensiones acuosas donde el fármaco se encuentra suspendido en forma de partícula micrónica en un medio acuoso. En este contexto, el Capitulo 3 explora la aplicación del método de una sola etapa DELOS-susp para la obtención de suspensiones acuosas de fármacos insolubles en agua de tamaño micrónico.

Por último, con el objetivo de expandir el uso de los fluidos comprimidos, la parte final de esta Tesis ha estado dedicada a la investigación y caracterización a nivel molecular de sistemas tipo microemulsión sin surfactantes formados en mezclas "agua/disolvente orgánico/CO_2" a alta presión. Estos líquidos nanoestructurados se pueden considerar como prometedores disolventes respetuosos con el medioambiente y como plantillas para la preparación de materiales nanoparticulados.

Contents

1

Introduction and Objetives

1.1 Introduction

Modern drug discovery techniques dating from the late 80's and early 90's,(e.g. advances in automated synthesis, innovative high-throughput screening methods, introduction of combinatorial chemistry) are biased towards drugs with high lipophilicity, leading to a number of poorly water-soluble drug candidates that is constantly increasing [1, 2, 3, 4]. In the 90's, it was generally acknowledged that approximately 40% of the new drug compounds screened were poorly water soluble [5], this value has not change over the years [6], and the percentage can approach 90% if compound selection is not design with diligence [7]. At present, it is estimated that about 40% of the drugs being in the development pipelines are poorly soluble, even up to 60% of compounds coming from synthesis are poorly soluble and that 70% of the potential drug candidates are discarded due to low bioavailability before they ever reached the pharmaceutical department [8].

The main reason of these large percentages of poorly soluble drugs candidates is the drug-like structures that result from optimization of specific binding to target receptors or enzymes. As a consequence, drug candidates are highly lipophilic, have huge molecular

weights and lots of substitutions [9]. Hydrophilicity and lipophilicity are two contradicting and often competing prerequisites necessary for the success of a commercial drug [10]: high lipophilicity helps in transporting molecules across biological membranes and plays an important role in its biological activity and metabolism, but also renders a water insoluble compound [11]. Since dissolution is the first step in the absorption of the drugs, poor aqueous solubility is one of the major hurdles in the development of new compounds [6]. Therefore, increasing the dissolution rate of poorly water soluble drugs is an important and significant challenge to the pharmaceutical industry in order to maximize absorption [12]. Hence, research of strategies for drug dissolution rate enhancement is of high interest [13].

The physical properties of Active Pharmaceutical Ingredients (APIs) such as size, degree of crystallinity and shape have the potential to impact the bioperformance of drugs, particularly for low-solubility compounds, where the rate-limiting-step in drug uptake may be the dissolution of the API in the gut [14]. From the bioavailability perspective, small particles are preferred as they provide faster dissolution. As a general rule, broad or bimodal particle-size distributions should be avoided and narrow distributions with an optimal mean size are desired [14]. Morphology of crystalline solids can also influence dissolution rate and biological availability of drugs and other properties such as packing density, agglomeration and re-dissolution [15, 16]. Moreover, particle shape also influences downstream operations as separating, washing and drying crystals [17]. Finally, crystallinity confers various advantages during isolation, processing and storage of the drug, such as better impurity, improved handling characteristics, such as sticking and flow and, in the majority of cases, better physical and chemical stability [14].

This Thesis deals with two poorly water soluble drugs: a widely known poor soluble drug, ibuprofen, and a recently discovered poor water soluble active compound, 4-benzyl-2-(naphtalen-1-yl)-1, 2, 4-thiadiazoline-3, 5-dione. Different techniques have been applied with the objective of increasing its bioavailability. In the following, a brief introduction of each compound is presented.

* **Ibuprofen**

Ibuprofen (2-(4-isobutyl-phenyl)-propionic acid)(Figure 4.12) is a widely used Non-Steroidal Anti- Inflammatory (NSAI), antipyretic and anti-rheumatic drug [18]. It was discovered in the 1960s in the U.K. and until nowadays is indicated for the relief of pain and

fever by millions of people in the whole world [19]. It is considered a model compound for poorly soluble drugs, being its solubility in water 0.049 mg/mL. Its LogP value (the octanol/water partition) is 3.14 [20]. The advantages of ibuprofen over other NSAIs are its high efficacy and safety. It should be noted that ibuprofen is a relatively safe substance only when used at low, analgesic dose (up to 1600mg/day) [21]. It is an enantiomeric compound, being the *S*-form the therapeutic active form, although the racemic mixture is the commercialized, as the *R*-enantiomer does not entail any secondary effects and a 60% of this enantiomer is metabolized in the human body into the *S*-form [22]. No polymorphism has been found [18].

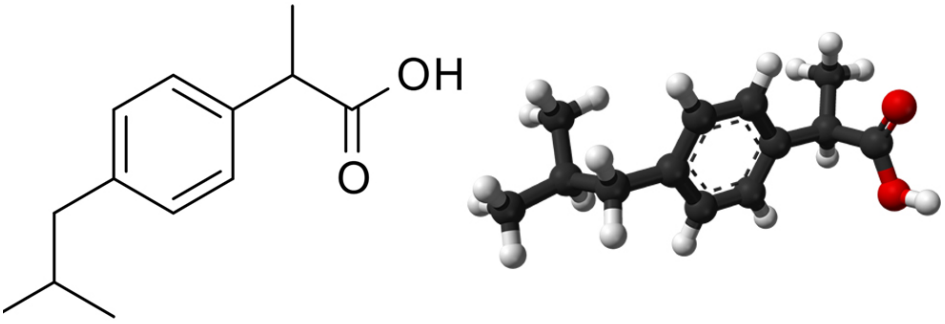

Figure 1.1: Molecular structure of (R,S)-ibuprofen

Due to its very poor solubility in water, ibuprofen presents very low bioavailability and a bad dissolution profile after oral administration [23, 24]. In addition, flowability and compressibility are bad, is readily prone to capping and has tendencies to stick to tablet punches during compression [25]. The pharmacokinetics of ibuprofen have been extensively studied [26]. Considering the Biopharmaceutical Classification System, (BCS) [27], which classifies drug substances into four categories according to their solubility and permeability properties (Figure 1.2), ibuprofen belongs to Class II. For these drugs, that exhibit low solubility but reasonable membrane permeability, the dissolution rate is the limiting factor for the drug absorption rate. In view of its importance as a pain reliever, still several research efforts are focusing on improving the physical, chemical and mechanical properties of ibuprofen.

∗ **4-benzyl-2-(naphtalen-1-yl)-1,2,4-thiadiazoline-3,5-dione**

4-benzyl-2-(naphtalen-1-yl)-1,2,4-thiadiazoline-3,5-dione, from now on, the thiadi-

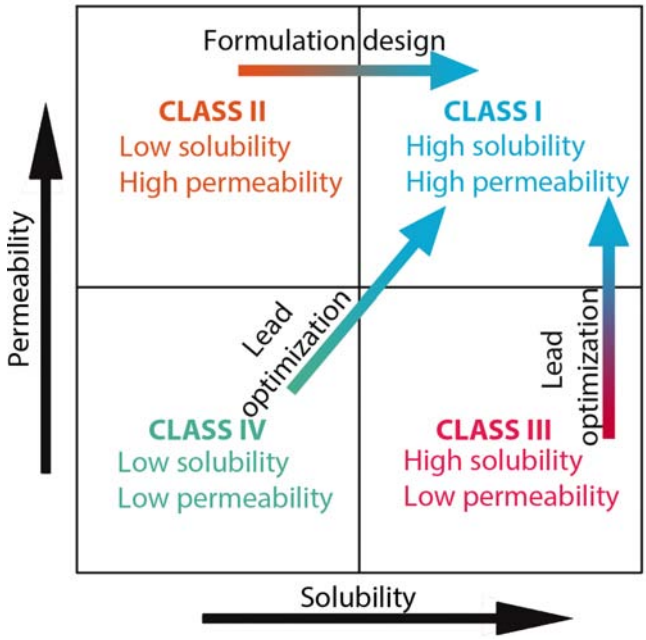

Figure 1.2: Biopharmaceutical classification system of drugs. Adapted from [1].

azoline derivative NP or NP, is a newly discovered poorly water-soluble anti-Alzheimer drug (logP= 4.3) (Figure 1.4). This drug presents a very fast one-face preferential growth that makes it to crystallize as very large needles. This type of morphology is usually undesirable in pharmaceutical crystallizations as hinders the effective application of several downstream operations such as particle handling, filtration, drying, milling and compaction [28].

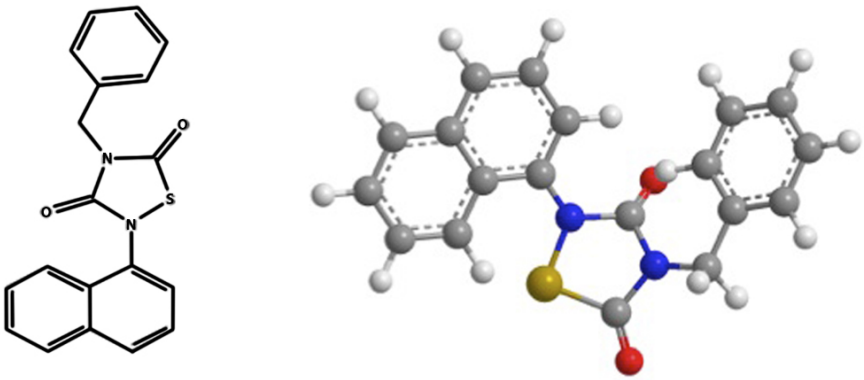

Figure 1.3: Molecular structure of NP drug

When NP is crystallized from conventional cooling, the precipitate consists of elongated needles as the SEM image of Figure 1.4a depicts, and as a consequence, the drug presents a cotton-like macroscopic appearance (Figure1.4b).

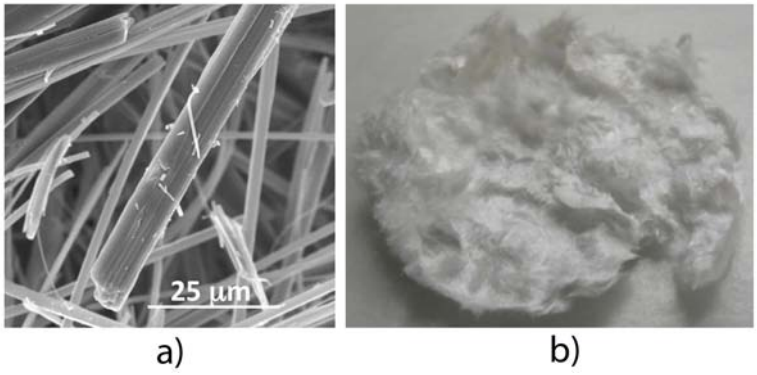

Figure 1.4: a) SEM image of the needle-like crystal of NP, b) Cotton-like physical appearance of NP after crystallization from conventional cooling.

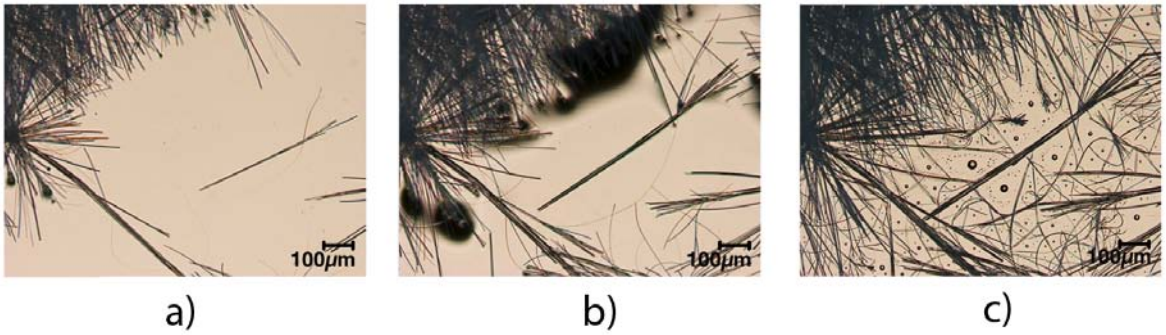

Figure 1.5: Optical microscopy images of the crystal growth of NP from evaporation of an acetonitrile solution, a) t = 0 sec., b)t = 15 sec., c) t = 30sec.

The conventional crystallization of NP from acetonitrile evaporation was monitored by optical microscopy. In this way, it was possible to follow in real time the growth of the NP crystals and it was experimentally checked how fast NP crystals grow. Figure 1.5 presents a sequence of optical microscopy images showing the growth of NP crystals by evaporation from an acetonitrile solution. As it can be seen, NP crystals grow in the shape of very long needles.

Approaches to increase bioavailability of drugs

Poorly soluble molecules have been successfully formulated by a variety of techniques such as: solubilization in surfactant solutions; use of cosolvents; pH adjusted solutions; emulsions; liposomes; complexation with cyclodextrins; and solid dispersions [29, 30]. However, most of these techniques require a large amount of additives limiting their use from a safety perspective [31, 10]. This outlook is driving pharmaceutical companies to search for fast, robust and reliable methods for the delivery of insoluble drugs.

Between the different available approaches for enhancing the dissolution rate of a drug, micronization and the creation of liquid formulations are among the most useful and promising approaches [9]. In fact, one of the major advancements in the pharmaceutical and drug delivery sector in the last fifteen years has been the recognition of the benefits obtained when poorly soluble actives are formulated as micro or submicron particles [7].

Techniques used to produce particles with a controlled particle size can be categorized into two major classes: top-down and bottom-up technologies.

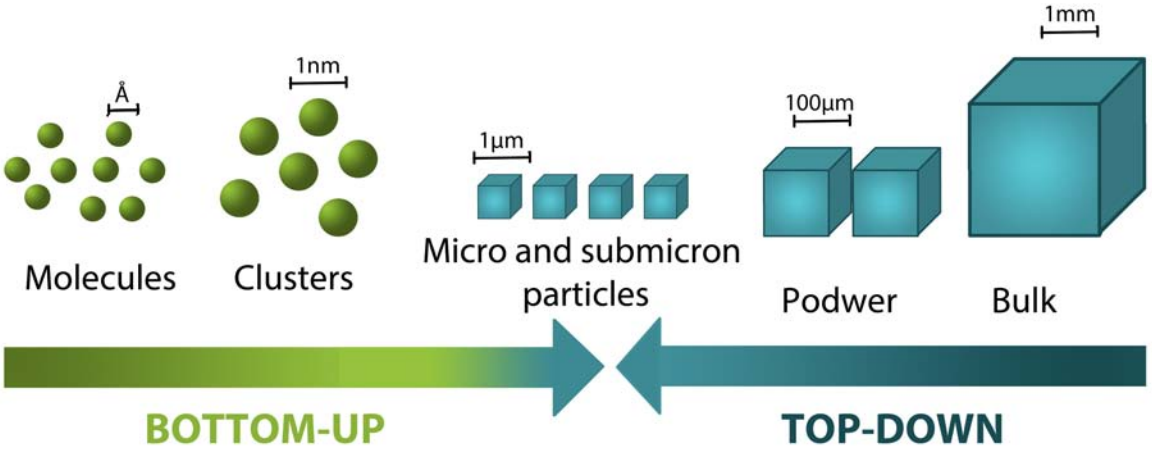

Figure 1.6: Approaches to produce micro and submicron particles.

Top-down approaches mainly comprise mechanical comminution (crushing, grinding and milling) and high pressure homogenization. Although these techniques are widely used, their limitations include: long preparation time, difficulty in achieving a narrow size distribution, high energy input, contamination and adverse effects of the high shear and temperature on the chemical and physical stability of the materials. The top-down approach has been hugely useful on the commercial scale, however, it has some inherent

drawbacks that impede their application for micronization of several APIs such as thermolabile compounds, cotton-like solids and waxy materials. These facts highlight the need of seeking for new alternative process.

Bottom-up procedures, where micron and submicron materials are built from their constituent units (molecules, macromolecules, polymers) by synthetic or self-assembly procedures, provide access to form particles with extremely well defined physicochemical characteristics (size, morphology and internal structure). With precisely controlled bottom-up processes it is possible to prepare, in a single engineering operation, solid particles with a narrow particle size distribution. Bottom-up process have further advantages like low energy requirements, simpler instrumentation, they are less expensive and usually can be operated at lower temperature [20, 32]. Nevertheles, this approach is still not established commercially.

One of the most widely used bottom-up procedures for the preparation of micron and submicron particulate APIs is precipitation [33]. Precipitation and crystallization are usually mixed terms, Mulling differentiates them and claims that precipitation is a fast crystallization, although it could also imply a non reversible process [34]. In general terms, precipitation or crystallization is a transient non-equilibrium process associated with a phase change leading to crystal formation. The driving force for this process is supersaturation (β) [35]. The degree of supersaturation is the ratio of the drug concentration in the solution to its solubility in that solution at that particular condition.

In any bottom-up process involving precipitation from solution, particle size, particle size distribution, morphology, and internal structure (polymorphs, solvates, etc.) are strongly dependent on the evolution of supersaturation (β) during precipitation (Figure 1.7). The supersaturation rate drives nucleation rate and crystal growth at each point of the solution [35]. For instance, in those precipitation process where large levels of supersaturation are attained rapidly (trace A of Figure 1.7) and where there is a homogeneity of this profile throughout the bulk solution, nucleation phenomena will dominate crystal growth, and very small and essentially mono dispersed particles will be produced. Conversely, in those cases when the β profile is more similar to trace B of Figure 1.7, the solute in solution is depleted by both nucleation and crystal growth mechanisms and, accordingly, large crystals are formed, with broad particle size distribution [36, 37].

Those precipitation process that occur far from equilibrium conditions, where large levels of β are achieved very fast, precipitation will be favored by kinetic factors rather than thermodynamic ones. In contrast, precipitations that take place near equilibrium

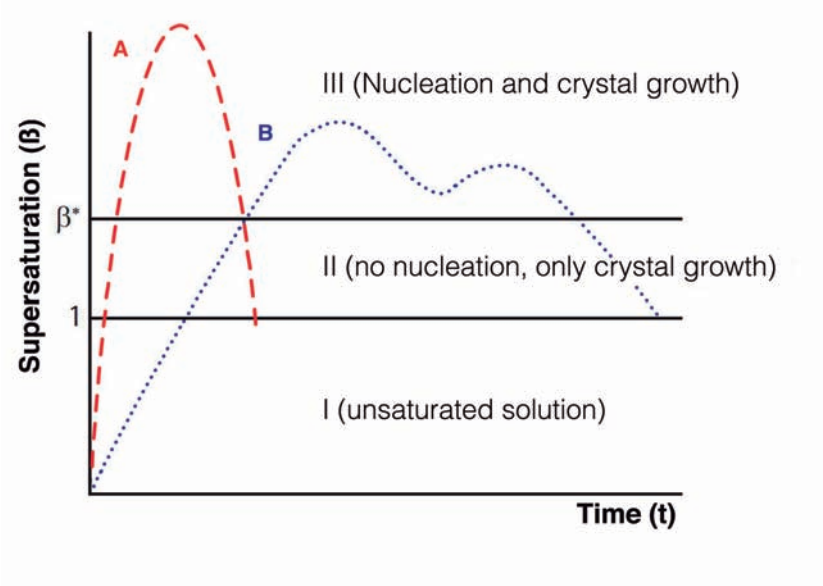

Figure 1.7: Qualitative supersaturation profiles corresponding to a crystallization process where nucleation phenomena are dominant over crystal growth (trace A) or crystal growth is dominant over nucleation (trace B). β is the ratio between the actual concentration (C_i) and the saturation concentration, or solubility (Cs),of the solute to crystallize.

conditions, thermodynamic will govern the process, and thermodynamically stable internal structures are more likely to obtain [14].

Crystallization, as mentioned, is governed by both thermodynamic and kinetic factors, which are often difficult to control. Thermodynamics determines the maximum yield achievable and the chemical composition of the crystalline phase. These two crystallization outputs can be modified by changing temperature, pressure and the initial and final equilibrium states involved in the crystallization procedure. Cooling/heating rates, mixing regime, vessel design and cooling profiles can deeply impact the final characteristics of the active compound, such as particle size and crystallinity.

Precipitation from conventional liquid solvents exploits temperature or compositional variations where the rate-limiting step is related to the thermal conductivity or mass transfer of the medium. In conventional crystallizations, efficient stirring systems are required to appropriately transmit the temperature and compositional changes through the whole solution with the aim of achieving large values of β homogeneously all over the system. Mixing efficiency affects the supersaturation achieved and thereby greatly influences particle size and distribution pattern. Hence, as in large-scale applications stirring efficien-

cies are usually very poor, very low and heterogenous supersaturation profiles are obtained [38] (Figure 1.8). As a consequence, in industry, very large particles are obtained and down-stream operations are required, which can damage the crystalline product or can be problematic to apply. [35, 39].

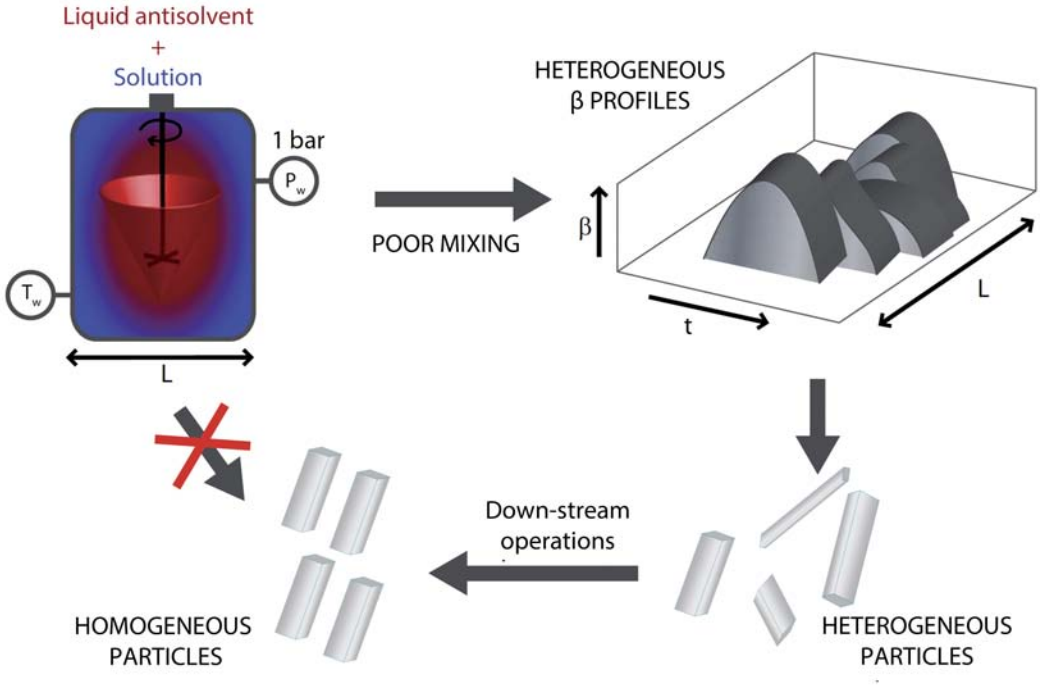

Figure 1.8: Schematic representation of a conventional precipitation process based on composition changes, in which poor mixing between solvent and antisolvent promotes low and heterogeneous supersaturation (β) degrees, generating large and heterogeneous particles that need further processing.

Apart from this, conventional precipitation techniques entail other shortcomings: thermal and chemical degradation of products, trace residues, solvent-voids, inter-batch particle size variability, and excessive solvent use and disposal [35]. Hence, strict regulations on the use of organic solvents and their residual level in the active compounds also present a major limitation to the application of precipitation from conventional liquids [40, 41]. Pharmaceutical industry is one of the industries with the higher E-factor, being the E factor the actual amount of waste produced in the process [42], defined by the ratio of the mass of waste per unit of product:

$$E-factor = \frac{total waste(kg)}{product(kg)} . \tag{1.1}$$

In an effort to reduce the use of volatile organics, pharmaceutical research has focused on the seek of alternative techniques for material processing. Therefore, the new paradigm for pharmaceutical industry is to develop robust processing platforms in an environmentally responsible manner with a high control of process parameters to produce APIs with will defined product characteristics such as particle size and shape.

Compressed Fluids (CFs)-based technologies appeared in the early 1980s and have created great expectations in the pharmaceutical industry due to the special features of CFs that could be exploited. CFs are defined as substances that at normal conditions of pressure (P) and temperature (T) exist as gases but with increased pressure can be converted into liquids or supercritical fluids. The supercritical state is achieved when they are exposed to conditions above their critical pressure (Pc) and temperature (Tc). A single phase is formed and density greatly varies with small changes in pressure and temperature close or above the critical point (Figure 1.9). These types of fluids often have liquid-like densities and, hence, solvating characteristics that are similar to those of liquids, but, at the same time, they also present gas-like mass transfer properties. These special characteristics start to take place at conditions below but near the critical point (subcritical region). Table 1.1 shows the physicochemical properties of a CF compared with those of liquid and gas.

As reflected in Table 1.1 density, viscosity, diffusion coefficient, and heat conductivity

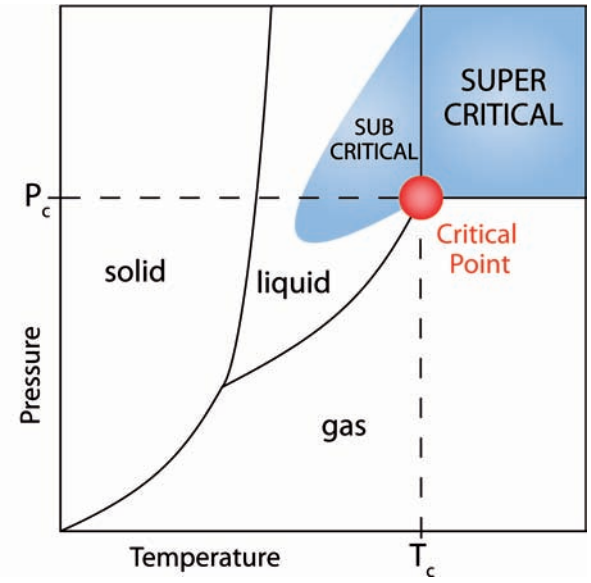

Figure 1.9: P-T Phase diagram of CO_2.

Table 1.1: Chacteristics of compressed fluids compared to those of liquid and gas.

Property	Liquid	CF	Gas
Density (kg/m^3)	1000	200-900	0.6-1
Viscosity (μPa.s)	10^{-3}	$10^{-}5$-10^{-4}	10^{-5}
Diffusion Coefficient (m^2/s)	$<10^{-9}$	10^{-7}-10^{-8}	10^{-5}
Heat conductivity(W/mK)	$<10^{-1}$	10^{-3}-10^{-1}	10^{-3}

values of are between those for liquid and gas. The density of a CF is either the same or close to that of a liquid, which allows CFs to enhance solubility more than gas could. In contrast, because its diffusion coefficient is close to that of a gas, the viscosity of a CF is much lower than that of a gas. These higher diffusivities, lower viscosities and lower surface tension enhance reaction rates. In addition, these physical properties of a CF, such as density, viscosity, diffusion coefficient, and heat conductivity, can be varied by slightly changing the temperature and pressure around critical point [9]. Moreover, residual solvent removal by CFs exploits the great diffusivity of the compressed gas as well as the easy evaporation of organic solvent into the supercritical phase [41].

Other benefits of CFs technologies are linked to the reduced complexity of the process which stems from a decrease in the number of steps as well as to the improved process understanding and control while the processing conditions are relatively mild [41]. Traditional methods for the production of drug microparticles require numerous manufacturing steps that are not required in case of CFs techniques. This brings a huge simplification and better control of the process.

The most widely used CF is CO_2, which is non-toxic, non-flammable, cheap and easy recyclable. It has gained considerable attention during the past few years as a green substitute to organic solvents in industrial processing.

A specific advantage of CFs that should be underlined is the almost instantaneous pressure variation transmission that takes place in CFs, which leads to uniform conditions in the whole solution. In CF-based processes, propagation of the pressure perturbation is correlated to the speed of sound, in contrast to conventional techniques, where the rate-limiting step is the propagation of temperature and compositional changes. This extremely fast transmission of pressure changes permits the easy, fast and homogeneous transmission of diffusion, solvent power and density through the whole solution. As a

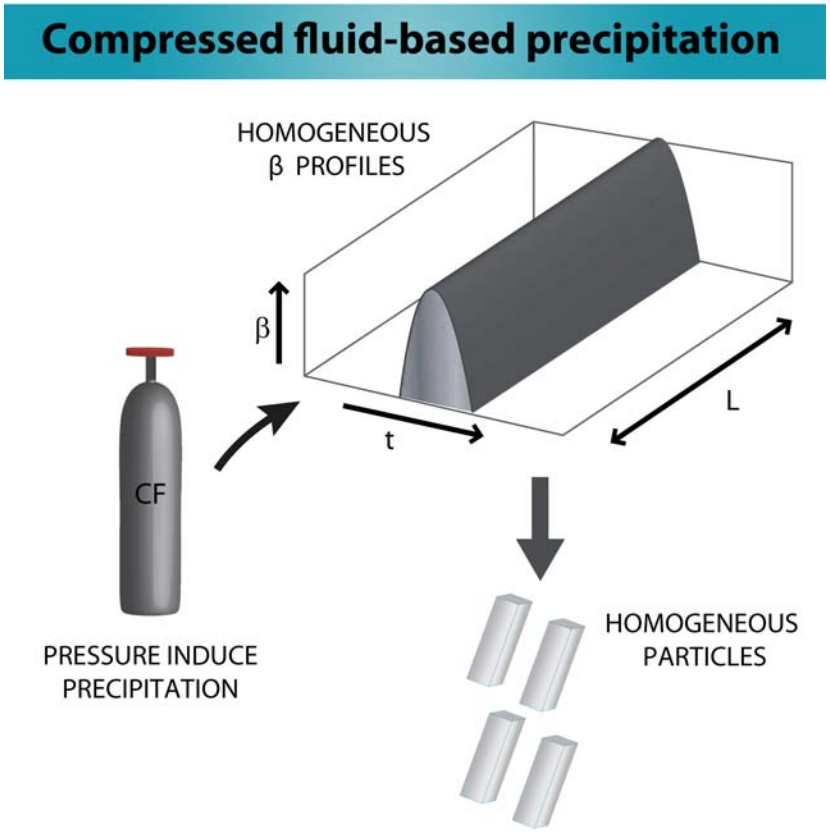

Figure 1.10: Schematic representation of the homogeneous supersaturation (β) profiles usually achieved by CF-based methods, which result in uniform particles in a single step.

consequence, large levels of supersaturation are attained rapidly and homogeneously through the bulk solution and hence, nucleation phenomena will dominate crystal growth, and very small particles will be produced (Figure 1.10). When using CFs as solvents or co-solvents, large levels of supersaturation which are homogeneous throughout the system are obtained and, as a consequence, uniform micro and nanoparticulate materials without the need of further downstream operations are obtained [35].

In contrast to conventional particle formation methods, where a larger particle is originally formed and then comminuted to the desired size, CF technology involves growing the particles in a controlled manner to attain the desired morphology [40]. This means that the rigid solid particle, once formed, does not have to undergo the thermal and mechanical stresses. This feature makes compressed fluid technology amenable to produce biomolecules and other sensitive compounds in their native pure state [40].

There are different available CF-based technologies for the preparation of APIs with

controlled physical properties which will be introduced in the following Chapters of this Thesis. *Nanomol* group (ICMAB-CSIC), where the present Thesis has been conducted, developed a method based on the use of CO_2-expanded solvents ten years ago. CO_2-expanded solvents are mixed solvents composed of compressed CO_2 (cCO_2) dissolved in an organic solvent. By varying the CO_2 composition, a continuum of liquid media ranging from the neat organic solvent to cCO_2 is generated, the properties of which can be adjusted by tuning the operating pressure. For example, a large amount of CO_2 favors mass transfer and, in many cases, gas solubility, and the presence of polar organic solvents enhances the solubility of solid and liquid solutes. CO_2-expanded solvents have been shown to be optimal solvents in a variety of roles including inducing separations, precipitating fine particles, facilitating polymer processing, and serving as reaction media for catalytic reactions. Process advantages include ease of removal of the CO_2, enhanced solubility of reagent gases (compared to liquid solvents), fire suppression capability of the CO_2, and mild process pressures (tens of bars). Reaction advantages include higher gas miscibility compared to organic solvents at ambient conditions, enhanced transport rates due to the properties of dense CO_2, and between 1 and 2 orders of magnitude greater rates than in neat organic solvent or cCO_2. Environmental advantages include substantial replacement of organic solvents with environmentally benign dense-phase CO_2. Thus, CO_2-expanded solvents have emerged as important components in the optimization of chemical processes [43].

From a technical view, CF particle design technology, as it applies to production of pharmaceutical active ingredients, is in its infancy [9]. Although large-scale commercial use of CF technology has been successfully used to decaffeinate coffee and tea, as well as extract spices, hops, and flavoring, it has not yet become the first choice technology for particle design in the pharmaceutical industry. The reason behind this may be the cost of installing Good Manufacturing Practices (GMP)-compliant equipment, and the relatively limited experience of most manufacturers with commercial production scale-up of this type of technology. A study published [44] at the beginning of the century on scale-up for particle formulation cast a positive light on the idea. The study offers evidence that commercial-scale CF facilities can be successful not only for the food and dry cleaning industries, but also for pharmaceutical particle design. Therefore, industry may slowly be realizing that GMP compliance is not a true obstacle to CF processing. In addition, it has been demonstrated before that large capacity plants, with optimized design and operation, lead to prices that are very often, and surprisingly for many people, of the same

order of magnitude as those related to classical processes submitted to similar constraints in terms of environmental and consumer protection. Moreover, there are also cases where compressed fluids permit to make products or operations that cannot be realized by any other means [45]. Use of cutting-edge technologies such CF can lead to great improvements in the commercialized production methods for particle formulation. The end result will be enhanced drug bioavailability, which will improve the overall performance of the drug, and more environmentally friendly manufacturing methods.

1.2 Objectives

- This Phd Thesis aims to improve the knowledge of CO_2-expanded solvents for the controlled precipitation of two poorly soluble drugs: the widely known ibuprofen and a newly discovered drug, which its precipitation from conventional cooling methods yields very long needles and, as a result, the drug presents a cotton-like appearance, which hinders its micronization by conventional techniques.

- Commercial application of CO_2-expanded solvent-based precipitation technology requires predictability, consistency and reproducibility of the final physical properties of the drugs precipitated. For this, a detail and comprehensive understanding of the influence of all the relevant process parameters and the CO_2-expanded solvent fundamentals is essential. In light of this need, one of the aims of the present Thesis is to gain more knowledge of all the mechanisms that occurs in a CO_2-expanded solvent-based precipitation method for the production of finely dispersed solids and liquid suspensions of poorly water soluble drugs.

- In addition, although CFs present unique properties, one limitation for the application of CO_2-based process is the low solubility of many compounds in CO_2. Based on this, this Thesis also aims to extend the use of cCO_2 by preparing microemulsion-like systems composed of water and CO_2-expanded solvents, which can be considered universal green solvents. This new systems can potentially be used as nano templates.

Bibliography

[1] A. Fahr and X. Liu, "Drug delivery strategies for poorly water-soluble drugs," *Expert Opinion on Drug Delivery*, vol. 4, no. 4, pp. 403–416, 2007.

[2] S. Venkatesh and R. Lipper, "Role of the development scientist in compound lead selection and optimization," *Journal of Pharmaceutical Sciences*, vol. 89, no. 2, pp. 145–154, 2000.

[3] C.-K. Kim and J.-S. Park, "Solubility enhancers for oral drug delivery: Can chemical structure manipulation be avoided?," *American Journal of Drug Delivery*, vol. 2, no. 2, pp. 113–130, 2004.

[4] S. Stegemann, F. Leveiller, D. Franchi, H. de Jong, and H. Lindén, "When poor solubility becomes an issue: From early stage to proof of concept," *European Journal of Pharmaceutical Sciences*, vol. 31, no. 5, pp. 249–261, 2007.

[5] T. Takagi, C. Ramachandran, M. Bermejo, S. Yamashita, L. Yu, and G. Amidon, "A provisional biopharmaceutical classification of the top 200 oral drug products in the united states, great britain, spain, and japan," *Molecular Pharmaceutics*, vol. 3, no. 6, pp. 631–643, 2006.

[6] C. Lipinski, "Poor aqueous solubility - an industry wide problem in drug discovery," *American Pharmaceutical Review*, vol. 5, no. 3, pp. 82–85, 2002.

[7] E. Merisko-Liversidge and G. Liversidge, "Nanosizing for oral and parenteral drug delivery: A perspective on formulating poorly-water soluble compounds using wet media milling technology," *Advanced Drug Delivery Reviews*, vol. 63, no. 6, pp. 427–440, 2011.

[8] L. Gao, G. Liu, J. Ma, X. Wang, L. Zhou, X. Li, and F. Wang, "Application of drug nanocrystal technologies on oral drug delivery of poorly soluble drugs," *Pharmaceutical Research*, vol. 30, no. 2, pp. 307–324, 2013.

[9] T. Yasuji, H. Takeuchi, and Y. Kawashima, "Particle design of poorly water-soluble drug substances using supercritical fluid technologies," *Advanced Drug Delivery Reviews*, vol. 60, no. 3, pp. 388–398, 2008.

[10] S. Verma, R. Gokhale, and D. Burgess, "A comparative study of top-down and bottom-up approaches for the preparation of micro/nanosuspensions," *International Journal of Pharmaceutics*, vol. 380, no. 1-2, pp. 216–222, 2009.

[11] D. Lewis, M. Jacobs, and M. Dickins, "Compound lipophilicity for substrate binding to human p450s in drug metabolism," *Drug Discovery Today*, vol. 9, no. 12, pp. 530–537, 2004.

[12] J. Hu, K. Johnston, and R. Williams III, "Nanoparticle engineering processes for enhancing the dissolution rates of poorly water soluble drugs," *Drug Development and Industrial Pharmacy*, vol. 30, no. 3, pp. 233–245, 2004.

[13] N. Rasenack and R. Müller, "Dissolution rate enhancement by in situ micronization of poorly water-soluble drugs," *Pharmaceutical Research*, vol. 19, no. 12, pp. 1894–1900, 2002.

[14] N. Variankaval, A. Cote, and M. Doherty, "From form to function: Crystallization of active pharmaceutical ingredients," *AIChE Journal*, vol. 54, no. 7, pp. 1682–1688, 2008.

[15] E. Moreno-Calvo, *On the polymorphism and structural characterization in the family of even saturated carboxylic acids.* PhD thesis, Universidad de Barcelona., 2008.

[16] K. Chow, H. Tong, S. Lum, and A. Chow, "Engineering of pharmaceutical materials: An industrial perspective," *Journal of Pharmaceutical Sciences*, vol. 97, no. 8, pp. 2855–2877, 2008.

[17] H. Cano, N. Gabas, and J. Canselier, "Experimental study on the ibuprofen crystal growth morphology in solution," *Journal of Crystal Growth*, vol. 224, no. 3-4, pp. 335–341, 2001.

[18] N. Rasenack and B. W. Muller, "Ibuprofen crystals with optimized properties," *International Journal of Pharmaceutics*, vol. 245, pp. 9 – 24, 2002.

[19] K. Adrjanowicz, K. Kaminski, Z. Wojnarowska, M. Dulski, L. Hawelek, S. Pawlus, M. Paluch, and W. Sawicki, "Dielectric relaxation and crystallization kinetics of ibuprofen at ambient and elevated pressure," *Journal of Physical Chemistry B*, vol. 114, no. 19, pp. 6579–6593, 2010.

[20] N. Rasenack, H. Steckel, and B. Muller, "Preparation of microcrystals by in situ micronization," *Powder Technology*, vol. 143-144, pp. 291–296, 2004.

[21] J. Bradley, K. Brandt, B. Katz, L. Kalasinski, and S. Ryan, "Comparison of an antiinflammatory dose of ibuprofen, an analgesic dose of ibuprofen, and acetaminophen in the treatment of patients with osteoarthritis of the knee," *New England Journal of Medicine*, vol. 325, no. 2, pp. 87–91, 1991.

[22] S. Adams, P. Bresloff, and C. Mason, "Pharmacological differences between the optical isomers of ibuprofen: evidence for metabolic inversion of the (-) isomer," *Journal of Pharmacy and Pharmacology*, vol. 28, no. 3, pp. 256–257, 1976.

[23] N. Kasim, "Molecular properties of who essential drugs and provisional biopharmaceutical classification.," *Mol Pharm*, vol. 1, no. 1, pp. 85–96, 2004.

[24] M. Lindenberg, S. Kopp, and J. Dressman, "Classification of orally administered drugs on the world health organization model list of essential medicines according to the biopharmaceutics classification system," *European Journal of Pharmaceutics and Biopharmaceutics*, vol. 58, no. 2, pp. 265–278, 2004.

[25] L. Seton, M. Roberts, and F. Ur-Rehman, "Compaction of recrystallised ibuprofen," *Chemical Engineering Journal*, vol. 164, no. 2-3, pp. 449–452, 2010.

[26] Y. Obidchenko, N. Khuchua, R. Abramovich, A. Savochkina, A. Karamyan, S. Barsegyan, Y. Khomyakov, M. Ovcharov, and V. Chistyakov, "Preparation of micronized ibuprofen substance and assessment of its bioavailability," *Pharmaceutical Chemistry Journal*, vol. 47, no. 7, pp. 382–386, 2013.

[27] G. Amidon, H. Lennernas, V. Shah, and J. Crison, "A theoretical basis for a biopharmaceutic drug classification: The correlation of in vitro drug product dissolution and in vivo bioavailability," *Pharmaceutical Research*, vol. 12, no. 3, pp. 413–420, 1995.

[28] J. Chen and B. Trout, "Computer-aided solvent selection for improving the morphology of needle-like crystals: A case study of 2,6-dihydroxybenzoic acid," *Crystal Growth and Design*, vol. 10, no. 10, pp. 4379–4388, 2010.

[29] F. Kesisoglou, S. Panmai, and Y. Wu, "Nanosizing - oral formulation development and biopharmaceutical evaluation," *Advanced Drug Delivery Reviews*, vol. 59, no. 7, pp. 631–644, 2007.

[30] V. Patravale, A. Date, and R. Kulkarni, "Nanosuspensions: A promising drug delivery strategy," *Journal of Pharmacy and Pharmacology*, vol. 56, no. 7, pp. 827–840, 2004.

[31] B. E. Rabinow, "Nanosuspensions in drug delivery," *Nature Reviews Drug Discovery*, vol. 3, no. 9, pp. 785–796, 2004.

[32] X. Zhang, Q. Xia, and N. Gu, "Preparation of all-trans retinoic acid nanosuspensions using a modified precipitation method," *Drug Development and Industrial Pharmacy*, vol. 32, no. 7, pp. 857–863, 2006.

[33] H. de Waard, W. Hinrichs, and H. Frijlink, "A novel bottom-up process to produce drug nanocrystals: Controlled crystallization during freeze-drying," *Journal of Controlled Release*, vol. 128, no. 2, pp. 179–183, 2008.

[34] J. Mullin *Crystallization*, 1993.

[35] I. Pasquali, R. Bettini, and F. Giordano, "Supercritical fluid technologies: An innovative approach for manipulating the solid-state of pharmaceuticals," *Advanced Drug Delivery Reviews*, vol. 60, no. 3, pp. 399 – 410, 2008.

[36] D. Horn and J. Rieger, "Organic nanoparticles in the aqueous phase - theory, experiment, and use," *Angewandte Chemie - International Edition*, vol. 40, no. 23, pp. 4330–4361, 2001.

[37] M. Löffelmann and A. Mersmann, "How to measure supersaturation?," *Chemical Engineering Science*, vol. 57, no. 20, pp. 4301–4310, 2002.

[38] B. Sinha, R. Müller, and J. Mschwitzer, "Bottom-up approaches for preparing drug nanocrystals: Formulations and factors affecting particle size," *International Journal of Pharmaceutics*, vol. 453, no. 1, pp. 126–141, 2013.

[39] E. Elizondo, J. Veciana, and N. Ventosa, "Nanostructuring molecular materials as particles and vesicles for drug delivery, using compressed and supercritical fluids," *Nanomedicine*, vol. 7, no. 9, pp. 1391–1408, 2012.

[40] C. Vemavarapu, M. J. Mollan, M. Lodaya, and T. E. Needham, "Design and process aspects of laboratory scale {SCF} particle formation systems," *International Journal of Pharmaceutics*, vol. 292, no. 1, pp. 1 – 16, 2005.

[41] I. Pasquali and R. Bettini, "Are pharmaceutics really going supercritical?," *International Journal of Pharmaceutics*, vol. 364, no. 2, pp. 176 – 187, 2008.

[42] R. Sheldon, "The e factor: Fifteen years on," *Green Chemistry*, vol. 9, no. 12, pp. 1273–1283, 2007.

[43] P. G. Jessop and B. Subramaniam, "Gas-expanded liquids," *Chemical Reviews*, vol. 107, no. 6, pp. 2666–2694, 2007.

[44] M. Perrut, "Supercritical fluids applications in the pharmaceutical industry," *S.T.P. Pharma Sciences*, vol. 13, no. 2, pp. 83–91, 2003.

[45] M. Perrut, "Supercritical fluid applications: Industrial developments and economic issues," *Industrial & Engineering Chemistry Research*, vol. 39, no. 12, pp. 4531–4535, 2000.

2

Micronization of APIs using compressed fluids

2.1 Introduction

2.1.1 Particle Engineering in the Pharmaceutical Industry

Pharmaceutical materials science is a discipline which deals with the application of physical principles common in materials science in areas such as drug delivery, control of the drug form, manufacture and processing of nanoscopic and microscopic particle systems, and the structure and properties of bulk powders and their assemblies for use in pharmaceutical applications [1]. This new area of material science arises from the urge of obtaining reproducible drugs with a specifically tailored form and size at the micro and nanoscale. This is a major issue that must be addressed by chemist, materials scientifics, engineers and pharmaceutical formulators.

Specific characteristics of particles such as size, surface, crystal structure and morphology are among the most important factors to control biopharmaceutical properties

of drug products [2]. Particle shape affects the efficiency of downstream processes (filtration, washing and drying). It also influences material properties such as the bulk density and the mechanical strength, which play a significant role in storage and handling. Acicular crystal habit is undesirable from a product manufacturing point of view because it entails poor powder flow properties, poor filtration characteristics, tendency to cake, and brittleness [3]. Brittle particles often fracture upon handling, which may result in a polydisperse particle size distribution which it is unfavorable since they adversely affect powder mixing phenomena, provide poor content uniformity, and afford the possibility of particle segregation in mixed materials [4]. Furthermore, pharmaceutical powders with an acicular habit are typically cohesive and present a high compressibility [5]. A high compressibility is indicative of a non-free flowing powder [6], which makes product tableting difficult and inefficient. The shape of grown crystals depend on the internal structure of crystals (e.g. space group, intramolecular and intermolecular bonding) and on the external conditions of growth (e.g. temperature, pressure, supersaturation, solvents, additives or impurities) [7].

Particle size and shape can influence a large variety of important physical properties, manufacturing processability and quality attributes of active pharmaceutical pharmaceutical ingredients (APIs) including:

- Dissolution rate and bioavailability of active pharmaceutical ingredients
- Drug release rate for sustained and controlled release formulations
- In vivo particle distribution and depositions
- Absorption rate and clearance time, especially for aerosols and different colloid systems designed for targeted drug delivery
- Content and dose uniformity and other properties related to the physicochemical stability
- Aerosoization behavior and performance of respiratory formulations
- Flow and packing properties, mixing and segregation of powders, rheological characteristics of liquid ans semisolid formulations
- "Grittiness" (grainy perception) of solid particles in chewable tablets, dermal ointments and creams

All these properties ultimate affect the safety and efficacy of drugs [8]. One of the most critical properties to the performance of a drug in humans is its plasma concentration profile, frequently referred to as bioavailability. **Bioavailability** is the fraction of administered dose of drug that reaches systemic circulation and is an important pharmacokinetic property of the solid-state of the drug. Hence, the formulation needs to be optimized to ensure that sufficient drug will be available to engage the target in humans and be efficacious.

As claimed in the Introduction of this Thesis (Chapter 1), micronization is a suitable approach to successfully enhance bioavailability of drugs when the dissolution velocity is the rate limiting step, that is for drugs belonging to Class II of the Biopharmaceutical Classification system. The main reason for the increased dissolution velocity, and thus improved bioavailability, for microparticles is by surface area enlargement: size reduction leads to an increased surface area and hence, according to the Noyes-Whitney [9] equation to a better dissolution velocity. The Noyes-Whitney equation derives from the Fick's law and it is expressed as:

$$\frac{dC}{dt} = \frac{D * A * (C_S - C_b)}{Vh}, \tag{2.1}$$

in which dC/dt is the dissolution rate of a drug formulation, D is the diffusion coefficient, A is the surface area of drug exposed to the dissolution media, C_S is the saturation solubility of the drug, C_b is the concentration of drug in solution, V is the volume of the dissolution media, and h is the thickness of the diffusion layer at the solid-liquid interface. The diffusion layer, h, should be small for small particles [10]. As it is reflected in this expression (equation 2.1), the dissolution rate (dC/dt) of a drug is directly proportional to its surface area (A), hence, decreasing particle size is a successful approach for increasing dissolution of drugs.

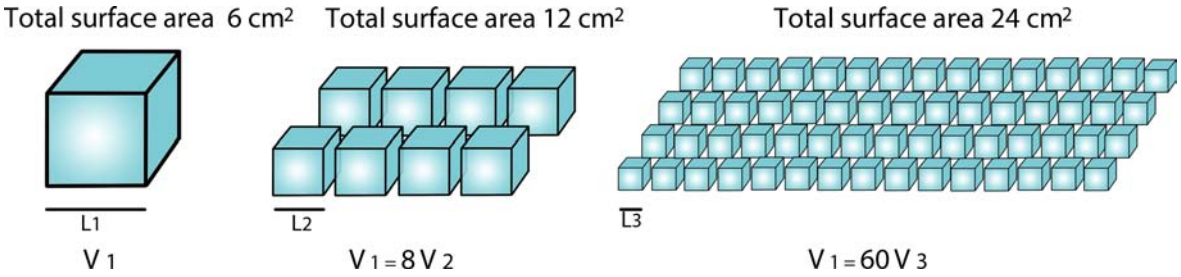

Figure 2.1: Surface enlargement.

Commercially used processes for micronization include mechanical milling, recrystallization, solid dispersion, freeze drying, and spray drying. However, these processes have limitations that include organic solvent use, thermal degradation, large residual solvent content, and difficulties in controlling particle size and size distribution during processing. These limitations affect drug particle stability, powder flow properties, and efficiency of the delivery system [11].

Current practices of API particle-size control often involve some type of size reduction subsequent to crystallization (Figure 2.2) in order to achieve some or all of the following objectives: break up needles or elongated rods into smaller aspect ratio particles, reduce the mean particle size significantly from that achieved during crystallization, reduce batch-to-batch variations, or create a more monodisperse distribution of sizes. This size reduction often implies micronization by mechanical disruption process either by milling techniques, such as jetmilling, milling in a pearl-ball-mill, or by high-pressure homogenization. The physical properties of drugs strongly influence the performance of these techniques and they are not suitable for thermolabiles, waxy or materials with low packing density, such as needle-like particles.

However, dry milling (pin or jet milling) has a number of liabilities resulting from the mechanical disruption process that can alter the surface properties as a thermodynamically activated surface is created [12]. Other disadvantages are:

* serious industrial hygiene concerns due to dust generation
* crystal form/crystallinity may be impossible to preserve across the milling step
* the product from dry milling is often rich in fines and/or highly electrostatic making downstream processing difficult
* is a very expensive operation

These drivers are leading the industry to adopt strategies that incorporate particle size and shape control into the final crystallization directly so that terminal dry milling can be eliminated from factory processes. As mention in the Introduction (Chapter 1) compressed fluid technology is an outcome of such research with particular emphasis in green synthesis and particle formation.

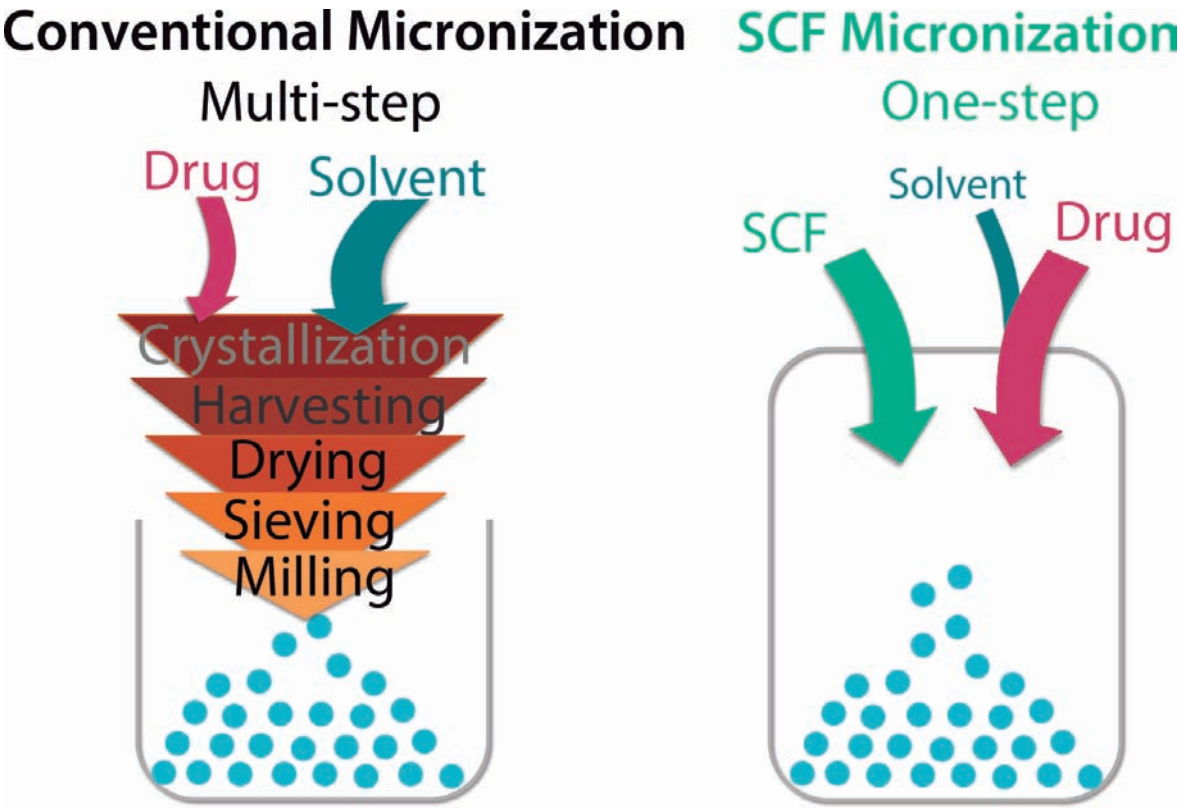

Figure 2.2: Steps required in conventional micronization vs Single step supercritical fluid micronization.

2.1.2 Crystallization of microparticulate APIs using compressed fluids

As mentioned in the Introduction (Chapter 1), the most widely used compressed fluid (CF) is CO_2 because it is nontoxic, nonflammable and easy recyclable. Apart from being considered a green solvent [13], the moderate critical parameters of CO_2 (P_c = 7.4 MPa, T_c = 304.1K) together with its low price and high availability make CO_2-based technology very attractive from an economical perspective [14]. Processes using CO_2 are developed in a non- oxidizing atmosphere and without the need for the application of high shear forces, which makes them particularly suitable for the processing of thermally, chemically or physically labile materials, such as biological compounds, chemical intermediates and pharmaceuticals. In this sense, precipitation technologies using compressed CO_2 (cCO_2) hold a great deal of promise in the pharmaceutical industry [15].

The physicochemical properties of compressed CO_2 (cCO_2) are key factors in particle design. In particular, solubility in cCO_2 is the major prerequisite for designing particles

using this dense gas as a crystallization solvent media.

To choose a process for particle design, the first thing to consider is the solubility of the substance to be crystallized in the compressed fluid. The choice between different methods will then be made considering the desired particle size, shape and structure, processing costs and production scale [16]. The study of the molecular constituents phase behavior in pure CO_2 or CO_2-expanded solvents becomes crucial, and constitutes an important first step towards successful achievement of a particulate material. One of the most effective methods for performing such studies implies the use of a high pressure variable volume cell equipped with windows that allow visualization of its interior. Solubility measurements help to prevent time and economic expenses derived from trial-and-error procedures and constitute a valuable tool to select the most convenient CF-based process for the preparation of particulate materials.

As one of the main objectives of using CO_2 is to avoid the presence of organic solvents in the processing of compounds, the study of the phase behavior in pure CO_2 is usually the first step when performing solubility studies. A certain amount of the compound of interest is placed inside the high pressure phase analyzer at the working conditions of temperature and pressure. The addition of CO_2 into the cell could lead to three different scenarios: the progressive dissolution of the solid in CO_2, the swelling of the CO_2 inside the solid or neither situation. This last case is the most common behavior for the major of drugs, polymers and polar substances. In the latter, further studies in CO_2-expanded mixtures would be required [17].

In order to get the solubility curve of a compound in the mixture of organic solvent and CO_2, the solubility of the compound in the pure organic solvent and in pure CO_2 need to be measured, as well as the solubility of the compound in the mixture of organic solvent/CO_2 at different CO_2 concentrations. One of the most widely used method to measure the solubility of a compound in a CO_2-expanded mixture is called the **Vanishing method** [18] which it is explained in detail in Section 6.2.2 of the Experimental Part. Examples of solubility curves are depicted in Figure 2.3 where it is shown the very different scenarios that can occur when adding CO_2 to a solution of a solid in an organic solvent. The behavior is defined by the minimum composition from which the CO_2 starts to provoke the precipitation of the compound, such value can be extracted from the intersection of the solubility curve with the ideal dilution line of the compound in the organic solvent/CO_2 mixture. This intersection is defined as the limit molar fraction of CO_2 (x_L), as above this value, CO_2 will cause the precipitation of the drug. The ideal dilution line

defines the expected solubility variation in an ideal process. In an ideal dilution, solubility in a mixture of solvents varies linearly with the mixture composition.

The solubility behavior of ibuprofen in CO_2-expanded acetone shows that CO_2 acts as a cosolvent until molar fractions of 0.82 (Figure 2.3a), whereas in the case of naproxen (Figure 2.3b), the addition of CO_2 over a solution of the drug in acetone causes the precipitation of the drug, revealing the antisolvent character of CO_2 from very low molar fractions of CO_2 (x_{CO_2}) [19]. Moreover, CO_2 can show a synergic behavior with the organic solvent, as was observed in the solubility behavior of hexamethylenetetramine in CO_2-expaned ethanol (Figure 2.3c) [20].

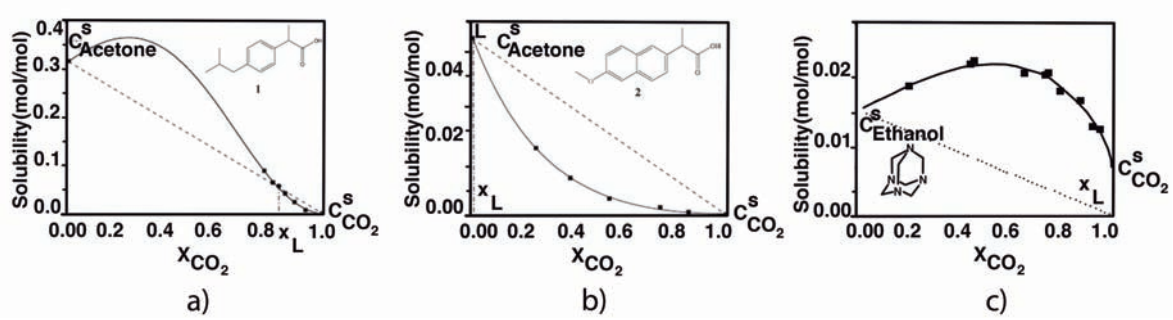

Figure 2.3: Solubility curves of a) ibuprofen, b) naproxen in CO_2-expanded acetone at 10 MPa and 298 K and c) hexamethylenetetramine in CO_2-expanded ethanol at 10MPa and 313K. Dashed lines represent the ideal dilution line, which connects linearly the solubility values of the compound in the organic solvent and in CO_2. x_L is the molar fraction of CO_2 where the solubility curve cross the ideal dilution line.

On the basis of the different solubility behaviors that a solute might have in pure CO_2 or in mixtures of CO_2-organic solvents, several precipitation processes have been developed to produce micro and nanoparticulate APIs in a single step as it is depicted in Figure 2.4. These precipitation processes can be classified into different groups depending on whether the CF, usually CO_2, acts as a solvent, antisolvent, solute or cosolvent with respect to the material to precipitate .When CO_2 is used as a solvent, the size distribution and morphology of the particles produced are a function of the concentration of the materials in CO_2 and the subsequent expansion conditions. In contrast, the CO_2 anti-solvent process is based on the change in the solubilization power of a solvent that results from adding CO_2 to it, as well as the miscibility of that solvent in CO_2 [21].

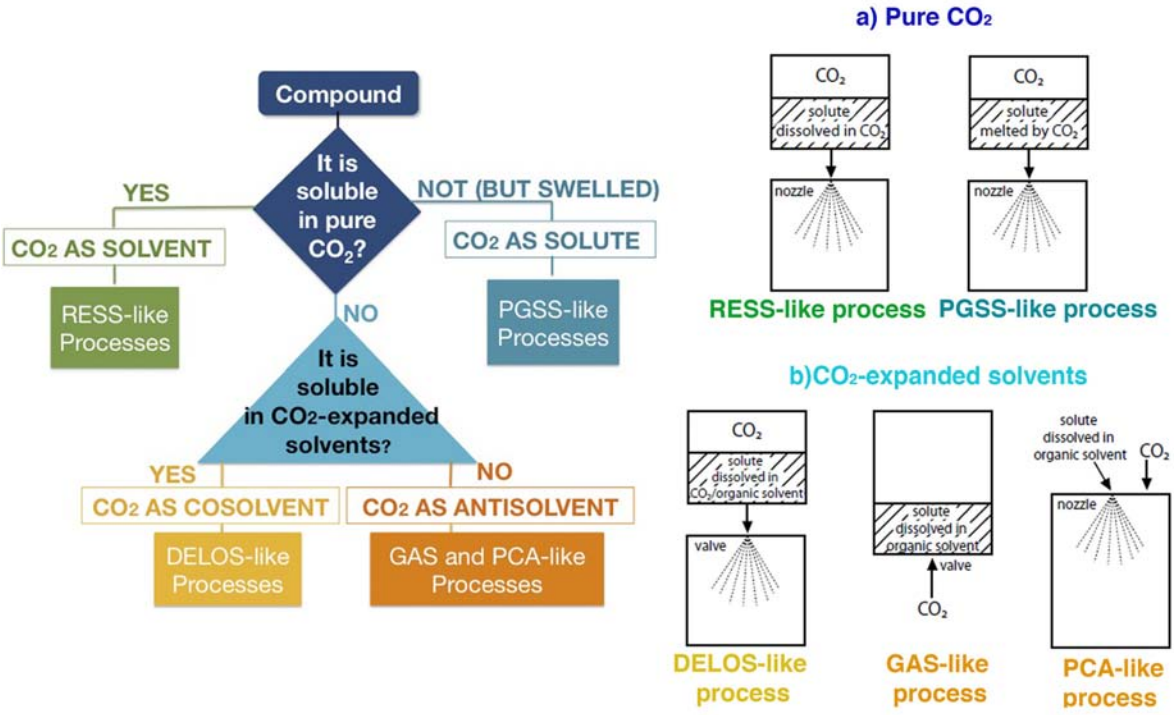

Figure 2.4: CF-based processes using either pure CO_2 or CO_2-expanded solvents. Adapted from [15].

- **CF as a Solvent: Rapid Expansion of Supercritical Solutions (RESS) process**

  Here, the solute is first solubilized in the supercritical fluid. The solution is then expanded across a nozzle or capillary at supersonic velocities. The rapid expansion leads to supersaturation of the solute due to an abrupt decrease of the dense fans solvating power and subsequent precipitation of virtually contaminant-free particles. The RESS process has been demonstrated to produce contaminant-free micro particles ranging from a few microns to several hundred microns, but some examples in the literature report nanometric particles using appropriate nozzles [22, 23, 24]. The RESS process has also been applied for coprecipitation of solutes [25]. The facts that affect particle size and morphology in the RESS process include the length/diameter ratio of the expansion device, the RESS time scale dictated by the expansion trajectory from the preheater and the expansion device, and particle agglomeration during free jet expansion [16]. A major limitation of the RESS process is that, at moderate temperatures and pressures (60°Cand 300 bars), the solubility of

compounds in CO_2 is on the order of 0.01wt% or less. Indeed, the high temperatures that are often required make this process unsuitable for labile polymers and drugs. A large amount of fluid is needed to produce a small yield, hence, RESS process is a comparatively costly technique.

- **CF as a solute: Particles from Gas Saturated Solutions (PGSS) process**

  As the solubility of compressed gases in liquids and solid-like polymers is usually high and much higher than the solubility of such liquids and solids in the compressed gas phase, the PGSS process consists in solubilizing supercritical CO_2 in melted or liquid-suspended substances, leading to a so-called gas-saturated solution/ suspension. When this solution is rapidly depressurized through a nozzle, microparticles can be formed due to the reduction in temperature and atomization experienced by the gas saturated solution during the expansion, which leads to the solidification of the melt in a micro particulate form. Advantages of PGSS process include the lack of necessity for the solute to be soluble in CO_2 and the absence of solvents. However, its main limitation is the melting of the compound, which can be problematic for heat- sensitive molecules. In order to tackle this problem, some drugs have been processed with polyethylene glycol 4000, which dissolves the drugs and lowers their melting point allowing its precipitation at milder conditions.

- **CF as an antisolvent**

  cCO_2 is a relatively poor solvent for most polymers and pharmaceutical compounds, therefore, these relatively low solubilities are exploited in this process wherein the solute of interest is dissolved in a conventional solvent to form a solution. The preferred ternary phase behavior is such that the solute is virtually insoluble in compressed cCO_2 while the solvent is completely miscible with cCO_2 at the recrystallization process temperature and pressure. The advantage of processes using CO_2 as an antisolvent in comparison to conventional precipitation techniques is that powders may be produced at ambient temperatures, in a low shear environment and with a low level of oxygen exposure. All these considerations are relevant for the production of drug and protein powders. It also has the advantages of having a higher solute throughput and flexibility of solvent choice. Antisolvent techniques are probably the most used for the micronization of pure active drugs and polymers from particles sizes ranging from nanometers to microns. The solute can be recrys-

tallized in two ways:

- In the Gas Anti-Solvent (**GAS**) process a batch of solution is expanded several-fold by mixing with dense CO_2 in a vessel. Because the CO_2 expanded solvent has a lower solvent strength that the pure solvent, the mixtures become supersaturated, forcing the solute to precipitate or crystallize as micro particles.
- The Precipitation with Compressed Anti-solvents (**PCA**) process, involves the spraying of solution through a nozzle as fine droplets into compressed CO_2. Using PCA-like methods, precipitates with a high residual solvent content are generally achieved and lengthy drying periods are usually required, which often leads to particle agglomeration and aggregation. This inconvenience can be reduced by promoting a better mass transfer between the supercritical antisolvent and the solution during its spraying, which can be achieved by favoring intensive mixing between both fluids, for example, using an ultrasonic nozzle.

- **CF as a co-solvent**

  In contrast to antisolvent techniques, DELOS (Depressurization of an Expanded Solution) process takes advantage of the cosolvent behavior that CO_2 can present over solutions of compounds in certain organic solvents [26]. In this method, CO_2 is added to an organic solution of the compound(s) to precipitate, resulting in a new pressurized solution, usually at pressures lower than 10MPa, in which the solvent medium is formed by the CO_2-expanded mixture. The rapid evaporation of the CO_2 upon depressurization of the solution generates an abrupt, fast and homogeneous cooling that provokes the straightforward precipitation of the solute as micro or submicronparticles. This abrupt and homogeneous temperature reduction produced during the depressurization of the CO_2-expanded solution generates a pronounced and very uniform increase of the supersaturation in every point of the solution, favoring the assembling of solute molecules through homogeneous primary nucleation rather than by crystal growth, and promoting the formation of micro or submicron sized particles with narrow particle size distributions and exceptional supramolecular structural homogeneity. The use of CO_2-expanded solvents instead of pure CO_2 offers numerous advantages for novel process development including enhanced solubilities of polar organic compounds and tunability of their solvent properties [17]. DELOS method takes profit of the advantages of

CO_2-based processing while avoiding the use of severe working conditions. This methodology use milder conditions of pressure (10MPa) and temperature (308K) than most of the described methodologies. Lower temperatures allow the processing of heat-labile compounds, while milder pressures would reduce the capital cost of a high-pressure plant when scaling up the process.

In Table 2.5 is gathered comparative data from different CO_2-based precipitation process.

Method	CO_2 behaviour	Working Pressure (MPa)	Stirring efficiency	Complex equipment	CO_2 Consumption*	Obs.
RESS	Solvent	>20	No	Nozzles	10^3-10^4	Limited solubility
GAS	Anti-solvent	5-10	Yes	No	1-20	Complex scale-up
PCA	Anti-solvent	6-30	No	Nozzles	1-50	Complex scale-up
PGSS	Solute	8-20	Yes	No	0.1-1	Limited solubility
DELOS	Co-solvent	5-10	No	No	1-20	Easy scale-up

*Kg CO_2 per kg drug precipitated.

Figure 2.5: Comparison of different CO_2-based techniques.

In DELOS, CO_2 acts as a cosolvent, which allows to work with more concentrated solutions than in technologies using pure CO_2. This makes possible to precipitate higher amounts of polar and high molecular weight compounds than in RESS process, working at lower pressures. In addition, this method is suitable for drugs with low melting point or for polymers that are not able to absorb high quantities of CO_2. In comparison to other CF crystallization techniques, like RESS and PCA, DELOS process requires mild working pressures, which is a crucial parameter in the economical evaluation of the process for industrial applications. In cases when CO_2 acts as anti solvent, the most suitable processes are GAS and PCA. The PGSS method can only be applied when drugs melt and can dissolve a significant amount of CO_2 at the working conditions.

The collection of particles in DELOS in performed in a filter at atmospheric pressure, however in PCA and GAS technologies, the collection is conducted at high pressure, and therefore the operation of such processes in a continuous mode is much more compli-

cated. Another important parameter when comparing CO_2-based technologies is the complexity of the facilities. It is important to bear in mind that as working pressure increases, the cost associated to the high-pressure equipment is also increased, especially when scaling-up. In this way, DELOS is presented as a promising alternative as it does not required high pressures. The working pressures in GAS method are very similar to the ones employed in DELOS, however, in GAS precipitation, the formation of the particles relies on the efficient stirring of the mixture, which makes the scalability more complex and increase the final cost. In PGSS, PCA and RESS the need of a nozzle also hampers the scalability of the process.

2.1.3 DELOS process

DELOS method procedure consists of three stages which are depicted in Figure 2.6. First, the solid to be crystallized is dissolved in an organic solvent at atmospheric pressure and working temperature (T_W) to form a solution with an initial concentration (C_i) which is charged into the high-pressure vessel. Second, the initial solution is pressurized up to the working pressure (P_W) by the addition of a given amount of CO_2, expressed by the CO_2 molar fraction of the mixture organic solvent/CO_2 (x_W). In this second stage, the solute concentration (C_W) should remain below the saturation limit in the CO_2-expanded mixture. That is, the solute is soluble in the CO_2-expanded mixture showing a single liquid phase. Finally, the solution is depressurized from the working pressure (P_W) to atmospheric pressure, through a nonreturn simple valve. During the depressurization, CO_2 evaporates very rapidly from the solution producing a large, fast, and extremely homogeneous decrease of the solution temperature down to a final temperature (T_F). The particles precipitated, due to this temperature decrease, are filtrated at atmospheric pressure. The equipment and protocols used in the present Thesis for DELOS experiments are described in Section 6.3.2 of the Experimental Part.

DELOS process is suitable for the preparation of drugs as micro and nano particulate materials, when CO_2 behaves as a co-solvent in the mixture of the drug in the CO_2-expanded solvent at the working conditions of pressure and temperature. Therefore, it is essential to have a good understanding of the solubility behavior of the compound of interest in the appropriate CO_2-expanded solvent system for optimal design of a successful DELOS experiment. Another requirement for an adequate DELOS experiment is that the solubility of the drug in the organic solvent should strongly depend on temperature.

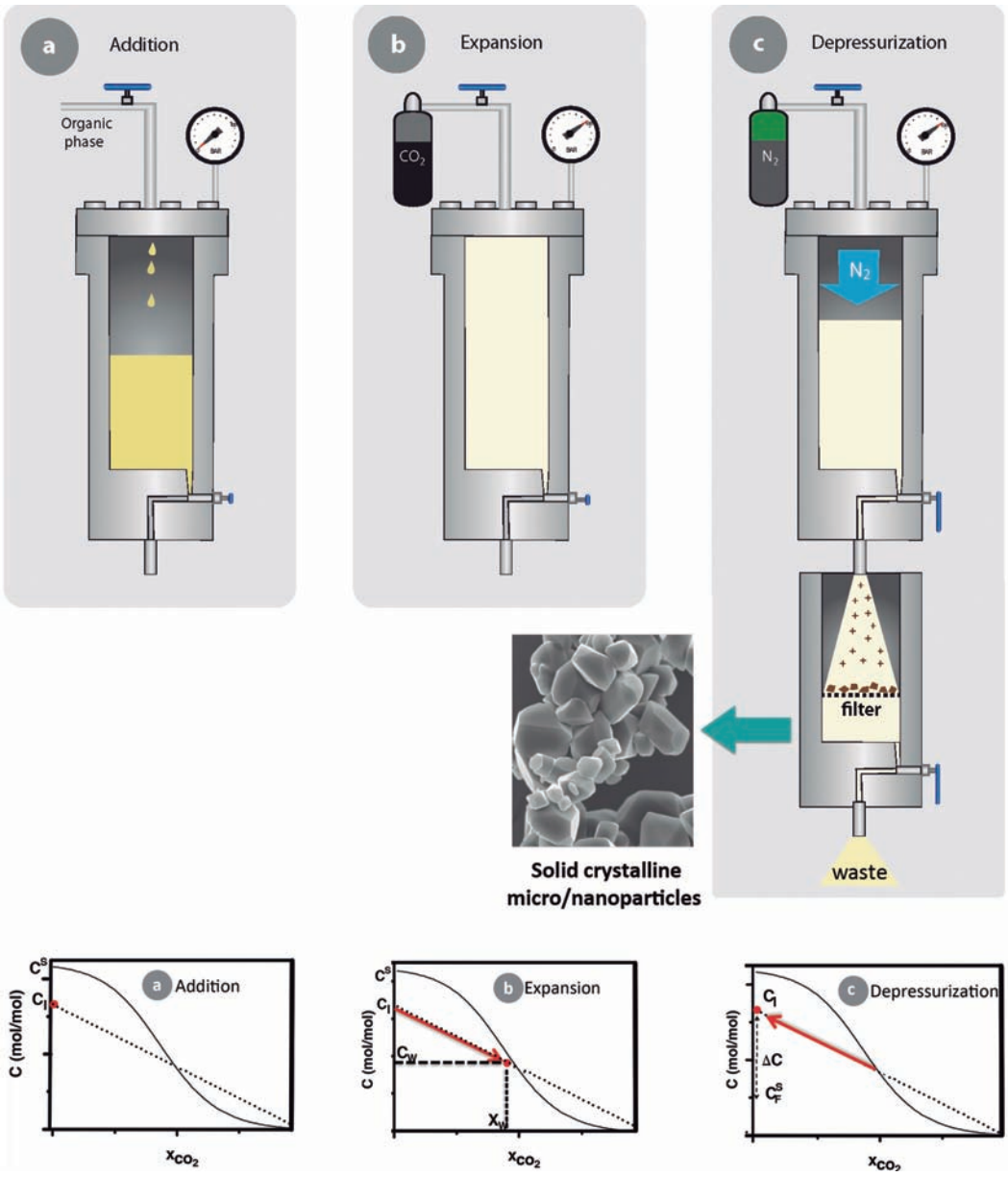

Figure 2.6: Steps in the DELOS process

Hence, apart from knowledge of the phase behavior of the drug in the CO_2-expanded solvent, information regarding the solubility dependence with temperature of the drug in the organic solution is also essential.

Thermodynamical considerations of DELOS method

Differently from conventional cooling crystallization processes, it can be assumed in this case, the final temperature (T_F) obtained after depressurization is reached before primary nucleation takes place. Therefore, as schematized in Figure 2.6, the initial solute concentration is re-establish ($C_F = C_i$). The magnitude of the temperature decrease, defined as $\Delta T = T_F\text{-}T_W$ determines the yield and the characteristics of the crystalline particles produced. It has been demonstrated that changes on the flow rate through the depressurization valve and on the working pressure (P_W) keeping the molar fraction of CO_2 constant (x_W), do not affect ΔT [27]. This result is very important from a practical point of view since it allows to reduce P_W to a much lower value than those used in other high pressure crystallization techniques, without affecting the yield neither the final characteristics of the precipitate. The magnitude of the temperature decrease is determined by the nature of the solvent employed in the process and the CO_2 content (x_W) of the expanded solution before its depressurization. During the depressurization of the expanded solution, CO_2 goes from the liquid state at P_W to the vapor state at atmospheric pressure. Since DELOS process is an adiabatic process, the heat required for the CO_2 vaporization must be extracted from the liquid solution and as a consequence, the solution experience the large, abrupt and homogenous decrease of temperature [27]. The heat required (q_R) for the vaporization of CO_2 is the vaporization enthalpy:

$$q_R = \Delta H_{vap} \cdot n_{CO_2} \,, \tag{2.2}$$

where ΔH is the vaporization enthalpy and n_{CO_2} is the number of CO_2 moles. As this is an adiabatic process, the heat required for the vaporization of CO_2 should be the same as the extracted heat (q_E):

$$q_E = q_R \,. \tag{2.3}$$

The extracted heat is given by:

$$q_E = n_{(dis)} \cdot Cp_{(dis)} \cdot \Delta T \,, \tag{2.4}$$

where $n_{(dis)}$ is the moles of the solution and $Cp_{(dis)}$ is the specific heat of the solvent. Hence, as a consequence, the decrease in temperature (ΔT) experienced by the solution depends on the organic solvent and the mass of solvent as well as the molar fraction of CO_2:

$$\Delta T = \frac{\Delta H_{vap} \cdot n_{CO_2}}{n_{(dis)} \cdot C_{p(dis)}} \,. \tag{2.5}$$

It can be inferred from expression 2.5, that as larger is the CO_2 content (n_{CO2}), larger will be the temperature decrease ΔT.

Under the conditions of DELOS crystallization, it could be considered that the difference between the initial concentration of the compound in the organic solution (C_i), and the solute solubility in the organic solvent at the final temperature reached after depressurization (C_F^S) is the maximum supersaturation achieved (ΔC =C_I-C_F^S). Thus, the higher ΔC, the higher the maximum supersaturation attained, and nucleation will be more favored than crystal growth provoking the crystallization of small particles. The process parameters that affect ΔC are the initial concentration of the compound in the organic solvent (C_i) and the CO_2 content (x_W), as the latter will determine the final temperature achieved after depressurization (T_F) and this value will define the solubility of the compound in the organic solution (C_F^S). The higher the x_W and C_i, the higher the supersaturation attained, and hence, smaller the particles produced. However, in most cases,x_W and C_i can not be increased unlimited, as in order to achieve successful crystallization experiments, the experimental conditions must ensure that the CO_2-expanded mixture in stage b of the DELOS process (see Figure 2.6) is in the liquid region, along or close below the solubility curve. Only in the cases where the addition of CO_2 provokes a synergic enhancement of the solubility in the organic solvent, both parameters can be increased unlimited. Figure 2.7 depicts the example of a solubility curve (blue line) of the compound in a CO_2-expanded mixture where CO_2 acts as a cosolvent. In this case, the solubility line limits the values of x_W and C_i. The dashes lines are the working lines of the different experimental conditions representing the addition of pure CO_2 over an initial solution of the compound in the organic solvent with a defined C_i. If C_i is increased (from experiment A to experiment B), the maximum x_W should be lower in order to be in the single phase region of the solubility curve as Figure 2.7 shows.

A recent study carried out in *Nanomol* [28] reveals that it is possible to predict the relative specific weight of the process parameters on the supersaturation ratio, and therefore, on particle characteristics by simply determining the solubility variation of the compound to be crystallized with temperature at atmospheric pressure. This study was conducted over the precipitation of cholesterol and aspirin performed along the solubility curve and was designed to compare the weight of x_W and C_i parameters on the supersaturation achieved and on particle characteristics, and to discern which parameter yields a more important decrease in particle size.

Figure 2.8 shows, in the temperature range studied, that aspirin solubility in acetone

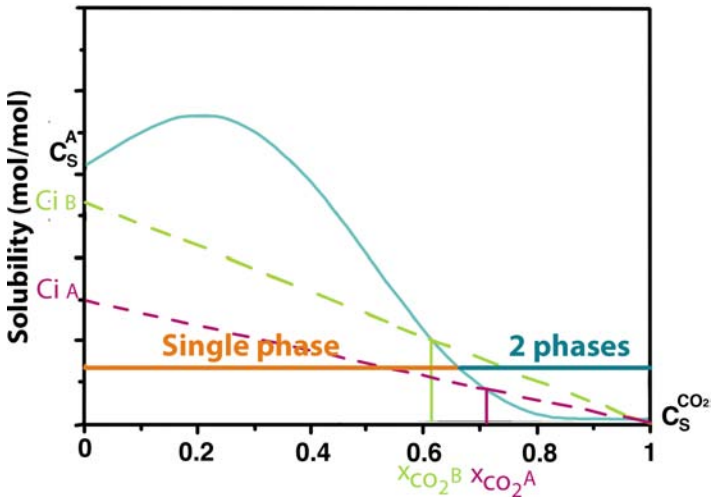

Figure 2.7: The solubility curve (blue line) of the compound in the CO_2-expanded solvent limits the maximum values of x_w and C_I possibles in order to be in the single-phase region

decreases linearly with decreasing temperature whereas solubility of cholesterol in acetone decreases exponentially with temperature. Therefore, in aspirin experiments, achieving a lower depressurization temperature results in a remarkably lower solubility at T_F. Hence, a low temperature exerts a strong impact on the final supersaturation during depressurization ($\Delta C = C_I - C_F^S$). In contrast, in the case of cholesterol, the solubility variation in acetone shows an exponential behavior, with no significant variation of solubility at temperatures below 275 K. In this case, increasing the CO_2 content of the mixture to reach a lower T_F will not result in a significant increase of the supersaturation attained, and the variation of the initial concentration C_i will produce a more pronounced effect on the supersaturation achieved in the crystallization. In cholesterol experiments, the difference in supersaturation is governed by the difference in the initial concentration. Therefore, the effect of increasing C_i in cholesterol precipitations and increasing x_W in aspirin experiments was translated into the obtaining of smaller particles in both cases.

Thus, the study of the solubility variation of the compound to be crystallized with temperature at atmospheric pressure and the solubility in the CO_2-expanded mixture allows to choose the most suitable working parameters and to tune the final characteristics of the particles precipitated.

DELOS process was developed in 2001 in *Nanomol* group, where this Thesis has been carried out. Since its discovery, it has been possible to obtain micronized particles of 1,1-bis-(n-butylamino)-9,10-anthraquinone (colorant solvent blue 35) with a high degree

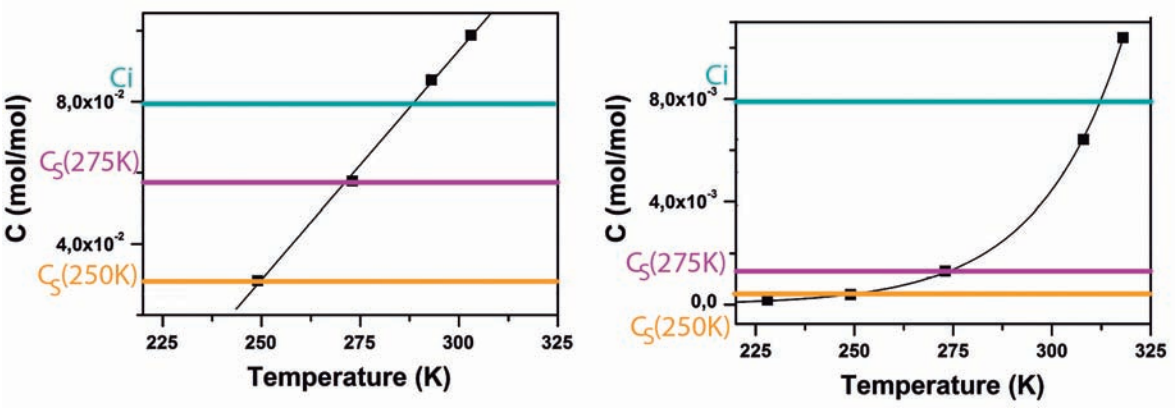

Figure 2.8: Solubility of aspirin (ASP) (left) and cholesterol (COL) (right) in acetone as a function of temperature

of crystallinity and reducing the particle size two orders of magnitude in comparison to the particles produced by conventional cooling crystallization technique from methanol solutions [26]. The feasibility of DELOS method to process active pharmaceutical ingredients (ibuprofen, cholesterol, aspirin, naproxen) as finely divided powders with narrow size distribution, high crystallinity degree, high polymorphic purity and free from residual solvent has also been demonstrated. Moreover, it has been confirmed that DELOS process is a kinetically controlled crystallization in which high supersaturation levels are rapidly achieved. This fact makes this process especially indicated for obtaining kinetically controlled polymorphs of exceptional polymorphic purity. In addition, recently, a new polymorph of β-sitosterol has been discovered, which was more crystalline than the native form, though its precipitation by DELOS process [29].

It is clear from all theses studies that the feasibility and performance of DELOS process has been extensively demonstrated. Hence, this chapter is devoted to the the development of systematic procedures with two main objectives: the optimization of thermodynamic parameters, that will be explored in the first section of the chapter, and the second part will be focused on understanding how the crystallization of molecules with very high precipitation kinetics takes place under DELOS method.

2.2 DELOS method for the precipitation of ibuprofen as microparticles

Ibuprofen, as it is considered a model for poorly-soluble water compounds, has been processed by several conventional methods with the aim of reducing its particle size and thus achieve an increase in its bioavailability. Particle size reduction of ibuprofen is often difficult to achieve during dry milling, particularly below the reported brittle-ductile transition particle size of 854 μm [30] as ibuprofen is known to show great ductility [31], although recent findings suggest that submicron sized micronized product is achievable by wet milling [32, 33]. There are several examples in the literature of milled ibuprofen [34, 35]: it has been micronized by air jet milling [36] and also by a continuous fluid energy mill [36]. The micronization of drugs using mills, as explained previously, is extremely inefficient, producing particles with broad size distribution and that can be afflicted with impurities due to abrasion [37].

Ibuprofen has been extensively studied by Müller et al. [12, 38, 39]. They achieved a dissolution enhancement with an *in situ* process of micronization of the drug. This process is called **the solvent change method** and consists of forming a dispersion by instantaneously mixing two liquids in the presence of a stabilizer. Then, the dispersion is spray-dried to dry the already formed particles. The particles obtained using this method are in the range of microns, however, the process requires the aid of stabilizing agents. In this method, the generation of particles relies on the efficient mixing of the two solvents and as mentioned in the Introduction of this Thesis (Chapter 1), the scaling-up of effective mixing entails many obstacles.

Several authors have reported micronization of ibuprofen using **supercritical fluid crystallization techniques**, as they have a huge potential for producing micron-sized particulate materials in a single step [40]. The most widely used procedure has been RESS [41]. However, the RESS process operates at high pressures and requires complex atomization systems for precipitating significant amounts. In this situation, a multi-nozzle system or the use of a porous sintered disk through which pulverization occurs are required. In both cases, particle size distribution is not easy to control, and may be much wider than in the case of a single nozzle. There is still a big challenge in the scaling-up of the RESS process [42]. Another considerable limitation of RESS process for micronization of ibuprofen lies in the too low solubility of the compound in pure CO_2. The filtration of the

solid at high pressure also entails some experimental difficulties. Attending to these drawbacks, DELOS method introduces some advantages: the solubility of ibuprofen in several CO_2-expanded solvents (ethanol, acetone, acetonitrile) is much higher than in pure CO_2, hence, more quantities of the product can be crystallized. The scaling-up of this method is very simple since this procedure does not require neither complex agitation systems nor sophisticated atomization apparatus, conversely as in RESS process. In addition, the simpler equipment and lower pressures of DELOS introduce economic advantages.

The feasibility of producing microparticles of ibuprofen by DELOS has already been demonstrated [28]. However, up to now, there is not a deep understanding of the thermodynamics behind the precipitation of ibuprofen by DELOS, which should allow to control process parameters in order to obtain higher yields and narrower particle size distribution.

2.2.1 Thermodynamic Analysis of DELOS precipitation of ibuprofen

The relationship between supersaturation and particle size is one of the most important for engineering and optimization of the precipitation process. The nucleation rate increases exponentially with supersaturation [43]. As stated before, in DELOS, the $\Delta C = C_I - C_F^S$ is the maximum supersaturation that can be achieved. Thus, in order to promote nucleation phenomena, a proper design of a DELOS crystallization should define a set of working conditions such to obtain the maximum supersaturation attainable.

The solubility curves of Ibuprofen in CO_2-expanded ethanol, acetone and acetonitrile were measured previously in *Nanomol* under the framework of the PhD Thesis of Dr. Muntó [44]. Figure 2.9 depicts the phase diagram for Ibuprofen in CO_2-expanded acetontrile (a), ethanol (b) and acetone (c) at 298 K and at 10 MPa in terms of the concentration of ibuprofen as a function of the CO_2 concentration in the solvent mixture in a solute-free basis. Over the solubility curves is the two-phase region, where the system is composed of a solid phase and a liquid phase. Under the curve is the single-phase region where ibuprofen is dissolved in the CO_2-expanded mixture. The phase boundary in the three cases has a sigmodal shape. Attending to this type of solubility curve, the two process parameters that affect the supersaturation, x_W and C_i can not be increased unlimited. Hence, the following section endeavors to study the specific weight of these process parameters on the maximum supersaturation (ΔC) that could be attained and, as a consequence, on the final characteristics of ibuprofen particles.

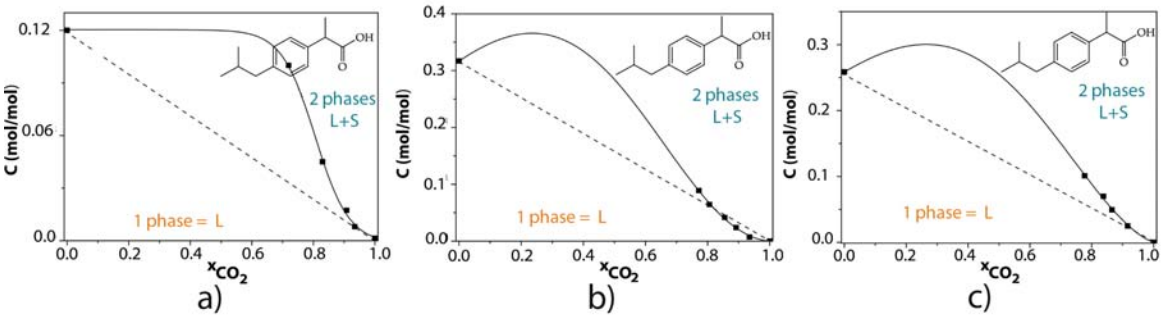

Figure 2.9: Solubility curves of Ibuprofen in CO_2-expanded a)acetonitrile, b)ethanol and c)acetone at 10MPa and 298K.

The solubility behavior of ibuprofen in the mixtures of CO_2 with ethanol, acetone and acetonitrile is known, however, there is a lack of information regarding the solubility evolution of ibuprofen in those organic solvents at atmospheric pressure with decreasing temperature. Therefore, the main objective of this section is to investigate this solubility behavior in order to elucidate which process parameters (x_W and C_i) govern the supersaturation.

The solubility evolution of ibuprofen with temperature in ethanol, ethyl acetate and acetone was measured following the experimental procedure detailed in Section 6.2.1 of the Experimental Part and the values obtained are depicted in Figure 2.10. Although the solubility curve of ibuprofen in CO_2 -expanded ethyl acetate is not determined, Dr. Muntó proved that it is feasible to process ibuprofen through DELOS using ethyl acetate as solvent. As can be ascertained from Figure 2.10, ibuprofen is very soluble in these systems and solubility variation shows an exponential decay in all solvents. Therefore, as in the case of cholesterol, the best way to enhance the supersaturation is to increase the initial concentration (C_i) as this parameter will stronger influence supersaturation than x_W.

A series of experiments were designed aiming to decrease particle size distribution and to increase crystallization yield. Based on the previous remarks, it was chosen to work with almost saturated solutions of ibuprofen.

The relationship between the actual concentration (C_i) and the solubility at the working temperature (C_s) is defined by β_i, which is calculated by:

$$\beta_i = \frac{C_i}{C_s}\,. \tag{2.6}$$

Hence, as it was decided to work with almost saturated solutions of ibuprofen, the value of

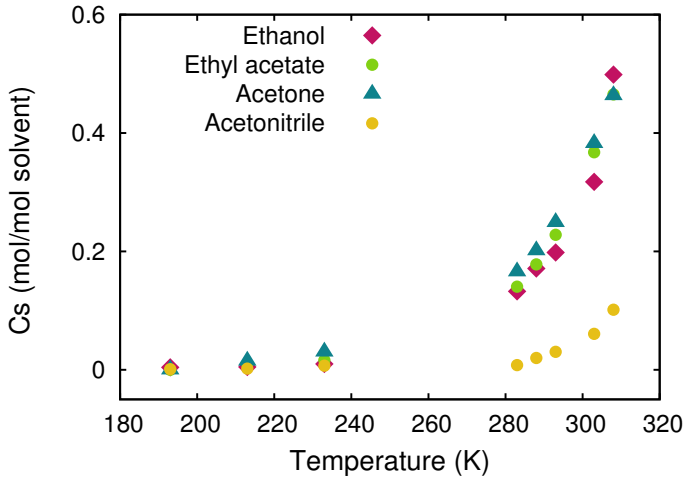

Figure 2.10: Solubility of ibuprofen in different organic solvents as a function of temperature

β_i was fixed at 0.9 for all the DELOS precipitation experiments from different organic solvents. Dr. Muntó conducted her experiments at a value of β_i of 0.6. Table 2.1 summarizes the process operation parameters (x_W, organic solvent) of all the conducted experiments as well as the final temperature reached after depressurization, when crystallization occurs, and the corresponding absolute supersaturation (ΔC) attained during depressurization. All the experiments were conducted at P_W = 10 MPa and T_W = 298 K.

Experiments 1 and 2 were carried out keeping all the process parameters constant except x_W. It can be inferred how the increase in the molar fraction of CO_2 is translated into a lower T_F. Moreover, the effect of the nature of solvent is also reflected in the temperature decrease experienced by the solution. The values presented in Table 2.1 indicate that the temperature decrease is different for each solvent.

In all the experiments, finely divided powders with micrometric size of highly crystalline ibuprofen were obtained as it is reflected in the X-ray powder diffraction spectra depicted in Figure 2.11. However, in the experiment using ethanol (experiment 4) the amount of solid collected in the filter was very low and not enough to perform a proper characterization. The precipitated solid instead of remaining in the filter, passed trough it and stayed in the mother liquor. This can be rationalized assuming that the particles produced are smaller than the pore size of the filter (200 nm) which might be possible considering the high supersaturation obtained in the experiment 4. Another hypothesis for such a low collection of solid can be found in the crystallization kinetics of ibuprofen

Table 2.1: DELOS experiments for the precipitation of Ibuprofen from different CO_2-expanded solvents.

Exp.	Solvent	C_i [a] (mol/mol)	x_W [b]	T_F [c] (K)	ΔT [d] (K)	C_F^S [e] (mol/mol)	ΔC [f] (mol/mol)
1	Acetone	0.28	0.74	261	-37	0.078	0.208
2	Acetone	0.28	0.82	250	-48	0.052	0.234
3	Ethyl acetate	0.25	0.83	241	-57	0.026	0.227
4	Ethanol	0.23	0.84	248	-50	0.029	0.204
5	Acetonitrile	0.06	0.80	248	-50	0.045	0.018

DELOS Experiments at 298 K and 10 MPa using different solvents, [a]initial concentration of Ibuprofen in the organic solvent, [b]CO_2 molar fraction, [c]Temperature reached after depressurization, [d]Difference from the working temperature to the final temperature,[e]Solubility of Ibuprofen in the organic solvent at the final temperature,[f] Supersaturation.

in ethanol.

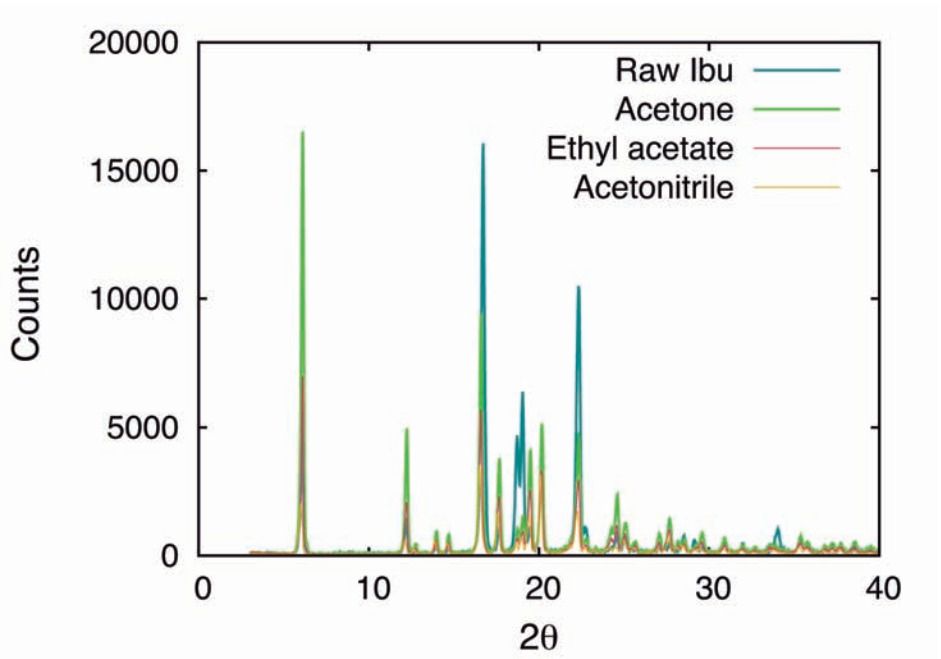

Figure 2.11: X-ray powder diffraction spectra of the raw ibuprofen and the ibuprofen precipitated by DELOS using acetone, ethyl acetate and acetonitrile.

Table 2.2: DELOS crystallization of outcome: Particle size distribution and Yield.

Experiment	Solvent	ΔC(mol/mol)[a]	Size distribution (μm)[b]			UI[c]	Yield (%)[d]
			d(0.1)	d(0.5)	d(0.9)		
1	Acetone	0.20	3.38	9.76	24.14	14	60
2	Acetone	0.23	2.84	6.78	14.37	19	78
3	Ethyl acetate	0.22	3.36	8.27	24.25	13	47
4	Ethanol	0.20	-	-	-	4	
5	Acetonitrile	0.01	3.99	13.04	46.86	8	64

[a]Supersaturation, [b]Volumetric particle size distributions expressed in percentiles of 10, 50 and 90% of accumulated volume, [c]Uniformity index is defined as d(10)/d(90)*100,[d]DELOS yield expressed in % of recovered mass.

The outcome of the crystallization experiments is displayed in Table 2.2. Particle size distribution has been measured by Light Scattering following the experimental procedure detailed in Section 6.4.1 of the Experimental Part.

The smaller and narrower particle size distribution and the higher yield corresponds to experiment 2. In this experiment, the supersaturation achieved is higher than in experiment 1 and the experiments of Dr.Muntó. In all the experiments performed in this Thesis the supersaturation has been increased with respect to the experiments conducted during her Thesis, and thus, smaller particles with better yields have been achieved. Nevertheless, the most significant decrease in particle size and increase in yield was achieved using acetone as organic solvent. This fact highlights the relevance of choosing the appropriate solvent for a successful crystallization. Khan and Jiabi [45] precipitated ibuprofen using methods such as cooling hot solutions of the drug and precipitation of crystals of drug solutions from different organic solvents. They also obtained the smallest particles sizes (and consequently the highest dissolution rates) when using ethanol and acetone.

The experiments reported in Table 2.1 were repeated in similar conditions, obtaining analogous output.

The morphology of the precipitated obtained was characterized by Scanning Electron Microscopy following the experimental protocol presented in Section 6.4.2 of the Experimental Part. Crystal shape also depends on the solvent employed as Figure 2.12 reveals.

As can be seen in Figure 2.12, ibuprofen particles present a high agglomeration. For

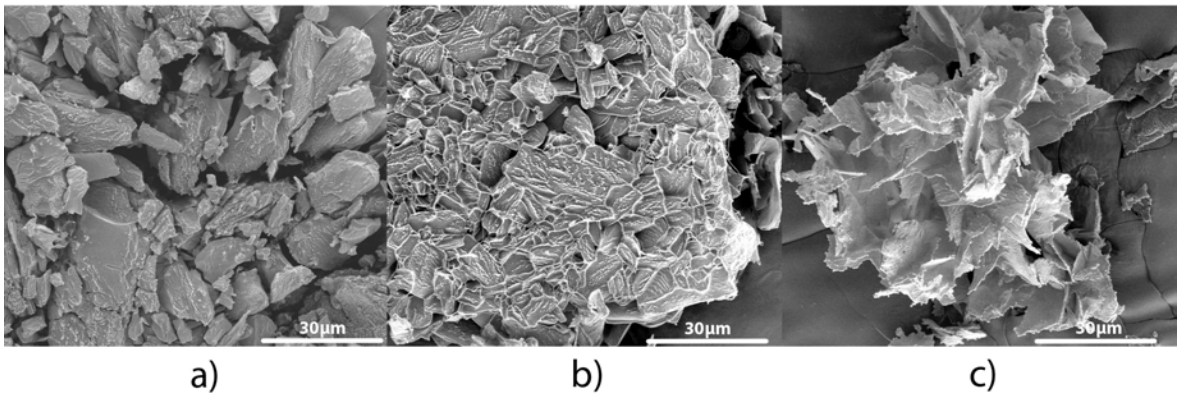

Figure 2.12: SEM images of ibuprofen precipitated through DELOS when using a) ethyl acetate, b) acetone and c) acetonitrile

this reason, in order to properly assess the difference in morphology observed when using different organic solvents, ibuprofen particles were further characterized by a microscope-based particle characterization system Morpholgi 3G. Morpholgi 3G is an imaging system that analyzes particles based on pictures of each one taken by the microscope. It measures size and shape of particles by static image analysis technique. The data acquisition (images of each particle) was carried out over a liquid suspension. The particles were suspended in water with 0.01% vol. of Tween 80 and sonicated for 5 min, hence, agglomeration of particles was averted. Section 6.4.3 gathers a more detail description of the equipment used and the complete protocol required for sample preparation.

The main difference with Light Scattering technique is that Morphologi 3G measures the perimeter of the particles as well as the length and width of the particle. In this case, particle size is measured in number of particles. The software also allows to compare the shape of different particles.

Figure 2.13 displays the mean size of the particles from experiments using acetone, ethyl acetate and acetonitrile, expressed as number distribution and volume distribution. As can be ascertained, the values obtained are in agreement with the reported values from Light Scattering measurements.

More relevant information is reported in Figure 2.14 where the comparison of the three samples is depicted. This comparison tells us that particles obtained using acetone and ethyl acetate are very similar between them and the ones obtained from acetonitrile differ from the two other. The difference between the particles is related to their circular-

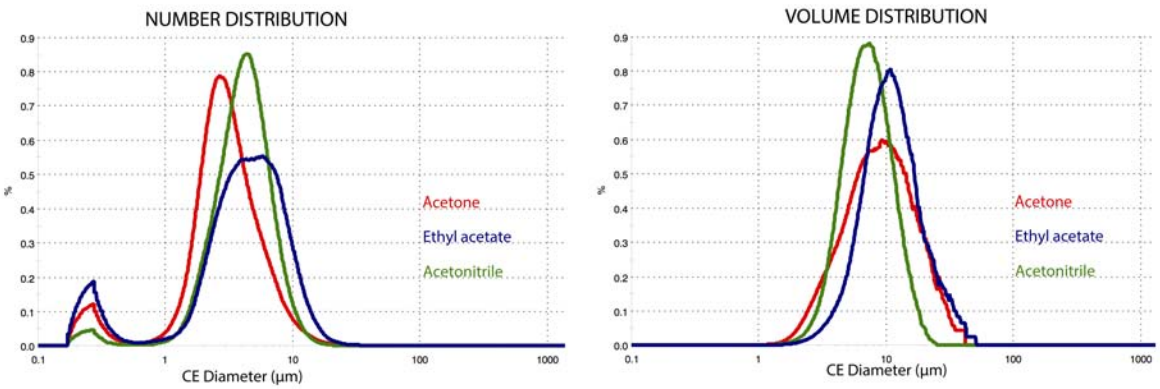

Figure 2.13: Particle size expressed as equivalent diameter in number and in volume distribution of ibuprofen particles precipitated by DELOS using acetone, ethyl acetate and acetonitrile.

ity.

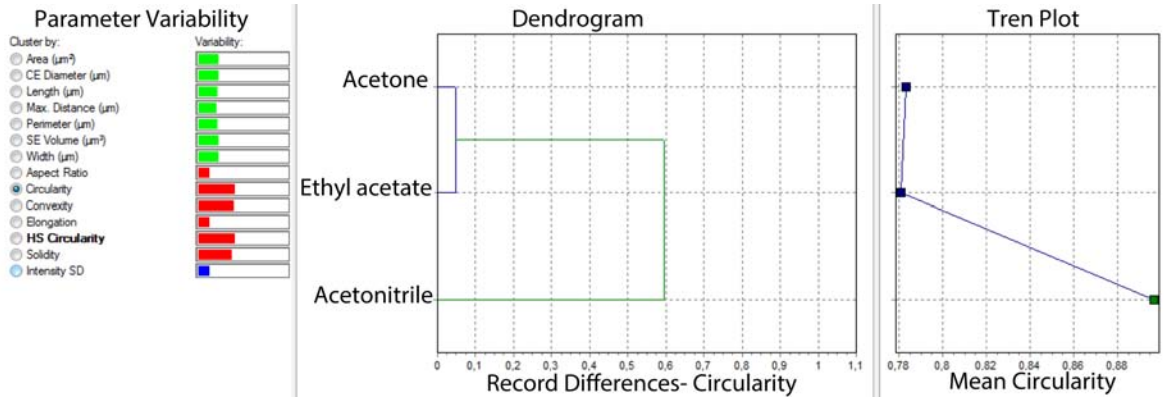

Figure 2.14: Comparison of of ibuprofen particles precipitated by DELOS using acetone, ethyl acetate and acetonitrile.

Figure 2.15a compares the circularity calculated by the Software for the three samples. Circularity is the ratio of the circumference of a circle equal to the object's projected area to the perimeter of the object:

$$Circularity = \frac{2 \cdot \sqrt{\pi \cdot Area}}{Perimeter}. \tag{2.7}$$

As mention, circularity of particles from acetone and ethyl acetate is very similar and acetonitrile particles present a higher circularity value. Another important parameter is the

aspect ratio, defined as the relation between the width of the particle to the length. The aspect ratio of the different particles is depicted in Figure 2.15b and it is inferred that the more elongated particles are the ones obtained when using ethyl acetate as solvent.

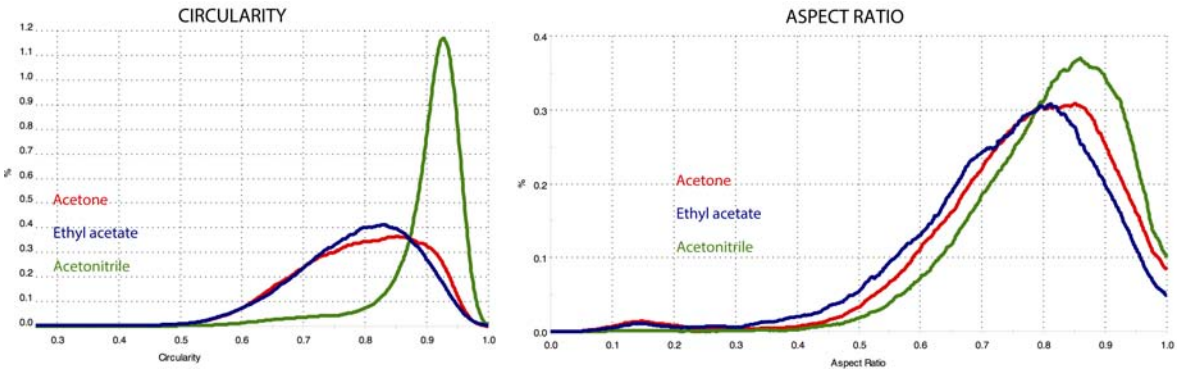

Figure 2.15: Circularity and aspect ratio of ibuprofen particles precipitated by DELOS using acetone, ethyl acetate and acetonitrile.

Finally, a representative selection of images of the particles taken by Morphologi 3G is disclosed in Figure 2.16, where the shape of ibuprofen particles is clearly seen. Ibuprofen particles precipitated by DELOS using acetone and ethyl acetate yield more elongated and rectangular particles compared to the particles obtained by DELOS precipitation from CO_2-expanded acetonitrile that are more squared.

Several authors have also seen differences in the morphology of the ibuprofen particles precipitated using different organic solvents [45, 46, 38, 47]. However, the morphology of ibuprofen particles does not affect the dissolution profile [48], therefore is not a characteristic of the drug that need to be optimized.

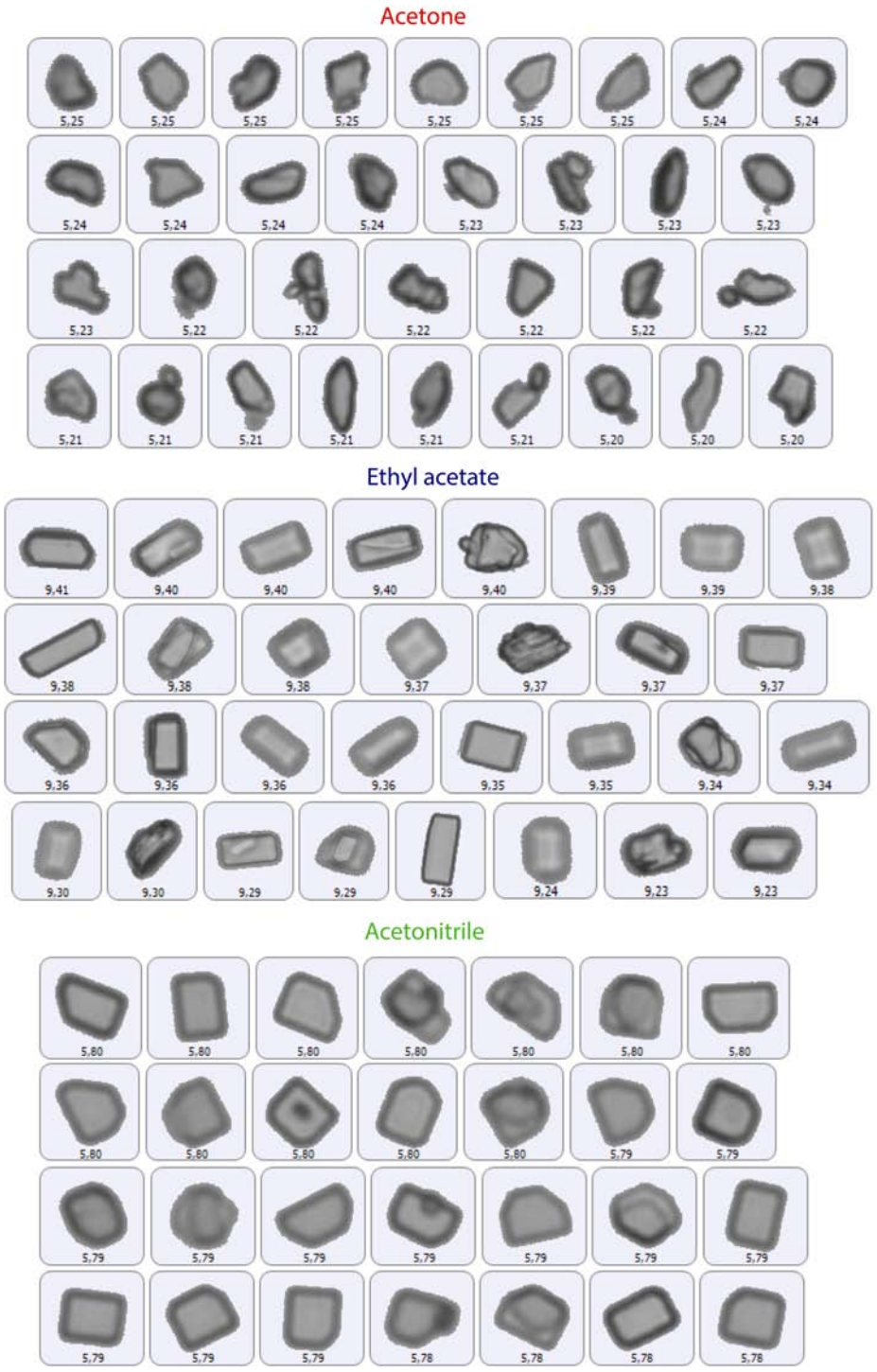

Figure 2.16: Images of ibuprofen precipitated through DELOS when using acetone, ethyl acetate and acetonitrile

2.2.2 Summary

- The solubility variation of ibuprofen in various organic solvents with temperature has been measured in order to assess which process parameter govern supersaturation. The solubility variation in all the solvents presents an exponential decay with decreasing temperature, hence an increase in the initial concentration will have a stronger impact on the supersaturation attained in DELOS precipitation process than x_W.

- DELOS crystallization experiments starting from very concentrated solutions of ibuprofen were conducted, obtaining highly crystalline finely dispersed micro particulate solids except when starting from ethanol.

- Yield and particle size characteristics of ibuprofen precipitated by DELOS can be tuned by the initial concentration and the solvent nature. It has been possible to obtain smaller particles and to increase DELOS yield in ibuprofen DELOS precipitations in comparison to previous DELOS experiments performed in *Nanomol* group.

2.3 Micronization of the thiadiazoline derivative NP from CO_2-expanded solvents

As described in more detail in the Introduction of this Thesis (Chapter 1), 4-benzyl-2-(naphtalen-1-yl)-1,2,4-thiadiazoline-3,5-dione, from now on, the thiadiazoline derivative NPor NP, is a highly hydrophobic substance which has shown therapeutic activity against Alzheimer disease. This compound crystallizes as very long needles and as a consequence cotton-like solids are obtained, which are extremely difficult to micronize by top-down methodologies.

In the present Thesis, and under the frame of a collaborative project with the company NOSCIRA, it was investigated the viability of crystallizing this drug from CF-based methodologies with the objective of producing micro-particle of NP, which can be easily formulated as injectables.

The determination of the solubility of the drug in different organic solvents as well as in CO_2-expanded mixtures is the first step in the assessment of the feasibility of processing NP via CO_2-based methodologies.

2.3.1 Solubility behavior of NP

Solubility of NP in organic solvents

The solubility of the NP compound was measured in different organic solvents (belonging to Class 1, 2 and 3 according to the European Pharmacopeia[1]). Table 2.3 gathers solubility values of the drug measured at atmospheric pressure at 298 and 313 K following the experimental protocol described in Section 6.2.1 of the Experimental Part.

Solubility of NP in CO_2-expanded mixtures

As mentioned in the Introduction of this Chapter (see Section 2.1.2), in order to select the best approach to process a compound by compressed fluid precipitation techniques, the solubility behavior of the drug in CO_2 or in CO_2- expanded mixtures should be determined. Wubbolts [49] described the Vanishing method (see Section 6.2.2 of the Experimental Part) for the determination of the solubilities of solids in CO_2-expanded solvents

[1] ICH Harmonised Tripartite Guideline, Impurities: Guidelines for residual solvents, ICH Steering Committee Meeting, 1977.

Table 2.3: NP Solubility in different organic solvents at 295 K and 313 K

Solvent	C_s (mol/mol)·10^3	
	T=298 K	T=313 K
Acetone	11.65	11.21
Acetonitrile	3.90	4.68
Ethyl acetate	6.45	8.81
Ethanol	0.34	0.52

as well as the modeling of such data. This method is based on the visual determination of the disappearance of the last crystal when known amounts of a co-solvent or a clear solution are added to supersaturated mixtures of different compositions. The concentration of the compound at the Vanishing point represents the solubility of the solute in the CO_2-expanded solvent at a given x_{CO_2}.

In the present work, it has been investigated the solubility behavior of NP in CO_2-expanded acetone and in CO_2-expanded acetonitrile at 10 MPa at different CO_2 contents and at two different temperatures: 298 K and 313 K. The solubility curves are depicted in Figure 2.17. Solubility values and the fitting curves are displayed in the Appendix of this Thesis.

As can be inferred from Figure 2.17, CO_2 acts as an anti-solvent over solutions of NP in acetone and acetonitrile at 298 K. In the "acetone/CO_2/NP" system, the phase boundaries shifted upwards with increasing temperature, leading to a high solubility of NP in the expanded mixture. However, for all range of CO_2 molar fractions (x_{CO_2}), CO_2 behaves as an anti-solvent over NP solutions in acetone and acetonitrile. In the system "acetonitrile/CO_2/NP" the increase in temperature is reflected in an increase in the miscibility region of the 3 components, and at low CO_2 concentrations, CO_2 acts as a co-solvent. The intersection of the phase boundary with the ideal dilution line is at molar fractions of CO_2 of 0.4.

These findings showed that the most suitable techniques to process NP are the ones taking advantages of the anti-solvent behavior of CO_2 over the mixture. Based on this, it was proposed to investigate the precipitation of NP through compressed antisolvent methods.

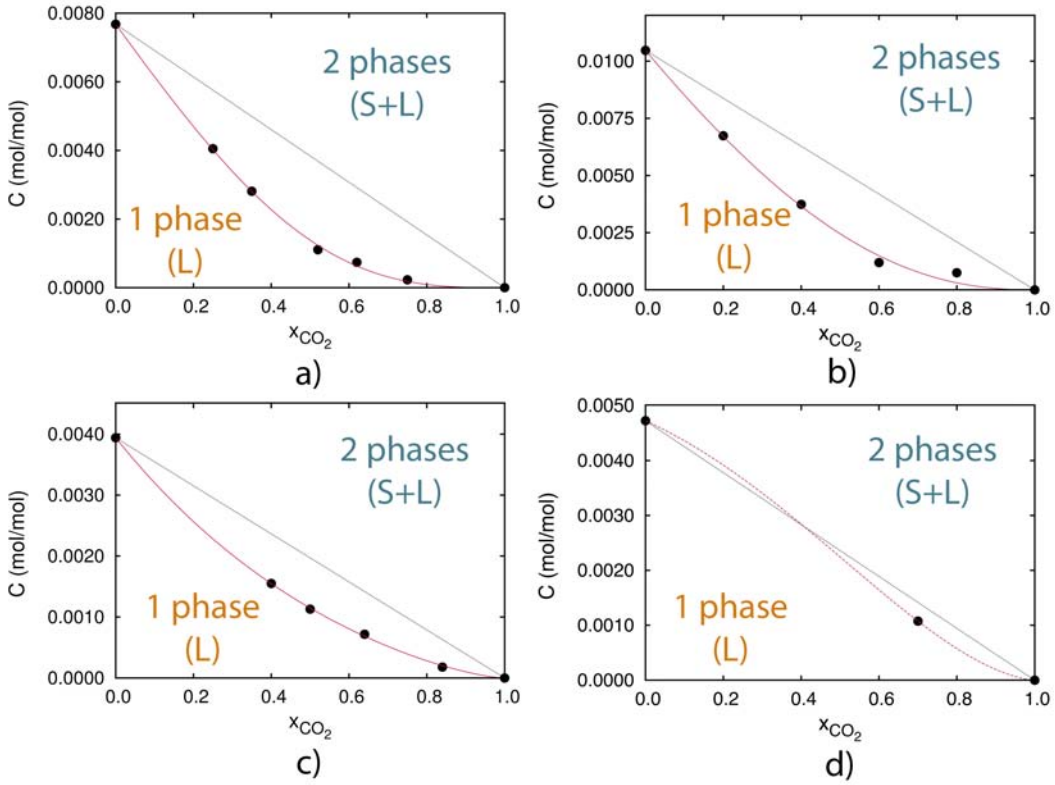

Figure 2.17: Solubility variation of NP at 10 MPa in a) CO_2-expanded acetone at 298 K, b) CO_2-expanded acetone at 313 K, c) CO_2-expanded acetonitrile 298 K and d) CO_2-expanded acetonitrile 313 K. The experimental values are represented by black dots, the dashed line is the solubility variation in an ideal dilution process. The pink lines are the fitted solubility curve.

2.3.2 Preparation of NP micro particles using Compressed Antisolvent Precipitation method.

In a Precipitation with Compressed Anti-solvent (PCA) process, an organic solution of the compound to precipitate is injected through a nozzle into a reactor previously brought to the operating conditions of pressure (P_W), temperature (T_W) and molar fraction of CO_2 (X_W). The antisolvent effect of the compressed CO_2, which rapidly diffuses into the sprayed solution, causes the precipitation of the solute, which is filtered at high pressure inside the reactor (see Figure 2.18).

Successful compressed antisolvent precipitation requires, not only the insolubility of the solute in the organic solvent/CO_2 mixture, but also the complete miscibility between

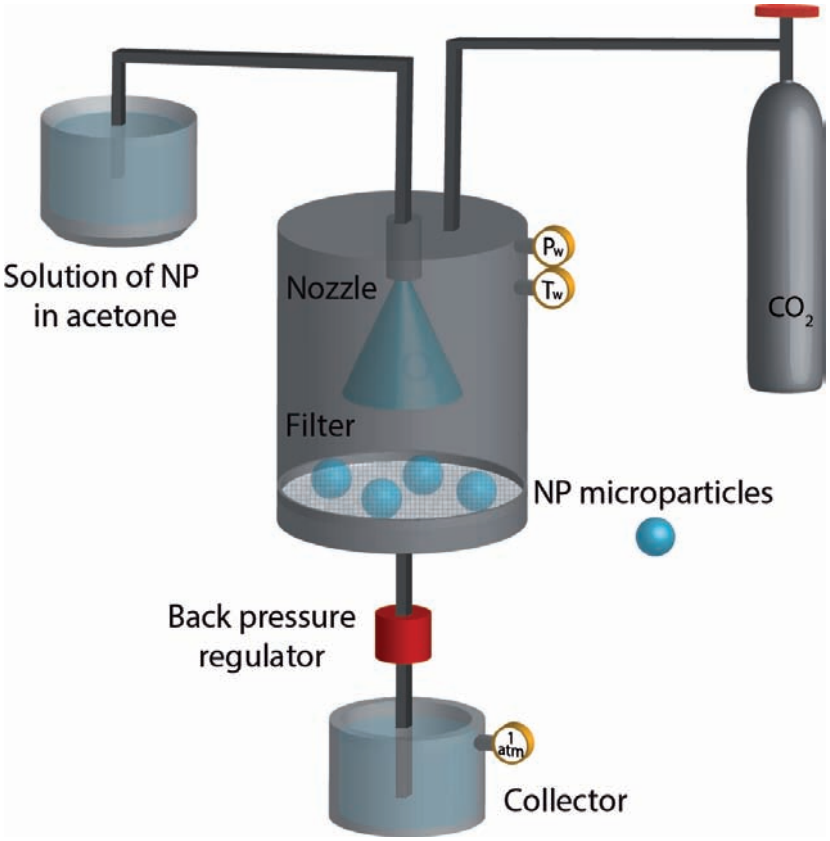

Figure 2.18: Schematic representation of a PCA process. Adapted from [15].

the liquid solvent and the compressed antisolvent. Considering the solvent- antisolvent binary system, this condition is achieved by working at P_W larger than that of the mixture critical point (MCP), which differs in more or less extent from that of pure CO_2 (Tc = 7.39 MPa, Pc = 304.3 K) depending on the nature and % of organic solvent present in the mixture. According to the data reported in the literature [50], for the acetone/CO_2 mixture the Pc and Tc for the mixture composition of interest (high molar CO_2 fractions) are approximately 9 MPa and 323 K. Based on these data, all experiments were performed at P_W over the critical pressure of the organic solvent/CO_2 systems used and therefore, conditions of complete miscibility between solvent-antisolvent should have been achieved. However, it should also be considered that the presence of a solute can modify the vapour-liquid equilibria (VLEs) of the binary system, in general, moving the MCP of the ternary system towards higher pressures compared to that for the corresponding binary one [51, 52]. However, as the phase behavior of NP in CO_2-expanded acetone and acetonitrile is known, it was experimentally checked that in the range of possible operating conditions, the mix-

tures of organic solvent and CO_2 presented a single liquid phase. The phase is liquid in some experiments as the working temperature is lower than the critical temperature of the mixture.

A series of experiments were designed in order to check the feasibility of PCA for the one-step preparation of micro particulate NP and are displayed in Table 2.4.

Table 2.4: PCA experiments for the precipitation of NP.

Exp.	Solvent	CO_2 State[a]	T_w[b] (K)	β_i[c]	C_i(mol/mol)$*10^3$[d]	x_W[e]	Yield(%)[f]
1	Acetone	Liquid	298	1	7.70	0.96	70
2	Acetone	Supercritical	313	0.7	7.70	0.96	80
3	Acetone	Supercritical	313	1	11.21	0.96	90
4	Acetone	Liquid	298	0.7	5.27	0.96	25
5	Acetone	Supercritical	313	0.7	7.70	0.90	100
6	Acetone	Supercritical	313	0.7	7.70	0.80	No solid
7	Acetonitrile	Supercritical	313	0.7	3.28	0.90	No solid

PCA Experiments performed at 10 MPa using different solvents, [a] state of CO_2, [b] working temperature, [c] Initial saturation C_i/C_S, [d] initial concentration,[e] molar fraction of CO_2,[f] Yield expressed as %of mass recovered.

In experiments 6 and 7 no solid was precipitated as the experimental conditions are close to the phase boundary. In the rest of experiments, a precipitate with cotton-like appearance was obtained. The solid was characterized by SEM following the experimental protocol described in detail in Section 6.4.2. Representative SEM images of the PCA solids are shown in Figure 2.19. SEM micrographs reveal the existence of long needle-like particles and hence, the solid keeps the cotton-like macroscopic appearance of the raw material. Light Scattering measurement were performed over some representative solids following the experimental protocol explained in Section 6.4.1. The particle size distribution of the solids was approximately between d(0.1) = 2μm, d(0.5) =10μm, d(0.9) = 40μm, values that are in agreement with the long needles observed by SEM.

As it is not possible to avoid the undesired cotton-like appearance and the precipitation of NP as very long needle-like particles, it was proposed to explore the viability of precipitating NP using another CO_2-based method, the DELOS platform. Therefore, the next section is dedicated to investigate the feasibility of using DELOS for the precipitation of NP as a micro particulate material.

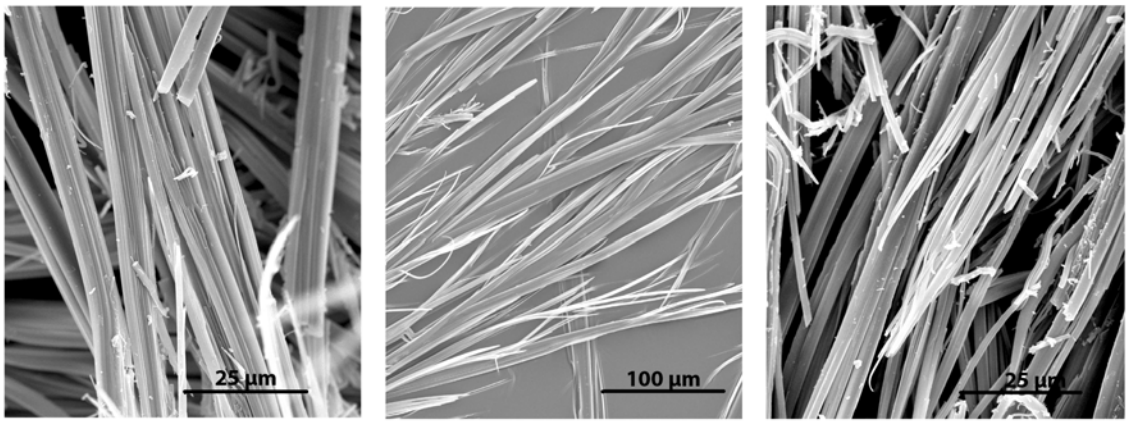

Figure 2.19: SEM images of the solids obtained through PCA experiments 1 (a), 4 (b) and 5 (c).

2.3.3 Preparation of NP microparticles using DELOS method.

As mentioned in Section 2.1.3, it is essential to have a good understanding of the solubility behavior of the compound to precipitate in the CO_2-expanded mixture, but also, in order to elucidate if the drug will be able to precipitate by the large, abrupt and homogenous decrease of temperature that occurs in DELOS and to evaluate the specific weight of the operational parameters on the final characteristics of the drug. Attending to this conclusion, in the following Section, the solubility dependence of NP in acetone and acetonitrile with temperature is evaluated.

Solubility variation of NP in organic solvents with temperature

The solubility evolution of NP with decreasing temperature in acetone and acetonitrile was experimentally measured following the experimental protocol described in Section 6.2.1 and Figure 2.20 depicts the tendency. The solubility values are reported in the Appendix. In both cases, NP shows a decay of the solubility with decreasing temperature. At temperatures lower than 273 K, however, solubility does not undergo any significant change. Therefore, it is feasible to precipitate this drug by the large, abrupt and homogenous decrease of temperature that takes place in DELOS.

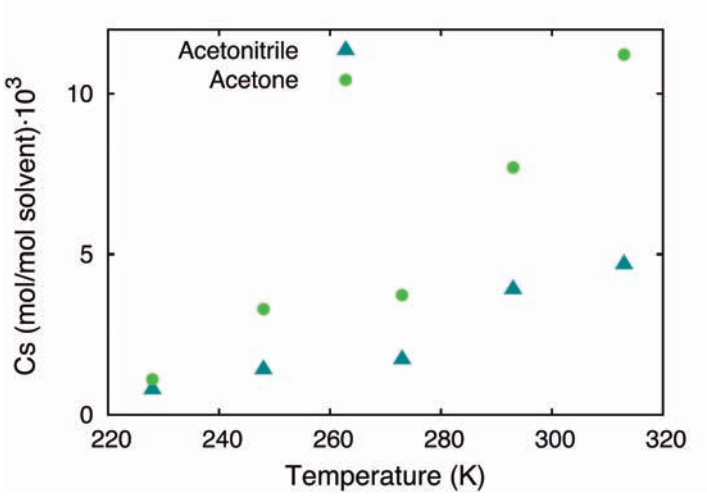

Figure 2.20: Evolution of the solubility of NP in acetone and acetonitrile with temperature.

DELOS precipitation of the thiadiazoline derivative NP

Table 2.5 presents the operational conditions of DELOS crystallization experiments of NP. In all the experiments, particles of NP were successfully obtained for the first time by DELOS. It can be checked how as the x_W is increased, lower temperatures are reached. Most of the experiments conducted started from acetonitrile at 313 K as the cosolvent behavior of CO_2 ,and hence, the range of variation of x_W and C_i is larger.

Table 2.6 summarizes the outcome of crystallization experiments. Yields, particle size distribution measurements and microscopic studies by SEM have been done following the experimental protocols presented in Sections 6.3.2, 6.4.1 and 6.4.2 of the Experimental Part, respectively.

Experiments 8 and 9 were carried out using CO_2-expanded acetone. In these two experiments, the yields obtained are very low and particle size of the solids precipitated are larger than the ones obtained when using CO_2-expanded acetonitrile. Based on these two facts, the use of acetone for processing NP by DELOS has been rejected. As occurs with ibuprofen crystallizations, the nature of the solvent employed plays an important role in the final characteristics of the solid obtained.

In acetone experiments (8 and 9) there is a correlation between the supersaturation attained during depressurization (ΔC) and particle size of the particles obtained. In experiment 9, performed at higher C_i , a higher supersaturation is achieved and as a consequence smaller particle sizes and higher yields are obtained.

Table 2.5: DELOS experiments for the micronization of NP starting from different temperatures, initial concentrations (β_i), x_W using acetone (ACE) or acetonitrile (ACN) as organic solvents and the yields obtained.

Exp.	Solvent	T[a] (K)	C_i[b] (β_i[c]) $\cdot 10^3$(mol/mol)	x_W[d]	ΔT[e] (K)	C_F^S[f] $\cdot 10^3$(mol/mol)	ΔC[g] $\cdot 10^3$(mol/mol)
1-2	ACN	298	2.87(0.7)	0.47	43	1.56	1.31
3	ACN	313	3.75(0.8)	0.59	70	1.25	2.50
4	ACN	298	2.05(0.5)	0.58	65	0.94	1.11
5-6	ACN	313	4.69(1)	0.46	55	1.56	3.13
7	ACN	313	4.69(1)	0.36	51	1.56	3.13
8	ACE	313	5.8(0.5)	0.36	50	2.86	2.75
9	ACE	313	8.98(0.8)	0.5	55	2.64	6.34

DELOS Experiments using different solvents and at [a]different working temperatures,[b]initial concentration of NP in the organic solvent (mol/mol), [c]Supersaturation ratio,[d]CO_2 molar fraction, after depressurization,[f] Solubility of NP in the organic solvent at the final temperature (mol/mol), [e]Temperature reached, [g]Supersaturation attained expressed as mass difference (mol/mol).

Table 2.6: DELOS crystallization outcome: particle size distribution and yield (η).

Exp.	Solvent	ΔC[a] $\cdot 10^3$(mol/mol)	Size distribution (μm)[b] d(0.1)	d(0.5)	d(0.9)	UI[c]	Yield(%)[d]
1-2	ACN	1.31	1.26	3.67	15.41	8	55
3	ACN	2.50	1.17	4.45	28.37	4	85
4	ACN	1.11	0.97	2.34	7.72	13	35
5-6	ACN	3.13	1.16	3.10	14.9	7	65
7	ACN	3.13	1.18	3.13	11.79	10	55
8	ACE	2.75	1.29	4.42	23.02	5	10
9	ACE	6.34	1.12	2.99	13.21	8	20

[a]supersaturation attained as mass difference (mol/mol) [b]Volumetric particle size distributions expressed in percentiles of 10, 50 and 90%, [c]Uniformity index is defined , as d(10)/d(90)*100, [d]Yield expressed as % of mass recovered.

In experiments from CO_2-expanded acetonitrile, it has been possible to precipitate NP microparticles with particle size distribution below 10 μm for the very first time. However, in this set of experiments (1-7) there is no clear correlation between the experimental conditions that result in the highest supersaturation (experiments 6-8) and particle size and yields of the precipitates. Even though, values of particle size distribution are very promising, as a very substantial reduction in size has been achieved : 10% of the particles in volume are below 1.4 μm and 50% are below 5 μm.

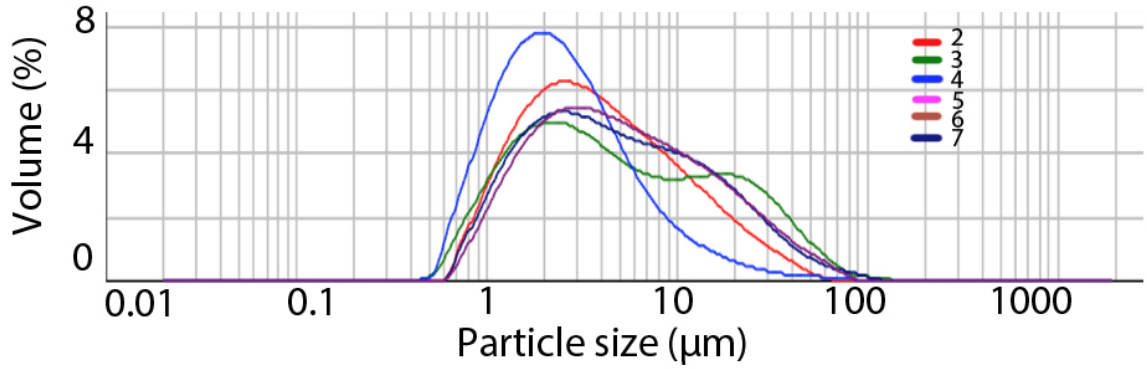

Figure 2.21: Comparision of the particle size distribution obtained in the experiments 2-7.

As it is depicted in Figure 2.21, particle size distribution of the previous experiments (2-7) shows the presence of two different particle populations, one smaller centered at around 2 μm and another with lager size centered at around 10-20 μm depending on the experiment. The global contribution of the latter population to the final particle size distribution changes from experiment to experiment regardless of the process parameters.

The morphological characterization of the particles of NP obtained in this set of experiments was done by SEM. In all experiments, small needle-like particles, as the ones depicted in Figure 2.22 were obtained. By careful inspection of the SEM images, two different sizes can be noticed and the same conclusion from the Light Scattering results can be withdrawn. A wide size distribution has a deceptively low dissolution rate due to the presence of large particles at the end to the distribution. Therefore, this type of particles size distribution should be averted. A narrow particle size distribution is always preferable as this means that particles are more homogenous and this is translated into a higher bioavailabilty.

The presence of two populations of particle size in the solids obtained by DELOS

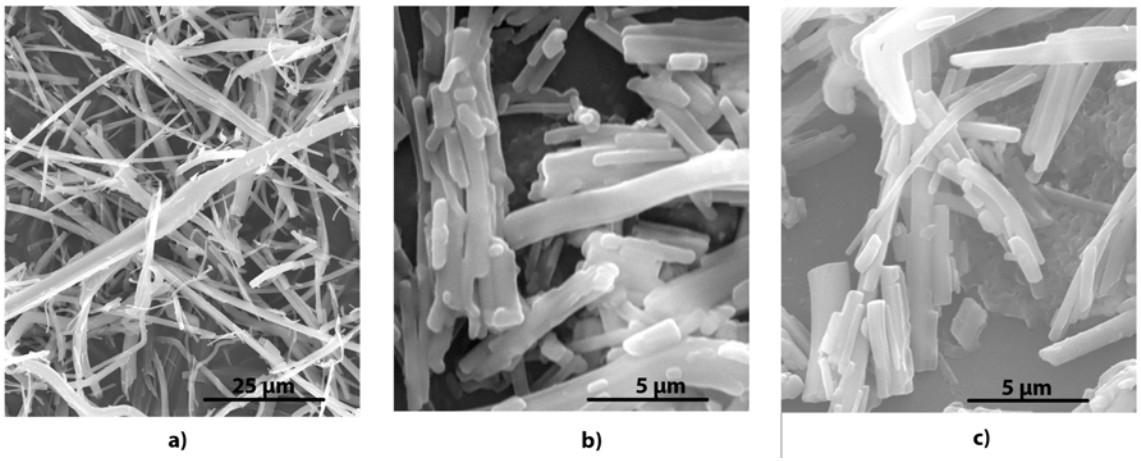

Figure 2.22: SEM images of NP precipitated through DELOS. Experiments 3 (a), 6 (b) and 8 (c).

method reveals that particles are being formed by more than one process [53]. A possible explanation of this phenomenon is that, a second particle growth can occur during filtration and drying of the solids. This uncontrolled growth of the crystals should occur after nucleation takes place, as there is no clear evidence between the operational variables and the outcome of the experiments. It is important to bear in mind that, as mentioned in the Introduction of this Thesis (Chapter 1), NP crystals present a very fast kinetics, that results in the formation of very long needles, hence, the tendency of NP particles to grow is very high.

In order to overcome the presence of these two populations, it was proposed to use quenching agents that could stop the growth of the nucleus formed just after depressurization occurs.

2.3.4 Use of organic solvents as growth inhibitors

The first approach followed to avert the uncontrolled growth of the NP after depressurization was to use specific organic solvents as growth inhibitors. Some organic solvents can interact with specific sites of the NP molecule avoiding its crystal growth. The use of modifiers to selectively change crystal growth kinetics during crystallization is a general processing strategy that can be easily used to modify crystal size and shape [53]. It is reported the strong influence of solvents on the habit of crystalline materials, however the role played by solvent-surface interactions in enhancing or inhibiting crystal growth

is still not completely resolved [54, 55]. Reverchon et al. investigated the effect of using urea in supercritical anti-solvent precipitation of adipic acid. Urea was found to be very effective in modifying the crystal shape and size of the acid.

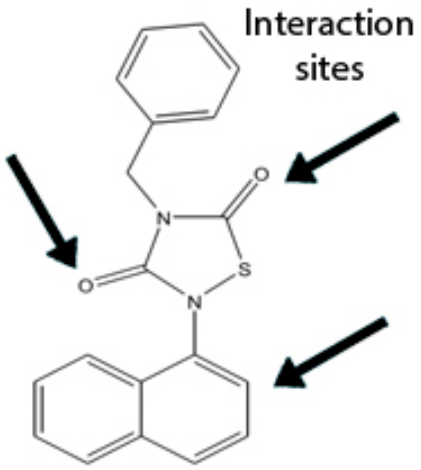

Figure 2.23: Potential interaction sites of NP molecule.

Hence, paying attention to the molecular structure of NP (Figure 2.23), two interaction sites have been identified: the carbonyl groups and the aromatic ring, which control the formation of hydrogen bonds and the π-π interactions, respectively. Based on these observations, it was proposed to use organic solvents of different nature that could potentially interact with these specific sites of the molecule.

Use of alcohols as potential the thiadiazoline derivative NP crystal growth inhibitors

It is widely recognized that alcohols are adequate solvents for the establishment of hydrogen bonds (and dipole-dipole interactions). Hence, solvent selection was conducted based on the hydrogen bonding capacity of different alcohols.

A possibility of comparing physico-chemical properties of solvents is to use the Kamlet-Taft classification that uses several parameters to describe them. In our particular case, α and π^* are of special importance. The former correspond to proticity or hydrogen-bond donating ability and ranges from 0 to 1. Protic solvents have values higher than 0.5 and aprotic ones below 0.5. Whereas π^* constant provides a quantitative empirical measure of the nonspecific part of van der Waals interactions. π^* is related to the molecular dipole moment [56, 57, 58, 59].

Table 2.7 presents the solvents selected with their corresponding solvatochromic values and the solubility of NP in them at 313 K. Acetonitrile is included for comparison purposes.

Table 2.7: Alcoholic organic solvents chosen as potential growth inhibitors of NP crystals and their corresponding solvatochromic values. The solubility of NP at 313 K in the solvents is also presented. Acetonitrile is included as a reference

Solvent	α [a]	π^* [b]	C_s(mol/mol)·10^3 [c]
Methanol (MeOH)	0.98	0.60	0.5
Ethanol (EtOH)	0.86	0.54	0.5
Isopropanol(IPA)	0.76	0.48	0.6
n-Butanol(n-BuOH)	0.84	0.47	1.2
Acetonitrile (ACN)	0.19	0.75	4.6

[a] evaluates the hydrogen-bonding contribution, [b] π^* provides information of the nonspecific part of the van der Waals interactions, [c] solubility on NP in the solvent at 313 K.

The α and π^* values of the alcohols chosen are very similar among them and very different compared to acetonitrile's parameters, which means that the effect of these solvents on the precipitation of NP could be different of the ones produced by acetonitrile.

The solubility of NP in the mixtures alcohol/acetonitrile at different compositions and at 298 and 313 K was assed. The results are depicted in Figure 2.24 and the solubility values are disclosed in the Appendix of this Thesis. As can be inferred from the values presented in Table 2.7, solubility of NP in pure alcohols is very low in comparison to the solubility in acetonitrile. Hence, as expected, solubility of NP in mixtures alcohol/acetonitrile increases as the mixture gets richer in acetonitrile. The increase in temperature is also translated in an increase of solubility. In rich acetonitrile mixtures (x_{ACN} higher than 0.5) at 313 K (see Figure 2.24b) a synergetic enhancement of the solubility is observed. This synergetic enhancement also occurs for the mixture n-butanol/acetonitrile at 298K and at x_{ACN} higher than 0.7, reaching its maximum at x_{ACN} = 0.9 (Figure 2.24a). At both temperatures, NP presents the highest solubility in the mixture n-butanol/acetonitrile and the lowest in the methanol mixture. Nevertheless, the solubilities in the mixtures are high enough to be used as solvents in the DELOS process. Hence, all the chosen alcohol/ ace-

tonitrile mixtures are suitable to prepare micron and sub-micron particles of NP using CO_2-expanded solvents.

The first set of experiments was done using the mixture ethanol/acetonitrile at different compositions of the mixture as a mean to evaluate the effect of alcohol concentration in particle characteristics of DELOS precipitates. Table 2.8 displays the experimental conditions of this serie of DELOS crystallizations. In this case, experiments 5-6 were taken as a reference experiment as are the ones that attained the higher supersaturation (ΔC) during depressurization. These experiments were conducted using acetonitrile at 313K and 10MPa, $\beta_i = 1$, $x_W = 0.47$.

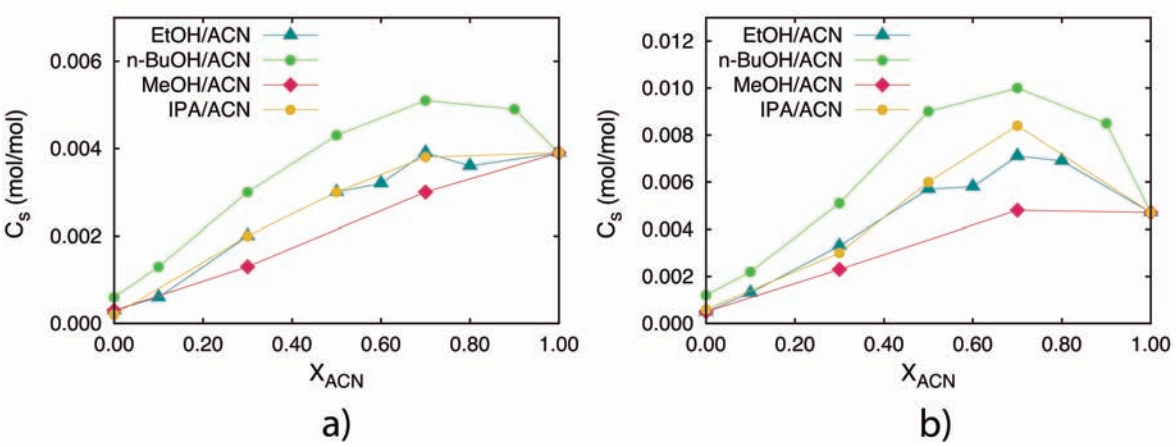

Figure 2.24: Solubility of NP in different mixtures alcohol/acetonitrile at a) 298 K and b) 313 K. The lines are a visual tool.

Although DELOS yields are high in most of the experiments, precipitate was found in the mother liquors in all the experiments except in experiments 10 and 12. Figure 2.25 shows representative images of the SEM characterization of the solid collected in experiments 10-15 where, once again, the presence of two types of particle size distributions were detected: submicron needle-like particles and very long and thin fibers.

However, Light Scattering results reveal a high variability in between measurements of the same sample, as Table 2.9 displays. As it is described in Section 6.4.1, the proper sampling consists of measuring 3 replicas of the same solid. In the solids obtained using alcohols as potential growth inhibitors, the variation between each replica is considerably important. This means that the particles obtained are very heterogenous. The variability in particle size in between the same samples occurs for all the DELOS experiments performed using mixtures of ethanol/acetonitrile as solvent. Despite this great variability,

Table 2.8: DELOS experiments using different mixtures of ethanol/acetonitrile mixtures.

Experiment	ACN:EtOH (molar relationship)[a]	$C_i \cdot 10^3$[b] (β_i[c])	x_W[d]	Yield[e](%)
10	80:20	6.9(0.99)	0.53	53
11	60:40	5.4(0.95)	0.48	58
12	50:50	5.6(0.98)	0.52	67
13	30:70	3.0(0.95)	0.49	64
14	10:90	1.2(0.94)	0.48	30
15	10:90	1.2(0.94)	0.67	75

DELOS Experiments at 313 K and 10 MPa using a mixture of acetonitrile and ethanol as solvent, [a]the proportion between the two solvents is expressed as molar relationship(mol/mol),[b]initial concentration of NP in the mixture of solvents,[c]Initial Supersaturation ratio,[d]CO_2 molar fraction, [e]Yield expressed as %of mass recovered.

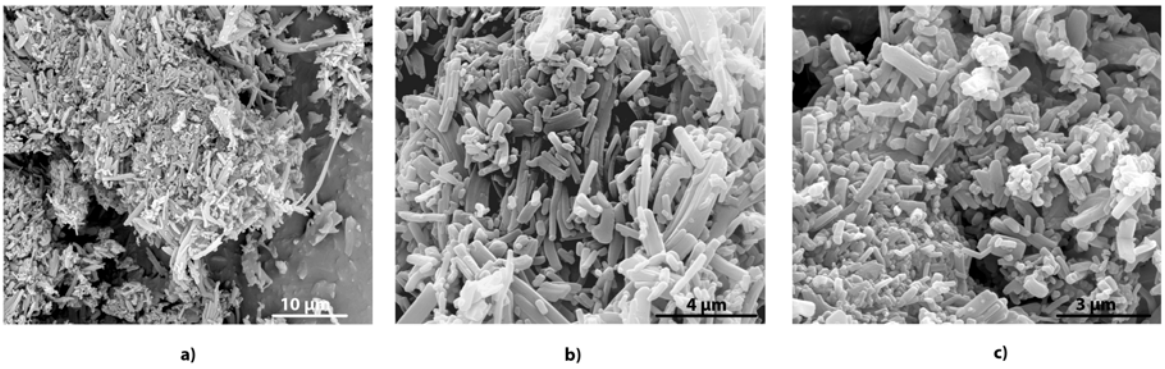

Figure 2.25: SEM images of NP precipitated from ethanol/acetonitrile mixture from experiment 13.

the best results in terms of particle size distribution were obtained in the solid precipitated through the experiment 13, using the molar relationship Acetonitrile/EtOH 30/70.

Figure 2.26 compares particle size distribution of the solid obtained from 30/70 acetonitrile/ethanol mixture and pure acetonitrile. The red curve corresponds to the solid obtained without ethanol, and the green, dark blue and navy blue to the different samples from the same solid. It is clearly seen the great variability of particle size distribution of the solid obtained in the presence of ethanol. The green curve is centered at a smaller particle size that the red one, which means that some of the NP crystal are smaller when

Table 2.9: Particle size distribution of different samples of the solid obtained in experiment 13.

Sample	Size distribution (μm)[a]		
	d(0.1)	d(0.5)	d(0.9)
13 A	0.6	1.4	4.4
13 B	0.8	1.9	7.9
13 C	1.3	5.9	38.8
13 D	1.5	6.4	40.4

[a]Volumetric particle size distributions expressed in percentiles of 10, 50 and 90%.

using ethanol. Hence, it can be assumed a possible growth inhibition effect of EtOH, although, another phenomenon should occur after depressurization that makes some NP particles to grow. One possible reason that could explain this observed behavior is that as NP is not soluble in ethanol, an antisolvent precipitation may occur while NP is still in contact with the mother liquor. Indeed, as acetonitrile is more volatile than ethanol, it is very likely that an ethanol enrichment of the mother liquor could occur. This difference in volatility could produce preferential paths in the cake during drying of the particles. If the drying is not homogenous for the whole cake, differences in the growth of particles in between the same sample can occur.

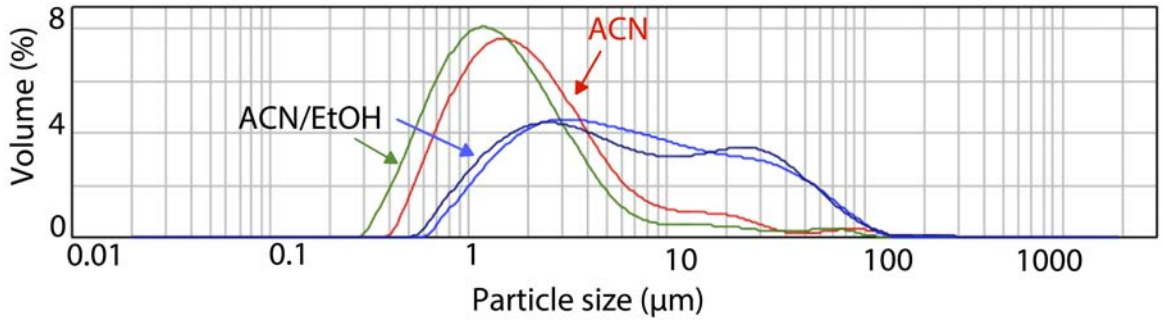

Figure 2.26: Comparison of the particle size distribution of the solid obtained using acetonitrile (red) and the solid precipitated from the 30/70 Acetonitrile/EtOH mixture (green, dark blue and navy blue.)

Summarizing, it has been possible to precipitate NP from CO_2-expanded ethanol/

acetonitrile mixtures. Ethanol may behave as a growth inhibitor although there is still a second unknown process of growth of NP crystals. The best results, in terms of particle size distribution, were obtained using the mixture ethanol/acetonitrile 30:70 at 313 K. It was at this composition of the mixture ethanol/acetonitrile where NP presents its higher value of solubility.

Attending to this observation, the next step was to move to other mixtures of alcohol/ acetonitrile. Prior to perform DELOS crystallizations using other alcohols and as a mean to gain more knowledge of the system under study, the solubility curve of NP in CO_2-expanded methanol/ acetonitrile mixture and in CO_2-expanded n-butanol/ acetonitrile was measured. These two solvents are the ones where NP presents its lowest and highest values of solubilities, respectively. The composition of the mixture alcohol/ acetonitrile was fixed to 30:70 based on the ethanol/ acetonitrile results and also because at this molar relationship, the synergist enhancement of solubility occurs for the rest of the mixtures at 313K. The solubility curves were performed following the same experimental protocol as the solubility curves of NP in the CO_2-expanded acetonitrile and acetone which is described in Section 6.2.2 of the Experimental Part and are depicted in Figure 2.27. The experimental values and the fitting curves are reported in the Appendix of this Thesis. In both curves, CO_2 acts as a cosolvent until molar fractions of CO_2 of around 0.5 and as anti-solvent at higher molar fractions. The behavior of CO_2 in the mixtures of alcohol/acetonitrile is very similar to the behavior in pure acetonitrile (Figure 2.17). Therefore, these mixtures are suitables for using them as solvents in DELOS method. As the solubility of NP in ethanol and isopropanol has values in between the solubility in methanol and in n-butanol, and as the solvatochromic parameters of the four solvents are very close to each other, it was assumed that the behavior of CO_2 in ethanol and in isopropanol should be very similar to the solubility curves measured.

The different mixtures 30:70 (molar relationship) alcohol/ acetonitrile at 313 K and 10 MPa are suitable for micronization of NP. Table 2.10 discloses the experimental conditions of the conducted DELOS crystallization using the above described mixtures. The experiment 13 performed using the mixture acetonitrile/ethanol 30/70 molar relationship, which is the one that produce the smallest particles, is included for comparison purposes.

In experiments 16-18 it was feasible to precipitate NP through DELOS with appropriate yields. Except in the case of the mixture methanol/acetonitrile, in the rest of the experiments precipitate was found in the mother liquor. Nevertheless, SEM images shows (Figure 2.28) that it was not possible to avoid the presence of long fibers in the solids ob-

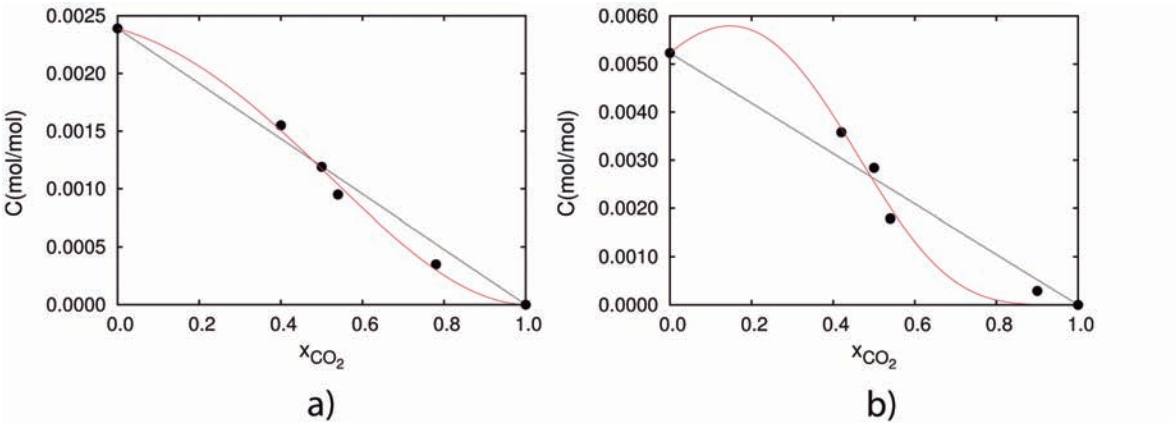

Figure 2.27: Solubility curves of NP in a) CO_2-expanded metanol/acetonitrile 30:70 and b) CO_2-expanded n-butanol/acetonitrile 30:70 at 313 K and 10 MPa.

tained using alcohols as growth inhibitors.

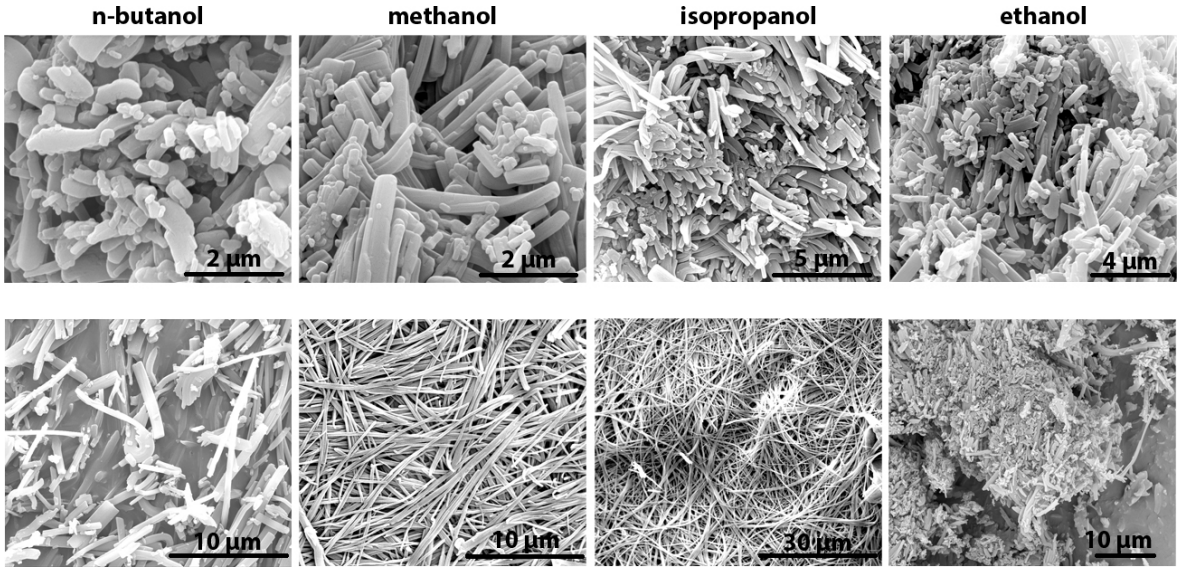

Figure 2.28: SEM images of the solid precipitated using mixtures of alcohol/acetonitrile

Light scattering measurements (Figure 2.29) confirm the observations drawn from the SEM images. The comparison of particle size distributions obtained in DELOS crystallization using different alcohol/acetonitrile mixtures reveals that the crystal growth of NP is sensitive to the nature of the alcohol employed, as the shape of particle size distribution varies from one mixture to another. However, in none of the mixtures studied the presence of the long fibers has been averted. The first particle size distribution is centered at

Table 2.10: Experimental conditions of DELOS crystallizations using alcohol/acetonitrile (30:70 molar relationship).

Experiment	Solvent	Molar relationship[a]	$C_i \cdot 10^3 (\beta_i)^b$	$x_W{}^d$	Yield (%)[e]
10	Ethanol	30:70	3.0(0.95)	0.49	64
16	n-Butanol	30:70	4.0 (0.99)	0.52	53
17	Methanol	30:70	2.4 (0.98)	0.55	70
18	Isopropanol	30:70	2.4(0.99)	0.55	53

DELOS Experiments at 313 K and 10 MPa using a mixture of acetonitrile and alcohol as solvent, [a]the proportion between the two solvents is expressed as molar relationship, [b]initial concentration of NP in the mixture ofNP in the mixture of solvents (mol/mol), [c]Initial Supersaturation ratio, [d]CO_2 molar fraction, [e]Yield expressed as %of mass recovered.

around 2 μm for all the mixtures, however, as mentioned, the weight of the second population of particles depends on the alcohol employed.

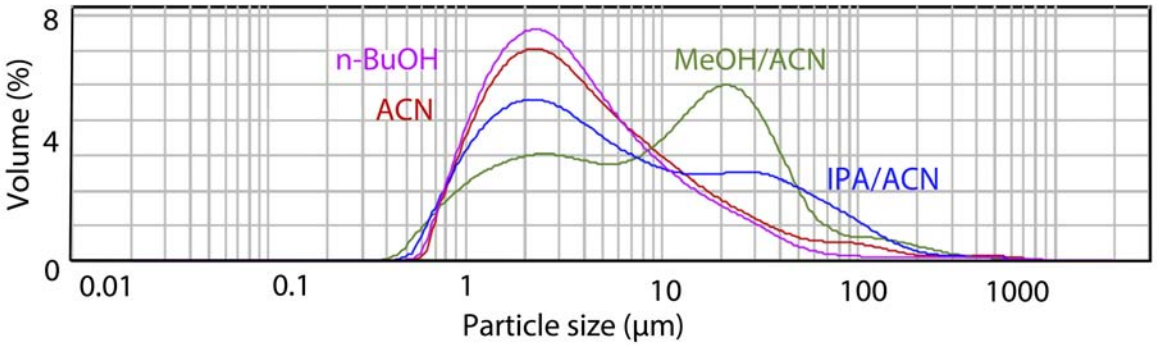

Figure 2.29: Particle size distribution of the solid precipitated using mixtures of alcohol/acetonitrile.

Use of toluene and anisole as growth inhibitors

As the alcohols used do not behave as growth inhibitors of NP particles, it was thought to investigate the effect of using other types of solvents for avoiding the second growth mechanism of NP crystals. Until now, the best results regarding particle size distribution has been obtained in the presence of pure acetonitrile, an organic solvent with a high affinity for dipole-dipole interactions. Attending to this fact, this section comprise a preliminary study using other organic solvents which can easily establish dipole-dipole interactions or π - π interactions.

Anisol and Toluene were the chosen solvents and their solvatochromic parameters are disclose in Table 2.11 as well as the solubility of NP in these solvents at 313 K.

Table 2.11: Organic solvents chosen as potential growth inhibitors of NP crystals and their corresponding solvatochromic values. The solubility of NP at 313 K in the solvents is also presented. Acetonitrile is included as a reference.

Solvent	α^a	π^{*b}	$C_s \cdot 10^{3c}$
Anisole	0.00	0.73	38
Toluene	0.00	0.54	15
Acetonitrile (ACN)	0.19	0.75	4

[a]evaluates the hydrogen-bonding contribution, [b]π^* provides information of the nonspecific part of the van der Waals interactions, [c]solubility on NP in the solvent at 313 K(mol/mol).

As reflected in the α values from Table 2.11, neither anisole nor toluene have the capacity of forming hydrogen bonds, however, both exhibit a high polarizability.

The solubility of NP in both solvents is very high. A new set of experiments were conducted using anisole and toluene as potential growth inhibitors. Table 2.12 displays the experimental conditions of these experiments.

However, as reflected in the values from Table 2.12, no solid was precipitated when using anisole and toluene as pure solvents. This can be rationalized taking into account the high solubility of NP in these organic solvents. Based on this, it was proposed to examine the viability of using mixtures of acetonitrile with these solvents. In the case of the mixture acetonitrile/anisole, NP was precipitated by the anti-solvent effect of the addition of CO_2, so it was explored the possibility of using anisole with another type of solvent. Some

Table 2.12: Experimental conditions of DELOS crystallizations using toluene and anisole as solvents.

Experiment	Solvent	$C_i \cdot 10^{3\,a}(\beta_i)^{\,b}$	$x_W{}^c$	Yield (%)^d
19	Anisol	38 (1)	0.55	0
20	n-Butanol	14 (0.9)	0.41	0

DELOS Experiments at 313 K and 10 MPa using pure anisole or toluene,^{a}initial concentration of NP in the solvent(mol/mol), ^{b}Initial Supersaturation ratio, ^{c}CO_2 molarfraction, ^{d}Yield expressed as % of mass recovered.

preliminary experiments were conducted and the experimental conditions are summarized in Table 2.13. Nevertheless, as can be checked from Light Scattering results (Figure 2.30) and SEM characterization (Figure 2.31), the particle size distribution is not improved when adding toluene or anisole in comparison to pure acetonitrile.

Table 2.13: Experimental conditions of DELOS crystallizations using mixtures of toluene/acetonitrile, anisole/acetonitrile and n-butanol/anisole as solvents.

Experiment	Solvent	Molar rel.(mol/mol)^a	C_i(mol/mol)$10^{3\,b}(\beta_i{}^c)$	$x_W{}^d$	Yield (%)^e
21	Anisole/Acn	30:70	8.81(1)	0.55	0
22	Anisole/n-But.	30:70	29.41(1)	0.55	21
23	Toluene/Acn	5:95	8.1(1)	0.51	40

DELOS Experiments at 313K and 10MPa using mixtures of organic solvents, ^{a}expressed as molar relationship(mol/mol), ^{b} initial concentration of NP in the solvent, ^{c} Initial Supersaturation ratio,^{d} CO_2 molar fraction, ^{e} Yield expressed as %of mass recovered.

Therefore, whereas these organic solvents have the ability to form hydrogen bonds or present a high polarizability, it can be concluded that the use of organic solvents as growth inhibitors can not be considered a successful approach as the final properties of NP particles have not been improved in terms of size, particle size distribution neither shape.

The next approach proposed for avoiding this undesired growth of NP crystals was to use water as a quenching agent. As a consequence the DELOS-susp method for the production of suspensions were defined. DELOS-susp is a modification of DELOS for

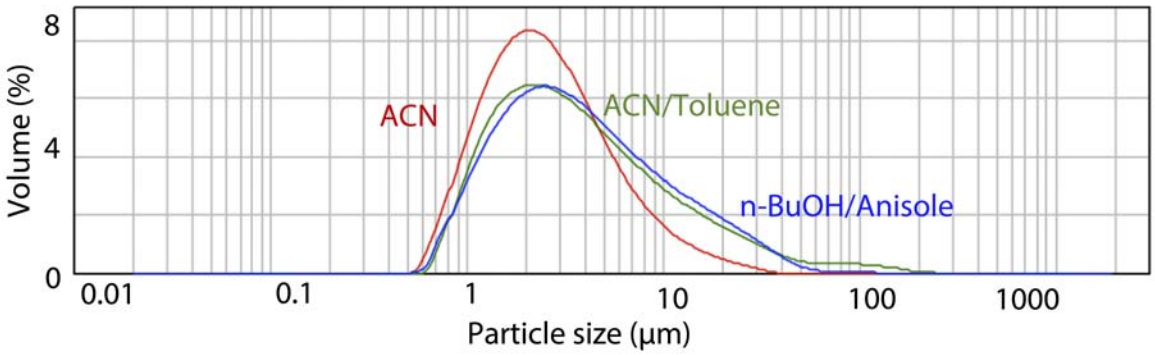

Figure 2.30: Particle size distribution of the solid precipitated using mixtures of toluene/acetonitrile and n-butanol/anisole as solvents.

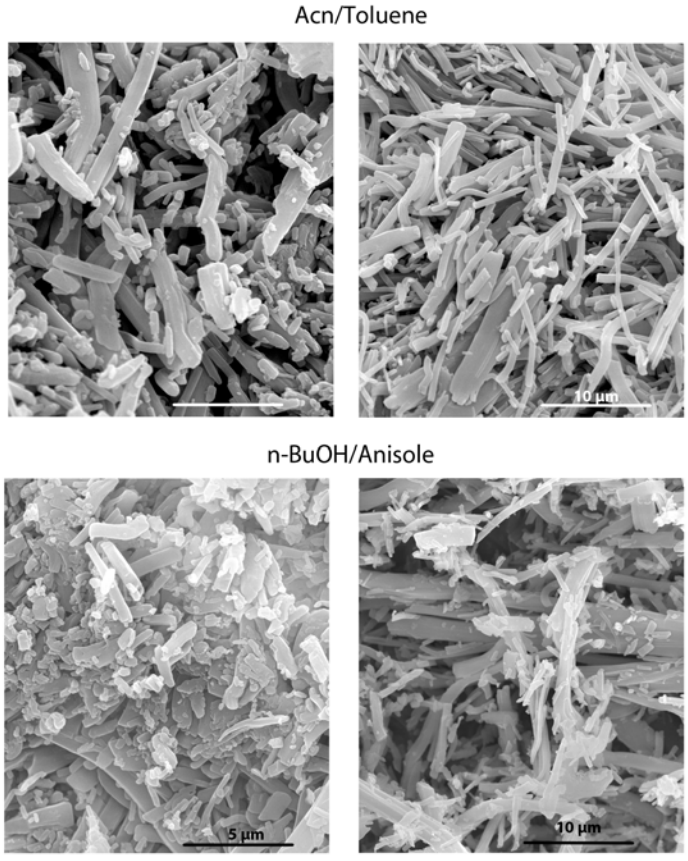

Figure 2.31: SEM images of the solid obtained from DELOS precipitations using mixtures of toluene/acetonitrile and n-butanol/anisole as solvents.

the obtaining of dispersed systems such as vesicular formulations, by performing the depressurization step of the CO_2-expanded solution over an aqueous flow. Using this novel method, it has been possible to obtain highly stable nanovesicles [60] [61] [62].

2.3.5 Summary

- The phase behavior of NP in CO_2-expanded acetone and CO_2-expanded acetonitrile has been measured as the solubility of NP in pure acetone and acetonitrile was suitable for processing it by CO_2-based methodologies.The solubility curves of NP in the expanded mixtures reveal that compressed anti solvent techniques are the most appropriate for processing NP. However, by PCA, NP crystallizes as very long needles and the mechanical properties of the final powder are not improved.
- The precipitation of NP by DELOS has been achieved and it has been possible to decrease particle size using acetonitrile as organic solvent. The solid obtained is a finely dispersed powder (see Figure 2.32). In this case, the thermodynamic analysis used for enhancing the properties of the final drug is not valid as there is a second phenomenon of uncontrolled growth of NP crystals.
- The use of organic solvents (alcohols and aromatic compounds) as growth inhibitors to avoid this undesired crystal growth has not been successful as the final properties of the particles have not been improved with respect to using pure acetonitrile.

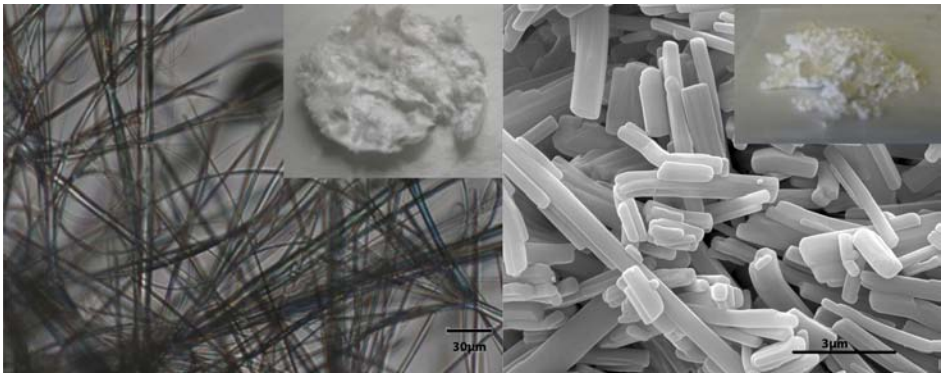

Figure 2.32: Comparison of NP precipitated by evaporation from acetonitrile evaporation and NP obtained by DELOS using acetonitrile as organic solvent. The upper images show the corresponding macroscopic appearance of the solids obtained.

Bibliography

[1] K. Byrappa, S. Ohara, and T. Adschiri, "Nanoparticles synthesis using supercritical fluid technology - towards biomedical applications," *Advanced Drug Delivery Reviews*, vol. 60, no. 3, pp. 299–327, 2008.

[2] I. Pasquali, R. Bettini, and F. Giordano, "Solid-state chemistry and particle engineering with supercritical fluids in pharmaceutics," *European Journal of Pharmaceutical Sciences*, vol. 27, no. 4, pp. 299 – 310, 2006.

[3] D. Jarmer, C. Lengsfeld, K. Anseth, and T. Randolph, "Supercritical fluid crystallization of griseofulvin: Crystal habit modification with a selective growth inhibitor," *Journal of Pharmaceutical Sciences*, vol. 94, no. 12, pp. 2688–2702, 2005.

[4] H. Brittain, S. Bogdanowich, D. Bugay, J. DeVincentis, G. Lewen, and A. Newman, "Physical characterization of pharmaceutical solids," *Pharmaceutical Research*, vol. 8, no. 8, pp. 963–973, 1991.

[5] S. Beach, D. Latham, C. Sidgwick, M. Hanna, and P. York, "Control of the physical form of salmeterol xinafoate," *Organic Process Research and Development*, vol. 3, no. 5, pp. 370–376, 1999.

[6] K. Nagel and G. Peck, "Investigating the effects of excipients on the powder flow characteristics of theophylline anhydrous powder formulations," *Drug Development and Industrial Pharmacy*, vol. 29, no. 3, pp. 277–287, 2003.

[7] J. Lu and J. Ulrich, "Improved understanding of molecular modeling - the importance of additive incorporation," *Journal of Crystal Growth*, vol. 270, no. 1-2, pp. 203–210, 2004.

[8] B. Shekunov, P. Chattopadhyay, H. Tong, and A. Chow, "Particle size analysis in pharmaceutics: Principles, methods and applications," *Pharmaceutical Research*, vol. 24, no. 2, pp. 203–227, 2007.

[9] A. Noyes and W. Whitney, "The rate of solution of solid substances in their own solutions," *The Journal of the American Chemical Society*, vol. 19, no. 12, pp. 930–934, 1897.

[10] R. Müller, C. Jacobs, and O. Kayser, "Nanosuspensions as particulate drug formulations in therapy: Rationale for development and what we can expect for the future," *Advanced Drug Delivery Reviews*, vol. 47, no. 1, pp. 3–19, 2001.

[11] J. Hu, K. Johnston, and R. Williams III, "Nanoparticle engineering processes for enhancing the dissolution rates of poorly water soluble drugs," *Drug Development and Industrial Pharmacy*, vol. 30, no. 3, pp. 233–245, 2004.

[12] N. Rasenack and R. Müller, "Dissolution rate enhancement by in situ micronization of poorly water-soluble drugs," *Pharmaceutical Research*, vol. 19, no. 12, pp. 1894–1900, 2002.

[13] E. Beckman, "Green chemical processing using CO2," *Industrial and Engineering Chemistry Research*, vol. 42, no. 8, pp. 1598–1602, 2003.

[14] M. Poliakoff, J. Fitzpatrick, T. Farren, and P. Anastas, "Green chemistry: Science and politics of change," *Science*, vol. 297, no. 5582, pp. 807–810, 2002.

[15] E. Elizondo, J. Veciana, and N. Ventosa, "Nanostructuring molecular materials as particles and vesicles for drug delivery, using compressed and supercritical fluids," *Nanomedicine*, vol. 7, no. 9, pp. 1391–1408, 2012.

[16] J. Jung and M. Perrut, "Particle design using supercritical fluids: Literature and patent survey," *The Journal of Supercritical Fluids*, vol. 20, no. 3, pp. 179 – 219, 2001.

[17] P. G. Jessop and B. Subramaniam, "Gas-expanded liquids," *Chemical Reviews*, vol. 107, no. 6, pp. 2666–2694, 2007.

[18] F. Wubbolts, O. Bruinsma, and G. Van Rosmalen, "Measurement and modelling of the solubility of solids in mixtures of common solvents and compressed gases," *Journal of Supercritical Fluids*, vol. 32, no. 1-3, pp. 79–87, 2004.

[19] M. Munto, N. Ventosa, S. Sala, and J. Veciana, "Solubility behaviors of ibuprofen and naproxen drugs in liquid "co2-organic solvent" mixtures," *Journal of Supercritical Fluids*, vol. 47, no. 2, pp. 147–153, 2008.

[20] S. Sala, N. Ventosa, T. Tassaing, M. Cano, Y. Danten, M. Besnard, and J. Veciana, "Synergistic enhancement of the solubility of hexamethylenetetramine in subcritical co2-ethanol mixtures studied by infrared spectroscopy," *ChemPhysChem*, vol. 6, no. 4, pp. 587–590, 2005.

[21] T. Yasuji, H. Takeuchi, and Y. Kawashima, "Particle design of poorly water-soluble drug substances using supercritical fluid technologies," *Advanced Drug Delivery Reviews*, vol. 60, no. 3, pp. 388–398, 2008.

[22] M. Turk, P. Hils, B. Helfgen, K. Schaber, H. Martin, and M. Wahl, "Micronization of pharmaceutical substances by the rapid expansion of supercritical solutions (ress): a promising method to improve bioavailability of poorly soluble pharmaceutical agents," *The Journal of Supercritical Fluids*, vol. 22, no. 1, pp. 75 – 84, 2002.

[23] C. Domingo, E. Berends, and G. Van Rosmalen, "Precipitation of ultrafine organic crystals from the rapid expansion of supercritical solutions over a capillary and a frit nozzle," *Journal of Supercritical Fluids*, vol. 10, no. 1, pp. 39–55, 1997.

[24] S. Cihlar, M. Tuerk, and K. Schaber, "Submicron particles of organic solids by rapid expansion of supercritical solutions," *Journal of Aerosol Science*, vol. 30, no. Suppl. 1, pp. S355–S356, 1999.

[25] B. Subramaniam, R. A. Rajewski, and K. Snavely, "Pharmaceutical processing with supercritical carbon dioxide," *Journal of Pharmaceutical Sciences*, vol. 86, no. 8, pp. 885–890, 1997.

[26] N. Ventosa, S. Sala, J. Veciana, J. Torres, and J. Llibre, "Depressurization of an expanded liquid organic solution (delos): A new procedure for obtaining submicron- or micron-sized crystalline particles," *Crystal Growth and Design*, vol. 1, no. 4, pp. 299–303, 2001.

[27] N. Ventosa, S. Sala, and J. Veciana, "Delos process: A crystallization technique using compressed fluids - 1. comparison to the gas crystallization method," *Journal of Supercritical Fluids*, vol. 26, no. 1, pp. 33–45, 2003.

[28] S. Sala, A. Cordoba, E. Moreno-Calvo, E. Elizondo, M. Munto, P. E. Rojas, M. A. A. Larrayoz, N. Ventosa, and J. Veciana, "Crystallization of microparticulate pure polymorphs of active pharmaceutical ingredients using CO2-expanded solvents," *Crystal Growth & Design*, vol. 12, no. 4, pp. 1717–1726, 2012.

[29] E. Moreno-Calvo, F. Temelli, A. Cordoba, N. Masciocchi, J. Veciana, and N. Ventosa, "A new microcrystalline phytosterol polymorph generated using co2-expanded solvents," *Crystal Growth and Design*, vol. 14, no. 1, pp. 58–68, 2014.

[30] R. Rowe and R. Roberts, "The mechanical properties of powders," *Advanced in Pharmaceutical Sciences*, pp. 1–62, 1995. cited By 1.

[31] M. Shariare, N. Blagden, M. de Matas, F. Leusen, and P. York, "Influence of solvent on the morphology and subsequent comminution of ibuprofen crystals by air jet milling," *Journal of Pharmaceutical Sciences*, vol. 101, no. 3, pp. 1108–1119, 2012.

[32] A. Bhakay, M. Merwade, E. Bilgili, and R. Dave, "Novel aspects of wet milling for the production of microsuspensions and nanosuspensions of poorly water-soluble drugs," *Drug Development and Industrial Pharmacy*, vol. 37, no. 8, pp. 963–976, 2011.

[33] L. Peltonen and J. Hirvonen, "Pharmaceutical nanocrystals by nanomilling: Critical process parameters, particle fracturing and stabilization methods," *Journal of Pharmacy and Pharmacology*, vol. 62, no. 11, pp. 1569–1579, 2010.

[34] Y. Obidchenko, N. Khuchua, R. Abramovich, A. Savochkina, A. Karamyan, S. Barsegyan, Y. Khomyakov, M. Ovcharov, and V. Chistyakov, "Preparation of micronized ibuprofen substance and assessment of its bioavailability," *Pharmaceutical Chemistry Journal*, vol. 47, no. 7, pp. 382–386, 2013.

[35] X. Han, L. Jallo, D. To, C. Ghoroi, and R. Dave, "Passivation of high-surface-energy sites of milled ibuprofen crystals via dry coating for reduced cohesion and improved flowability," *Journal of Pharmaceutical Sciences*, vol. 102, no. 7, pp. 2282–2296, 2013.

[36] X. Han, C. Ghoroi, D. To, Y. Chen, and R. Dave, "Simultaneous micronization and surface modification for improvement of flow and dissolution of drug particles," *International Journal of Pharmaceutics*, vol. 415, no. 1-2, pp. 185–195, 2011.

[37] N. Rasenack, H. Hartenhauer, and B. MÃijller, "Microcrystals for dissolution rate enhancement of poorly water-soluble drugs," *International Journal of Pharmaceutics*, vol. 254, no. 2, pp. 137–145, 2003.

[38] N. Rasenack and B. Muller, "Properties of ibuprofen crystallized under various conditions: A comparative study," *Drug Development and Industrial Pharmacy*, vol. 28, no. 9, pp. 1077–1089, 2002.

[39] N. Rasenack, H. Steckel, and B. Muller, "Preparation of microcrystals by in situ micronization," *Powder Technology*, vol. 143-144, pp. 291–296, 2004.

[40] M. Perrut, J. Jung, and F. Leboeuf, "Enhancement of dissolution rate of poorly-soluble active ingredients by supercritical fluid processes: Part i: Micronization of neat particles," *International Journal of Pharmaceutics*, vol. 288, no. 1, pp. 3 – 10, 2005.

[41] A. Hezave and F. Esmaeilzadeh, "Micronization of drug particles via ress process," *Journal of Supercritical Fluids*, vol. 52, no. 1, pp. 84–98, 2010.

[42] U. T. Lam, *Bioparticle engineering Using Dense Gas Technologies*. PhD thesis, The University og New South Wales, 2009.

[43] F. Wubbolts, *Supercritical Crystallization: Volatile Components as (Anti-) Solvents*. PhD thesis, Technische Universiteit Delft, 2000.

[44] M. Munto, *Micro- i nanoestructuracio de materials moleculars funcionals amb fluits comprimits: Desenvolupament de metodologies de preparacio i estudis fisicoquoimics*. PhD thesis, UAB, 2009.

[45] G. Khan and Z. Jiabi, "Preparation, characterization, and evaluation of physicochemical properties of different crystalline forms of ibuprofen," *Drug Development and Industrial Pharmacy*, vol. 24, no. 5, pp. 463–471, 1998.

[46] H. Garekani, F. Sadeghi, A. Badiee, S. Mostafa, A. Rajabi-Siahboomi, and A. Rajabi-Siahboomi, "Crystal habit modifications of ibuprofen and their physicomechanical characteristics," *Drug Development and Industrial Pharmacy*, vol. 27, no. 8, pp. 803–809, 2001.

[47] H. Cano, N. Gabas, and J. Canselier, "Experimental study on the ibuprofen crystal growth morphology in solution," *Journal of Crystal Growth*, vol. 224, no. 3-4, pp. 335–341, 2001.

[48] N. Rasenack and B. W. Muller, "Ibuprofen crystals with optimized properties," *International Journal of Pharmaceutics*, vol. 245, pp. 9 – 24, 2002.

[49] F.E.Wubbolts, *Supercritical Crystallization-Volatile Components as (Anti-)Solvents*. PhD thesis, Technische Universiteit Delft, 2000.

[50] J. Todd Reaves, A. Griffith, and C. Roberts, "Critical properties of dilute carbon dioxide + entrainer and ethane + entrainer mixtures," *Journal of Chemical and Engineering Data*, vol. 43, no. 4, pp. 683–686, 1998.

[51] E. Reverchon and I. De Marco, "Supercritical antisolvent micronization of cefonicid: Thermodynamic interpretation of results," *Journal of Supercritical Fluids*, vol. 31, no. 2, pp. 207–215, 2004.

[52] E. Reverchon and I. De Marco, "Supercritical antisolvent precipitation of cephalosporins," *Powder Technology*, vol. 164, no. 3, pp. 139–146, 2006.

[53] J. Mullin *Crystallization*, 1993.

[54] M. Lahav and L. Leiserowitz, "The effect of solvent on crystal growth and morphology," *Chemical Engineering Science*, vol. 56, no. 7, pp. 2245–2253, 2001.

[55] J. Ter Horst, R. Geertman, and G. Van Rosmalen, "The effect of solvent on crystal morphology," *Journal of Crystal Growth*, vol. 230, no. 1-2, pp. 277–284, 2001.

[56] M. Kamlet, R. Doherty, M. Abraham, Y. Marcus, and R. Taft, "Linear solvation energy relationships. 46. an improved equation for correlation and prediction of octanol/water partition coefficients of organic nonelectrolytes (including strong hydrogen bond donor solutes)," *Journal of Physical Chemistry*, vol. 92, no. 18, pp. 5244–5255, 1988.

[57] M. Kamlet and R. Taft, "The solvatochromic comparison method. i. the alfa-scale of solvent hydrogen-bond acceptor (HBA) basicities," *Journal of the American Chemical Society*, vol. 98, no. 2, pp. 377–383, 1976.

[58] M. Kamlet, J. Abboud, and R. Taft, "The solvatochromic comparison method. 6. the pi scale of solvent polarities," *Journal of the American Chemical Society*, vol. 99, no. 18, pp. 6027–6038, 1977.

[59] R. Taft, J.-L. Abboud, M. Kamlet, and M. Abraham, "Linear solvation energy relations," *Journal of Solution Chemistry*, vol. 14, no. 3, pp. 153–186, 1985.

[60] L. Ferrer Tasies, E. Moreno Calvo, M. Cano-Sarabia, M. Aguilella Arzo, A. Angelova, S. Lesieur, S. Ricart, J. Faraudo, N. Ventosa, and J. Veciana, "Quatsomes: Vesicles formed by self-assembly of sterols and quaternary ammonium surfactants," *Langmuir*, vol. 29, no. 22, pp. 6519–6528, 2013.

[61] E. Elizondo, E. Moreno, I. Cabrera, A. Cordoba, S. Sala, J. Veciana, and N. Ventosa, "Liposomes and other vesicular systems: Structural characteristics, methods of preparation, and use in nanomedicine," *Progress in Molecular Biology and Translational Science*, vol. 104, pp. 1–52, 2011.

[62] M. Cano-Sarabia, N. Ventosa, S. Sala, C. Patio, C.o, R. Arranz, and J. Veciana, "Preparation of uniform rich cholesterol unilamellar nanovesicles using CO2-expanded solvents," *Langmuir*, vol. 24, no. 6, pp. 2433–2437, 2008.

3

DELOS-susp for the preparation of pharmaceutical suspensions

3.1 Introduction

3.1.1 Micro-suspensions as Drug Delivery Systems

Dispersed systems, such as suspensions, emulsions and liposomes, consist of systems of at least two phases: the substance that is dispersed known as the dispersed or internal phase, and the continuous (or) external phase. These systems are widely used in various industrial sectors, such as pharmaceuticals, foodstuffs, cosmetics, agriculture, polymers, chemicals and ceramics [1] (Figure 3.1). In order to successfully penetrate the market, the structural characteristics of these systems must be tailorable to provide high quality products.

A well established strategy to increase bioavailability of poorly water soluble drugs is the creation and formulation of well dispersed micro- and submicroscale drugs suspended in an aqueous solution, so called suspensions [2]. Pharmaceutical micro- sus-

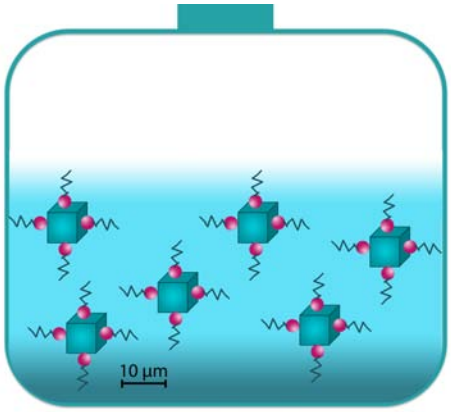

Figure 3.1: Scheme of a stable aqueous suspension.

pensions are a two phase systems composed of micro-scale particulate drugs suspended in a continuous liquid media.

Micro-suspensions can be used for compounds that are water insoluble but which are soluble in oils and can also be used to successfully formulate compounds that are insoluble in both water and oil. These suspensions overcome delivery issues for poorly water soluble compounds by obviating the need to dissolve them, and by maintaining the drug in a preferred crystalline state with a particle size sufficiently small for pharmaceutical acceptability. In addition, utilization of the dense, solid state confers an additional advantage of higher mass per volume loading. This is crucial when a high dosing is required. Moreover, the suspension technology has subsequent revealed secondary benefits that are now beginning to be realized: the particulate nature of the dosage form might offer alternative pharmacokinetic profiles in intravenous delivery that can offer less toxic and more efficacious regimes. Moreover, as explained in Chapter 2, micronization of poorly soluble drug increases its dissolution rate, thereby addressing a number of issues related to poor oral bioavailability. The solid state of the drug offers solutions to issues of chemical stability [3, 4]. By suspending the drugs as micro or nanoparticles, one can achieve a dose that is higher than that of a solution, which is thermodynamically limited by the aqueous solubility of the drug [5, 1, 6, 4].

Since the last two decades, production and stabilization of pharmaceutical suspensions has been an effective focus of pharmaceutical industry [4].

Aqueous forms of micro and submicron particles require special formulation techniques to optimize the properties of the drugs. An important target in this context is the

conversion of the generally coarse crystalline product into the finest particulate dispersion possible [7].

The available techniques to produce suspensions are very similar to the methods to produce microparticles of APIs and hence can be also categorized into two major classes: top-down (milling) and bottom-up (precipitation and chemical reaction) technologies, as depicted in Figure 3.2.

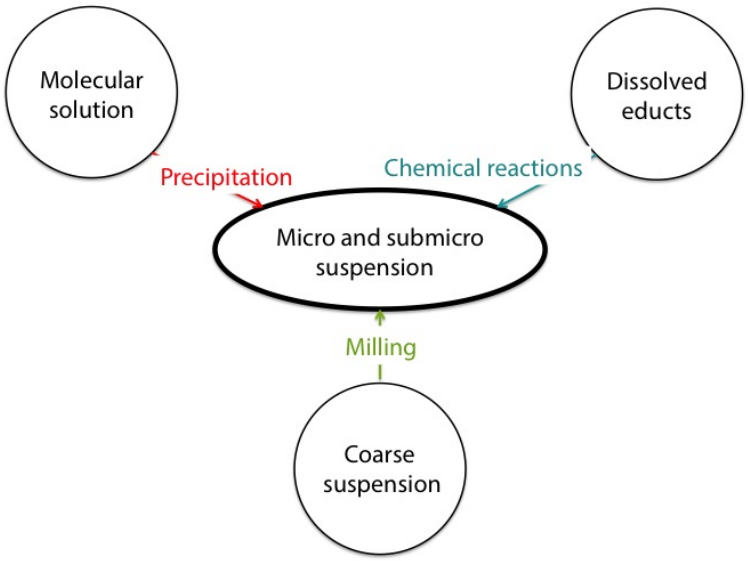

Figure 3.2: Methods for the preparation of micro and submicronparticles. Adapated from [7].

Top-down approaches are disintegration methods applicable to coarse suspensions. There are two basic disintegration technologies for preparation of aqueous suspensions:

- Pearl/ball milling

  In pearl/bal milling, the coarse suspension is loaded into a milling container containing milling pearls from, i.e. glass, zircon oxide or special polymers such as hard polystyrene derivatives. The pearls are moved by a stirrer, the drug is ground to nanocrystals in between the pearls [8]. This is the basic technology developed by G. Liversidge and coworkers, who patented it under the name of NanoCrystals®. This patent-protected technology was developed in 1990 and was formerly owned by the company NanoSystems, recently acquired by Elan. To produce NanoCrystals®, the

drug powder is dispersed in a surfactant solution and the obtained suspension undergoes a pearl milling process for hours to several days. The first products on the market using this technology were Rapamune and Emend and were launched in 2002 and 2003, respectively. A general problem of pearl mills is the potential erosion of material from the milling pearls leading to product contamination. Scaling up with pearl mills is possible; however, there is a certain limitation in the size of the mill due to its weight [8].

- High Pressure homogenization:

  The second most frequently used disintegration method is milling by high pressure homogenization. In the high pressure homogenization technique, the coarse drug suspension is forced under pressure through a valve that has a nano aperture. Typical pressures applied are between 100 and 1500 bars. As the drug suspension passes through the nano aperture with high velocity, the static pressure is decreased, leading to the formation of small gas bubbles, which implode as they exit the valve. The cavitation forces created breakdown the drug particles. It is not possible to obtain the desired particle size for many drugs in a single homogenization cycle.

  When producing suspensions using homogenization methods, the most important technologies are: Microfluidizer technology and Piston-gap homogenization.

  The Microfluidizer technology is a jet stream principle. The suspension is accelerated and passes with a high velocity through an especially designed homogenization chamber. There are two types of chambers: a) a Z-type chamber, where the suspension changes a few times the direction of its flow leading to particle collision and shear forces. In the second type of chamber, b) the Y-type, the suspension stream is divided into two streams which then collide frontally. A disadvantage of the technology is the large number of passes through the microfluidizer required to achieve the desired particle size.

  Piston-gap homogenization was developed in the middle of the 1990s by Müller and coworkers and was patented under the name DissoCubes®. In this technology, the drug powder is dispersed in an aqueous surfactant solution and subsequently forced by a piston through a tiny homogenization gap with pressures ranging up to 4000 bar. The width of the homogenization gap depends on the viscosity of the suspension and the applied pressure and usually ranges from 5 to 20 μm. The re-

sulting high streaming velocity of the suspension causes an increase in the dynamic pressure which is compensated by a reduction in the static pressure below the vapor pressure of the aqueous phase. Formation of gas bubbles occurs because the water starts boiling at room temperature. These gas bubbles collapse immediately when the liquid leaves the homogenization gap at atmospheric pressure [9]. Figure 3.3 presents a typical piston gap homogenizer.

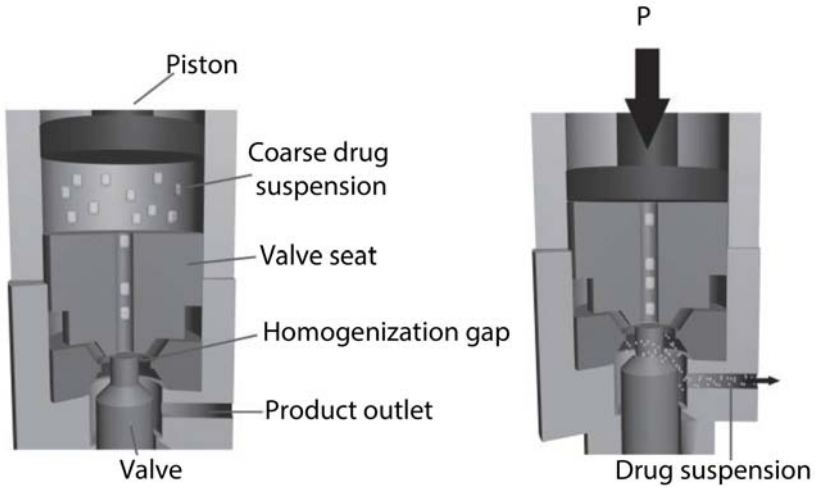

Figure 3.3: Basic principle of high pressure homogenization using a piston gap homogenizer. Adapated from [10].

Milling processes are in principle unsuitable for the production of micro dispersed systems with narrow size distribution since with decreasing particle size it becomes increasingly more difficult to use the applied mechanical energy in the form of shearing and cavitation forces. Moreover, the unavoidable milling element abrasion contaminates the final product and is difficult to separate, especially in active compound formulations. All media milling processes involve high energy input [11]. In general, in top-down process considerable heat is generated which may cause degradation of heat sensitive APIs. Milling has been shown to cause mechanical activation at drug particle surfaces [12].

In spite of these disadvantages, milling processes do find widespread use in the formulation of poorly soluble active compounds [13, 14] since alternative technologies which could deliver micro and submicron particles are essentially still in the development stage [15].

In contrast to top-down techniques, **bottom-up** methods generate micro and submicron particles by building them from drug molecules in solution. This can be achieved by

controlled precipitation (or crystallization). These processes can occur in the bulk solution or in droplets, depending on the technique [9].

Particle production by bottom-up processes is an area of growing interest as the number of marketed products employing nanotechnology is expected to increase. Although specific production techniques vary, they converge at the point of controlling the particle growth kinetics through mixing rate during precipitation or evaporation rate of the droplets [7].

Formation of a stable suspension with the smallest particle size requires high nucleation rate but low growth rate. Both process rates are dependent on supersaturation as explained in Chapter 1, therefore, high-supersaturation conditions are chosen for rapid nucleation.

Precipitation is the traditional approach to produce nano and microsized drug materials, but has the problem of a possible uncontrolled particle growth. The company Baxter introduced a combination technology called NANOEDGE, where precipitation is followed by a second high energy step, typical high pressure homogenization.

The precipitation processes from homogeneous solution with suitable process control allow the preparation of extremely fine particulate dispersions. These technical advantages also make precipitation processes particularly attractive from an economic viewpoint. For the manufacturing of micro- and submicrosuspensions, precipitation conditions are chosen so as to minimize particle size.

Figure 3.4 gives a general overview of precipitation and condensation processes for the production of organic micron or submiconparticles in aqueous media. The starting point of the three groups of methods is a molecularly dispersed solution of the API.

The individual process disclosed in Figure 3.4 differs in respect to the adjustment of the temporal supersaturation profile as well as in the choice and function of the additives. Process I and II employ lipophilic solvents and particle size restriction occurs through an emulsion step as an intermediate stage and is adjusted mechanically by homogenization [16]. In process III, the formation of micron and submicron particles takes place through a transient emulsion phase which forms spontaneously. When hydrophilic and fully water-miscible solvents are used (process IV and V), particle formation takes place by precipitation, according to nucleation and crystal growth or at extremely high supersaturation by spinodal phase separation. In each case, agglomeration can take place.

Except in the case of lipophilic solvents (process I and II) particle size distribution is controlled by the level of the adjustable supersaturation as well as by surfactant additives.

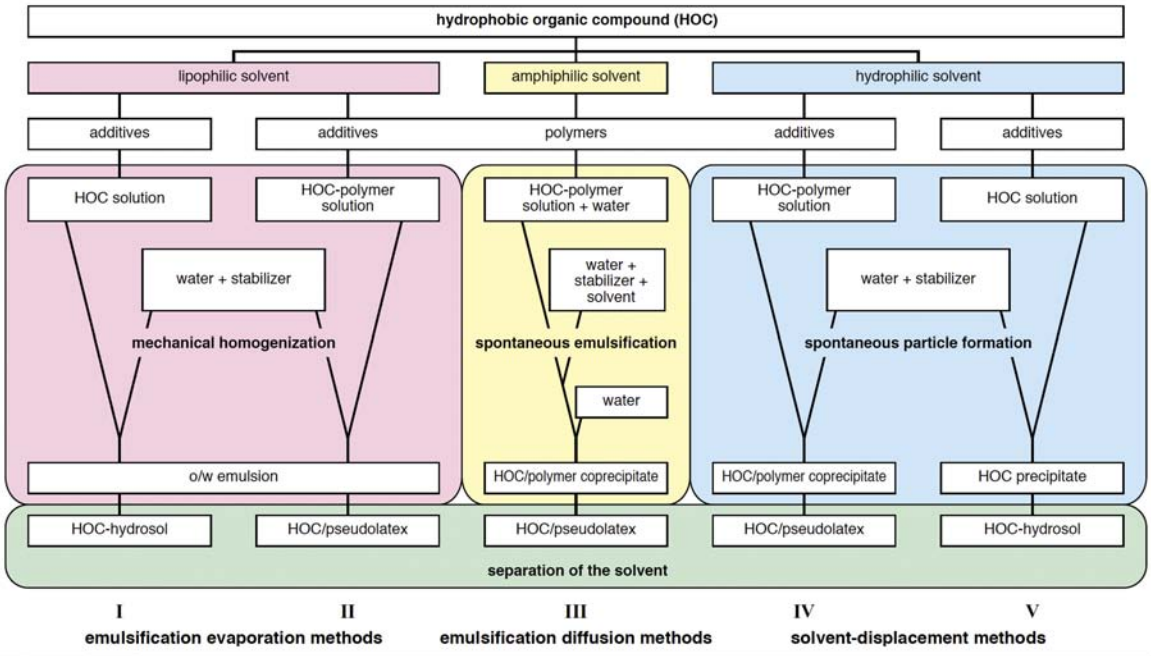

Figure 3.4: Precipitation and condensation processes for the preparation of organic micro and submicronsuspensions. Adapted from [7].

Only in process I and V, particle formation takes place by pure precipitation processes. In the other variants, a pseudo latex system is formed though physical condensation of dissolved macromolecules [7].

Conventional precipitation process also entails some problems by the generation of various unstable polymorphs, hydrates and solvates during processing. In addition, these approaches involve the use of solvents which are usually difficult to remove completely [2]. Moreover, though bottom-up approaches have shown promise, considerable gaps exist and more work is required before these techniques can be commercialized [17].

As mentioned in the Introduction of this Thesis, the scaling-up of conventional precipitation techniques comprises several difficulties, and cCO_2 based technology emerges as a very promising approach for the production of micro dispersed systems at large scale. The two most popular cCO_2-based methods are RESOLV and RESAS [18, 19, 20]. These processes consist of a simple modification of the RESS method for preparing stable suspensions. As described in Chapter 2, RESS methodology effectiveness relies on the solubility of the active compound in cCO_2, that it is usually very low.

The development of versatile methods for the preparation of stable aqueous suspen-

sions of poorly soluble drugs is still a major challenge, despite the extensive effort based on traditional techniques [4]. While the uncountable benefits of producing pharmaceutical nanosuspensions have been and continue to be explored, the methods to produce them have not been well established.

The possibility and ability for large-scale production of a delivery system or a dosage form is the essential prerequisite for its introduction to the pharmaceutical market. It is pointless to have a very neat delivery system but no possibility to produce it on a large scale to supply the market [6]. Moreover, it is well established that the method of manufacture can significantly impact the formation and stability of suspensions and hence their overall performance [11].

In light of this need, this Chapter is devoted to explore new ways to manufacture stable pharmaceutical micro- and submicron suspensions in a fast, safe and predictable manner, which is still a requirement in the pharmaceutical industry.[4]. In the following, a small introduction regarding the stability of suspensions and the role of surfactants in the obtaining of aqueous suspensions is presented.

3.1.2 Stability of aqueous suspensions

Stability issues associated with suspensions have been widely investigated and can be categorized as physical and chemical stability. Drug particles can either settle down or cream up in the formulation medium depending on their density relative to the medium [21] (Figure 3.16).

Role of surfactants in aqueous suspensions

Finely dispersed particles in an aqueous phase have a high tendency to agglomerate together leading to the formation of larger aggregates [1]. Aggregation of particles lowers the stability of the systems and the crisis is even more severe when a suspension contains a high concentration of particles [22, 23]. A surfactant (a contraction of the term surface-active agent) literally means active at a surface. The name amphiphile is sometimes used synonymously with surfactant. The word is derived from the Greek word *amphi*, meaning both, which relates to the fact that all surfactants consist of two parts, one soluble in a specific fluid (lyophilic part) and one which in insoluble (lyophobic) (see Figure 3.6) [24]. The relation of both parts of the surfactant is described by the hydrophile-lipophile balance, (HLB) which is a number between 0 and 40 indicative of the emulsification be-

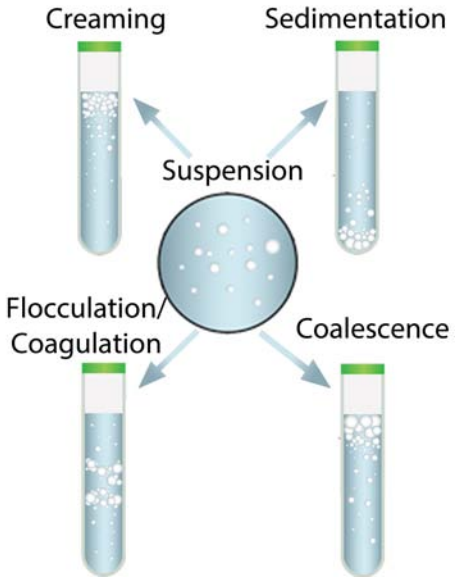

Figure 3.5: Common destabilization mechanism of suspensions.

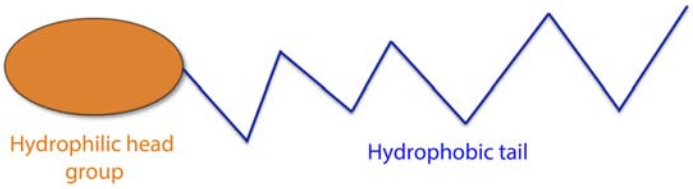

Figure 3.6: Schematic representation of a surfactant.

havior and it is related to the balance between the hydrophilic and lipophilic portions of the molecules.

A surfactant is a substance that, when present at low concentration in a system, has the property of adsorbing onto the surfaces or interfaces of the system and of altering to a marked degree the surface or interfacial free energies of those surfaces (or interfaces). The term interface indicates a boundary between any two immiscible phases; the term surface denotes an interface where one phase is a gas, usually air. The interfacial free energy is the minimum amount of work required to create that interface [25]. The interfacial (or surface) tension is also a measure of the difference in nature of the two phases meeting at the interface (or surface). The greater the dissimilarity in their natures, the greater the interfacial (or surface) tension between them. A surfactant is therefore a substance that at

low concentrations adsorbs at some or all of the interfaces in the system and significantly changes the amount of work required to expand those interfaces [26].

It is thought that surfactants inhibit crystal growth and aggregation of particles in suspensions by adsorbing on the crystal surfaces [22, 23, 27]. There are two main mechanisms through which colloidal suspensions can be stabilized in both aqueous and non-aqueous medium, i.e. electrostatic repulsion and steric stabilization [28, 29, 3, 21]. These two mechanisms can be achieved by adding ionic and non- ionic stabilizers into the medium, respectively. Amphiphilic non-ionic stabilizers are usually utilized to provide steric stabilization which is dominated by solvation effect. As the non-ionic stabilizers are introduced into suspensions, they are absorbed onto the drug particles through an anchor segment that strongly interacts with the dispersed particles, while the other well-solvated tail segment extends into the bulk medium [21].

As mentioned, the adsorption of polymers and surfactants at the growing interface reduces the interfacial surface energy and hence, inhibits particle growth. When particles of a drug are formed, a new surface area is created, which necessitates a free-energy (ΔG) cost defined by:

$$\Delta G = \gamma_{s/l} * \Delta A \,, \tag{3.1}$$

in which $\gamma_{s/l}$ is the interfacial tension and ΔA is the new area formed. This arises because water molecules incur fewer attractive forces with other water molecules when located at a free surface. The system prefers to reduce this increase in surface area by either dissolving incipient crystalline nuclei, in the case of precipitation, or by agglomerating small particles, regardless of their formation mechanism. This tendency is resisted by the addition of surface-active agents, which, as explained above, reduce the $\gamma_{s/l}$ and therefore the free energy of the system (Figure 3.7).

Nucleation is the key step in a crystallization process [30]. Effective stabilizers for bottom-up preparation methods should have the ability to promote the rate of nucleation. Surfactants and polymers, apart from decreasing the surface tension of the system, increase the the viscosity of a solution at any temperature [31]. This decrease in surface tension and increase in viscosity enhance nucleation rate. This can be rationalized bearing in mind the nucleation rate expression according to the classical theory of homogenous nucleation [32]:

$$J = A * exp(-\frac{B}{lnS^2}) \,, \tag{3.2}$$

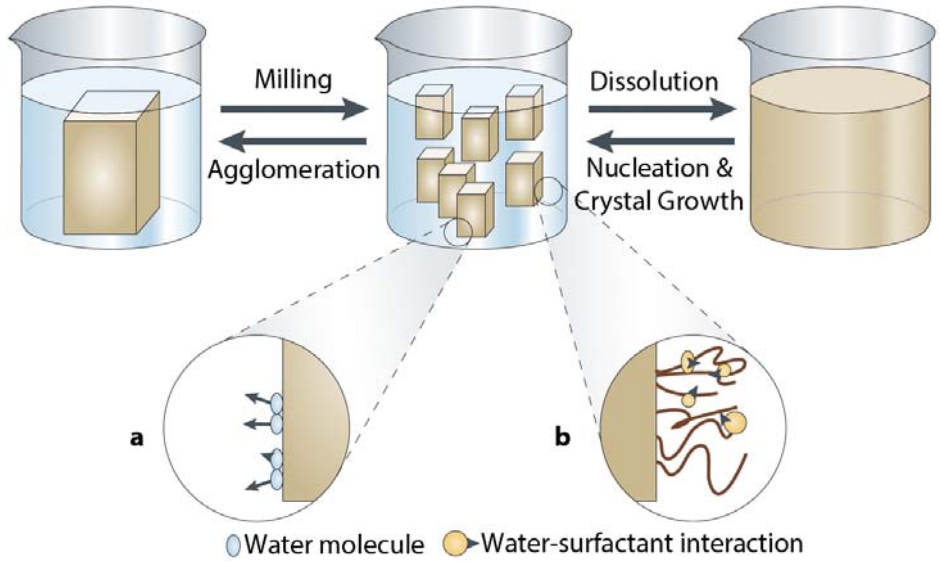

Figure 3.7: Creation and stabilization of microparticles from the perspective of surface energetics: a) In the case of unfavorable energetics, hydrophobic crystal surface directly contacting water molecules leads to crystal agglomeration, because, as shown by the arrows, water molecules are energetically driven to leave the surface. b) A surfactant-stabilized crystal surface reduces interfacial tension by allowing attractive mater-surfactant interactions.The crystal surface is stabilized and shows reduced tendency to agglomerate.Adapted from [3].

where J is the nucleation rate, S is the supersaturation, A is

$$A = N_0 * \upsilon \,, \tag{3.3}$$

being N_0 the number of molecules of solute per unit volume and υ the frequency of molecular transport to the solid-liquid interface,

$$\upsilon \approx \frac{kT}{3\Pi {a_0}^2 \eta} \,, \tag{3.4}$$

where η is the viscosity and a_0 is the mean effective diameter of the diffusing species. And B in expression (3.2) is

$$B = \frac{16\Pi\sigma^3 {\upsilon_s}^2}{3k^3T^3} \,, \tag{3.5}$$

where σ is the surface tension at the solid-liquid interface, k is the Boltzmann constant, υ_s is the volume of a solute molecule and T is the temperature. According to equations 3.2 and 3.5, a decrease in surface tension increases the nucleation rate, and as a result,

particle size decrease [33, 34]. Based on expression (3.4), an increase in viscosity reduces the number of collisions and decreases the rate of mass transfer from the solution to the growing solid-liquid interface as a result of diffusion [31].

The addition of surfactants and polymers as stabilizers can greatly improve the stability of a drug suspension system [35, 36, 37], however, unfortunately, there exists no systematic technique to determine the effectiveness of additives a priori. Therefore, due to a lack of predictability, stabilizers are typically chosen empirically or using heuristics. In addition, there are no high throughput means to test the effectiveness of various stabilizers. Currently, there are a few studies incorporating theoretical predictions of stabilizer effectiveness, in particular, models proposed to explain the enhancement of stability by additives, and a study on the stabilization of covalent metal nano-scale crystals [38], but none for small pharmaceutical crystals. Furthermore, no models exist to compare the stabilization capabilities of using multiple stabilizers simultaneously, therefore leaving the possibility of additive synergism unexplored [39].

3.2 Development of a DELOS-susp procedure for the preparation of aqueous suspensions

DELOS-susp method arises as a novel and promising methodology for the preparation of colloidal molecular micro and nanoparticles in an eco-efficient manner [40, 41]. In this Thesis, it is explored for the first time the use of DELOS-susp for the preparation of aqueous suspensions.

Taking advantage of the versatility of the DELOS method, a simple modification was introduced after the depressurization stage, keeping the simplicity of the process intact. In this new platform, called DELOS-susp, the CO_2-expanded solution is depressurized into an aqueous phase instead of passing through a filter (Figure 3.8). The explanation behind this modification is to inhibit the undesired particle growth and agglomeration that can take place after depressurization during filtration of particles. During filtration, the nucleus are still in contact with the mother liquors and therefore they can continue growing. Mechanistically, the liquid at the receiving end of the rapid depressurization that occurs in DELOS, could suppress particle growth of the precipitate.

As depicted in Figure 3.8, the first and second stage of DELOS-susp procedure are the same as in DELOS method (see Figure 2.6 of Chapter 2) and are the following: the API is dissolved in a conventional organic solvent at atmospheric pressure and at working temperature (T_W). The solution is charged into the high pressure vessel, which has been previously driven to the working temperature (T_W). CO_2 is then added to obtained a volumetric expanded solution of the API at T_W and at high pressure (P_W) with a given molar fraction of CO_2 (x_W). Finally, this CO_2-expanded solution is depressurized from P_W to atmospheric pressure over a continuous aqueous flow, giving a aqueous suspension of the drug.

Experimental protocol and equipment

The equipment adapted in this Thesis for preparing suspensions is schematized in Figure 3.9. This set-up comprises a 300mL reactor where CO_2 is pumped through a high pressure pump (B-1), which head is cooled by a cooling unit. Before entering the high pressure vessel, CO_2 is heated to the working temperature (T_W) using a heat exchanger (TIC). The amount of CO_2 added to the reactor through valve V1-b is measured by a mass flowmeter (FCO2). The vessel temperature is controlled using an external fluid heating

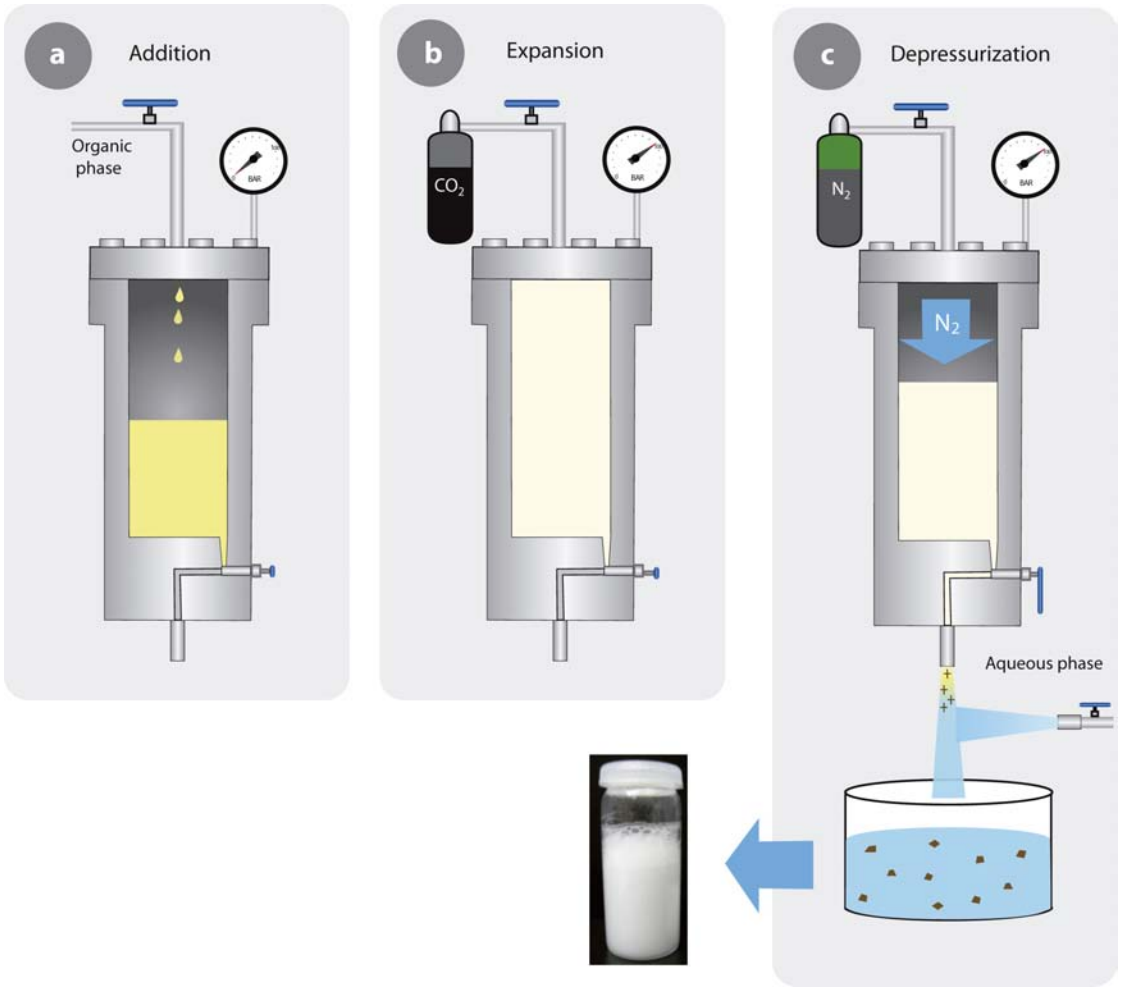

Figure 3.8: Schematic representation of the DELOS-susp method for the preparation of micro- and submicrosuspensions. A) Addition of a liquid organic solution of the compound to be crystallized inside the vessel at atmospheric pressure, P_{atm}, and working temperature, (T_W). B) Addition of CO_2 for the formation of a CO_2-expanded liquid solution at P_W and T_W and certain molar fraction of CO_2 (x_W). Stirring favors the rapid mixing between CO_2 and the organic solution. C) Rapid depressurization of the CO_2-expanded solution from P_W to P_{atm} over an aqueous phase for the formation of micro suspensions.

jacket. After the vessel there is a filter (F-1) pressurized at P_W. This filter collects particles that could precipitate due to the anti-solvent effect of the addition of CO_2 when the experimental working conditions are very close to the binodal line. This filter is connected to the depressurization valve (V8) which is remotely controlled with a computer. After the depressurization valve there is a T-mixer, where the depressurized solution is co-currently

mixed with the aqueous phase. During depressurization the aqueous phase is pumped at a constant flow by a peristaltic pump (B-3). The aqueous suspension is collected in a plastic bucket (T).

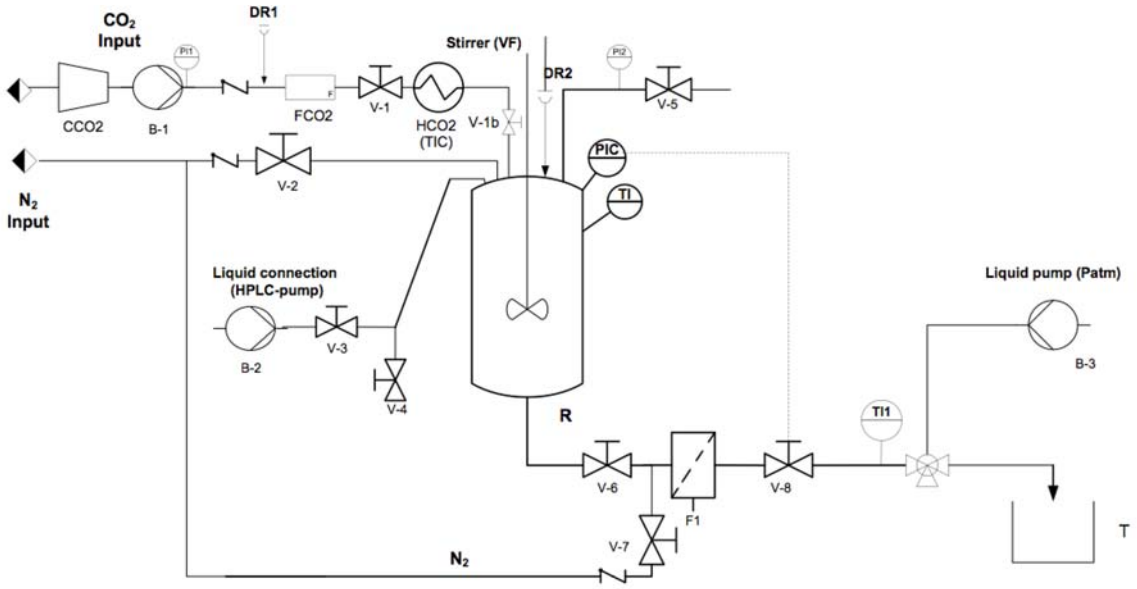

Figure 3.9: Schematic representation of the DELOS-susp set-up for the preparation of micro- and submicrosuspensions.

The distance between the depressurization valve and the T-mixer has kept constant as well as the flow at which the aqueous phase is pumped during depressurization.

The experimental protocol followed for the preparation of micro and submicron suspensions of APIs is the following:

1. A certain volume (V_I) of an initial solution of the compound to be crystallized in organic solvent with a specific C_i is added to the high pressure vessel at atmospheric pressure and at the working temperature (T_W).

2. After 30 minutes, once the solution has achieved T_W, the vessel is pressurized with compressed CO_2 through valve V-1b, producing a volumetric expanded liquid solution with the desired molar fraction of CO_2 (x_W) at the working pressure (P_W). The stirring is switched on during the addition of CO_2 to favor the mixing between cCO_2 and the organic solution.

3. The system "solute/organic solvent/CO_2" is left to equilibrate during at least 1hour.

4. Filter F-1 is pressurized at P_W . Valve V-6 is opened to connect the pressurized filter F-1 with the vessel. Filter F-1 collects any precipitate formed due to the antisolvent behavior of CO_2 that could take place.

5. The CO_2-expanded solution is then depressurized from P_W to atmospheric pressure though valve V-8 into the T-mixer where it is mixed with a certain volume of an aqueous phase (V_{aq}) which is being pumped with a specific flow (F). A current of nitrogen at P_W is used as embolus to push down the expanded solution in order to maintained constant pressure in the reactor during depressurization.

6. The mixing of the depressurized solution with the aqueous phase leads to the formation of aqueous suspensions.

3.3 Preparation of aqueous suspensions of the thiadiazoline derivative NP by DELOS-susp

DELOS-susp method emerges as a promising approach to tackle the uncontrolled growth of NP crystal that occurs after depressurization of the CO_2-expanded solution in DELOS process. Although it is not exactly clear from the experimental results explained in Chapter 2 what is the mechanism that cause this phenomenon, it is very common in precipitation that agglomeration of the particles occurs during filtration of the particles [18]. This agglomeration can cause a variety of issues including crystal growth [21]. The following section is devoted to explore this new alternative of DELOS platform for the preparation of stable aqueous micro and submicro-suspensions of NP crystals.

In order to validate DELOS-sups method for the production of aqueous suspensions of NP and to asses the quenching effect of water after depressurization, two DELOS-susp preliminary experiments were designed on the basis of the DELOS crystallization experiments which had the highest yield and which produced the smallest particles. Experiment DELOS 3 was the one with the highest yield and the experimental conditions of experiments 5-6 produced the particles with the smallest particle size (see Section 2.3.3 and Table 2.5.) These DELOS crystallizations were conducted at T_W= 313 K and P_W= 10 MPa using acetonitrile as organic solvent. Experiment DELOS 3 was carried out at β=0.8 whereas experiment DELOS 6 carried out at a higher initial concentration and hence at a higher initial supersaturation, β_i=1. The molar fraction of CO_2 in experiment 3 was x_W=0.6 and in experiment 6, x_W=0.4.

As mentioned, the experimental procedure of DELOS-susp is the same of DELOS for the two first stages and the difference of both process relies on the third stage: In DELOS-susp, the CO_2-expanded solution is depressurized through a one-way automatic valve into a T mixer, to which a current of water is co-currently pumped with a certain flow (F= 500 mL/min). The huge, rapid and homogeneous cooling due to CO_2 venting during depressurization extremely reduces the solubility of NP in acetonitrile, causing the nucleation of the active, whose growth is partially quenched by the current of water leading to the formation of a microsuspension.

Table 3.1 discloses the operational conditions of the conventional DELOS experiments and the new DELOS-susp experiments.

In both DELOS-susp experiments, aqueous suspensions of NP were obtained for the

Table 3.1: DELOS-susp experiments designed based on DELOS experiments.

Experiment	C_i*10^3 [a]	β_i [b]	x_W [c]	Yield (%) [d]	Size distribution (μm) [e]		
					d(0.1)	d(0.5)	d(0.9)
DELOS 3	3.75	0.8	0.59	85	1.10	4.45	28.37
DELOS-susp 1	3.75	0.8	0.65	95	1.2	5.00	30.15
DELOS 6	4.69	1	0.4	66	1.16	3.10	14.90
DELOS-susp 2	4.65	1	0.45	92	1.1	3.80	19.65

All experiments were conducted at P_W =10 MPa and T_W = 313 K. [a] initial concentration of NP in acetonitrile in mol/mol, [b] $\beta_i = C_i/C_S$, [c] molar fraction of CO_2, [d] yield expressed as % os mass recovered. [e] Volumetric particle size distributions expressed in percentiles of 10, 50 and 90%.

first time. However, these suspensions were not stable and the solid settled down very fast.

To delucidate if DELOS-susp yields smaller particles of NP than DELOS, both suspensions were filtered under vacuum to characterize the solids recovered. The particles filtrated were dried under vacuum and measured by Light Scattering and SEM following the procedures described in detail in Sections 6.4.1 and 6.4.2 of the Experimental Part respectively. Figures 3.10 and 3.11 display each characterization.

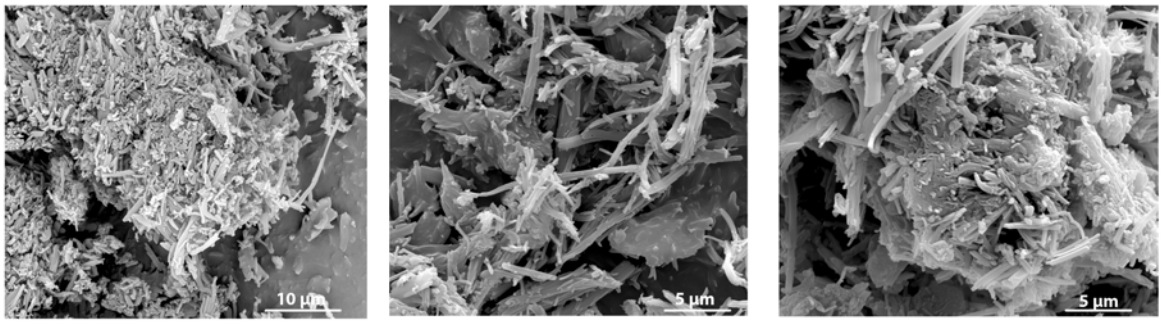

Figure 3.10: Comparison of representative SEM pictures of the NP particles obtained though DELOS (a, experiment 3) and after filtration of the suspensions obtained by DELOS-susp: b) experiment 1 and c) experiment 2.

The SEM images of the solids obtained after filtration and drying of the NP suspensions show us two types of particles homogeneously distributed. Both particles are needle-

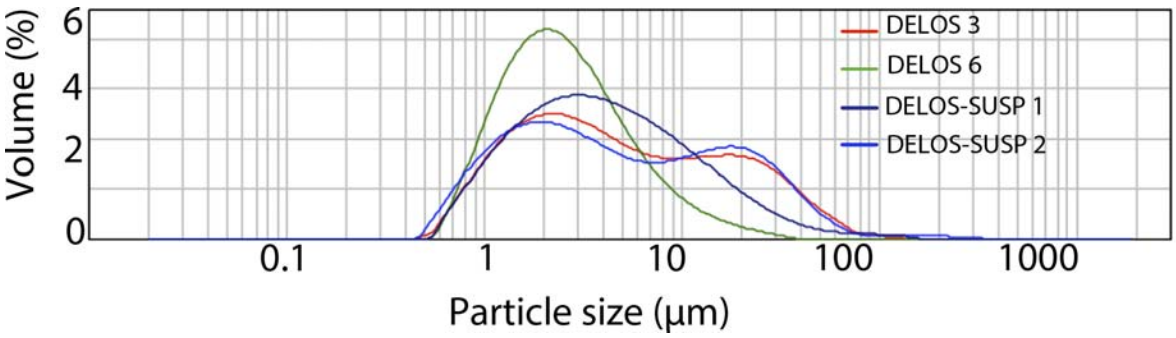

Figure 3.11: Comparison of particle size distribution of the solids obtained by experiments DELOS 3 and 6 to the solids obtained after filtration and drying under vacuum of the suspensions produced by DELOS-susp.

like particles. There is a population of submicron particles very similar to the one observed in DELOS experiments and another composed of larger needles with a equivalent sphere diameter of 20 μm.

Light Scattering results present a difference in between the two samples obtained by DELOS-susp. It can be clearly seen in Figure 3.11 that the solid produced in DELOS-susp experiment 1 is composed of a broad but unimodal particle size distribution, whereas, the solid obtained in DELOS-susp experiment 2 has a bimodal particle size distribution. The second peak of the distribution presents an average size of 20μm. This second peak could reflect a phenomena that occurs after depressurization and can be attributed to the difference in the DELOS yield of both DELOS-susp experiments. Experiment DELOS-susp 2 is conducted at the same experimental conditions that DELOS experiment 6, which yield was 66%. Therefore, 34% of the initial NP does not precipitate by the large and abrupt decrease in temperature produced in DELOS and, as a consequence, remains in the mother liquor (upper part of Figure 3.12). It can be assumed that the NP molecules that do not precipitated due to the abrupt decrease in temperature, crystallized by anti-solvent precipitation when the active compound enters the water current. In experiment DELOS-susp 1, which is performed as DELOS experiment 3 (yield 85%), this phenomenon takes place in much lower magnitude as the amount of NP that stays in the mother liquor is smaller as the DELOS precipitation yield obtained is higher. Hence, the resulting particle size distribution is broad but unimodal.

As a mean to understand this difference in particle size distribution and to prove the above mentioned hypothesis, a experiment were conducted which is schematized in Fig-

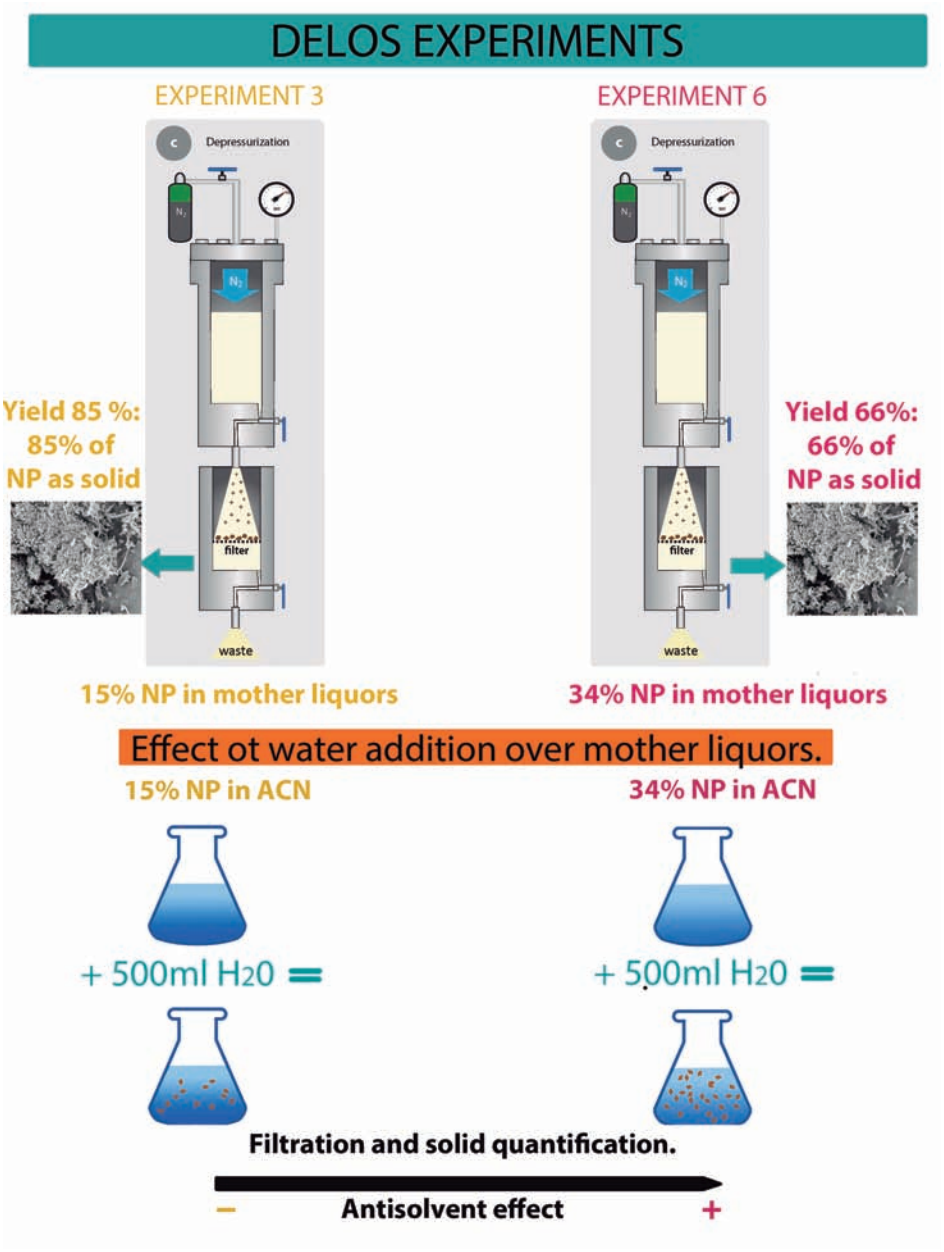

Figure 3.12: Two solutions with the amount of NP that does not precipitate in DELOS experiment were prepared. Then, the same amount of water used in DELOS-susp (500 mL) was added. NP precipitated by anti-solvent effect of water. The suspensions were filtered and the solids were dried and weighted to assess the amount of NP that precipitate by anti-solvent.

ure 3.12.

The amount of solid that does not precipitated by the large and abrupt decrease of

temperature was estimated based on the corresponding DELOS yields. Therefore, in experiment DELOS 3, the DELOS yield is 85%, expressed as recovered mass in the filter in relation to the initial mass of NP charged into the vessel. Hence, the difference is the amount of NP that remains in the mother liquor: 15%. For experiment DELOS 6, this amount is higher (34%) as the DELOS yield is lower (66%). As the initial amount of NP dissolved in acetonitrile (C_i) is known for both conditions, it is possible to estimate the concentration of NP in the mother liquor. Two acetonitrile solutions with these concentrations of NP were prepared. And then, to reproduce what might occur in experiments DELOS-sups 1 and 2, 500 mL of water was added to those solutions. In both cases, a precipitate was observed because NP crystallized by anti-solvent precipitation. The new suspensions obtained were filtered and dried to measure the amount of solid that crystallize by the anti-solvent behavior of water. This simple test allows the quantification of the antisolvent precipitation yield. The DELOS-susp yield is the sum of the DELOS yield plus the anti-solvent yield. The values of the yields of the DELOS-susp experiments presented in Table 3.1 are calculated following this procedure.

In experiment DELOS-susp 1, where most of the solid precipitated by the large, abrupt and homogenous decrease in temperature, a unimodal particle size distribution was achieved as can be checked in Figure 3.11. Hence, attending to these preliminary results, in order to conduct a successful DELOS-susp experiment, the experimental conditions must ensure the maximum DELOS yield possible. In light of this conclusion, for the preparation of aqueous suspensions of APIs by DELOS-susp, the experimental conditions should guarantee the maximum DELOS yield to avoid at the highest extend the possibility of obtaining anti-solvent precipitation of the drug when the depressurized solution is quenched by the aqueous flow.

The comparison between particle size distribution of the DELOS experiment 3 and DELOS-susp experiment 1 (Figure 3.11) reveals that, for the same experimental conditions, DELOS-susp performs better in terms of particle size reduction, as a unimodal distribution is achieved. This could be explained considering that the addition of water at the end of the depressurization could inhibit crystal growth of NP particles.

Considering these promising results, it was proposed to improve the stability of the suspensions by the addition of surfactants that could avoid crystal growth and agglomeration of the crystals in suspensions.

3.3.1 Preparation of aqueous suspensions of the thiadiazoline derivative NP using surfactants

In the course of the development of a stable micro- and submicrosuspension formulation of NP, various surfactants were screened to achieve the desired particle size, with a narrow distribution in size and to prevent agglomeration. The selection of surfactants and the concentration used in each experiment was based on previous experience of Noscira or based on information reported in the literature. However, as NP is a newly discovered drug, there is no previous experimental data in the literature referring to the behavior of this drug.

The surfactants selected were dissolved in the water phase over which was depressurized the CO_2-expanded solution of NP, in accordance to the DELOS-susp protocol described in Section 6.5.2 of the Experimental Part. The surfactants chosen are briefly described below, including some specific properties such as molecular weight, molecular structure and the hydrophile - lipophile balance, (HLB), which was previously described.

Description of the surfactant used

- **Gelurice® 44/14:** It is produced by the reaction of hydrogenated palm kernel oil and polyethylene glycol, PEG 33. It contains PEG 33 esters (mainly PEG mono- and dilaurate, i.e; esters of PEG with C12 chains either at one end only or at both ends), glycerides (mainly mono-, di- and trilaurin, i.e. the triglyceride with C12 chains), unreacted PEG 33, and a small amount of glycerol. Gelucire 44/14 possesses surfactant properties [42, 43, 44]. [].
  - Average Molecular weight = 300 -1500 g/mol
  - HLB = 14
- **Poloxamer F-127:** Also known as Poloxamer 407, it belongs to the category of hydrophilic non-ionic surface active polyoxyethylene - polyoxypropylene - polyoxyethylene block copolymers (Pluronics) [45, 45, 46].
  - Average Molecular weight = 9840 -14600 g/mol
  - HLB = 18
- **Hydroxypropyl methylcellulose, HPMC:** is a coating agent and film-former used as an inactive ingredient in the pharmaceutical industry. It has also been used as

a rate-controlling polymer for sustained-release dose forms. Hypromellose is considered an inert ingredient. It has a high viscosity [47, 48, 49, 50].

  - Average Molecular weight = 324.284 g/mol
  - HLB = 10

- **Polyvinylpyrrolidone (PVP):** is a water-soluble polymer that results from the polymerization of vinylpyrrolidone. Different chain lengths yield in different viscosities. It is one of the most interesting and versatile polymers used in the pharmaceutical industry [51, 52].

  - Average Molecular weight = 2500-2 500 000 g/mol

- **Sodium dodecyl sulfate (SDS):** It is also known as Sodium Lauryl Sulfate (SLS). It is an anionic surfactant naturally derived from coconut and/or palm kernel oil. It usually consists of a mixture of sodium alkyl sulfates, mainly the lauryl [53, 54, 55, 56].

  - Average Molecular weight = 288.379 g/mol
  - HLB = 40

- **Polysorbate 80:** Also known as Tween 80, is a common hydrophilic nonionic excipient used in the pharmaceutical industry.

  - Average Molecular weight = 1310 g/mol
  - HLB = 15

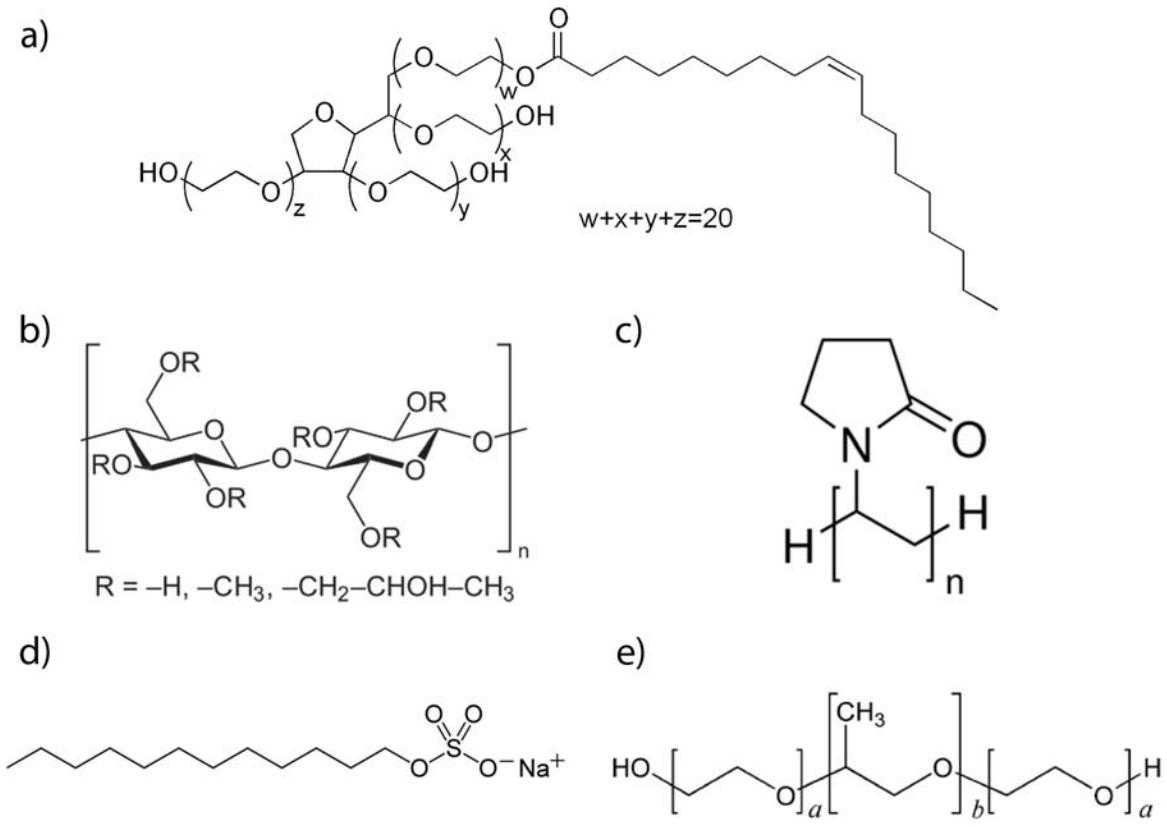

Figure 3.13: Molecular structure of the surfactants employed: a) Polysorbate 80 , b) HPMC, c) PVP, d) SDS and e) Poloxamer F-127. The molecular structure of Gelurice® 44/14 is not reported.

Preparation of aqueous suspensions of the thiadiazoline derivative NP by DELOS-susp in the presence of surfactants

Following the same DELOS-susp protocol described in Section 6.5.2 of the Experimental Part and the same equipment as in the preparation of suspensions of NP in the absence of surfactants (see Section 6.5.1 of the Experimental Part for more details), a new set of experiments were designed to evaluate the effect of the addition of surfactants in the aqueous phase over the structural characteristics of NP particles of the suspensions. The unique difference introduced in the experimental protocol is that instead of pumping pure water, an aqueous solution of the surfactant is used to quench the depressurized

solution (see Figure 3.14).

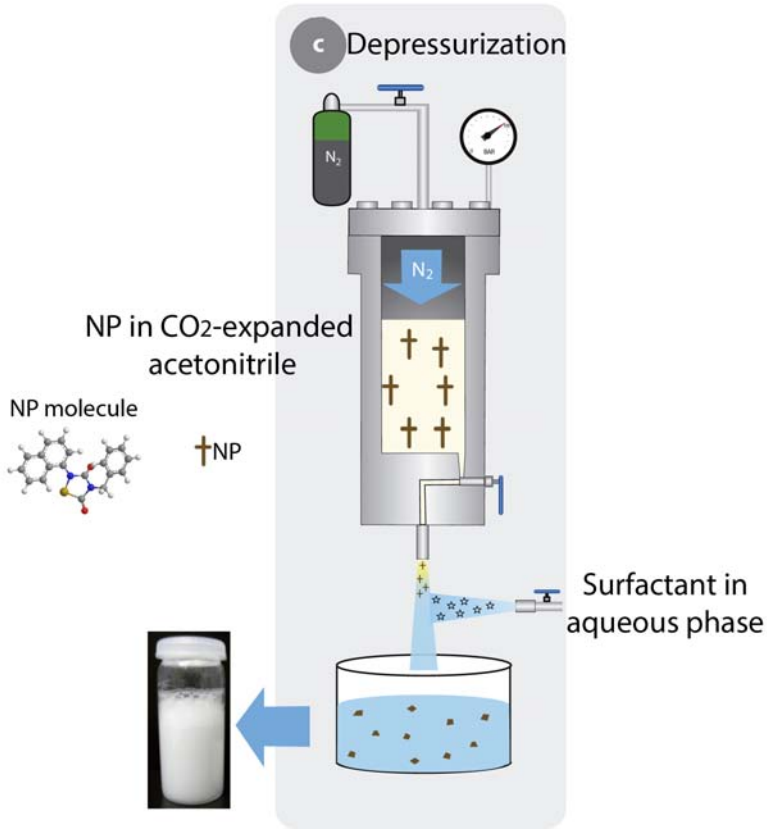

Figure 3.14: Addition of surfactant in the aqueous flow during depressurization.

The experiments designed to study the influence of the nature of the surfactant on the stability and particle size reduction of NP crystals are displayed in Table 3.2 as well as the reference DELOS-susp experiment without surfactant, experiment 1. This set of experiments were performed at the same processing variables as the ones used in experiment 1 as those ones ensure the maximum DELOS yield. The experimental conditions are the following: temperature (T_W= 313 K), pressure (P_W= 10 MPa), CO_2 content (x_W= 0.65), water flow (F= 500 mL/min) and the initial concentration of NP in acetonitrile (C_i= 3.75*10^{-3} mol/mol). As mentioned before, the new variable introduced is the surfactant employed.

In all the experiments, milky suspensions of NP were obtained, with a much higher macroscopically stability than the suspensions prepared in the absence of surfactants (experiment 1), as can be seen in Figure 3.15.

The stability of the aqueous suspensions of the thiadiazoline derivative NP obtained

Table 3.2: DELOS-susp experiments for evaluating the impact of the surfactant for the preparation of NP aqueous suspensions.

Experiment	Surfactant	Surfactant/NP ratio (g:g)[a]
1	-	-
3	Gelurice® 44/14	0.77:1
4	Poloxamer F-127	0.8:1
5	HPMC	0.8:1
6	PVP	1:1
7	SDS	0.8:1
8	Tween80	0.8:1

DELOS-susp experiments performed at T_W = 313 K, P_W =10 MPa, x_W= 0.65 and F=500 mL/min for testing the influence of various surfactants, [a] amount of surfactant expressed as grams of surfactant per gram of NP.

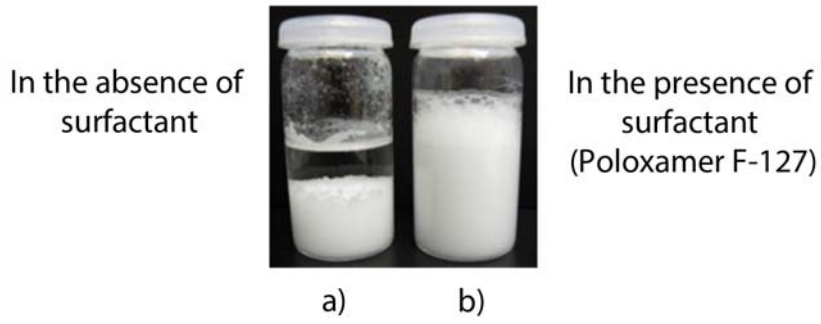

Figure 3.15: Comparsion of the macroscopic appearance of two aqueous suspensions of NP obtained through DELOS-susp in the absence of surfactant (experiment 1) and in the presence of Poloxamer F-127 (experiment 4).

by DELOS-susp were optically monitored and particle size distribution of particles were measured by Light Scattering. The results of both characterizations are displayed in Table 3.3. The macroscopic appearance of the suspensions of NP in the presence of Poloxamer F-127, Gelurice® 44/14, HPMC and Tween80 are the same: they are stable and homogenous milky aqueous suspensions. On the other hand, suspensions obtained with PVP and SDS are not stable as NP particles tend to cream up. SDS is an ionic surfactant, which exerts an electrostatic repulsion among particles. PVP is a nonionic surfactant but be-

Table 3.3: Comparison of particle size distribution results of the microsuspensions obtained by DELOS-susp using different surfactants.

Experiment	Surfactant	Macroscopic stability[a]	Size distribution (μm)[b]		
			d(0.1)	d(0.5)	d(0.9)
1	-	✗✗	9.2	23.6	51.5
3	Gelurice® 44/14	✓	3.3	9.4	23.0
4	Poloxamer F-127	✓	0.6	1.6	5.5
5	HPMC	✓	1.4	5.2	17.1
6	PVP	✗	1.6	8.2	22.8
7	SDS	✗	1.2	3.8	17.6
8	Tween80	✓	0.9	2.4	8.0

[a]Optical monitored macroscopically stability, [b] Volumetric particle size distributions expressed in percentiles of 10, 50 and 90% of NP suspensions after 10 min of US.

cause of their dipolar resonance form, it also shows some of the properties of zwitterionics. Zwitterionic surfactants may present both positive and negative charges at their surface [26]. The rest of the surfactants utilized are non-ionic polymers, which confer a steric repulsion [3](Figure 3.16). In the case of stabilizing NP particles in aqueous suspensions produced by DELOS-susp, non-ionic polymers are more suitable than the ionic surfactant SDS and the polymer PVP, which shows some zwitterionic properties. SDS and PVP, at the concentrations used (1:1 and 0.8:1 surfactant/NP (g:g) respectively) are not acceptable for the preparation of stable aqueous suspensions of NP.

The mechanics of the surfactant-stabilized suspensions can be considered from the perspective of potential energy. If particles approach each other too closely, they will agglomerate. This must be prevented to ensure a stable system. Energetically, this requires the placement of a sufficiently high energy barrier at relatively long separation distances to prevent particles coming too close together. A non-ionic polymeric surfactant coats the surface with a hydrophobic chain and permits a hydrophilic tail to project into the water. This provides the necessary repulsive barrier between two neighboring particles. In the case of the aqueous suspensions of NP, agglomeration of particles is prevented by adding some non-ionic surfactants, whereas the addition of the ionic surfactant SDS or the polymer PVP, which exhibits some properties of zwitterionics, makes NP particles to

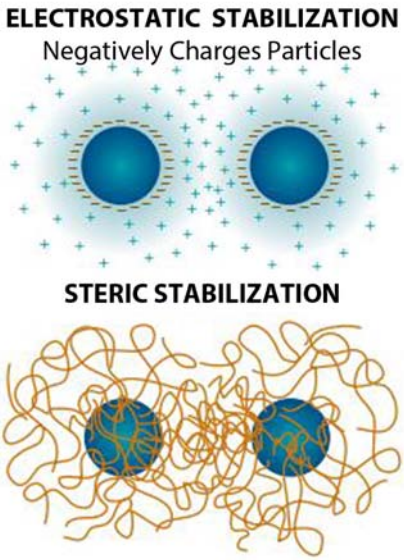

Figure 3.16: Steric and electric stabilization. Adapted from [21].

flocculate and cream up.

Particle size and size distribution has been the key parameters used for evaluating the physical stability of micro and submicrosuspensions of NP [21]. Microsuspensions of NP were characterized by Laser Scattering following the experimental protocol explained in Section **??** of the Experimental Part and the results obtained are disclosed in Table 3.3. The Light Scattering protocol was exactly the same as the one used to characterized particle size distribution of the the solids obtained by DELOS and the ones collected by filtration of the suspensions obtained by DELOS-susp in the absence of surfactants.

For comparison purposes, the values of particle size distribution of the suspension obtained without surfactant after 10 minutes in a sonication bath is included. Particle size measurements reveal that all the surfactants screened affect crystal growth of NP as the particles of the microsuspensions in the presence of surfactants are much smaller than the one without surfactant. Particle size of NP particle is reduced more than a half in the presence of any surfactant in comparison to the particles obtained in the absence of surfactant. Therefore, the use of surfactants is beneficial as all of them are able to reduce NP crystal growth. The surfactants that perform better in terms of particle size reduction are Tween 80 and Poloxamer F-127. Gelurice® 44/14, PVP, SDS and HMPC have approximately the same effect in crystal growth inhibition.

Although PVP and SDS are not able to stabilize the final microsuspensions at the same degree as the rest of surfactants, they exert an efficient impact in crystal growth, as can be checked by the small size of the particles obtained when these additives are used. Conversely, although the macroscopic appearance of the microsuspensions produced using HMPC and Gelurice® 44/14 are similar to the ones of Poloxamer F-127 and Tween80, particle size of these suspensions are very different. NP particles produced in the presence of HPMC and Gelurice® 44/14 are similar in size to the ones in the presence of SDS and PVP. HPMC and Gelurice® 44/14 are able to stabilize the final NP microsuspensions although their impact on particle size reduction is not relevant. The microsuspensions with the smaller particle size and narrower distribution were obtained using Poloxamer F-127 and surfactant Tween 80.

In order to elucidate which surfactant were the most appropriate for the production of stable micro and submicron aqueous suspensions of NP, Laser Scattering measurements of the as prepared microsuspensions in the presence of Tween80 and Poloxamer F-127 without sonicating the suspensions were performed and the results are disclosed in Table 3.4.

Table 3.4: Comparison of particle size distribution results of the microsuspensions obtained by DELOS-susp using Tween80 and Poloxamer F-127 before and after 10 min in a sonication bath.

Experiment-Surfactant	Size distribution (μm) [a]			UI[b]	Size distribution (μm)			UI
	0 min				10 min			
	d(0.1)	d(0.5)	d(0.9)		d(0.1)	d(0.5)	d(0.9)	
4-Poloxamer F-127	0.8	2.7	9.3	8.6	0.6	1.6	5.5	10.9
8-Tween80	4.8	21.3	81.0	5.92	0.9	2.4	8.0	11.25

[a] Volumetric particle size distributions expressed in percentiles of 10, 50 and 90% of NP suspensions without US and after 10 min of US and [b] Uniformity index is defined as d(10)/d(90)*100

The results displayed in Table 3.4 compare particle size distribution and how uniform is that distribution for the suspensions obtained in the presence of Poloxamer F-127 and Tween80 before and after being sonicated. As can be ascertained, the sonicated suspensions are ver similar between them as reflected by the Uniformity Index. However, the as prepared suspension in the presence of Tween 80 presents a larger particle size and a

wider distribution. The as prepared suspension obtained when using Poloxamer F-127 has a smaller and more homogenous particle size distribution. These last measurements confirm that the most appropriate surfactant for obtaining stable microsuspensions of NP is Poloxamer F-127.

The morphological characterization of the particles of the microsuspensions were performed by Scanning Electron Microscopy following the experimental protocol described in Section **??** of the Experimental Part and the micrographs are displayed in Figure 3.17. In all the pictures micro- and submicronparticles of needle-like shape are distinguished. The difference in between the solids relies on the proportion between submicron particles against the larger particles (15-25μm). Despite the nature of the surfactant employed, all NP particles precipitated as needle-like crystals. If the morphology of the particles remains the same and only a growth inhibition is observed, this means that the surfactant adsorption is similar on all the faces of the crystal [57].

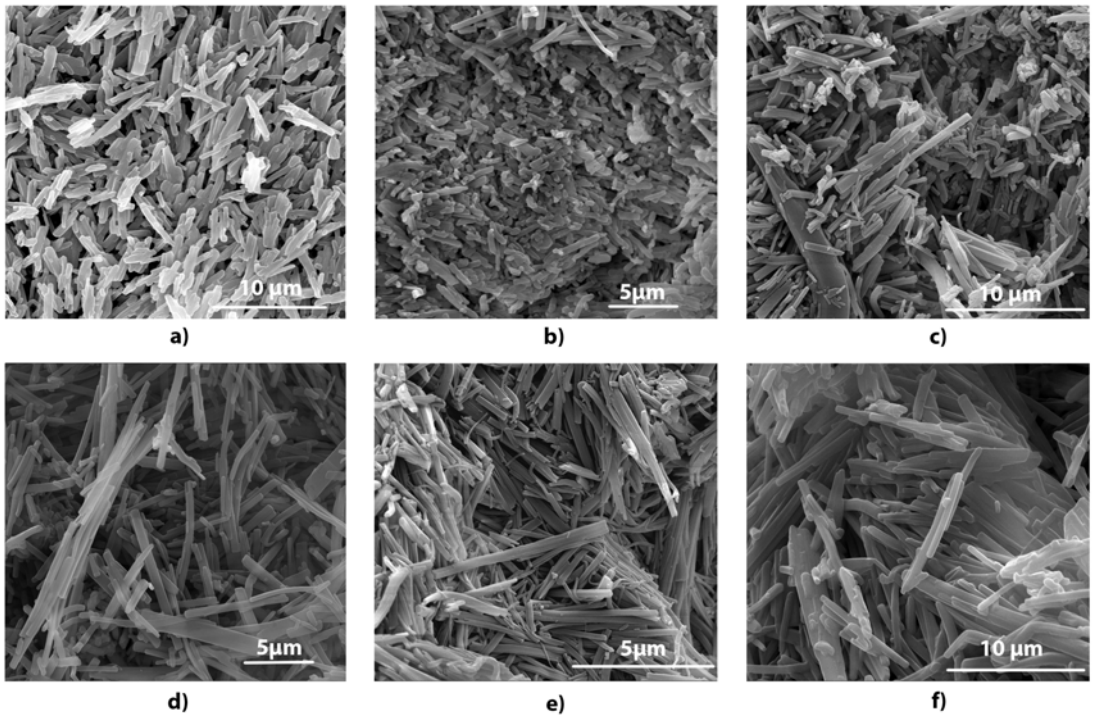

Figure 3.17: SEM images showing the influence of the surfactant employed: a) Gelurice® 44/14, b) Poloxamer F-127, c) HMPC, d) Tween80, e) SDS and f) PVP.

The mechanism of growth inhibition by polymers appears to be poorly understood. Although there are several reports in the literature on the inhibition of crystallization by

polymers, the mechanism is rarely discussed [57]. It is claimed that the role of stabilizer at the molecular level is an often overlooked aspect to the creation of pharmaceutical suspensions [58] and there is a lack of understanding their mechanism of action [59, 60, 61, 30]. This fact hinders the selection of a suitable stabilizer and makes this step pretty challenging. The challenge stems mainly from two aspects: (i) lack of fundamental understanding of interactions within suspensions and (ii) lack of an efficient and high throughput stabilizer screening technique. Selecting the anchor groups that interact strongly with the drug surface can be challenging due to the limited understanding of interactions between particles and stabilizers at molecular level. The current practice for stabilizer screening involves trial production of suspensions with different stabilizers, which could be burdensome and require vast amount of efforts especially with a large number of potential stabilizer candidates [21].

Influence of mixing surfactants.

Mixing a polymeric and an ionic surfactant could complement each other and enables combining electrostatic and steric mechanisms [3]. To test if it was possible to obtain a synergetic enhancement in the physico-chemical properties of NP microsuspensions, a experiment was designed mixing different types of surfactants (Table 3.5): the ionic surfactant SDS was mixed with the polymeric surfactant Poloxamer F-127, as this one was the one which performed better in terms of particle size reduction.

Table 3.5: DELOS-susp experiment for evaluating the effect of mixing surfactants

Experiment	Mix of surfactants	Surfactant/NP ratio (g:g)[a]
9	SDS+Poloxamer F-127	0.8/0.8:1

DELOS-susp experiments performed at T_W = 313 K, P_W = 10MPa, x_W = 0.65 and F = 500mL/min, [a] amount of surfactant expressed as grams of surfactant per gram of NP.

A stable milky microsuspension of NP was obtained, hence the addition of Poloxamer F-127 to SDS cancels the flocculation effect that SDS alone provokes in NP microemulsions. Particle size measurements of the microsuspensions as prepared and sonicated 10 min in an ultrasound bath are disclosed in Table 3.6.

The effect of mixing SDS+Poloxamer F-127 enhances the properties of NP microsuspensions in terms of particle size and particle size distribution with respect to the use

Table 3.6: Particle size distribution of the microsuspensions obtained in the DELOS-susp experiments for evaluating the effect of mixing surfactants before and after 10 min in a sonication bath.

Experiment	Surfactant	0 min (μm)[a]			10 min (μm)[b]		
		d(0.1)	d(0.5)	d(0.9)	d(0.1)	d(0.5)	d(0.9)
9	SDS+Poloxamer F-127	1.2	4.0	13.9	1.0	2.5	8.4
4	Poloxamer F-127	0.8	2.7	9.3	0.6	1.6	5.5

[a] Volumetric particle size distributions expressed in percentiles of 10, 50 and 90% of NP suspensions before and after 10 min in a sonication bath.

of SDS alone but Poloxamer F-127 still yields the best results in terms of particle size reduction. In many cases a combination of stabilizers is more beneficial [62], but there are other studies that demonstrated that a combination of ionic and non-ionic stabilizers is not always advantageous to enhance the properties of suspensions [63].

Once the screening of surfactants has been conducted and based on the promising results obtained preparing microsuspensions of NP using Poloxamer F-127, the following section of the chapter is devoted to the optimize the conditions of the experiments using this surfactant and to a more compendious characterization of the microsuspensions.

3.3.2 Influence of process variables on NP microsuspensions.

In this section, the influence of different process variables on the final characteristics of NP microsuspensions prepared by DELOS-susp using Poloxamer F-127 is studied. Particle size, morphology and stability were selected as the most important physicochemical parameters of NP microsuspensions.

Influence of the amount of water

All the previous experiments were conducted pumping the same amount of water cocurrently with the expansion of the compressed solution. A small tests was performed to elucidate what happened if the amount of water was increase almost double (Table 3.7).

The comparison of particle size distribution of the microsuspensions obtained from experiments using V_{aq} = 500mL (experiment 4) and V_{aq} = 900mL (experiment 10) as pre-

Table 3.7: DELOS-susp experiments for evaluating the effect of the amount of water.

Experiment	Amount of water (mL)
4	500
10	900

DELOS-susp experiments performed at T_W = 313 K, P_W =10 MPa, x_W = 0.65 and F = 500 mL/min for testing the influence of the water flow.

pared are depicted in Figure 3.18.

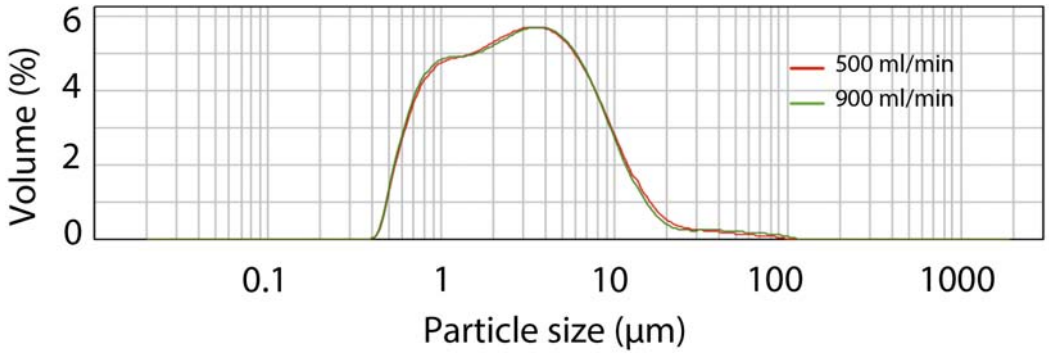

Figure 3.18: Influence of the water flow in the particle size distribution of the suspensions as prepared.

It can be ascertained from particle size distribution results (Figure 3.18) that the influence of increasing the amount of water does not have any impact on particle size distribution. What it is relevant for a successful precipitation by DELOS-susp is that water is co-currently being pump when the depressurization starts, so the solution of the compound is always quenched by the current of water.

The fact that the amount of water do not have any influence on particle size is a highly beneficial aspect as allows to change the concentration of the drug in the final microsuspensions keeping constant the particle size of the compound. Another important advantage of DELOS-susp in relation to other supercritical fluid based technologies such as RESOLV or RESAS, is that suspensions can be more loaded as the amount of the drug to precipitate does not depend on the solubility of such compound in CO_2, but in the solubility of the CO_2-expanded mixture, which is usually much higher.

Hence, the following experiments were conducted using V_{aq} = 500 mL of water and a constant flow of F = 500 mL/min, as in this way the microsuspensions will be more concentrated.

Influence of Poloxamer F-127 concentration and point of addition

Once the appropriate amount of water was defined, a set of experiments (Table 3.8) was designed to evaluate the effect of surfactant concentration utilized as well as the location of the surfactant. Poloxamer F-127 can be dissolved in the solution of NP in acetonitrile or can be placed in the current of water (see Figure 3.19). Experiments 1 and 4 are also presented for comparison purposes.

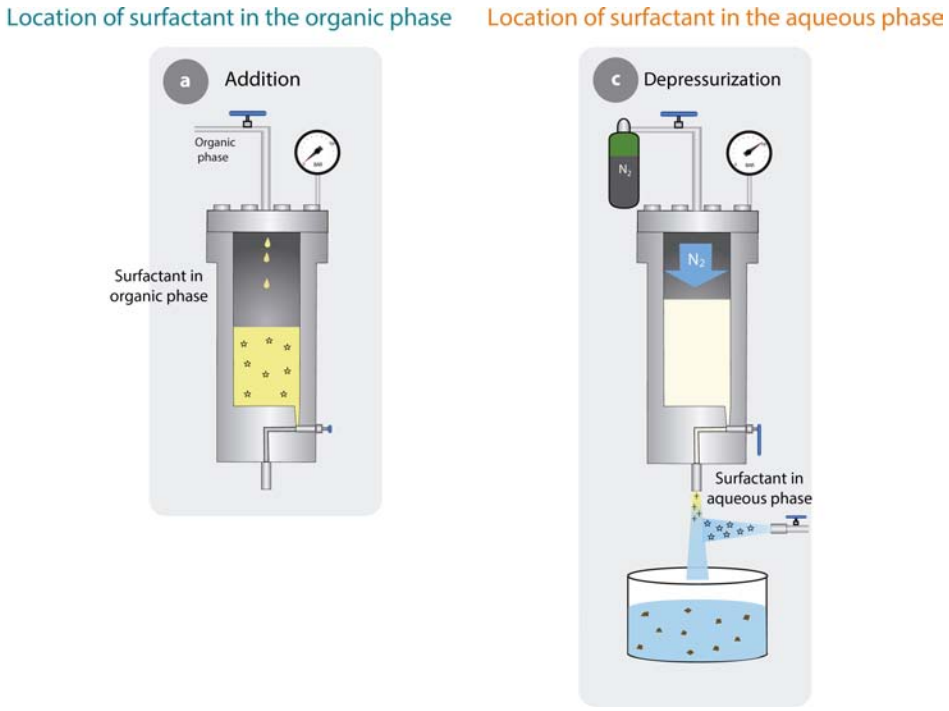

Figure 3.19: Possible location of Poloxamer F-127 :organic phase or aqueous phase.

The focus of suspension characterization was on particle size, morphology and stability. Tendency of NP particles to agglomerate has been evaluated by measuring particle size distribution before and after being sonicated and establishing a relation between uniformity index as prepared ($U.I_0$) and uniformity index after being sonicated 10 min

Table 3.8: DELOS-susp experiments for evaluating the effect of the amount and the location of Poloxamer F-127

Experiment	Amount of surfactant (g Polox:g NP)	Location of Poloxamer F-127	
		Organic phase	Aqueous phase
1	0:1	-	-
4	0.8:1	-	x
11	0.08:1	-	x
12	0.15:1	x	x
13	0.8:1	x	-
14	1.6:1	x	x
15	1.6:1	-	x

DELOS-susp experiments performed at T_W = 313 K, P_W = 10 MPa, x_W = 0.65 and F = 500 mL/min for testing the influence of the amount and location of Poloxamer F-127.

($U.I_{10}$). This new parameter has been defined as Agreggation Tendency (AT):

$$AT = \frac{U.I_0}{U.I_{10}} . \tag{3.6}$$

If particles tend to agglomerate, ($U.I_0$) and ($U.I_{10}$) will differ among them as the sonication bath will break the agglomerates. On the contrary, if particles do not agglomerate, the effect of the sonication bath will not be relevant and these two values will be similar.

In all the experiments presented in Table 3.8 milky homogenous and macroscopically stable aqueous suspensions of NP were produced.

Particle size of the suspensions were measured as prepared and after 10min in a sonication bath for comparison purposes with previous measurements and in order to calculate AT. The results obtained are disclosed in Table 3.9.

From the values presented in Table 3.9 some conclusions can be withdrawn: comparing experiment 1 and 11, it is inferred how a small addition of Poloxamer F-127 exerts a great impact on the macroscopic appearance of the suspensions and on particle size. Attending to the particle size distribution values of the suspensions without sonication, an increase in surfactant concentration is translated into a decrease of particle size. Nevertheless, there is a limit concentration and above that limit, 0.8:1 g Polx/NP, there is no more reduction in particle size. This result is highly relevant as the best relationship between the Poloxamer F-127 and NP has been found, and with this amount of surfactant

Table 3.9: Particle size measurements of NP suspensions prepared by DELOS-susp to evaluate the concentration and location of Poloxamer F-127.

Experiment	0 min (μm)[a]			$U.I_0$[b]	10 min (μm)[c]			$U.I_{10}$[d]	AT[e]
	d(0.1)	d(0.5)	d(0.9)		d(0.1)	d(0.5)	d(0.9)		
	-	-	-		9.2	23.6	51.1	18.00	
4	0.82	2.8	9.4	8.72	0.6	1.6	5.5	10.91	0.79
11	1.1	4.3	20.8	5.29	0.7	2.3	8.3	8.43	0.62
12	1.1	4.4	25.5	4.31	0.9	2.4	8.3	10.84	0.39
13	1.2	3.6	11.5	10.43	1.1	2.7	7.6	14.47	0.72
14	1.2	3.8	13.8	8.70	1.1	2.6	8.6	12.79	0.67
15	1.3	3.8	13.1	9.92	1.1	2.8	10.0	11.00	0.90

[a]Volumetric particle size distributions expressed in percentiles of 10, 50 and 90% of NP suspensions without ultrasound and [c]after 10 min of US,[b] [d]Uniformity index is defined as d(10)/d(90)*100 and [e] Aggregation Tendency is calculated as $U.I_0/U.I_{10}$.

is possible to obtain stable NP suspensions where particles are not aggregated. The existence of a maximum value of surfactant concentration from which particle size no longer changed with increasing surfactant concentration has already been observed [64].

Particle size distributions of the suspensions sonicated 10 min present values more similar between them. This means that when the agglomerates are broken, values of particle size of NP particles are closer to each other hence, growth inhibition is achieved with the smallest concentration of Poloxamer F-127, 0.08:1 g Polx/NP and the rest of the amount of Poloxamer F-127 avoids agglomeration of NP particles.

Uniformity Index reflects that the more homogeneous particle size distribution is obtained in experiment 13 as is in this experiments where $U.I$ presents the highest value. Uniformity index also reveals that after sonication, particle size distributions are more similar among them as $U.I$ values are closer to each other. As mentioned before, the higher the tendency of NP particles to agglomerate, the bigger the different between particle size distribution before and after the sonication bath, therefore, AT value will be smaller. If the tendency of NP particles to agglomerate is not very relevant, the effect of applying ultrasounds will not exert a strong impact on particle size distribution, therefore UI before and after ultrasounds should be similar among them, hence, AT will have

a value closer to 1. When the concentration of Poloxamer is 0.8:1 g Polx/NP the tendency of the particles to aggregate is smaller as when using ten time less concentration and this is reflected by a higher *AT* value.

Particle size distribution of the suspension in the presence of 0.08:1 g Polx/g NP after 10 min in a sonication bath is the same as the one of the suspension obtained using 0.8:1 g Polx/g NP as prepared. This means that the dispersion effect achieved after 10 min of a sonication bath is the same as the one obtained by adding tenfold amount of surfactant.

Table 3.9 highlights that the location of the surfactant does not affect the final properties of the microsuspensions as there is no important difference in particle size distribution. Based on this, in the upcoming experiments, the surfactant was always dissolved in the aqueous phase.

The concentration of the surfactant has proven to be one of the key parameters in stabilization and particle formation. The optimum concentration has been found, which is 0.8:1 g Polx/g NP, a higher concentration will not be translated into a smaller particle size. The growth inhibition is achieved using a lower concentration, 0.08:1 g Polx/g NP. However, with this amount of Poloxamer F-127, aggregation of NP particles is not avoided and the application of ultrasounds is required to achieve the same particle size as when using ten fold concentration of Poloxamer F-127.

3.3.3 Elimination of acetonitrile from NP microsuspensions: Filtration

As produced, suspensions contain acetonitrile (max. 20% vol.) that comes from the depressurization of the CO_2-expanded organic solution of NP into the aqueous phase during the DELOS-susp process. This excess of organic solvent needs to be reduced under 400 ppm, which is the maximum concentration of acetonitrile allowed by the European Pharmacopeia for acetonitrile as it belongs to Class II of organic solvents.

An easy way to remove the excess of acetonitrile is by vacuum filtration of NP microsuspensions. The filtration was carried out following the experimental protocol described in Section 6.8.1 of the Experimental Part. In order to measure particle size distribution by Light Scattering it is required to form a stable suspension. The solids filtrated are resuspended in pure water, however in order to form a stable suspension, the sample was sonicated in a bath during 10min, as Figure 3.20 depicts.

Table 3.10 displays particle size measurements of the solids obtained after filtration and drying of NP microsuspensions re-suspended in water and sonicated 10 min. Fil-

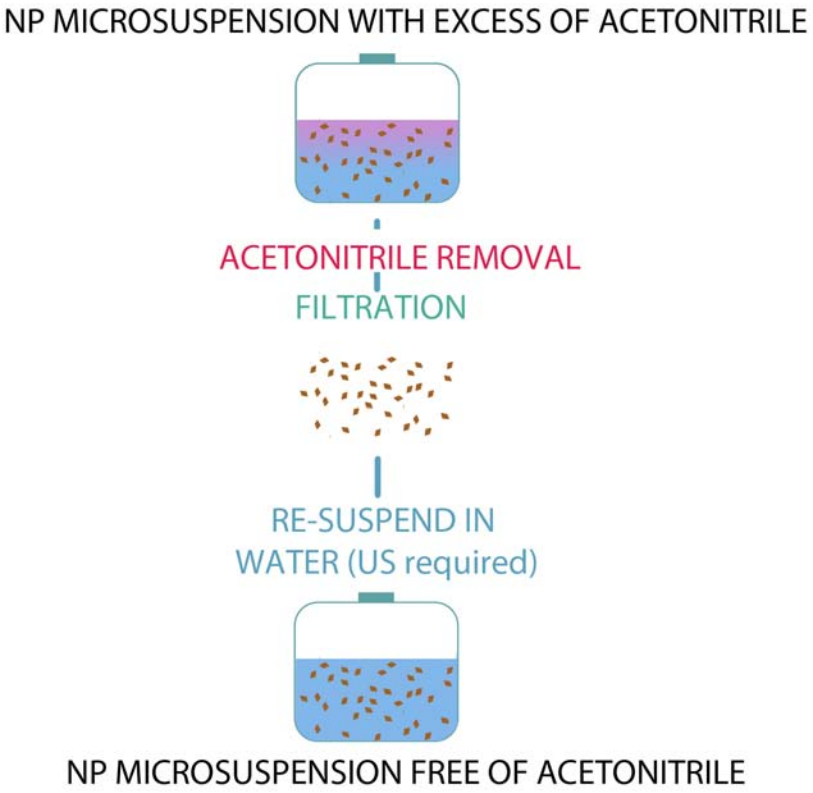

Figure 3.20: Removal of the excess of acetonitrile from NP microsuspensions by filtration. The application of 10 min of US are required to re-dispersed NP micro particles in pure water.

tration of the suspensions entails aggregation of particles and therefore in order to measure stable milky suspensions, it was required to apply ultrasounds. It can be ascertained comparing the size of the solids obtained from experiments 4 and 11 that the reduction in size observed in the microsuspensions when adding tenfold more surfactant is lost when samples are filtrated due to this agglomeration phenomena. Therefore, if the suspension is going to be filtrated and the preferable form of the drug is as dried powder, with a small quantity of surfactant (0.08:1 g Polx/g NP) is enough to stop crystal growth of NP crystals as the excess of Poloxamer is just essential for stabilizing the microsuspension and prevent particle agglomeration.

Depending on the final application, DELOS-sups method is a suitable platform for the preparation of stable aqueous suspensions of NP or dry powders of NP microparticles, that can be easily re-suspended in water after 10 min in a sonication bath. Generally,

Table 3.10: Particle size measurements of NP particles obtained after filtration and drying of the suspensions, resuspended in water and ultrasonicated for 10 min.

Experiment	Amount of surfactant (g Polox:g NP)	Particle size distribution (μm)[a]		
		d(0.1)	d(0.5)	d(0.9)
1	-	1.1	3.8	18.9
4	0.8:1	0.4	1.4	5.7
11	0.08:1	0.8	2.1	8.7
12	0.15:1	1.1	3.3	19.6
13	0.8:1	1.1	2.8	10.7
14	1.6:1	1.2	3.3	13.5
15	1.6:1	1.1	2.4	7.1

[a]Volumetric particle size distributions expressed in percentiles of 10, 50 and 90% of NP suspensions after 10 min of US

it is better to transport and storage drugs as powders than as suspensions. If, on the other hand, the final form preferable is in the form of aqueous suspensions of dispersed microparticles, a method to eliminate the organic solvent that do not alter the properties of the particles will be presented in future sections.

The fact that dispersions of microparticles can be post processed as a dry powder for solid dosage is a very interesting property for injectable products. These dried powders are designed to re-disperse into microparticles when placed in water or an alternate water-based environment. The ability of the dried powder to re-disperse into a non-aggregated microparticulate dispersions is critical to the development of a solid dosage form that maintains the benefits of this enabling delivery technology [5].

Based on this observation, there are two experimental conditions of interest: for applications where dried solids are preferred, experiment with the small amount of Poloxamer (experiment 11), and when suspensions are the chosen option, the experiment with tenfold more concentration of surfactant (experiment 4). Hence, the following characterization has been carried out for the suspensions obtained in those experiments.

3.3.4 Comprehensive characterization of NP microsuspensions

The following section endeavors to a more detailed characterization of NP microsuspensions regarding stability and reproducibility. In addition, two different methods for the elimination of acetonitrile has been developed for suspensions with the minimum amount of surfactant, 0.08 g Polx/NP (experiment 11) and for the tenfold Poloxamer F-127 concentration, 0.8 g Polx/NP (experiment 4).

Reproducibility of DELOS-susp method for the preparation of stable NP suspensions

One of the first thing to evaluate was the reproducibility of DELOS-susp for preparing stable suspensions of NP with the aid of Poloxamer F-127. Figure 3.21 depicts the superposition of particle size distribution of the suspensions and the solids obtained by filtration after performing twice experiments 4 and 11. The results reveal the robustness of the DELOS-susp method as solids and suspensions with the same particle size distribution are achieved.

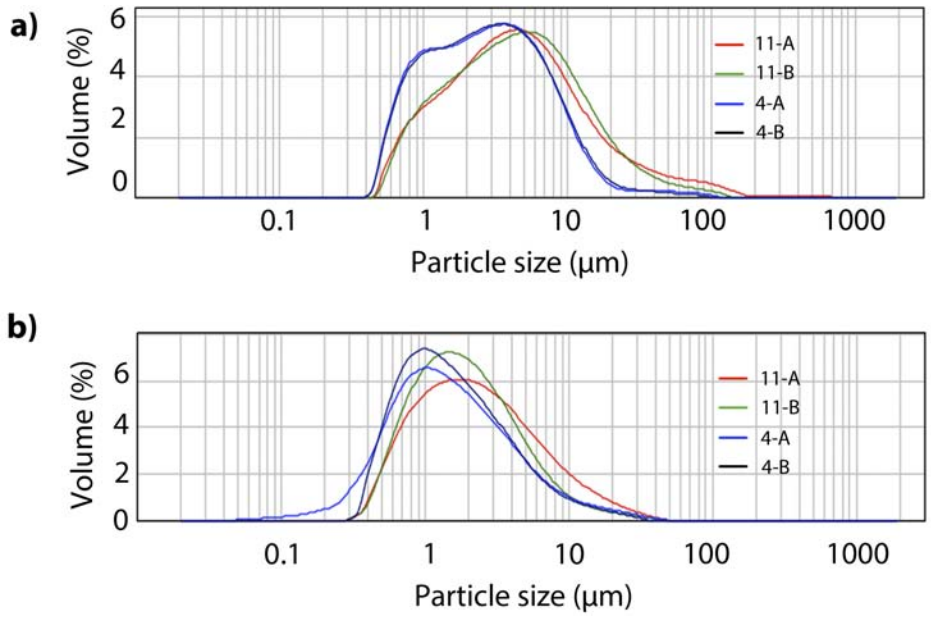

Figure 3.21: Reproducibility of DELOS-susp for the preparation of stable NP suspensions (a) and dried solid powders (b).

Role of the surfactant

In addition, as a mean to gain more knowledge of the effect of the addition of Poloxamer F-127 in the final properties of microsuspensions, a small test were further conducted. The solid obtained after filtration and drying of the suspension obtained by DELOS-susp without surfactant (experiment 1) were re-suspended in a solution of water with the same concentration of Poloxamer F-127 as the ones used in the DELOS-susp experiments in the presence of surfactants (Table 3.6). These new suspensions of NP were characterized by Laser Scattering and the values are displayed in Table 3.11.

Table 3.11: Particle size measurement of the solid obtained after filtration and drying of the suspension 1 and re-suspended in a solution of Poloxamer F-127 and water after 10 min of US.

Amount of surfactant (g Polx: g NP)	10 min (μm)[a]		
	d(0.1)	d(0.5)	d(0.9)
0.08:1	1.6	7.8	31.3
0.8:1	1.3	4.8	18.7
1.6:1	1.4	5.0	17.4

[a]Volumetric particle size distributions expressed in percentiles of 10, 50 and 90% of NP suspensions after 10 min of US

Particle size of the solid re-suspended in a solution of the polymer in water are much higher than when the polymer is added during depressurization. These results highlight that the Poloxamer F-127 confers immediate protection and is more effective when present at the time of creation of the new, fresh surface than if added afterwards [3].

Stability of suspensions

Stability is one of the critical aspects in ensuring safety and efficacy of drug products. Therefore, stability issues associated with drug suspensions deserve significant attention during pharmaceutical product development [21]. For pharmaceutical use, a suspension must have a minimal tendency to agglomerate, which could lead to the formation of a hard cake. The traditional method to evaluate sedimentation or creaming is by visual observation over a period of time [21]. Hence, suspensions were optical monitored during

2 days after their preparation. During this time, it was observed how NP particles settle down. However, particles are completely re-disperse into the suspension just by shaking manually. A suspension with slow sedimentation rate is acceptable, perhaps even preferable, provided the product is re-suspendable and homogeneous [3]. Apart from this optical monitoring, the dispersion rate of the particles from suspensions 4 and 11 was assessed using an equipment called Turbiscan and following the experimental protocol explained in Section 6.6.2 of the Experimental Part. Turbiscan is used to characterize the dispersion state of emulsions, suspensions, foams, etc. Changes in terms of size and concentration (such as creaming, sedimentation, flocculation or coalescence) are directly monitored. This technique consists in sending photons (light) into the sample. These photons, after being scattered many times by objects in suspension (droplets, solid particles, gas bubbles, ...) emerge from the sample and are detected by the measurement device of the Turbiscan. A mobile reading head, composed of a NIR diode and two detectors (transmission for transparent phases and backscattering for cloudy phases), scans a glass cell containing the sample. The measurement enables the quantification of several parameters linked to particles average diameter and volume fraction. The rate of sedimentation of a suspended phase depends on several factors which need to be controlled. Assuming that all dispersed particles are uniform in shape and size and that the particles are sufficiently far apart so that the movement of one does not affect the neighboring particles, the rate of sedimentation can be estimated by Stokes' equation [65]:

$$V = \frac{d^2 * (\rho_1 - \rho_2) * g}{18 * \eta_0}, \tag{3.7}$$

where V is the sedimentation rate, d the diameter of the suspended particles, ρ_1 the particles' density, ρ_1 is the density of the medium, g is the acceleration of gravity, and η_0 is the viscosity of the external phase. Although the Stokes' equation does not consider all the variables which affect the stability of a suspension, it gives an approximation of the settling rate and an appreciation of the variables governing the sedimentation process. For example, by reducing the particle size or by increasing the viscosity and density of the external phase, the rate of sedimentation can be retarded.

The Turbiscan software enables to calculate the sedimentation rate and it also gives a parameter called Turbiscan Stability Index (TSI) that permits to compare different samples. The smaller the TSI, the more stable the suspension is. Table 3.12 provides the TSI and the sedimentation rate for suspensions 4 and 11. TSI parameter allows a quantitative comparison of the stability of both samples and, as expected, the sample with the

smallest particles, suspension 4, is more stable against sedimentation than the one with higher particle, suspension 11. Nevertheless, both values are quite closed. Regarding the sedimentation rate, as expected, suspension 4, with smaller particles, presents a lower sedimentation rate.

Table 3.12: Turbiscan Stability Index and Sedimentation rate of suspensions 4 and 11 after 8 hours

Experiment	TSI	V (μm/min)
4	4.71	7.07
11	5.42	11.45

TSI = Turbsican Stability Index.

V = Sedimentation rate (μm/min)

Apart from these values, Turbiscan provides a profile of the suspension destabilization kinetics, where the evolution of the backscattering and transmitted flux over time and in relation to the height of the container where the sample is placed is recorded. Figure 3.22 depicts the profile of the backscattering intensity (y-axis) as a per centage relative to an external standard versus the height of the sample (x- axis in mm) along the time of measurement (8 hours).

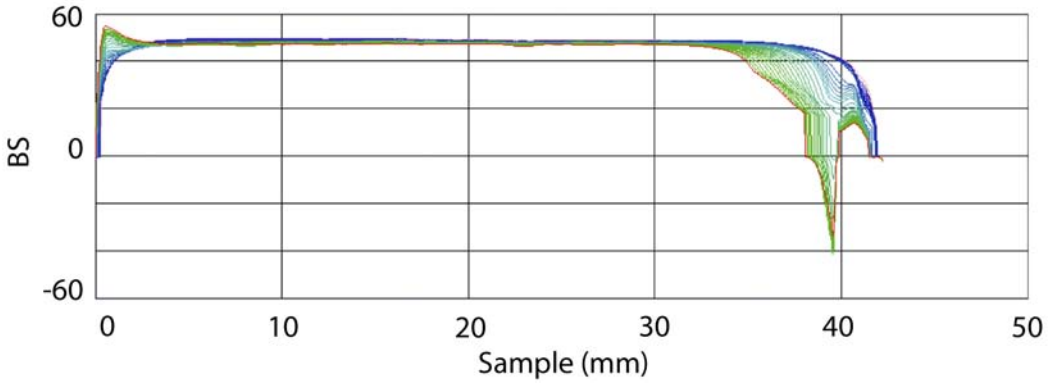

Figure 3.22: Evolution of the backscattering intensity flux for the height of the sample 4 during 8 hours.

Figure 3.22 tells us that particles in the sample are settling down during the measurement as it can be checked by the progressive fall in concentration (clarification) at the

sample top (around 40 mm). A fall in backscattering intensity means a decrease in concentration. Conversely, at the bottom of the sample, an increase in concentration is observed as the backscattering intensity increases with time. Figure 3.22 also reveals that particle size does not change during the measurement time as the backscattering intensity at the center area of the sample does not change. If particles tend to agglomerate during the measurement, a decrease in the backscattering will be recorded [66].

Apart from the stability against sedimentation and the confirmation that particles do not change during Turbiscan measurements (8 hours), the stability of the suspensions with time has been assessed. Particle size of the suspensions 4 and 11 was measured after one week, two weeks, one month and two months and the values of the distributions as prepared and after 2 months are compared in Table 3.13. From theses results, it can be inferred the high physical long-term stability with respect to particle size changes of the suspensions of NP prepared by DELOS-susp.

Table 3.13: Comparison of particle size measurements of the suspensions as prepared and after two months.

Experiment	As prepared (μm)[a]			After 2 months (μm)[b]		
	d(0.1)	d(0.5)	d(0.9)	d(0.1)	d(0.5)	d(0.9)
4	0.8	2.7	9.4	0.7	2.0	7.2
11	1.1	4.3	20.8	1.0	4.1	17.9

[a]Volumetric particle size distributions expressed in percentiles of 10, 50 and 90% of NP suspensions as prepared and [b] after 2 months.

This can be a consequence of the narrow size particle distribution. If particle size is uniform, there is no driving force for the well-known Ostwald ripening effect to occur (Figure 3.23). Ostwald ripening has been described for highly dispersed systems, which means a reduction in size of the finest particle fraction and their final disappearance combined with a simultaneously growth of larger particles. Reasons for the Ostwald ripening are the different saturation solubilities in the vicinity of different sized particles and the concentration gradient existing between them [21]. Moreover, this result also highlights the effect of the addition of the Poloxamer F-127 as the surfactant adhered to particles surfaces reduces the mass-transfer coefficient and hence, the ripening effect is also decreased.

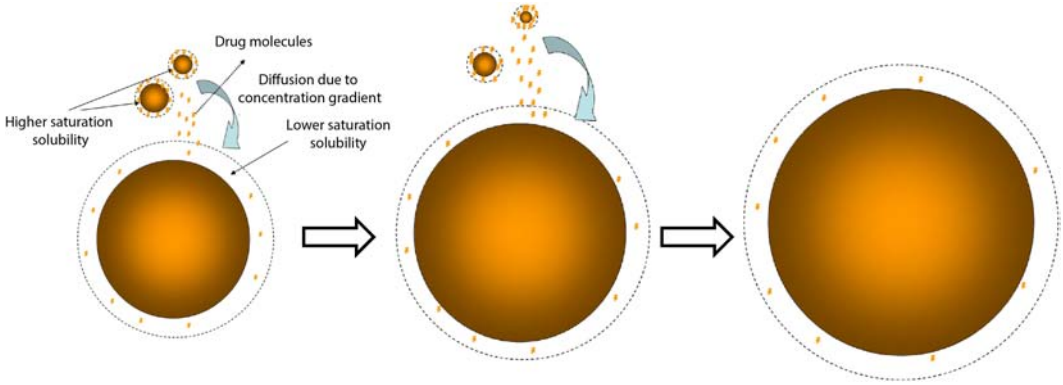

Figure 3.23: Schematic illustration of Ostwald ripening.

In addition, particulate samples of the microsuspensions prepared by DELOS-susp were highly crystalline and kept the same crystalline structure as in the raw material as can be checked in Figure 3.24. A highly crystalline powder compares favorably in terms of the physical stability, with the amorphous materials often obtained by milling.

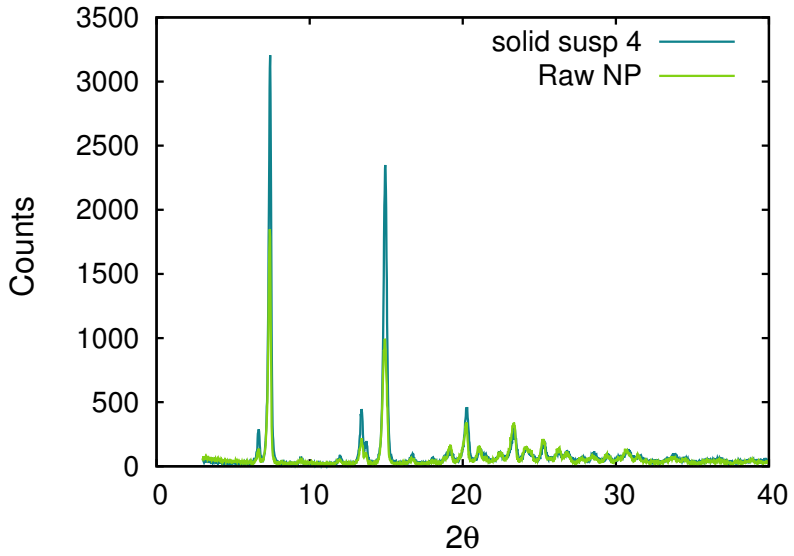

Figure 3.24: Comparison of the X-ray powder Difraction spectra of the raw NP and the processed by DELOS-susp, experiment 4.

3.3.5 *In vivo* experiments

The suspension free of acetonitrile obtained after filtration of NP suspension prepared with a concentration of 0.08 g Polox./ 1 g NP and re-suspended in water was used for an *in vivo* assay. Several suspensions of the thiadiazoline derivative NP in water prepared by different techniques were injected to monkeys, and the results were highly encouraging as the formulation prepared by DELOS-susps was the ones that yielded the highest dissolution velocity.

3.3.6 Acetonitrile elimination and quantification

The good results obtained *in vivo* encouraged us to investigate a different way to eliminate the acetonitrile from the suspensions obtained by DELOS-susp. Since filtering the suspensions promotes particle agglomeration, a different strategy like diafiltration and lyophilisation has been evaluated as depicted in Figure 3.25. Diafiltration should be applied in cases when liquid suspensions of NP are the preferable option. Lyophilisation and filtration, on the other hand, remove all the solvent and therefore, these techniques should be applied when solid particles are required. In the following, diafiltration and lyophilisation techniques are described and the final characteristics of free acetonitrile suspensions and dried solids are presented. The removal of acetonitrile by filtration and the characterization of the obtained dried particles and the free acetonitrile suspensions are already described in Section 6.8.1 of this Chapter.

Table 3.14 compares the efficacy of each technique in terms of removal of acetonitrile from suspensions, measured by Headspace-gas chromatography-flame ionization detection (HS-GC-FID) in collaboration with "Servei D'Anàlisi Química" of UAB. In the case of lyophilisation and filtration, the solids were re-suspended in water and a free acetonitrile suspensions of NP were obtained. These new suspensions were the ones measured.

Lyophilisation is the technique that yields better results regarding the elimination of acetonitrile from aqueous suspensions, nevertheless, the three methodologies applied remove successfully the excess of organic solvents according to the limits permitted by the European Pharmacopeia for acetonitrile as it belongs to Class II of organic solvents (400 ppm).

In addition, in order to assess the goodness of each technique, a more comprehensive characterization of the suspensions and the solids obtained after diafiltration and lyofilization respectively has been carried out.

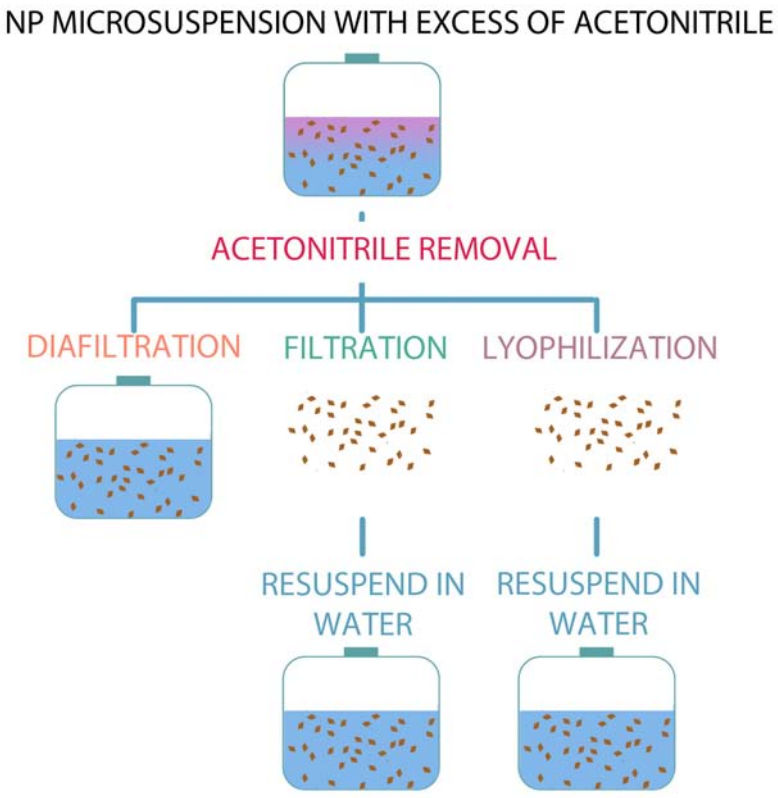

Figure 3.25: Different methods studied for acetonitrile removal.

Table 3.14: Acetonitrile content of NP suspensions obtained as prepared and after diafiltration, lyophilisation and filtration.

Experiment	(gPolx: gNP)	As prepared (ppm)	Filtration (ppm)	Diafiltration (ppm)	Lyophilisation (ppm)
4	0.8:1	»410	<10	25	<1
11	0.08:1	»410	<10	170	<1

Diafiltration

This methodology allows to change the dispersing medium of particles without changing their concentration during the process: acetonitrile/water dispersing medium was substituted by pure water, removing as a result the undesired acetonitrile from the formulation. Samples were pumped through a filtering column (for more details see Section 6.8.2 of the Experimental Part), that allowed acetonitrile and water molecules to pass

through while retaining NP particles. At the same time, pure water was introduced into the system in order not to concentrate the sample and replace the dispersing medium by water. The membrane of the column differentiate components based on size. Components larger than the membrane pore are quantitatively held back by the membrane while smaller components pass through the membrane structure along with the permeate. It is a continuous diafiltration in an airtight system and it is a self-regulating and constant flow process. The hollow fiber membrane and cross-flow filtration system provide faster and gentler separation that helps avoid membrane fouling and maximizes product recovery (see Figure 3.26)

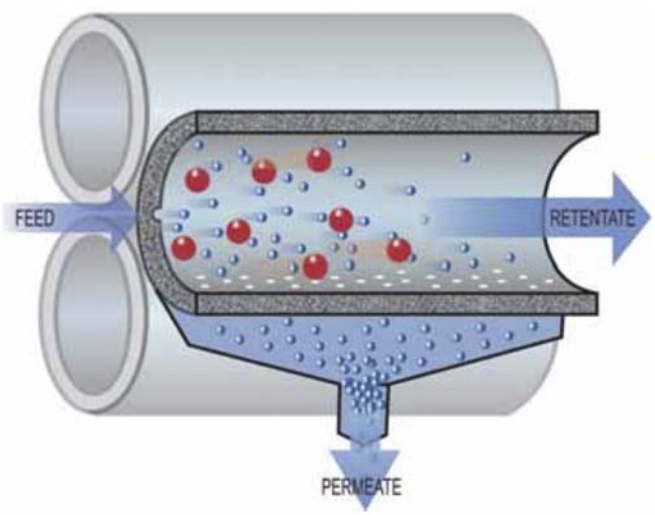

Figure 3.26: Schematic of hollow fiber membrane showing tangential cross flow diafiltration.

An aliquot of 10 mL of each suspensions was diafiltered. In order to successful remove acetonitrile, 6 diafiltration cycles (1 hour) are required. Samples were used without further modification. From sizes shown in Table 3.15, it is extracted that this process does not alter the characteristics of the original suspension and promotes mild conditions for the elimination of the organic solvent. As samples were diafiltered one month after its preparation, the comparison has done with the distribution measured after one month. In this case, the preparation of suspensions with a molar relation of 0.8:1 g Polx./g NP is preferable as it makes a difference since allows the achievement of desired particle sizes without using sonication. Diafiltration does not modify neither the particle size distribution neither the morphology of NP particles as Figure 3.27 depicts.

Table 3.15: Comparison of particle size distribution of NP suspensions after a month and after diafiltration.

Experiment	(g Polx: g NP)	US min[a]	After one month(μm)[b]			After diafiltration(μm)[c]		
			d(0.1)	d(0.5)	d(0.9)	d(0.1)	d(0.5)	d(0.9)
4	0.8:1	0	0.8	2.9	10.8	0.8	2.9	10.7
4	0.8:1	10	0.5	1.2	4.2	0.6	1.6	5.5
11	0.08:1	0	1.1	4.1	16.9	1.1	4.0	15.5
11	0.08:1	10	0.7	1.2	7.1	0.8	2.3	7.6

[a] minutes of ultrasounds, [a]Volumetric particle size distributions expressed in percentiles of 10, 50 and 90 after one month and [b]after diafiltration.

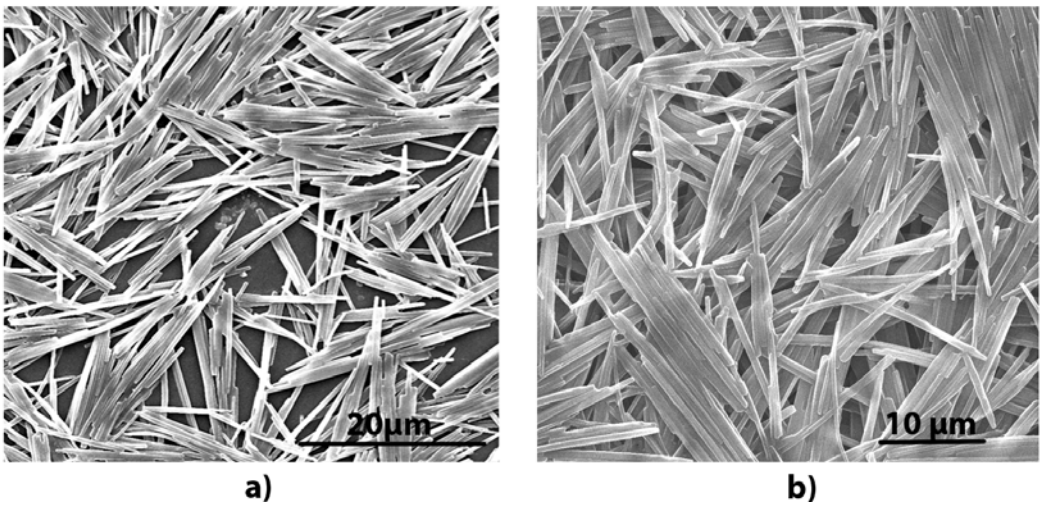

Figure 3.27: SEM micrographs of free acetonitrile suspension 4 after diafiltration (a) and before (b).

The stability of the free-acetonitrile suspensions were checked after one month of storage and particle size remains constant. Therefore, it can be concluded that diafiltration is a very suitable technique to remove the excess of acetonitrile from the suspensions prepared by DELOS-susp.

Lyophilisation

Lyophilisation or freeze-drying is often the preferred method of sample drying because a high level of dryness is achieved with low residual solvent levels. In addition, it allows to convert solutions or suspensions into solids of sufficient stability for distribution and storage. It is a process that consists of removing water from a frozen sample by sublimation and desorption under vacuum. A typical freeze-drying process consists of three stages; that is, freezing, primary drying, and secondary drying. Freezing is an efficient dessication step where most of the solvent, typically water, is separated from the solutes to form ice. Primary drying, or ice sublimation, begins whenever the chamber pressure is reduced and the shelf temperature is raised to supply the heat removed by ice sublimation. During primary drying, the chamber pressure is well below the vapor pressure of ice, and ice is transferred from the product to the condenser by sublimation and crystallization onto the cold coils/plates in the condenser. Secondary drying is the stage where water is desorbed from the freeze concentrate, usually at elevated temperature and low pressure. Some secondary drying occurs even at the very beginning of primary drying as ice is removed from a region, but the bulk of secondary drying occurs after primary drying is over and the product temperature has increased [67].

This process generates various stresses during freezing and drying steps [68, 69, 70]. This technique has been largely discussed in many articles devoted to liposomes formulations [71, 72], but very few recent articles are concerned with particles freeze-drying [73, 74]. Therefore, some authors have reported that, for these systems, some additives must be used in order to obtain successful results [75].

An aliquot of 1 mL was lyophilized following the experimental protocol described in Section 6.8.3 of the Experimental Part. The lyophilized samples (Figure 3.28a) were resuspended in 1 mL of water to keep the same concentration of NP in water as in the original suspension. In the case of sample 4, the solid was easily resuspended just shaking manually. However, the suspension was not stable and it was not possible to obtain a proper measurement of particle size and as a consequence the sample was sonicated. The solid obtained from sample 11 was not able to bere-suspended in water manually and it was sonicated for 10 minutes also (Figure 3.28b).

For an accurate comparison, an aliquot of 1 mL of the original suspensions was also sonicated for 10 min and measured by Light Scattering to avoid any undesired effect of a bigger influence of the sonication bath due to the smaller volume of the sample. (The vol-

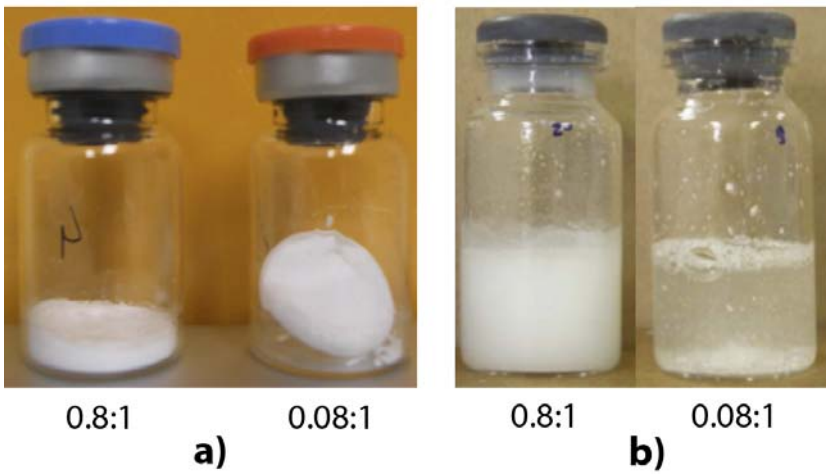

Figure 3.28: Samples lyophilized (a) and resuspended samples in water (b).

ume of the samples sonicated were always 5 mL.) Surprisingly, particle size distribution of both samples were smaller than the ones of the original suspensions. Figure 3.16 shows the SEM characterization of the solid lyophilized and the solid lyophilized re-suspended in water after 10 min of US. It can be inferred from the micrographs that after sonicating the suspension of the lyophilized solids re-suspended in water, particles of NP are broken.

Table 3.16: Light scattering result of the Lyophilized solids re-suspended in 1ml of water after 10 min of US and 1ml of the suspensions after 10 min of US.

Experiment	(gPolx: gNP)	Particle size distribution(μm)[a]		
		d(0.1)	d(0.5)	d(0.9)
4-Lyo	0.8:1	0.3	0.8	2.5
4	0.8:1	0.6	1.5	5.5
11-Lyo	0.08:1	0.4	1.0	3.1
11	0.08:1	0.9	1.6	5.2

4-Lyo and 11-Lyo are the solids after Lyophilization, [a]Volumetric particle size distributions expressed in percentiles of 10, 50 and 90.

It has been reported that freeze-drying of nanoparticles can break particles [75]. Moreover, lyophilization of NP suspensions were performed without the aid of additives. As it has been explained, this techniques is quite aggressive. Therefore, a proper optimization

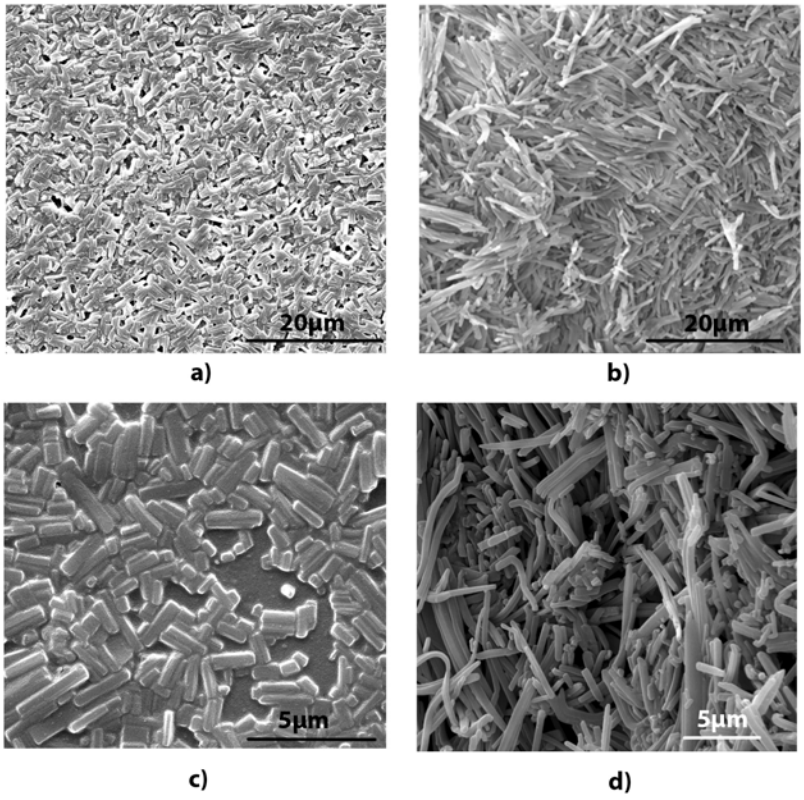

Figure 3.29: SEM micrographs showing the effect of ultrasounds on the lyophilized NP particles: a) and c) are the solids lyophilized after 10 min of US and b) and d) without applying US.

of the parameters of this procedure, as well as the use of cryogenic protectors, is required. The results presented here should be considered a preliminary step and a deeper study will be conducted soon.

3.3.7 Summary

- The feasibility of DELOS-susp for the preparation of stable aqueous suspensions of NP has been assessed. The effect of addition of water at the end of depressurization overcome the undesired growth of NP particles observed during DELOS precipitations.

- The suspensions prepared in the absence of surfactant were not stable and particles creamed. As a consequence, several surfactants were screened and the one which

performed better in terms of particle size reduction and stability was Poloxamer F-127.

- The effect of Poloxamer F-127 on particle size of NP crystal was evaluated: with a concentration of 0.08 g Polox: g NP, particle growth was avoided, however particles tend to agglomerate. Using tenfold concentration, agglomeration is averted.
- The robustness of DELOS-susp has been established for preparing stable aqueous suspensions of NP as well as for producing finely dispersed dried powders of this compound by filtration of the suspensions.
- Diafiltration of suspensions has been presented as a suitable method for removing the excess of acetonitrile when the final preferable form is aqueous suspensions.
- A preliminary study for the lyophilization of suspensions has been proposed. However, it was found that lyophilization performed at those conditions and without the aid of additives breaks NP particles.

3.4 Crystal growth morphology prediction for the thiadiazoline derivative NP crystal.

The conventional crystallization of NP from acetonitrile evaporation was monitored by optical microscopy, as explained in the Introduction of this Thesis (Chapter 1). In this way, it was experimentally observed how NP crystals present a one-face preferential growth and crystallize as very long needles. It has been possible to precipitate this drug as micro and submicroparticles with a particle size distribution centered at 1μm and with 90% (in volume) of the particles below 10μm by DELOS-sups in the presence of Poloxamer F-127. However, despite of the methodology applied and the surfactants employed, particles always crystallized in the shape of needle-like. As a mean to understand the crystal growth of this new drug, a morphology prediction of NP crystal was proposed using the molecular modeling software Materials Studio.

Morphology refers to the macroscopic appearance of a crystal. It is characterized by a set of surfaces and their relatives areas. The morphology of a crystal is determined by the slowest growing faces (often referred to as the morphologically important faces) as a consequence of the relative growth rates of the various faces of the crystal [32]. The growth rates of the different faces depend on the internal structure of the crystal, as well as external factors imposed on the crystal by crystallization conditions, such as supersaturation, impurities, temperature and the choice of solvents. The individual face growth kinetics depends to a different extent on supersaturation [57].

The morphology of crystalline solids influences their physical properties [76]. Since many physical properties of crystals are implicitly dependent on their shape, the morphology of crystalline solids can influence dissolution rate of chemicals and biological availability of drugs; filtration, grinding, dusting and handling, packaging and storage of crystalline products and, density and texture optimization, among others [77]. The rationalization of the relationship between crystal morphology and the arrangement of atoms in the bulk crystal lattice is of great interest in many areas of science.

3.4.1 Introduction to Morphology simulations.

The aim of morphology prediction is to simulate the habit of a single crystal of a crystalline material using its internal crystal structure. Morphology prediction is performed using the atomic structure of a crystal and a subsequently analysis of the relevant faces

in conjunction to surface chemistry. Three different methods are available within our resources to predict morphology from the knowledge of the crystal structure:

- **The Bravais-Friedel Donnay-Harker, BFDH Method:**

  The Bravais-Friedel Donnay-Harker, BFDH, laws are based on the crystal lattice and space group symmetry to generate an ordered list of possible growing faces versus their appearance importance and their relative growth rate [78]. The slowest growth rates occur at the faces with the largest interplanar spacing. The BFDH method use the Donnay-Harker rules to isolate the likely growth planes and then the Bravais-Friedel rules to deduce their relative growth rates. The relative growth rate of {hkl} forms on crystals is inversely proportional to the interplanar distance d_{hkl}. Therefore, the larger the d_{hkl}, the more pronounced is the morphological importance of the face, usually reflecting the weakest interactions between the face and the next group layer. This method, however, does not account for the composition of the crystal and position of crystallization units (atoms, ions or molecules) and their bonds. It does not consider atomic composition or molecule itself. For that reason, the strongest the bonding effect in the crystal, the less accurate the method is.

- **The Growth Morphology Method**

  The Growth Morphology [79] method assumes that the growth rate of a face is proportional to its attachment energy. That is, faces with the slowest attachment energy are the slowest growing and, therefore, have the most morphological importance. From the energy calculation and, hence, the growth rate, a center-to-planar distance is assigned to each face. It was proposed by Hartman and Perdok and Hartman and Bennema. This method considers the role of intermolecular forces in crystallization and tries to find relations between crystal structure and crystal morphology on an energy basis. The attachment energy method does not include thermodynamic (temperature and supersaturation) as well as kinetics effects of crystal growth on the final morphology. It attempts to provide a rough estimate of a generic morphology determined by the interactions between the molecules in the crystal.

- **The equilibrium morphology Method**

  Determines the the equilibrium morphology by the minimum of the surface energies for all relevant crystal faces at zero Kelvin.

In this work, the morphology prediction for the NP crystal has been conducted using the The Bravais-Friedel Donnay-Harker, BFDH, method as well as the The Growth Morphology method. During the growth morphology calculation, all possible surface configurations for a given growth face are screened and a number of energetic and geometric properties of theses surfaces are calculated. Out of the list of surface configurations, the most stable one will limit the growth rate of the surface and that surface will dominates the habit facet.

The atomic structure of the NP molecule has been determined from powder X-ray diffraction for the first time in a collaboration with Prof. Norberto Masciocchi from the Università dell' Insubria in Como, Italy.

The crystal morphology is calculated using force field technology. In order for a prediction to be successful, it is important to select an energy expression that is able to describe accurately all molecular fragments and the influence of intermolecular interactions in the crystal and at the surface.

3.4.2 Morphology prediction.

The growth morphology of NP has been predicted from its crystal structure via molecular modeling-based simulation techniques. The crystal structure, as mentioned, was determined from powder X-ray diffraction by Prof. Norberto Masciocchi and the crystallographic data is reported in Table 3.17.

Table 3.17: Crystallographic data of NP determined from PXRD.

Crystal System	orthorhombic
Space group	P_{212121}
Lattice parameters	a = 13.319
	b = 4.697
	c = 26.369
	α = 90 deg
	β = 90 deg
	γ = 90 deg

Before performing any morphology prediction that involves energetic considerations, it is very important to select an appropriate energy expression and verify that it is able

to accurately describe the crystal cell parameters, the molecular fragments and the intermolecular interactions in the crystal.

In this case, five available force-field has been tested: COMPASS, COMPASS II, CVFF, CVFF-nocroos-nomorse and PCFF [80] with forcefield assigned atomic point charges. The cell parameters predicted by Geometry optimization with the different force fields are presented in Table 3.18 as long as the errors in reproducing the experimental values.

Table 3.18: Cell parameters predicted by geometry optimization with different force fields and the errors in reproducing the experimental ones.

Cell parameter	COMPASS	COMPASSII	CVFF	CVFF-nocross-nomorse	PCFF
a	13.832	13.339	14.555	14.504	14.114
b	4.325	4.322	4.052	4.062	4.131
c	25.904	27.396	26.531	26.497	27.626
			$\alpha = \beta = \gamma = 90$ deg		
			Error (%)		
a	3.85	0.16	9.28	8.90	5.97
b	7.91	7.97	13.73	13.52	12.04
c	1.77	3.89	0.61	0.48	4.76

The results displayed in Table 3.18 show that all force fields reproduce the b parameter with the highest error. COMPASS II does the best job in reproducing the experimental structure. Figure 3.30 presents the optimized cell using COMPASS II forcefield.

The growth morphology of NP crystal structure is determined by the BFDH and the The Growth Morphology Method using the COMPASS II forcefield. Figure 3.31 depicts the morphology predictions using both methods respectively.

Both methods predict the same morphology and the simulated habit is needle-like, indicating that the b axis is intrinsically the fast-growing direction. The predicted morphology are in good agreement with the experimental morphology. The strong interactions Π - Π between the aromatic rings makes the crystal to growth following that direction. The predicted major faces and the associated percentage areas of the facets for NP crystal and the energy attachment of each face are given in Table 3.19. It can be checked how the face with the highest Attachment energy (absolute value),{0 1 1}, is the face that grows more and as a consequence, this is the face with the lowest surface area (each face 4% of the

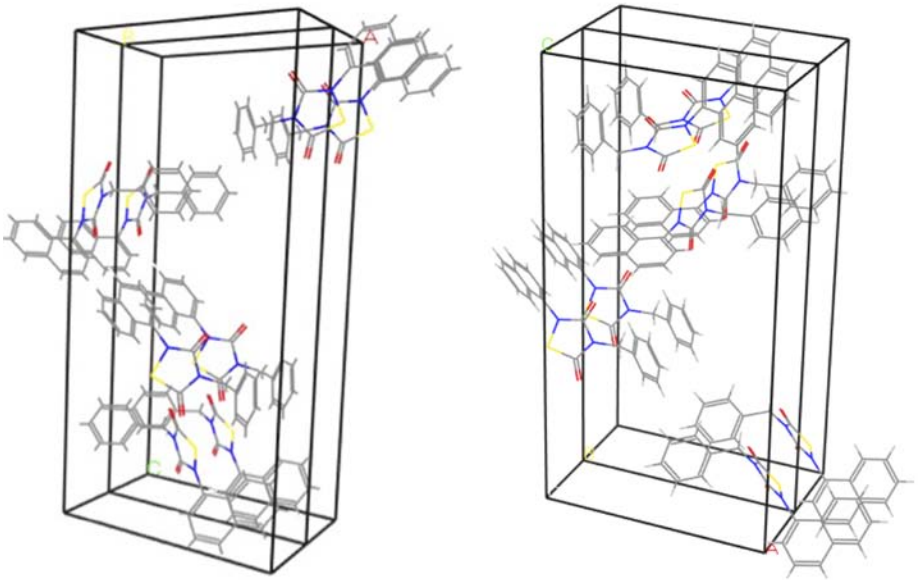

Figure 3.30: Optimize cell of NP crystal predicted by COMPASS II forcefield.

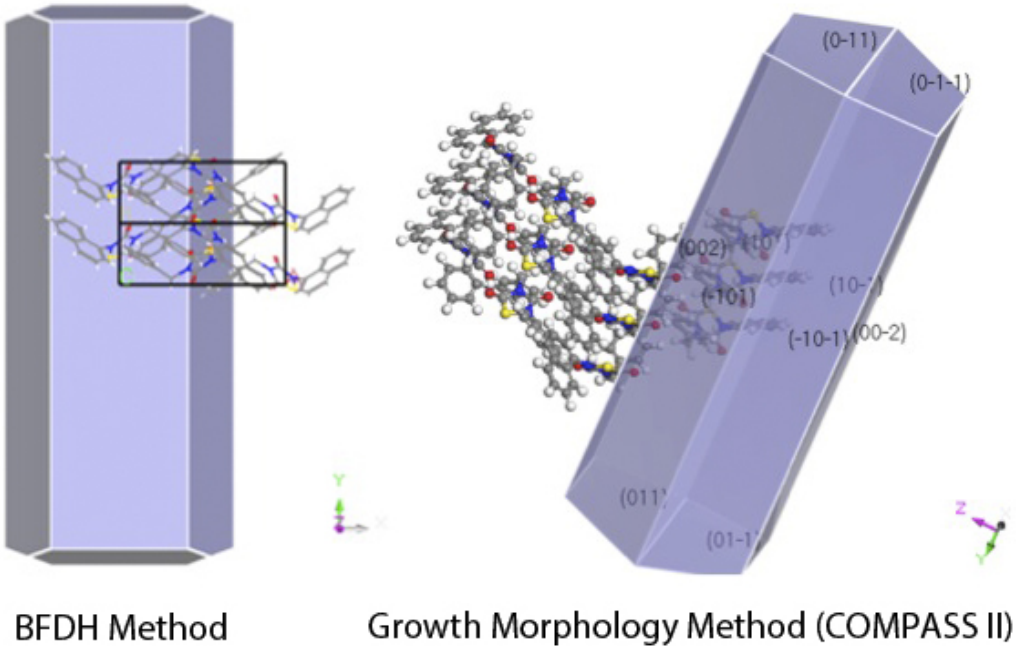

Figure 3.31: Predicted morphology of NP by the BDFH method and the Growth Morphology method using COMPASS II forcefield.

Table 3.19: Dominant crystal surfaces predicted from Crystal Morphology prediction using COMPASS II as force field for NP with the associated attachment energy and percentage of total area.

Face	Multiplicity	Eatt	% Area
{0 0 2}	2	-45.11	31
{1 0 1}	4	-53.42	53
{0 1 1}	4	-108.72	16

Eatt is the Attachment energy.

%Area is the percentage of the total area.

total area).

Once the crystal structure and the predicted morphology is known, new strategies for preventing crystal growth can be designed. However, several authors reported that in relation to the crystal surfaces and the molecular structures of the most effective stabilizer they found for several drugs, there appears to be no apparent pattern to choose the best additives for a particular drug [30, 59]. A more rigorous modeling involving calculation of binding energies for the adsorption of additives onto the crystal surface should be required to understand the mechanism by which the surfactants inhibits NP crystal growth. However, the difficulty in linking molecular level interactions between the stabilizer molecule and crystal surfaces is based on the complexity of these systems that comprises multiple components and the dynamic nature of the precipitation process itself.

3.4.3 Summary

- The morphology of the NP crystal has been predicted using two methods: the BFDH and the Growth Morphology Method.
- The selection of a proper forcefield that predict well the cell parameters is essential for a successful morphology prediction. For this reason, several forcefields has been assessed and the predicted lattice parameters have been compared. The best job in reproducing the experimental cell of NP was done by COMPASS II.
- The BFDH and the Growth Morphology Method using COMPASS II predicted a needle-like habit elongated along the b axis which is in good agreement with the experi-

mental morphology.

3.5 Preparation of aqueous suspensions of ibuprofen by DELOS-susp

DELOS-susp method has been proven to be a promising alternative for preparation of NP microsuspensions. Based on the encouraging results presented in Section 3.3, the next section of this Chapter is devoted to explore the feasibility of DELOS-susp for the preparation of stable suspensions of ibuprofen, a well known poor water soluble drug.

In DELOS-susp, the supercritical solution is expanded into a liquid media instead of passing through a filter and a dispersion of the drug in an aqueous media is obtained. Mechanistically, the liquid at the receiving end of the rapid depressurization that takes place in DELOS, could suppress particle growth of the precipitate as depicted in Figure 3.32.

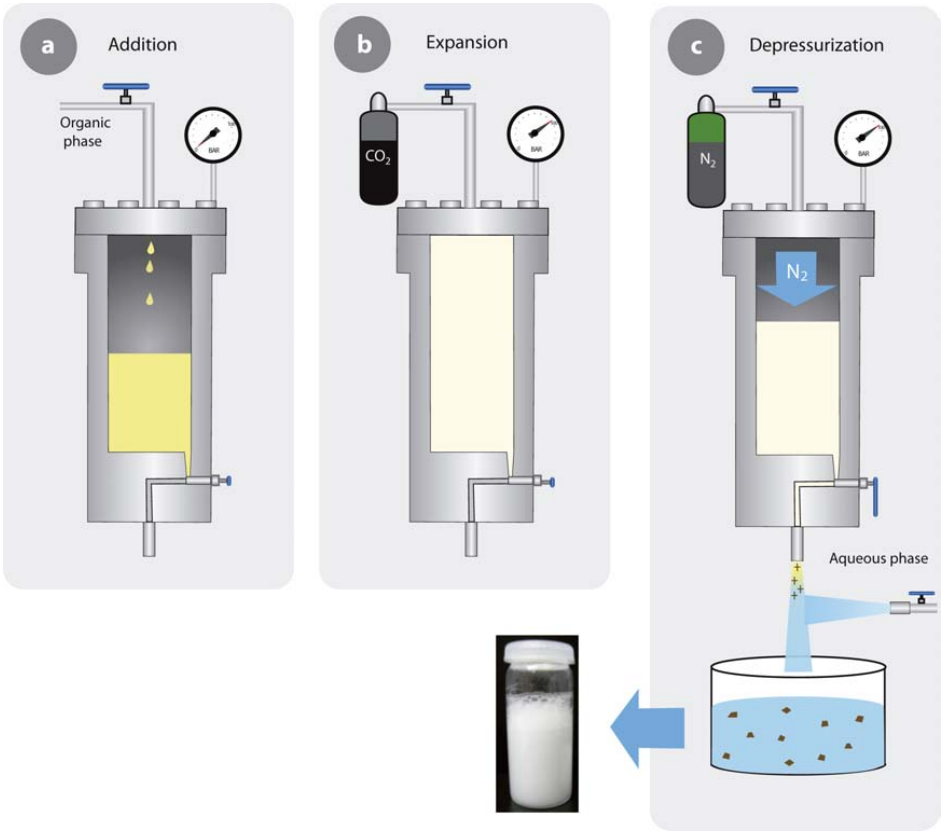

Figure 3.32: Schematic representation of the DELOS-susp method for the preparation of micro- and submicrosuspensions.

The production of stable micro and submicro-suspensions of drugs by DELOS-susp

involves the depressurization of a CO_2-expanded solution of the active compound over an aqueous phase. As depicted in Figure 3.32, the first and second stage of DELOS-sups procedure are the same as in DELOS methology (see Figure 2.6 of Chapter 2): the API is dissolved in a conventional organic solvent at atmospheric pressure and at working temperature (T_W). The solution is charged into the high pressure vessel once, previously driven to the working temperature (T_W). CO_2 is then added to obtained a volumetric expanded solution of the API at T_W and at high pressure (P_W) with a given molar fraction of CO_2 (x_W). Finally, this CO_2-expanded solution is depressurized from P_W to atmospheric pressure over a certain volume of aqueous media (V_{aq}) with a continuous aqueous flow (F) giving a aqueous suspension of the drug.

As revealed in Section 3.3, in order to circumvent anti-solvent precipitation of the poor water soluble drug when it enters the water current, experimental conditions must ensure the maximum DELOS yield possible.

In Section 2.2 of Chapter 2, the operation variables of DELOS for the precipitation of ibuprofen has been optimized. Hence, experiment 2, that was conducted at T_W = 298 K, P_W = 10 MPa, x_W = 0.82, using acetone as solvent and a C_i of ibuprofen in acetone of 0.28 mol/mol (β_i = 0.9), was chosen as a reference experiment for the preparation of stable suspensions by DELOS-susp because at those conditions the highest DELOS yield was achieved (Yield = 78%).

The selection of surfactant was carried out based on the promising results obtained with NP and studies reported in the literature [62]. The same proportions between drug and surfactant were evaluated. It is important to note that ibuprofen solubility in acetone is one order of magnitude higher than NP solubility in acetonitrile, therefore more concentrated suspensions were obtained although the current flow of the water were increased up to 700 mL/min. Table 3.20 collects the experiments conducted for the preparation of stable aqueous suspensions of ibuprofen by DELOS-susp.

In all the experiments conducted, aqueous suspensions of ibuprofen were produced. The suspension produced without the aid of surfactants were not stable and ibuprofen particles tend to cream up after 2 hours of its preparation (see Figure 3.33). The rest of ibuprofen suspensions, except the suspension obtained in the presence of HPMC using 0.8:1 g HMPC/ g Ibu (suspension 5) were milky homogenous and stable suspensions. The suspension obtained after experiments 5 consists of very big agglomerates. Therefore, this suspension was not characterize as it is not macroscopically homogenous.

Table 3.20: Experiments conducted for the preparation of micro and submicrosuspensions of Ibuprofen by DELOS-susp.

Experiment	Surfactant	Surfactant/IBU ratio (g:g)[a]
1	-	-
2	Poloxamer F-127	0.08:1
3	Poloxamer F-127	0.8:1
4	HPMC	0.08:1
5	HPMC	0.8:1
6	Tween80	0.08:1
7	Tween80	0.8:1

DELOS-susp experiments performed at T_W = 298 K, P_W = 10 MPa, x_W = 0.82 and F = 700 mL/min for preparing stable ibuprofen aqueous suspensions, [a] amount of surfactant expressed as grams of surfactant per gram of IBU.

Figure 3.33: Macroscopically comparison between the suspension of ibuprofen in the presence (a) and in the absence of surfactant (b).

∗ **Particle size distribution of ibuprofen suspensions**

The characterization of the suspensions prepared by DELOS-susp were analysed by Light Scattering using the protocol described in Section 6.4.1 of the Experimental Part just as prepared and applying 10 min of US and the results are presented in Table 3.21.

In the case of suspensions of ibuprofen, the presence of surfactants at those concentrations do not inhibit so much the crystal growth of ibuprofen particles and the effect of adding tenfold concentration of surfactant is negligible. Attending to the values of par-

Table 3.21: Particle size distribution of Ibuprofen suspensions prepared by DELOS-susp as prepared and after 10 min of US.

Experiment	As prepared (μm)[a]			10 min US (μm)[a]		
	d(0.1)	d(0.5)	d(0.9)	d(0.1)	d(0.5)	d(0.9)
DELOS 2	-	-	-	2.84	6.7	14.37
1	-	-	-	5.4	11.3	23.1
2	4.8	16.9	97.5	2.8	5.8	14.5
3	5.9	13.3	28.1	5.1	10.3	18.7
4	7.8	13.5	35.4	3.9	9.5	18.6
6	4.9	11.0	24.4	3.4	7.3	14.7
7	5.4	11.3	23.12	5.1	11.9	27.0

[a]Volumetric particle size distribution expressed in percentiles of 10, 50 and 90 as prepared and [a] after 10 min of ultrasounds.

ticle size distribution without applying ultrasounds, the best results are obtained when using Tween 80 at a concentration of 0.08:1 g Tween 80/ g Ibuprofen. After 10 min in an sonicated bath, the particle size distributions of the suspensions in the presence of Tween 80 and Poloxamer F-127 are quite similar.

The suspension prepared using HPMC with the highest concentration was not homogenous and therefore it was not further characterized. The one using ten times less of HMPC yields the bigger particle size distribution. In addition, as can be ascertained from Figure 3.34, HMPC alters the morphological aspect of ibuprofen particles. There are previous studies that highlights that HMPC displays poor stabilizing performance citeVanEerdenbrugh2009,Jongen2000.

∗ Characterization of ibuprofen micro particles obtained by filtration of the micro-suspensions

As in the case of NP, the suspensions contained an excess of acetone and therefore were filtered and dried. The solids obtained were characterized by SEM and by Light Scattering following the experimental procedure detailed in Sections 6.4.2 and 6.4.1 respectively. For Light Scattering measurements, the dried ibuprofen powders were resuspended in pure water. In order to have a stable suspension that could be characterized,

suspensions were sonicated 10 min.

As Figure 3.34 shows, the morphology of ibuprofen particles does not change as a function of the surfactant used as except for the solids precipitated using HPMC. It has been reported that HPMC induces different morphologies [34].

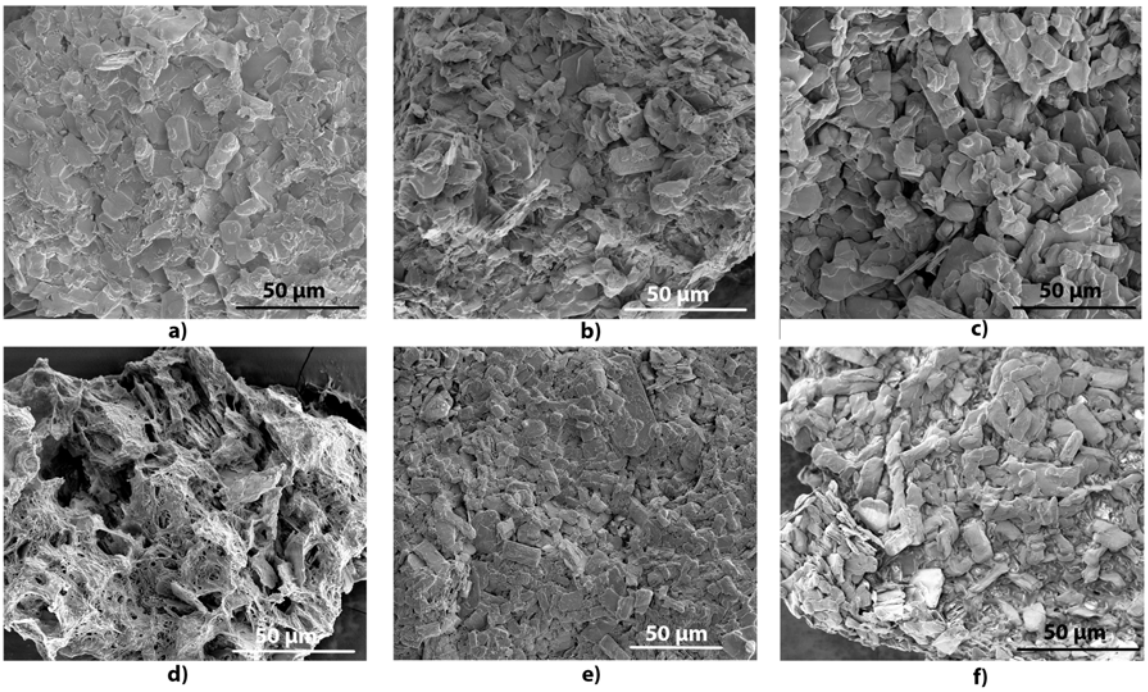

Figure 3.34: SEM images of the ibuprofen obtained after filtration and drying of the suspensions prepared by DELOS-susps in the absence of surfactant, experiment 1(a), and employing surfactants: experiments 2-7 from Table 3.20.

The particle size measurements of ibuprofen particles re-suspended in pure water are presented in Table 3.22. The free-acetone ibuprofen aqueous suspensions obtained present similar particles size distributions as the ones containing acetone after 10min of ultrasounds. The preparation of stable suspensions of ibuprofen should be regarded as a preliminary study. More experiments changing the surfactant nature and concentration should be design in order to obtain smaller ibuprofen particles, as in this case, the size is not improved in comparison to DELOS precipitation of ibuprofen.

Table 3.22: Particle size distribution of the solids of Ibuprofen resuspended in water.

Experiment	10 min US (μm)[a]		
	d(0.1)	d(0.5)	d(0.9)
1	2.5	7.1	19.5
2	2.8	5.8	14.2
3	2.8	6.1	12.7
4	2.3	4.4	7.8
6	2.5	5.3	9.9
7	3.0	6.3	11.7

[a]Volumetric particle size distribution expressed in percentiles of 10, 50 and 90 as prepared after 10 min of ultrasounds.

3.5.1 Summary

- The feasibility of preparing stable aqueous suspensions of ibuprofen by DELOS-susps has been demonstrated. However, the additives screened and the concentrations employed do not exert a significant impact on the crystal growth of ibuprofen.
- The best results in terms of particle size reduction has been achieve using Tween 80.
- HPMC does not display good stabilizing properties and it also modifies ibuprofen crystal morphology.
- The preparation of stable suspensions of ibuprofen can be considered a preliminary study, a more comprehensive screening of surfactant and concentrations is essential in order to reduce particle size of ibuprofen.

Bibliography

[1] R. H. Muller and K. Peters, "Nanosuspensions for the formulation of poorly soluble drugs: I. preparation by a size-reduction technique," *International Journal of Pharmaceutics*, vol. 160, no. 2, pp. 229 – 237, 1998.

[2] V. Patravale, A. Date, and R. Kulkarni, "Nanosuspensions: A promising drug delivery strategy," *Journal of Pharmacy and Pharmacology*, vol. 56, no. 7, pp. 827–840, 2004.

[3] B. E. Rabinow, "Nanosuspensions in drug delivery," *Nature Reviews Drug Discovery*, vol. 3, no. 9, pp. 785–796, 2004.

[4] P. Pathak, M. Meziani, T. Desai, and Y.-P. Sun, "Nanosizing drug particles in supercritical fluid processing," *Journal of the American Chemical Society*, vol. 126, no. 35, pp. 10842–10843, 2004.

[5] E. Merisko-Liversidge, G. G. Liversidge, and E. R. Cooper, "Nanosizing: a formulation approach for poorly-water-soluble compounds," *European Journal of Pharmaceutical Sciences*, vol. 18, no. 2, pp. 113 – 120, 2003.

[6] R. Müller, C. Jacobs, and O. Kayser, "Nanosuspensions as particulate drug formulations in therapy: Rationale for development and what we can expect for the future," *Advanced Drug Delivery Reviews*, vol. 47, no. 1, pp. 3–19, 2001.

[7] D. Horn and J. Rieger, "Organic nanoparticles in the aqueous phase - theory, experiment, and use," *Angewandte Chemie - International Edition*, vol. 40, no. 23, pp. 4330–4361, 2001.

[8] C. M. Keck and R. H. Müller, "Drug nanocrystals of poorly soluble drugs produced by high pressure homogenisation," *European Journal of Pharmaceutics and Biopharmaceutics*, vol. 62, no. 1, pp. 3 – 16, 2006.

[9] H.-K. Chan and P. Kwok, "Production methods for nanodrug particles using the bottom-up approach," *Advanced Drug Delivery Reviews*, vol. 63, no. 6, pp. 406–416, 2011.

[10] J.-U. Junghanns and R. Mu, T. Muller, "Nanocrystal technology, drug delivery and clinical applications," *International Journal of Nanomedicine*, vol. 3, no. 3, pp. 295–309, 2008.

[11] S. Verma, R. Gokhale, and D. Burgess, "A comparative study of top-down and bottom-up approaches for the preparation of micro/nanosuspensions," *International Journal of Pharmaceutics*, vol. 380, no. 1-2, pp. 216–222, 2009.

[12] R. Huttenrauch, S. Fricke, and P. Zielke, "Mechanical activation of pharmaceutical systems," *Pharmaceutical Research*, vol. NO. 6, pp. 302–306, 1985.

[13] G. Liversidge and K. Cundy, "Particle size reduction for improvement of oral bioavailability of hydrophobic drugs: I. absolute oral bioavailability of nanocrystalline danazol in beagle dogs," *International Journal of Pharmaceutics*, vol. 125, no. 1, pp. 91–97, 1995.

[14] B. H. L. B. Rainer H. Müller, Simon Benita, ed., *Emulsions and Nanosuspensions for the Formulation of Poorly Soluble Drugs.* Medpharm„ 1998.

[15] D. Horn and J. Rieger, "Organic nanoparticles in the aqueous phase - theory, experiment, and use," *Angewandte Chemie - International Edition*, vol. 40, no. 23, pp. 4330–4361, 2001.

[16] R. Müller, S. Gohla, and C. Keck, "State of the art of nanocrystals - special features, production, nanotoxicology aspects and intracellular delivery," *European Journal of Pharmaceutics and Biopharmaceutics*, vol. 78, no. 1, pp. 1–9, 2011.

[17] S. Verma, Y. Lan, R. Gokhale, and D. Burgess, "Quality by design approach to understand the process of nanosuspension preparation," *International Journal of Pharmaceutics*, vol. 377, no. 1-2, pp. 185–198, 2009.

[18] S. Dalvi, M. Azad, and R. Dave, "Precipitation and stabilization of ultrafine particles of fenofibrate in aqueous suspensions by resolv," *Powder Technology*, vol. 236, pp. 75–84, 2013.

[19] P. Pathak, M. J. Meziani, T. Desai, and Y.-P. Sun, "Formation and stabilization of ibuprofen nanoparticles in supercritical fluid processing," *The Journal of Supercritical Fluids*, vol. 37, no. 3, pp. 279 – 286, 2006.

[20] L. Songtipya and A. Sane, "Effect of concentration and degree of saturation on co-precipitation of catechin and poly(l-lactide) by the resolv process," *Journal of Supercritical Fluids*, vol. 75, pp. 72–80, 2013.

[21] L. Wu, J. Zhang, and W. Watanabe, "Physical and chemical stability of drug nanoparticles," *Advanced Drug Delivery Reviews*, vol. 63, no. 6, pp. 456–469, 2011.

[22] A. Ain-Ai and P. Gupta, "Effect of arginine hydrochloride and hydroxypropyl cellulose as stabilizers on the physical stability of high drug loading nanosuspensions of a poorly soluble compound," *International Journal of Pharmaceutics*, vol. 351, no. 1-2, pp. 282–288, 2008.

[23] M. Sangalli, L. Zema, A. Maroni, A. Foppoli, F. Giordano, and A. Gazzaniga, "Influence of betacyclodextrin on the release of poorly soluble drugs from inert and hydrophilic heterogeneous polymeric matrices," *Biomaterials*, vol. 22, no. 19, pp. 2647–2651, 2001.

[24] B. K. Krister Holmberg, Bo Jönsson and B. Lindman, *Surfactants and Polymer in Aqueous Solution.* John Wiley & Sons, Inc., 2002.

[25] D. Myers, *Surfaces, Interfaces, and Colloids:Priniciples and Applications.* John Wiley & Sons, Inc., 1999.

[26] M. J. Rosen, *Surfactants and Interfacial phenomena.* Wilet-Interscience, 2004.

[27] W. Tiyaboonchai and N. Limpeanchob, "Formulation and characterization of amphotericin b-chitosan-dextran sulfate nanoparticles," *International Journal of Pharmaceutics*, vol. 329, no. 1-2, pp. 142–149, 2007.

[28] M. Nutan and I. Reddy, "General principles of suspensions," *Pharmaceutical suspensions: from formulation development to Manufacturing*, pp. 39–66, 2009.

[29] C.-J. Kim, "Surface chemistry and colloids," *Advanced Pharmaceutics: Physicochemical Principles*, pp. 193–256, 2004.

[30] S. Xie, S. Poornachary, P. Chow, and R. Tan, "Direct precipitation of micron-size salbutamol sulfate: New insights into the action of surfactants and polymeric additives," *Crystal Growth and Design*, vol. 10, no. 8, pp. 3363–3371, 2010.

[31] S. Dalvi and R. Dave, "Controlling particle size of a poorly water-soluble drug using ultrasound and stabilizers in antisolvent precipitation," *Industrial and Engineering Chemistry Research*, vol. 48, no. 16, pp. 7581–7593, 2009.

[32] J. Mullin *Crystallization*, 1993.

[33] K. Chari, B. Antalek, J. Kowalczyk, R. Eachus, and T. Chen, "Polymer-surfactant interaction and stability of amorphous colloidal particles," *Journal of Physical Chemistry B*, vol. 103, no. 45, pp. 9867–9872, 1999.

[34] N. Jongen, P. Bowen, J. Lematre, J.-C. Valmalette, and H. Hofmann, "Precipitation of self-organized copper oxalate polycrystalline particles in the presence of hydroxypropylmethylcellulose (hpmc): Control of morphology," *Journal of Colloid and Interface Science*, vol. 226, no. 2, pp. 189–198, 2000.

[35] A. Balakrishnan, B. Rege, G. Amidon, and J. Polli, "Surfactant-mediated dissolution: Contributions of solubility enhancement and relatively low micelle diffusivity," *Journal of Pharmaceutical Sciences*, vol. 93, no. 8, pp. 2064–2075, 2004.

[36] R. Thakur and R. Gupta, "Rapid expansion of supercritical solution with solid cosolvent (ress - sc) process: Formation of griseofulvin nanoparticles," *Industrial and Engineering Chemistry Research*, vol. 44, no. 19, pp. 7380–7387, 2005.

[37] M. Wulff, M. Aldën, and D. Craig, "An investigation into the critical surfactant concentration for solid solubility of hydrophobic drug in different polyethylene glycols," *International Journal of Pharmaceutics*, vol. 142, no. 2, pp. 189–198, 1996.

[38] L.-H. Zhu, L.-Z. Wang, H.-R. Li, Y. Lei, H.-H. Pan, and S.-J. Han, "Molecular dynamics simulation for dmf aqueous solution," *Acta Chimica Sinica*, vol. 61, no. 4, pp. 526–530, 2003.

[39] A. M. M. Cerdeira, *Production and Stabilization of Nnaosuspensions of Poorly Soluble Durg Substances.* PhD thesis, ETH Zurich, 2012.

[40] I. Cabrera, E. Elizondo, O. Esteban, J. Corchero, M. Melgarejo, A. Pulido, D. Cordoba, E. Moreno, U. Unzueta, E. Vazquez, I. Abasolo, S. Schwartz, A. Villaverde, F. Albericio, M. Royo, M.and Garcia Parajo, and J. Ventosa, N. Veciana, "Multifunctional nanovesicle-bioactive conjugates prepared by a one-step scalable method using co2-expanded solvents," *Nano Letters*, vol. 13, no. 8, pp. 3766–3774, 2013.

[41] M. Cano-Sarabia, N. Ventosa, S. Sala, C. Patio, C.o, R. Arranz, and J. Veciana, "Preparation of uniform rich cholesterol unilamellar nanovesicles using CO2-expanded solvents," *Langmuir*, vol. 24, no. 6, pp. 2433–2437, 2008.

[42] A. Da Fonseca Antunes, B. De Geest, C. Vervaet, and J. Remon, "Gelucire 44/14 based immediate release formulations for poorly water-soluble drugs," *Drug Development and Industrial Pharmacy*, vol. 39, no. 5, pp. 791–798, 2013.

[43] A. Svensson, C. Neves, and B. Cabane, "Hydration of an amphiphilic excipient, gelucire 44/14," *International Journal of Pharmaceutics*, vol. 281, no. 1-2, pp. 107–118, 2004.

[44] O. Chambin and V. Jannin, "Interest of multifunctional lipid excipients: Case of gelucire 44/14," *Drug Development and Industrial Pharmacy*, vol. 31, no. 6, pp. 527–534, 2005.

[45] S. Cafaggi, E. Russo, G. Caviglioli, B. Parodi, R. Stefani, G. Sillo, R. Leardi, and G. Bignardi, "Poloxamer 407 as a solubilising agent for tolfenamic acid and as a base for a gel formulation," *European Journal of Pharmaceutical Sciences*, vol. 35, no. 1-2, pp. 19–29, 2008.

[46] S. Khattak, S. Bhatia, and S. Roberts, "Pluronic f127 as a cell encapsulation material: Utilization of membrane-stabilizing agents," *Tissue Engineering*, vol. 11, no. 5-6, pp. 974–983, 2005.

[47] T. Gafourian, A. Safari, K. Adibkia, F. Parviz, and A. Nokhodchi, "A drug release study from hydroxypropylmethylcellulose (hpmc) matrices using qspr modeling," *Journal of Pharmaceutical Sciences*, vol. 96, no. 12, pp. 3334–3351, 2007.

[48] J. Siepmann and N. Peppas, "Modeling of drug release from delivery systems based on hydroxypropyl methylcellulose (hpmc)," *Advanced Drug Delivery Reviews*, vol. 64, no. SUPPL., pp. 163–174, 2012.

[49] P. Thapa and M. Ghimire, "Effect of drug solubility and polymer viscosity on in-vitro drug release from hpmc matrix tablet," *Indian Drugs*, vol. 42, no. 6, pp. 389–391, 2005.

[50] D. Zhou, D. Law, J. Reynolds, L. Davis, C. Smith, J. Torres, V. Dave, N. Gopinathan, D. Hernandez, M. Springman, and C. Zhou, "Understanding and managing the impact of hpmc variability on drug release from controlled release formulations," *Journal of Pharmaceutical Sciences*, vol. 103, no. 6, pp. 1664–1672, 2014.

[51] K. Chowdary, K. Rao, and R. Shaik, "Enhancement of solubility and dissolution rate of nimesulide by cyclodextrins, poloxamer and pvp," *International Journal of Chemical Sciences*, vol. 9, no. 2, pp. 637–646, 2011.

[52] L. Song, C.-N. Zhang, J. Liu, Y.-Q. Zhang, and S.-R. Guo, "Study on paa and pvp as drug delivery carriers," *Shanghai Jiaotong Daxue Xuebao/Journal of Shanghai Jiaotong University*, vol. 39, no. 10, pp. 1680–1684, 2005.

[53] J. Carvalho, F. Alves, T. Batista, F. Carvalho, P. Santiago, and M. Tabak, "Sodium dodecyl sulfate (sds) effect on the thermal stability of oxy-hbgp: Dynamic light scattering (dls) and small angle x-ray scattering (saxs) studies," *Colloids and Surfaces B: Biointerfaces*, vol. 111, pp. 561–570, 2013.

[54] S. Hejazi, M. Erfan, and S. Alireza Mortazavi, "Precipitation reaction of sds and potassium salts in flocculation of a micronized megestrol acetate suspension," *Iranian Journal of Pharmaceutical Research*, vol. 12, no. 3, pp. 239–246, 2013.

[55] B. Phani Kumar, S. Umayal Priyadharsini, G. Prameela, and A. Mandal, "Nmr investigations of self-aggregation characteristics of sds in a model assembled tri-block copolymer solution," *Journal of Colloid and Interface Science*, vol. 360, no. 1, pp. 154–162, 2011.

[56] D. Tulumello and C. Deber, "Sds micelles as a membrane-mimetic environment for transmembrane segments," *Biochemistry*, vol. 48, no. 51, pp. 12096–12103, 2009.

[57] S. Raghavan, A. Trividic, A. Davis, and J. Hadgraft, "Crystallization of hydrocortisone acetate: Influence of polymers," *International Journal of Pharmaceutics*, vol. 212, no. 2, pp. 213–221, 2001.

[58] F.S.Romanski, *The Production and stabilization of pharmaceutical nanosuspensions*. PhD thesis, New Brunswick Rutgers, The State University of New Jersey, 2011.

[59] S. Khan, M. Matas, J. Zhang, and J. Anwar, "Nanocrystal preparation: Low-energy precipitation method revisited," *Crystal Growth and Design*, vol. 13, no. 7, pp. 2766–2777, 2013.

[60] B. Van Eerdenbrugh, G. Van den Mooter, and P. Augustijns, "Top-down production of drug nanocrystals: Nanosuspension stabilization, miniaturization and transformation into solid products," *International Journal of Pharmaceutics*, vol. 364, no. 1, pp. 64–75, 2008.

[61] S. Verma, S. Kumar, R. Gokhale, and D. Burgess, "Physical stability of nanosuspensions: Investigation of the role of stabilizers on ostwald ripening," *International Journal of Pharmaceutics*, vol. 406, no. 1-2, pp. 145–152, 2011.

[62] I. Ghosh, S. Bose, R. Vippagunta, and F. Harmon, "Nanosuspension for improving the bioavailability of a poorly soluble drug and screening of stabilizing agents to inhibit crystal growth," *International Journal of Pharmaceutics*, vol. 409, no. 1-2, pp. 260–268, 2011.

[63] J. Lee, J.-Y. Choi, and C. Park, "Characteristics of polymers enabling nano-comminution of water-insoluble drugs," *International Journal of Pharmaceutics*, vol. 355, no. 1-2, pp. 328–336, 2008.

[64] M. Matteucci, M. Hotze, K. Johnston, and R. Williams III, "Drug nanoparticles by antisolvent precipitation: Mixing energy versus surfactant stabilization," *Langmuir*, vol. 22, no. 21, pp. 8951–8959, 2006.

[65] R. Chakraborti and J. Kaur, "Noninvasive measurement of particle-settling velocity and comparison with stokes' law," *Journal of Environmental Engineering (United States)*, vol. 140, no. 2, 2014.

[66] O. Mengual, G. Meunier, I. Cayre, K. Puech, and P. Snabre, "Characterisation of instability of concentrated dispersions by a new optical analyser: The turbiscan ma 1000," *Colloids and Surfaces A: Physicochemical and Engineering Aspects*, vol. 152, no. 1-2, pp. 111–123, 1999.

[67] X. Tang and M. Pikal, "Design of freeze-drying processes for pharmaceuticals: Practical advice," *Pharmaceutical Research*, vol. 21, no. 2, pp. 191–200, 2004.

[68] J. Sassone, E. Jo, L. Noguera, and J. Mullick, "Freeze-drying in pharma," *Pharmaceutical Manufacturing and Packing Sourcer*, no. SUMMER, pp. 46–50, 2009.

[69] F. Franks, "Freeze-drying of bioproducts: Putting principles into practice," *European Journal of Pharmaceutics and Biopharmaceutics*, vol. 45, no. 3, pp. 221–229, 1998.

[70] W. Abdelwahed, G. Degobert, S. Stainmesse, and H. Fessi, "Freeze-drying of nanoparticles: Formulation, process and storage considerations," *Advanced Drug Delivery Reviews*, vol. 58, no. 15, pp. 1688–1713, 2006.

[71] H. Talsma, M. Van Steenbergen, P. Salemink, and D. Crommelin, "The cryopreservation of liposomes. 1. a differential scanning calorimetry study of the thermal behavior of a liposome dispersion containing mannitol during freezing/thawing," *Pharmaceutical Research*, vol. 8, no. 8, pp. 1021–1026, 1991.

[72] K. Tanaka, T. Takeda, K. Fujii, and K. Miyajima, "Cryoprotective mechanism of saccharides on freeze-drying of liposome," *Chemical and Pharmaceutical Bulletin*, vol. 40, no. 1, pp. 1–5, 1992.

[73] C. Schwarz and W. Mehnert, "Freeze-drying of drug-free and drug-loaded solid lipid nanoparticles (sln)," *International Journal of Pharmaceutics*, vol. 157, no. 2, pp. 171–179, 1997.

[74] A. Saez, M. Guzm"Ãą"n, J. Molpeceres, and M. Aberturas, "Freeze-drying of polycaprolactone and poly(d,l-lactic-glycolic) nanoparticles induce minor particle size changes affecting the oral pharmacokinetics of loaded drugs," *European Journal of Pharmaceutics and Biopharmaceutics*, vol. 50, no. 3, pp. 379–387, 2000.

[75] M. Choi, S. Brianon, J. Andrieu, S. Min, and H. Fessi, "Effect of freeze-drying process conditions on the stability of nanoparticles," *Drying Technology*, vol. 22, no. 1-2, pp. 335–346, 2004.

[76] E. Moreno-Calvo, T. Calvet, M. Cuevas-Diarte, and D. Aquilano, "Relationship between the crystal structure and morphology of carboxylic acid polymorphs. predicted and experimental morphologies," *Crystal Growth and Design*, vol. 10, no. 10, pp. 4262–4271, 2010.

[77] E. Moreno-Calvo, *On the polymorphism and structural characterization in the family of even saturated carboxylic acids.* PhD thesis, Universidad de Barcelona., 2008.

[78] P. Bennema, "Morphology of crystals, past and future," *Science and Technology of Crystal Growth*, pp. 149–164, 1995.

[79] G. Clydesdale, K. Roberts, and R. Docherty, "Habit95 - a program for predicting the morphology of molecular crystals as a function of the growth environment," *Journal of Crystal Growth*, vol. 166, no. 1-4, pp. 78–83, 1996.

[80] H. Sun, "The compass force field: Parameterization and validation for phosphazenes," *Computational and Theoretical Polymer Science*, vol. 8, no. 1-2, pp. 229–246, 1998.

4

Surfactant-free microemulsion-like systems

4.1 Introduction

The most abundant and inexpensive solvents on earth are water and CO_2, which, in addition, are environmentally benign, non-toxic and non-flammable fluids. Based on this, systems containing both solvents offer new possibilities in replacement of more toxic solvents in fields like chemical processing, pharmaceutical, microelectronics, particle formation, organometallic catalysis, synthesis of polymers and so on.

Solvents based on liquid and supercritical CO_2 have evolved from pure CO_2, to CO_2-expanded solvents, complexing agents, micelles, and water/CO_2 microemulsions. The solvent quality of compressed CO_2 may be tuned with pressure and temperature. In light of the emergence of these new green systems, the following chapter is devoted to the description of new CO_2-based microemulsion-like systems containing water and organic solvents.

4.1.1 Microemulsions-like systems

Microemulsions are clear solutions of oil, water or other aqueous solutions and surfactants, with a rich variety of microstructures at the nanoscale level. They are thermodynamically stable, that is, for example, reversible to temperature cycles and they are transparent [1]. Microemulsions are isotropic, optically transparent and thermodynamically stable solutions. They were discovered by Schulman in the 1940s [2] and Winsor [3]. However, Mother Gardiner's recipe for washing woolen clothes in Australia predates this by 100 years. It comprises methanol, grated bar soap and a little eucalyptus oil. The most sophisticated modern washing detergents do to surpass it in effectiveness [4].

The first to call these solutions, consisting of water, oil, surfactant, and alcohol, "microemulsions" were Schulman et al. [5] in 1959. Another definition was given later by Danielsson and Lindman in 1981 [6]: a microemulsion is a system of water, oil and an amphiphile which is a single optically isotropic and thermodynamically stable liquid solution.

The term microemulsion was selected because of a fundamental misunderstanding of the nature of these systems. During a long period of time there were no agreed definition on what should constitute a microemulsion, but the term was used broadly to include several types of surfactant systems. A major reason for the confusion is due to the prefixes used to denote them, the term micro does not correlate to the size of the domains, which are on the nanoscale [7]. Nowadays, the fundamental understanding has matured into a considerable consensus and there are interesting applications of these systems in a variety of fields [1].

The extensive research on microemulsions was prompted by two oil crisis in the 1970s, when oil companies focused on the research of microemulsions because they could be used as a tool for optimizing oil recovery. Besides the economic interest, in the 1980s researchers took an interest in the understanding of phase behavior, the different nanostructures and the unique properties of microemulsions like their low interfacial tension [8].

At the nanoscopic scale, microemulsions are structured either as well defined nano droplets dispersed in a continuous media (water in oil (w/o) or oil in water (o/w)) [9, 2] or as bicontinuous structures [10, 11] (see Figure 4.1). Often, o/w microemulsions are abbreviated as L_1-phases, w/o as L_2-phases, and bicontinuous structures often as L_α-phases or sponge phases. Bicontinuous structures consist of networks of oil and water nanodomains separated and stabilized by a surfactant interfacial film. There is a huge

Table 4.1: Comparison between microemulsions and emulsions

Emulsions	Microemulsions
2 liquid phases	1 structure liquid phase
Thermodynamically unstable	Thermodynamically stable
Turbid aspect	Trasparent or translucent
Non spontaneous formation	Spontaneous formation
Micrometirc domain	Nanometric domains

diversity of other structures available: beside droplets, lamellar [12], random [13] or bicontinuous [14] nanostructures, a network of water tubes in an oil matrix or a network of oil tubes in a water matrix, have been identified. The microstructure is commonly reminiscent of random bicontinuous connected cylinders of oil in water or of water in oil and it is claimed that bicontinuos structures are more the rule than the exception. It is important to note that these are all dynamic aggregates [4] and that their net curvature is close to zero [8].

Another important phase classification was introduced by Winsor [3] who discovered four general types of phase equilibria:

- Winsor I: two phases in equilibrium, o/w structure and an almost pure upper oil phase.
- Winsor II: two phases in equilibrium, an aqueous phase containing surfactant and an upper w/o phase.
- Winsor III: three phase system consistint of a surfactant poor water phase, a bisontinuous middle phase and an almost pure upper oil phase.
- Winsor IV: classical single phase microemulsions that can be L_1, L_2 or L_α.

Microemulsions have been intensively studied during the last few years by many scientists and technologists. Most of the recent applications of microemulsions take advantage of the fact that, though macroscopically homogenous, microemulsions are heterogenous on the submicroscopic scale. The unique properties of microemulsions make them interesting for commercial products and technical processes. In particular, the high solubilizing power of microemulsion systems for organic and inorganic compounds favors

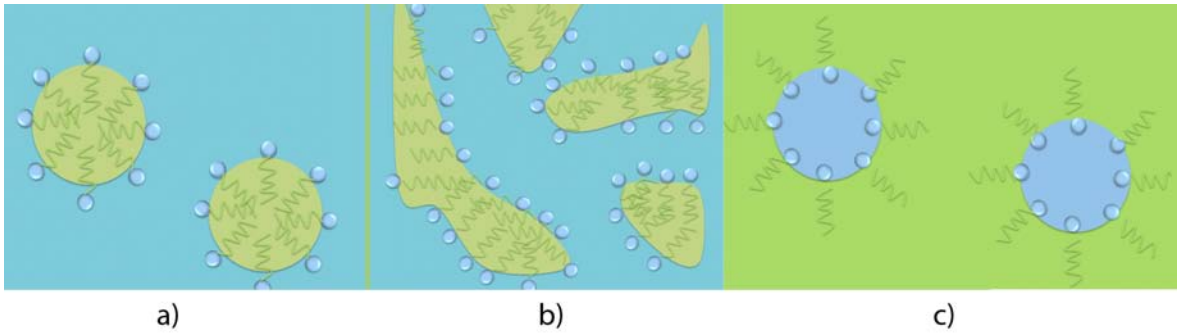

Figure 4.1: Different nano structures of microemulsions: a) oil-in-water, b) bicontinuous and c) water-in-oil.

their use as solvents for a large number of applications. The applications investigated at present range from classical fields like solubilisation media in food, cosmetic [15] and pharmaceutical industry [16], oil recovery [1], ground water remediation [17], soil cleanup [18] and organic chemistry, to new subjects like improvement of fuels or the use as decontamination media. Microemulsions have been used as chemical reactors because of their special interfacial properties which allow an intimate contact, at nanoscale level, of hydrophilic and hydrophobic domains [19]. The microemulsion route is very efficient in terms of stabilization of the products that can be dissolved in the different domains and in controlling their particle size.

Summarizing, microemulsions have attracted the attention of academia and industry since a long time because of their unique properties: they show thermodynamic stability, optical clarity and high solubilisation capacity [20], and they are isotropic with ultralow interfacial tensions [21]. Though they are macroscopically homogeneous solutions, an ordered structure can be found on the nanoscopic scale.

One problem of using conventional microemulsions is the separation and removal of solvent from products [19]. Additionally, microemulsions composed of conventional solvents could be formed and destroyed by composition and temperature changes, which require efficient stirring systems to ensure a homogeneous modification. In this sense, CO_2-based microemulsions emerge as a promising alternative to overcome these problem, as CO_2 used as solvent offers several advantages such rapid separation, easy removal of solvent and the introduction of pressure as a new operational parameter.

4.1.2 CO_2-based microemulsions-like systems

Water-in-CO_2 (W/C) microemulsions may be utilized as environmentally benign non-toxic solvents in chemical processes. The solvent quality of compressed CO_2 can be tuned with pressure and temperature to manipulate the properties of the microemulsion. The fluid properties of CO_2 such as density, and hence solvent quality, can be adjust by slightly changing temperature or pressure, which further enhances the ease of solvent removal through rapid evaporation. cCO_2 is generally a very poor solvent, especially for polar and high molecular weight solutes, and this limits its use in many potential applications [22]. One of the most promising approaches for enhancing the solubility of polar substances in cCO_2 is to form water CO_2-based microemulsions. CO_2 properties are much different from those of water [23], hence, water CO_2-based microemulsions can be considered as green universal solvents, what favors their use as solvents for a large number of purposes [24]. These organized fluids have the attractive characteristics of cCO_2 and the solvation properties of bulk water [25]. Over the past 40 years, a lot of effort has been put in the formation and characterization of CO_2-based microemulsions [26, 27, 28, 29, 23, 19].

Water and compressed CO_2 microemulsions have been widely used in many fields, such as chemical reactions, nano particle synthesis, extraction of hydrophiles and proteins [30]. Nevertheless, in order to become a viable green technology, the amount of surfactant required to form CO_2-based microemulsions need to be reduced until its minimum value.

Over the last three decades and among the more than 10.000 publications dealing with microemulsions (CO_2-based and conventional microemulsions), only few papers deal with the so-called surfactant-free microemulsions [31, 32, 33, 34, 35, 36, 37, 38, 39, 40]. Up to now, and as far as we know, it is only possible to form CO_2-based microemulsions with the aid of surfactants. This Thesis presents, for the first time, surfactant-free CO_2-based microemulsion-like systems.

4.1.3 Surfactant-free Microemulsion-like systems

The concept of surfactant-less microemulsions has been known for a long time. Strange observations dating back to the early XXth century about membrane enzyme reactions in lipid-less media, non-linear effects in evaporation of ternary mixtures [41], the polar paradox in oxidation rates of ternary fluids, as well as unexplained single phase ternary solutions that contain ethanol, led to the proposition in the seventies by the group of

Barden, [42] that *surfactant-less microemulsions* should go beyond a nice name to some strange unexplained behavior. This observed behavior of some homogeneous ternary fluids that can be reversibly phase separated by simple centrifugation, but correspond to a thermodynamic equilibrium in the phase diagram. The existence of surfactant-less microemulsions was very controversial at the beginning mainly due to the redundant argument that microemulsions were composed by at least a ternary system in which one component is an amphiphile, therefore, surfactant- less microemulsions could not exist.

In 1976 the group of Barden started an investigation with the aim to determine the effect of an interfacial environment on the properties of metal-ligand complexes [43]. In this work the system water/hexane was studied with hexadecyl-trimethylammonium perchlorate as surfactant and 2-propanol as cosurfactant. The objective was to characterize the system in absence of metals and ligands. In another set of studies, the phase behavior of the pseudo-ternary systems alcohol/ hydrocarbon/brine was examined [44, 45, 46]. The single phase areas were similar to those observed with surfactants. Also the determined interfacial tensions of these systems were similar to surfactant-based microemulsion systems. In 1981, Lara et al. explored the ternary system water/2-propanol/benzene with heat capacity measurements. Their experimental results supported the formation of systems similar to microemulsions. Also a bicontinuous structure was suggested [47].

Hence, in the late 1970s several groups found similar structures to microemulsions in systems in the abcense of surfactants. However, there was no continuation of these initial works. Some recent studies have tried to understand and explain the mechanism of the formation of these domains [37, 36]. Pfennig and Schott [48] published a study with computer simulations where the formation of nano-droplets in the close vicinity of the interface induced by mass transfer across these interfaces is described. In their simulation they found areas in a ternary system where stable nano-droplets were formed.

However, recent scattering experiments with light [31], X-rays and neutrons [49], gave proof of structures identical to standard micelles, which led to the conclusion that well-defined aggregates exist in ternary solutions containing two alcohols (ethanol and octanol). Some of these experiments also demonstrated that these structures are not caused by critical fluctuations, because the signals of different solution components give different q dependencies [50].

Another recent publication regarding surfactant - free microemulsion- like systems is the work published by Wang et al. They have reported a surfactant-free microemulsion - like system that comprises only an ionic liquid and water [51].

Though the literature concerning the structure and microenvironment of these surfactant -less microemulsions is quite scarce [40], these systems have the advantage of the absence of harmful surfactants facilitating the recovery of products and making them more environmentally friendly. The surfactant-less microemulsion systems have been shown to serve as an appropriate media for enzymatic reactions, [36] to be more suitable than microemulsions composed of surfactants for biocatalytic process [40, 35] and for the hydrolysis of chlorophyll [52].

Klossek et al. [49] also investigated the formation of surfactant less microemulsions in ternary mixtures that fulfill the following requirements : solvent 1 being miscible with solvent 2 and that additional component 3 is highly soluble in solvent 2 but not in solvent 1, which are the same pre requites as in our CO_2-based surfacatant-free microemulsion-like systems. This chapter deals with the formation and characterization of surfactant-free CO_2-based microemulsions-like systems that were observed studying the behavior of ternary mixtures composed of water and CO_2-expanded solvents.

4.2 Water/Acetone/CO_2 system

The first mixture studied has been the mixture composed of acetone/water/CO_2 at 10 MPa at different temperatures. Water and acetone are completely miscible and acetone expands greatly upon the addition of CO_2 [53]. However, as mentioned, water and CO_2 represent extremes of the solvent spectra, therefore the solubility of CO_2 in water is notably low. As described in the previous section, microemulsions are a single transparent phase systems, therefore, the knowledge of the phase behavior of the mixture is the preliminary step in the study of microemulsions.

4.2.1 High pressure phase equilibria

A break-through in the understanding of microemulsions was due to the determination of phase diagrams. Extensive work on phase diagrams contributed much to clarify the existence range of microemulsions and to relate phase behavior to molecular interactions [1].

High pressure phase equilibria have been a subject of rapidly increasing interest since the 90s. Mixtures containing carbon dioxide, water and an organic solvent are among the most extensively studied [54]. The phase behavior of ternary mixtures of water, acetone

and CO_2 at high pressure has been the subject of many studies revealing a high pressure fluid-fluid phase equilibrium [55, 56]. Therefore, according to a phenomenon called "salting out with a supercritical fluid", which was first described by Elgin and Weinstock in the late 50s, initially homogeneous mixtures of acetone and water can be split in two fluid phases by pressurization with CO_2 (Figure 4.2).

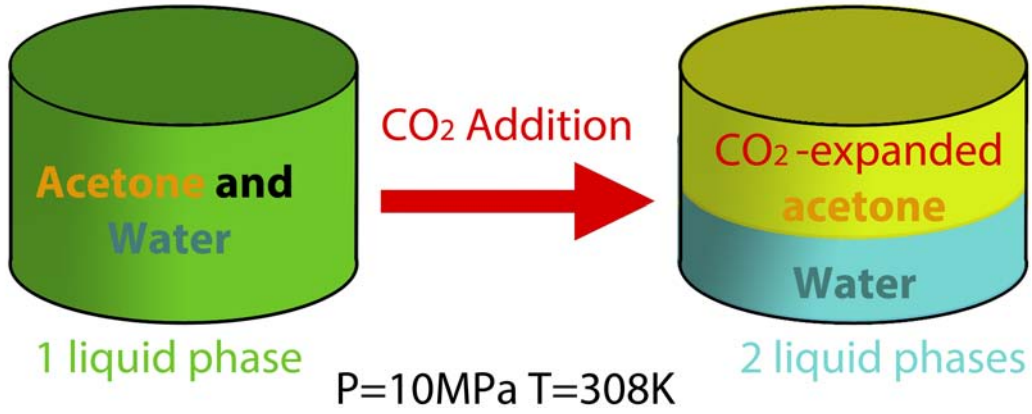

Figure 4.2: Salting out with a supercritical gas

A way to present the phase behavior within a ternary system is the Gibbs triangle, which is a equilateral triangle. Along the sidelines either the mass, volume, or mole fraction of the components are plotted. Every corner corresponds to the pure component. When the phase behavior is investigated as a function of temperature as well, the triangle is extended to the Gibbs Prism. In this case the Gibbs triangle is the basis and temperature the ordinate.

The phase behavior of the ternary system of water, acetone and CO_2 at high pressure is already reported in the literature [54].

In the framework of this Thesis, it has been optically monitored what happens upon the addition of CO_2 at constant pressure (10 MPa) to miscible mixtures of water and acetone at different molar proportions and at different temperatures: 298 K, 308 K and 238 K. The compositions at which the phase splits into two different phases, a dense water rich phase and a water lean light phase, have been measured following the experimental protocol described in Section 6.9.1 and using the Variable Volume cell, which is described in Section 6.2.2 of the Experimental Part. The addition of a substance isobaric and isothermally is possible by increasing the volume of the Variable Volume Cell.

Table 4.2 discloses the CO_2 molar fraction (x_{CO_2}) at which the single liquid phase

splits into two liquid phases. Figure 4.3 presents in a ternary diagram the experimentally measured compositions at which different initial mixtures of water/acetone/CO_2 splits into two phases at 10 MPa and different temperatures. The continuous lines represent the working lines, from initial mixtures of water and acetone (50/50, 60/40, 70/30 water/acetone molar relationship) upon the addition of pure CO_2 keeping constant pressure at temperature.

Table 4.2: Compositions of the ternary system water/acetone/CO_2 when the single phase breaks into two liquid phases at 10 MPa and different temperatures.

Water/Acetone (molar relationship)[a]	x_{CO_2} [b]		
	298K	308K	328K
50/50	0.17	0.18	0.20
60/40	-	0.14	-
70/30	0.10	0.12	0.14

[a]Water/Acetone molar relationship of the initial solution,

[b]CO_2 composition where the single phase breaks into 2 liquid phases.

As it is ascertained from Figure 4.3, an increase in temperature from 298 K to 308 K and to 328 K is translated into a decrease in the miscibility gap. As a consequence, the single phase region is increased, this means that at high temperature, more CO_2 is required to break the single phase.

The phase behavior of a system containing water, CO_2 and an organic liquid depends primarily on the hydrogen bonding tendency of the organic liquid [55]. Therefore, monitoring the evolution of hydrogen bonding is a powerful tool to get insights at the molecular level of the phase behavior of the ternary system which permits to relate phase behavior and molecular interactions. Vibrational spectroscopy probes the local environment of a molecule [57] and gives insights about the state of aggregation of the molecules. Hence, Raman Spectroscopy has been proven to be a valuable tool to investigate the nanostructre of several systems [58]. In this Thesis, Raman Spectroscopy has been used to characterize at the molecular level the effect of the addition of compressed CO_2 over a mixture of water and acetone, before the system separates into two liquid phases.

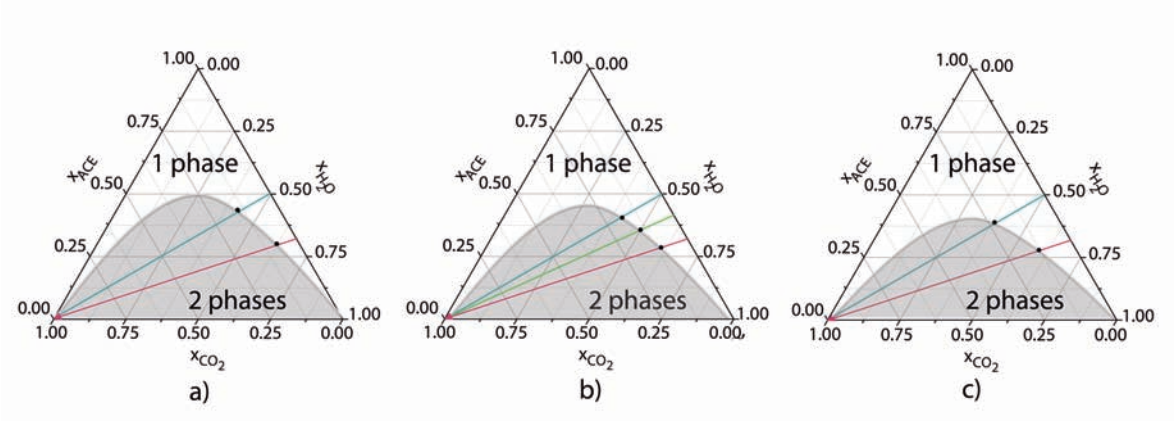

Figure 4.3: Ternary diagram of water/acetone/CO_2 at 10 MPa and at a) 298 K, b) 308 K and c) 328 K. The continuous lines represent the working lines of adding CO_2 to the initial mixtures of water/acetone: mixture 50/50 blue line, mixture 60/40 green line and mixture 70/30 pink line. The black dots represent the compositions where the single phase splits into 2 liquid phases (values from Table 4.2).

4.2.2 Raman Spectroscopy characterization of microemulsion-like systems

Raman spectroscopy provided evidence into the state of aggregation of water molecules in the ternary systems at high pressure. The Raman spectrum of the OH stretch vibration of the water molecules gives insights into the development of hydrogen bonding at a molecular level. Raman spectroscopy is probably the most important of the techniques which has been employed to obtain information relating the intra- and inter-molecular vibrational modes of liquid water. Liquid water may have as many as seven fundamental intramolecular vibrational distributions and as many as nine intermolecular vibrational distributions. The use of the term distributions refers to the fact that all modes are inhomogeneously broadened, i.e., the bond lengths and bond angles are widely distributed due to intermolecular interactions. The various Gaussian Raman OH-stretching components are thought to arise from various amounts of hydrogen bonding and their intensities change with rising temperature [59].

The formation and destruction of hydrogen bonds could be monitored by the signature of the OH-vibration band between 3000 and 3800 cm^{-1} for liquid water (also true for liquid alcohols). This band is sensitive for changes in temperature, pressure and composition over a wide range [58, 60]. Increasing pressure, decreasing temperature or concen-

trating the water content leads to an intensification of the hydrogen bonds and vice versa as Figure 4.4 presents.

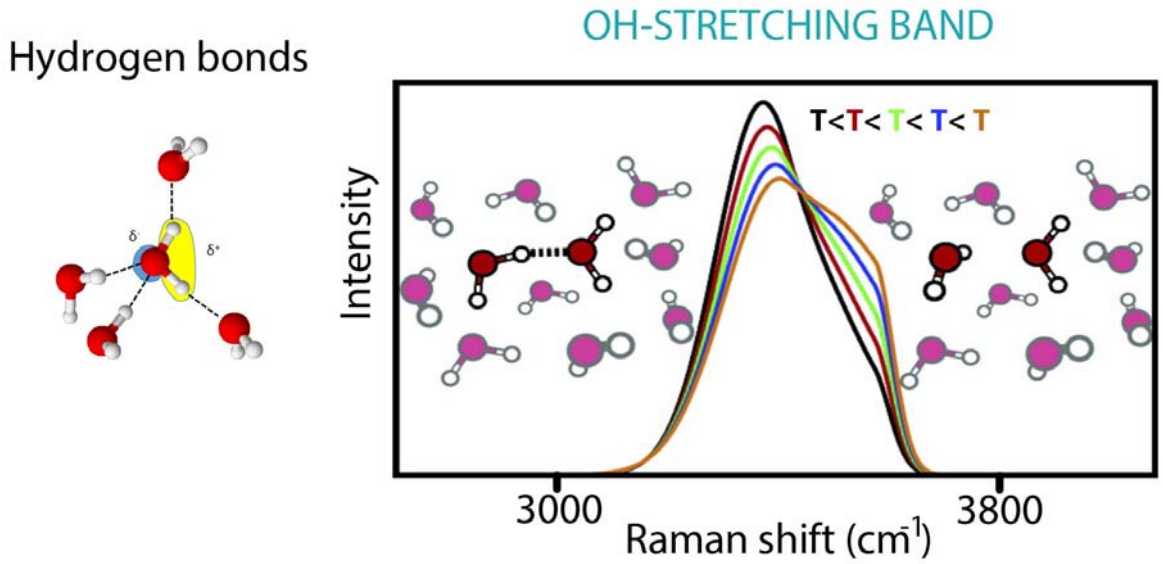

Figure 4.4: OH stretching band of water: as temperature increases, the mean distance between water molecules decreases which means there is a loosening of hydrogen bonds. This is reflected by an increase of the higher-frequency peak intensities. Conversely, when temperature decreases, water molecules are closer and there is an increase of the lower-frequency peak intensities.

The deconvolution of the OH-vibration band shows that the intensification of the hydrogen bonds is reflected by an increase of the lower-wavenumber peak intensities while a loosening of hydrogen bonds is reflected by an increase of the higher-wavenumber peak intensities [61]. Actually, the entire OH-vibration band between 3000 and 3800 cm^{-1} consists of several (the number and the central wavenumbers are debated [62]) peaks which make the detailed evaluation of the signal complex and the interpretation at least controversial [63]. Nevertheless, following the previously made remarks, there is a consensus in literature that contributions at high wavenumbers can be assigned to the least bonded molecules, and contributions at lower wavenumbers can be assigned to the hydrogen bonded molecules. These remarks are valid for infrared absorption spectroscopy as well as for Raman spectroscopy. Raman signals (here between 3050 and 3450 cm^{-1}) can be assigned to the hydrogen bonded water molecules (I_b) and the high wavenumber Raman signals (here between 3450 and 3850 cm^{-1}) can be assigned to the least bonded water

molecules (I_{nb}) . The wavenumber position of the temperature-isosbestic point [64] of the Raman OH stretch vibration of pure liquid water at 3450 cm^{-1} defines the border between bonded and least (here called *non-bonded*) Raman signals. Following the previously made remarks, the ratio of both intensities provides information regarding the development of the hydrogen bonds in the mixture. Hence, an OH ratio has been defined according to these observation:

$$R_{OH} = \frac{I_b}{I_{nb}} . \tag{4.1}$$

This ratio indicates the relation between the proportion of the more bonded water molecules and the less bonded water molecules (Figure 4.5). According to equation 4.1, the higher R_{OH} is, the stronger is the development of hydrogen bonds.

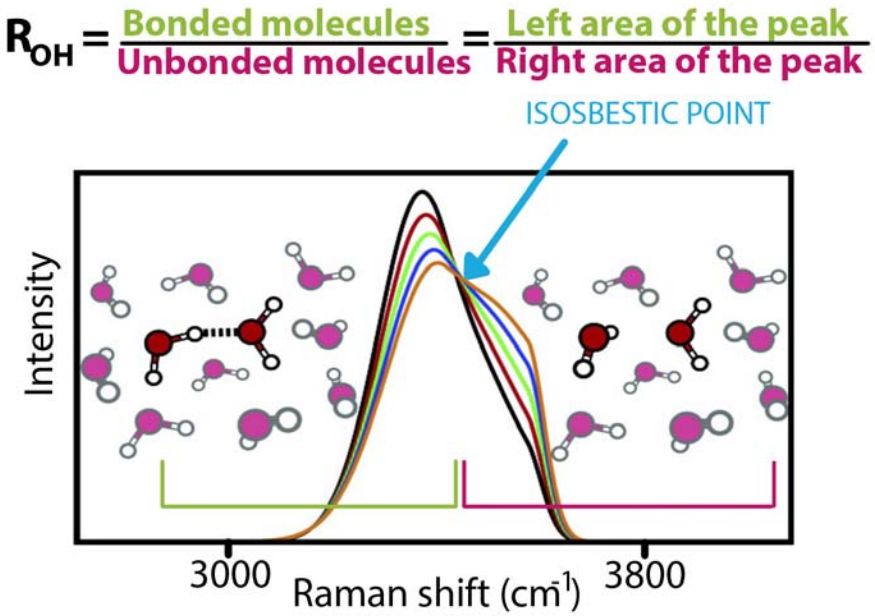

Figure 4.5: Representation of how the R_{OH} is obtained from the OH stretching band of water.

The advantage of the applied technique is its convenience. The detailed description of the Raman set-up, the acquisition of spectra and the treatment of those to calculate the R_{OH} is explained in Sections 6.9.4, 6.9.6 and 6.9.7, respectively.

4.2.3 Evolution of the R_{OH} in the Water/Acetone/CO_2 system

Initial mixtures of water and acetone have been diluted by adding a third component: CO_2 or acetone. The addition has been performed at 10 MPa and 308 K isobaric and isothermal following the experimental protocol described in Section 6.9.6 of the Experimental Part. The addition of CO_2 and acetone has been monitored by Raman Spectroscopy. Figure 4.6 depicts the OH stretching band of water upon the addition of CO_2 for the mixture 50/50.

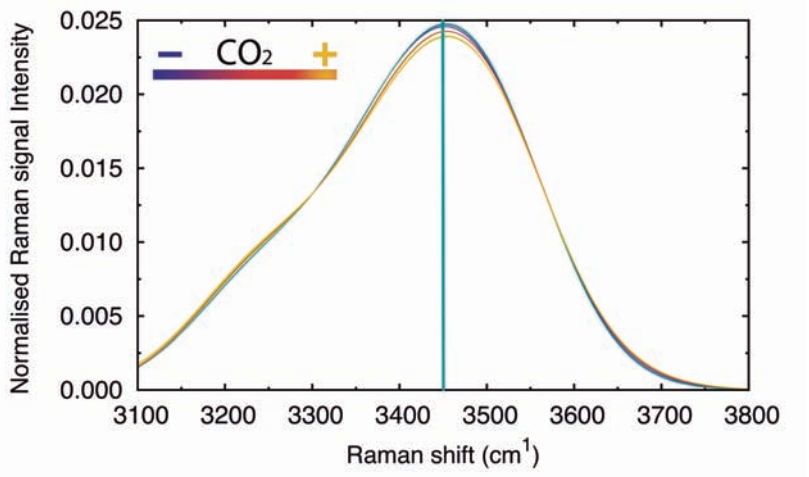

Figure 4.6: OH stretching band of water of the mixture water/acetone 50/50 upon the addition of CO_2. The blue line marks the point chosen to calculate the R_{OH} (temperature-isosbestic point of water).

The R_{OH} has been computed from the OH stretching vibration Raman signal of water (Figure 4.6) to monitor the evolution of the development of hydrogen bonding between water molecules, according to the methodology explained in detail in Section 6.9.7. Figure 4.7 plots the evolution of the R_{OH} when adding CO_2 and when additing acetone to initial mixtures of water/acetone 50/50 and 60/40 as a function of the molecular density of water (ρ_{H20}) defined as moles of water divided by the volume of the cell. ρ_{H20} gives information about the evolution of bulk water density upon the addition of CO_2 and the probability of a water molecule to be close to another water molecule.

When the initial mixtures of water and acetone are diluted with pure acetone, the evolution of the R_{OH} for the initial mixtures 50/50 and 60/40 is the same and the ratio linearly decreases, which means that the effective distance between water molecules decreases. Hence, the addition of acetone isobaric and isothermally to the initial mixture of

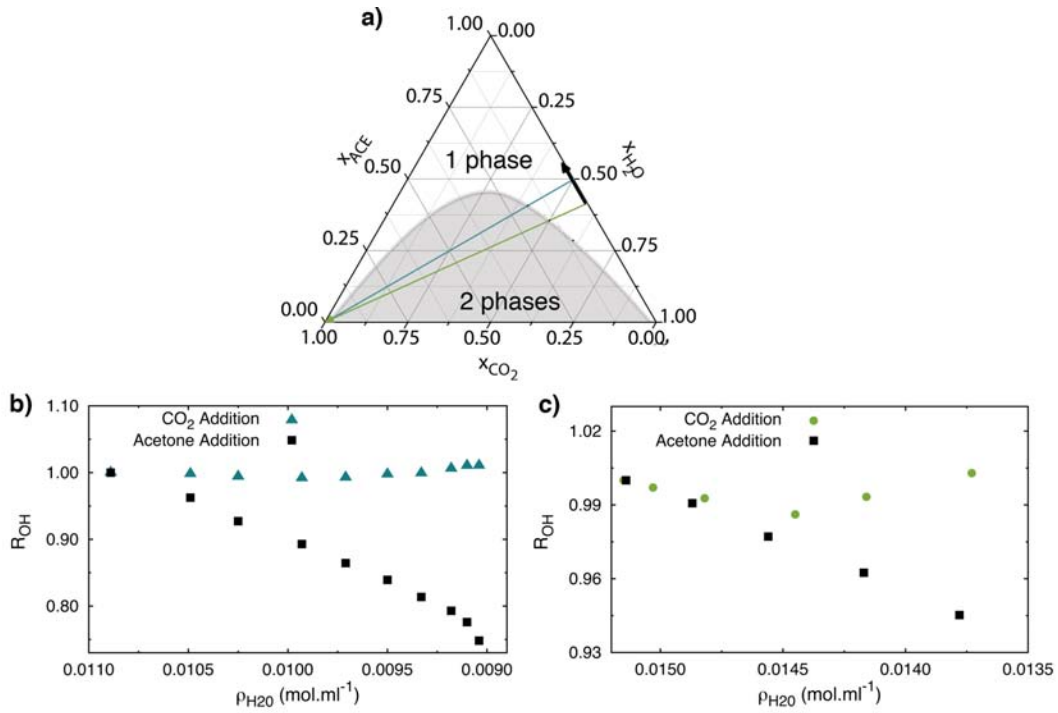

Figure 4.7: a) Composition evolution of the system upon progressive addition of acetone (black arrow) and CO_2 over the initial mixtures, 50/50 (blue line) and 60/40 (green line) represented in a ternary diagram. b) Comparison of the R_{OH} ratio as a function of the water density (water mols/cell volume) of the mixture 50/50 during the addition of CO_2 (blue triangles) and the addition of acetone (black squares) at 10 MPa and 308 K. c) Comparison of the R_{OH} ratio as a function of the water density (water mols/cell volume) of the mixture 60/40 during the addition of CO_2 (green dots) and the addition of acetone (black squares) at 10 MPa and 308 K.

water/acetone 50/50 and 60/40, dilutes the water molecules. However, the tendency of the R_{OH} upon the addition of CO_2 over these initial mixtures of water and acetone until phase separation occurs is different that in the case of the addition of acetone. The tendency of the R_{OH} for the addition of CO_2 to the mixtures 50/50 and 60/40 (water/acetone molar relationship) is the same for both mixtures. Small additions of CO_2 make R_{OH} to decrease, which means that the effective distance between water molecules increases (the proportion of less bonded molecules is increased). However, if the addition of CO_2 continues, R_{OH} increases until phase separation takes place. An increase of R_{OH} means that the effective distance between the water molecules is decreased. In other words, from a

certain point of the ternary mixtures (ρ_{H20}=0.01445 mol/mL,ρ_{H20}=0.0097mol/mL for the mixtures 60/40 and 50/50 respectively), the addition of CO_2 reduces the mean distance between water molecules, that is, water molecules tend to be more bonded forming clusters.

The R_{OH} ratio has also been calculated for the addition of CO_2 over the initial mixture 70/30 (water/acetone molar relationship). Figure 4.8 presents the evolution of the R_{OH} for the three initial mixtures 70/30, 60/40 and 50/50 at 10MPa and 308K.

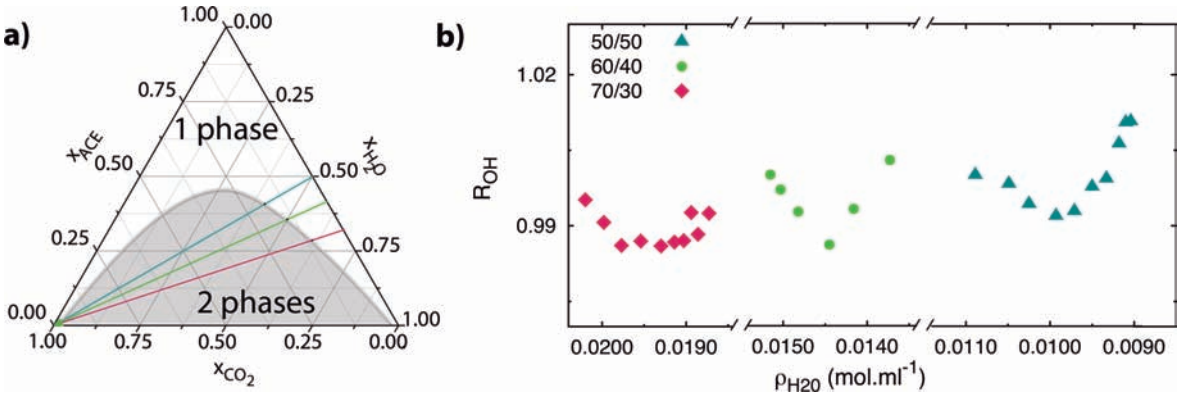

Figure 4.8: a) Composition evolution of the system upon progressive addition of CO_2 over the 3 initial mixtures, 50/50 (blue line), 60/40 (green line) and 70/30 (pink line) represented in a ternary diagram. b) Evolution of the R_{OH} ratio as a function of the water density (water mols/cell volume) of the mixtures 50/50 (blue triangles), 60/40 (green dots) and 70/30 (pink diamonds) during the progressive addition of CO_2 at 10 MPa and 308 K.

It can be ascertained that the tendency followed by the R_{OH} is the same for the there initial mixtures. In the mixture 70/30, from a ρ_{H20}= 0.01914mol/mL, the water molecules distance decreases, meaning that water molecules are more bonded.

If water molecules cluster to water-rich regions, other water-lean nanoscopic regions should exist with higher acetone and CO_2 content relative to the bulk. Therefore, although the system is a single transparent phase macroscopically homogenous, it presents an organization at the nanoscopic scale formed by domains of different nature. The system water/acetone/CO_2 at certain conditions of composition, temperature and pressure displays the physical characteristics of a surfactant-free microemulsion-like systems.

This phenomenom of forming water clusters is not observed when the initial mixtures are diluted with acetone instead of with CO_2 as can inferred from Figure 4.7.

Effect of Temperature over the microemulsion-like structure

In order to get more knowledge about the relation between phase behavior and molecular interactions of the ternary mixture composed of water/acetone/CO_2 and with the aim of gaining more understanding regarding the formation of water-rich clusters in the single phase region of this ternary mixture, the evolution of R_{OH} upon the addition of CO_2 over homogenous mixtures of water and acetone at different temperatures has been monitored. The experimental protocol followed is the same as the one used to characterize the system at 308 K and it is explained in detail in Section 6.9.6 of the Experimental Part.

The phase behavior of the systems at 298 K and 328 K has already been shown (see Figure 4.3). An increase in temperature from 308 K to 328 K is translated into a decrease of the miscibility gap and as a consequence the single phase region is enlarged, meaning, that at high temperature, more CO_2 is required to break the single phase. Conversely, as temperature decreases so does the solubility of the 3 components, and less CO_2 need to be added to split the single phase.

Figure 4.9 depicts the OH stretching band of water for the mixture 50/50 at 298 K (a) and at 328 K (b). As can be inferred, the shape of the OH band changes with temperature, and in agreement with the OH stretching band depicted in Figure 4.4, the left part of the peak decreases with increasing temperature.

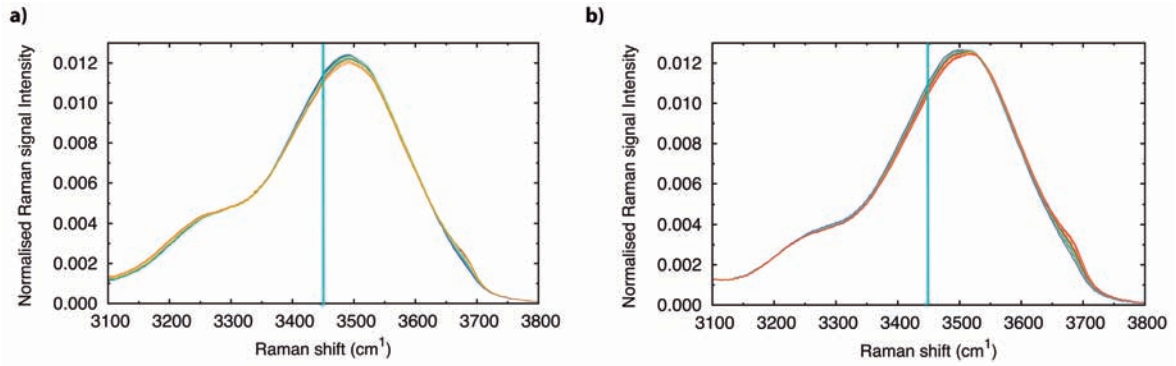

Figure 4.9: OH stretching band of water of the mixture water/acetone 50/50 upon the addition of CO_2 at 298 K (a) and at 308 K (b).

The R_{OH} evolution was monitored upon the addition of CO_2, in this case, only to the initial mixtures of water/acetone with a molar relationship of 50/50 and 70/30 and the measured tendency is plotted in Figure 4.10.

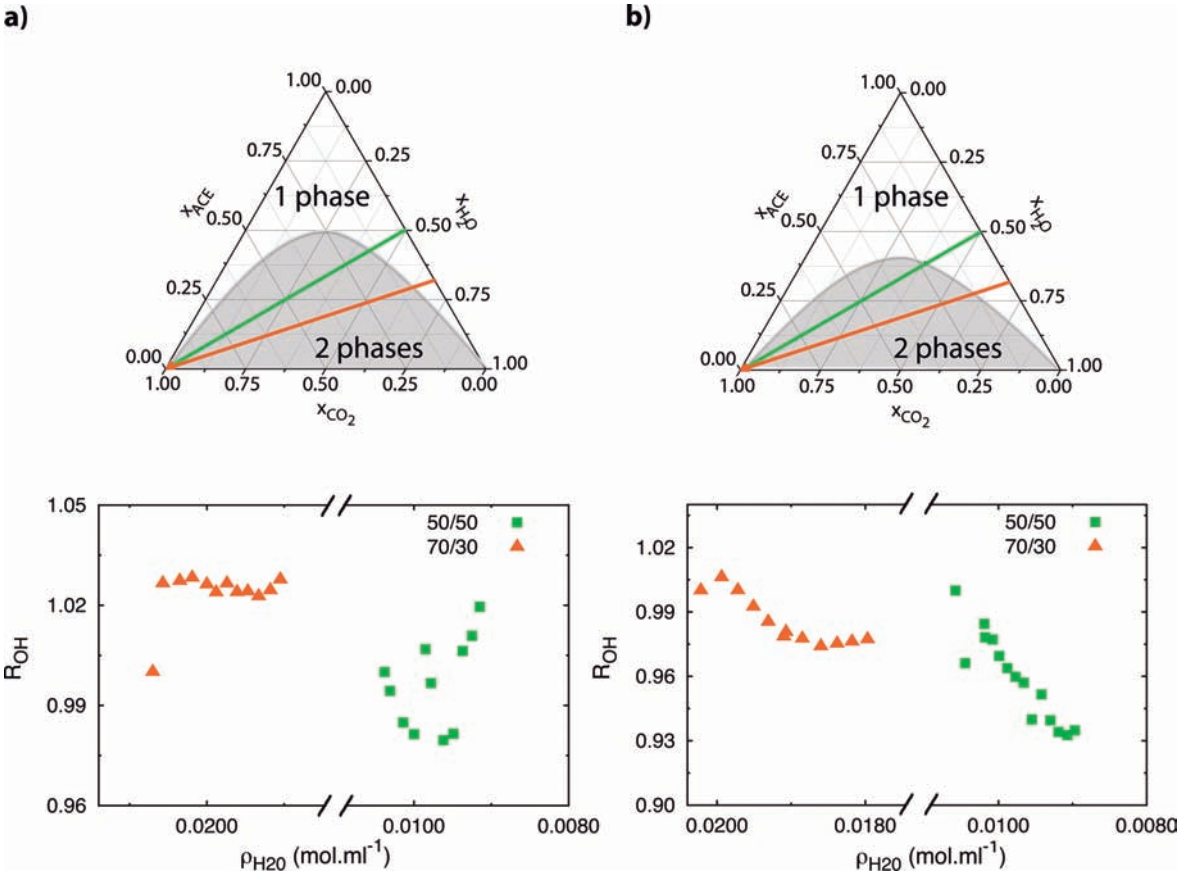

Figure 4.10: a) Upper: Composition evolution of the system upon progressive addition of CO_2 over the initial mixtures, 50/50 (green line) and 70/30 (orangeline) represented in a ternary diagram at 10 MPa and 298 K. Bottom: Evolution of the R_{OH} ratio as a function of the water density (water mols/cell volume) of the mixtures 50/50 (green squares) and 70/30 (orange triangles) during the progressive addition of CO_2 at 10 MPa and at 298 K and b) Composition evolution of the system upon progressive addition of CO_2 over the initial mixtures, 50/50 (green line) and 70/30 (orangeline) represented in a ternary diagram at 10 MPa and 328 K. Bottom: Evolution of the R_{OH} ratio as a function of the water density (water mols/cell volume) of the mixtures 50/50 (green squares) and 70/30 (orange triangles) during the progressive addition of CO_2 at 10 MPa and at 328 K.

The addition of CO_2 at 10 MPa and 298 K (Figure 4.10a) provokes two different scenarios depending on the amount of water in the initial mixture. For the equimolar mixture, the tendency of the R_{OH} is very similar to the one previously observed for the mixtures at 308K: small additions of CO_2 dilutes the water molecules, however, from a certain composition (ρ_{H20} = 0.096 mol/ml), the addition of CO_2 provokes the formation of water clus-

ters, as can be inferred from the increase of the R_{OH}. In the mixture 70/30, the decrease in the R_{OH} with small additions of CO_2 does not occur and therefore, water molecules tend to form clusters since the first addition of CO_2 to the initial mixture. Hence, it can be concluded from the evolution of the hydrogen bonding capacity of water that at 298 K, the liquid mixture presents a certain nanostructure in terms of domains of different nature. In the mixture 50/50, the nanostructuring appears at compositions of ρ_{H20} = 0.096 mol/ml until phase separation occurs. In the water richer mixture (70/30) the formation of nano domains takes place since the first addition of CO_2.

At high temperature (Figure 4.10b), CO_2 addition over the initial mixture 50/50 makes the water molecules to be less bonded as can be observed from the continuos decrease of the R_{OH}. Just before phase separation occurs, it can be seen a slight increase of the R_{OH} ratio, but much less pronounced that for the mixture at 308 K. The same conclusion can be withdrawn from the evolution of the R_{OH} ratio in the mixture 70/30. Therefore, the evolution of the R_{OH} ratio reveals that the microemulsion-like structure is not formed at 328 K where the miscibility of the 3 components is higher.

An important conclusion can be withdrawn from the comparison of the evolution of the R_{OH} at the three different temperatures for the initial mixtures studied. It is possible to relate the phase behavior of the system to the molecular interactions and to the state of aggregation of water molecules, as the most pronounced structuring occurs when the miscibility region is smaller.

4.2.4 Microemulsion-like solubilization capacity

In order to further support the hypothesis of the existence of water-rich and water-lean domains in a clear solution, the solubilization power of this microemulsion-like system was assessed. For this reason, a widely known poor water soluble compound, ibuprofen (see Chapter 1) was chosen as a non-water and non-CO_2 soluble compound (solubility of ibuprofen in water = $0.18{\cdot}10^{-5}$ mol·mol^{-1} [65] and solubility of ibuprofen in CO_2 = $0.13{\cdot}10^{-2}$ mol·mol^{-1} [66]). However, ibuprofen is known to present a high solubility in pure acetone and in CO_2-expanded acetone at the working conditions of temperature and pressure [67]. Figure 4.11 presents the solubility curve of ibuprofen in CO_2-acetone mixture at 10 MPa and 298 K, where it can be ascertained that CO_2 acts as a co-solvent for a wide range of CO_2 molar fractions. The solubilization experiment of ibuprofen in the microemulsion-like system is conducted at 308 K. An increase of temperature increases

the solubility of ibuprofen in the system.

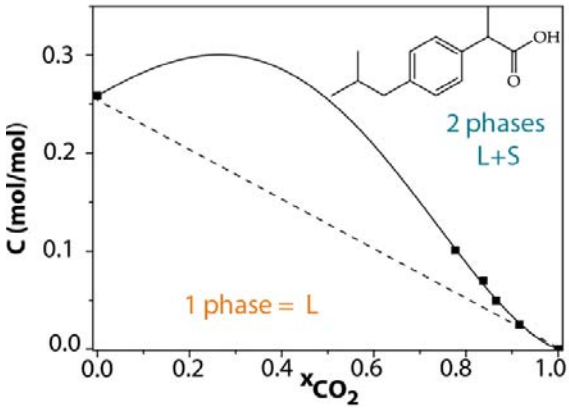

Figure 4.11: Solubility curve of ibuprofen in CO_2-expanded acetone at 10 MPa and 298 K [67].

The solubilization experiments were conducted in the High pressure Variable Cell described in Section 6.2.2 of the Experimental Part and following the experimental procedure presented in Section 6.9.8 of the same Chapter. Experiments were carried out at constant pressure (10 MPa) and temperature (308 K). Briefly, the experiments were conducted as the following: a certain solution of ibuprofen in acetone is prepared and charged into the High Pressure Variable Volume Cell, which was previously driven to the working temperature. Then, a certain volume of water was added to have the desired molar relationship between water and acetone. The addition of water provokes the precipitation of ibuprofen by its anti-solvent behavior. Then, CO_2 was added very slowly keeping pressure and temperature constant. The addition of a third component keeping pressure and temperature constant is possible thanks to the movable piston of the Variable Volume Cell that allows to increase the volume of the Cell. The addition is stopped when a single transparent phase is observed.

Ibuprofen is precipitated in the initial mixture of water/acetone, and by the addition of CO_2, it has been possible to dissolve it as a single transparent phase is obtained. This is unexpected as the dissolution is achieved by adding a solvent where ibuprofen is very poorly soluble. Hence, the solubilization of ibuprofen supports the conclusions obtained from the Raman spectroscopy characterization: the addition of CO_2 over initial mixtures of water/acetone provokes the structuration of the system at the nanoscale. As ibuprofen is neither soluble in water nor in CO_2, it should be dissolved in the water-lean domains of

the microemulsion-like system.

Figure 4.12 shows how from an initial state (a), where ibuprofen is precipitated in the mixture of water/ acetone, a single transparent phase is obtained by the addition of CO_2. The appearance of this single transparent phase reveals that ibuprofen is dissolved in the water-lean domains.

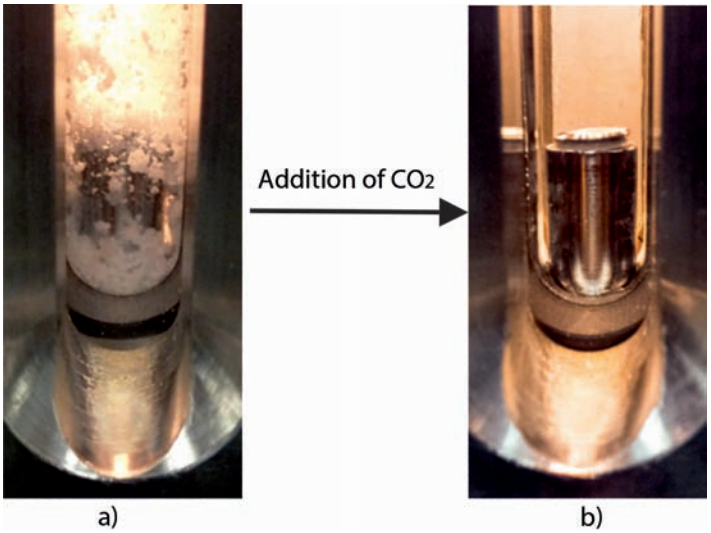

Figure 4.12: Microemulsion-like solubilization powder: ibuprofen is precipitated in the initial mixture of water/acetone (50/50) at 10 MPa and 308 K (a) and upon the addition of CO_2 a single transparent phase is obtained (b).

Table 4.3 discloses the different condition explored for the solubilization experiments for the 3 different molar compositions of water and acetone. For the mixture 60/40, two amounts of ibuprofen were dissolved. In all the experiments presented in Table 4.3 a single phase was obtained by the addition of CO_2.

Table 4.3: Ibuprofen solubilization in the domains of the microemulsion-like system

Experiment	Water/Acetone (molar relationship)	Ci(mol/mol)[a]
1	50/50	0.278
2	60/40	0.278
3	60/40	0.371
3	70/30	0.278

Solubilization of Ibuprofen in the domains of the microemulsion-like systems performed at P = 10 MPa and T = 308 K,[a] concentration of Ibuprofen in acetone expressed as mol/mol

4.2.5 Summary

- The phase behavior of the ternary system Water/Acetone/CO_2 at 10 MPa and at different temperatures (298 K, 308 K and 328 K) has been assessed. Homogeneous mixtures of water and acetone can be split into two liquid phases by the addition of CO_2 at high pressure. In addition, it has been experimentally proven how as temperature increases, miscibility of the three components increases.

- Raman Spectroscopy has been successfully used for monitoring the evolution of the hydrogen bonds of water during addition of CO_2 over initial mixtures of water and acetone. The OH stretching band of water turned out to be a very useful tool for evaluating the mean distance between water molecules during addition of CO_2 over initial mixtures of water and acetone until phase separation takes place. Based on this peak, a ratio has been defined (R_{OH}) which gives information of how bonded water molecules are.

- Raman Spectroscopy reveals that small additions of CO_2 increase the mean distance between water molecules. However, if the addition of CO_2 continues, but still in the single phase region, it has been assessed how water molecules tend to form clusters for the mixtures at 308 K. If there are water-rich regions in the single transparent phase, there should be other water-lean regions. Therefore, at certain conditions of pressure, temperature and composition this system presents a certain structure at the nanoscale while it is macroscoscopically homogeneous.

- The formation of this water-rich domains occurs for different initial compositions

of water and acetone at 10 MPa and 308 K. However, at higher temperature (328 K) where the single phase region is larger, the formation of water clusters does not take place. Conversely, at lower temperature (298 K), the nano structuring is enhanced and starts at smaller additions of CO_2. It has been demonstrated that it is possible to relate phase behavior with interactions at the molecular level.

- In order to support Raman Spectroscopy measurements, the solvation capacity of the water-rich and water-lean domains has been evaluated using a poor water soluble compound that also presents low solubility in CO_2, ibuprofen. It has been possible to dissolve high quantities of this drug in the water-lean domains, probing the salvation capacity of this microemulsion-like system.

4.3 Water/Acetonitrile/CO_2 system

It is very interesting to investigate, from a theoretical and practical point of view, if the formation of domains of clearly different composition in macroscopically homogenous mixtures of water/organic solvent/CO_2 at high pressures can occur in other ternary systems. Based on this, it was proposed to explore new possibilities of CO_2-based surfactant-free microemulsion-like systems. This section, therefore is dedicated to extend the possible ternary systems sensitive to form microemulsion-like structures.

The ternary system should fulfill the same conditions as the water /acetone/ CO_2 system. The acetonitrile/ water/ CO_2 was chosen because its high pressure phase behavior is very similar to the former. The water-acetonitrile mixture can be split into two phases upon the addition of CO_2: a dense water-rich phase and a lighter water-lean phase, richer in the mixture of CO_2-expanded acetonitrile, as in the case of the water/acetone/CO_2 ternary system [68]. Acetone and acetonitrile are both polar aprotic organic solvents with large dipole moments that can accept hydrogen bonds [69].

The same experimental protocol employed to determine the existence of nano domains of different nature in mixtures of water/acetone/ CO_2 at high pressure before phase separation was applied to characterize the new ternary system composed of water/ acetonitrile/ CO_2. The protocol is presented in Section 6.9.6 of the Experimental Part.

4.3.1 High pressure phase equilibria

As mentioned, knowledge of the phase behavior of the mixture at high pressure is essential. The ternary mixture water/acetonitrile/CO_2 is not so studied as the acetone one, and the phase equilibria at 10 MPa have not been found reported in the literature.

The addition of CO_2 was performed over initial mixtures of water and acetonitrile with the same molar proportion as in the case of acetone: 50/50, 60/40 and 70/30. The composition at which the single phase breaks into two separate phases, a dense water-rich phase and a light water-lean phase, has been measured following the same experimental protocol as in the previous ternary mixture, which is described in detail in Section 6.9.1 of the Experimental Part.

Figure 4.15 presents the high pressure ternary diagram of the water/acetonitrile/CO_2 system at 10 MPa and 308 K. The compositions at which the single phase breaks into two liquid phases are disclosed in Table 4.4. As it is shown, the miscibility region of the ternary

diagram is smaller than for the ternary diagram of water/acetone/CO_2 at the same conditions of pressure and temperature.

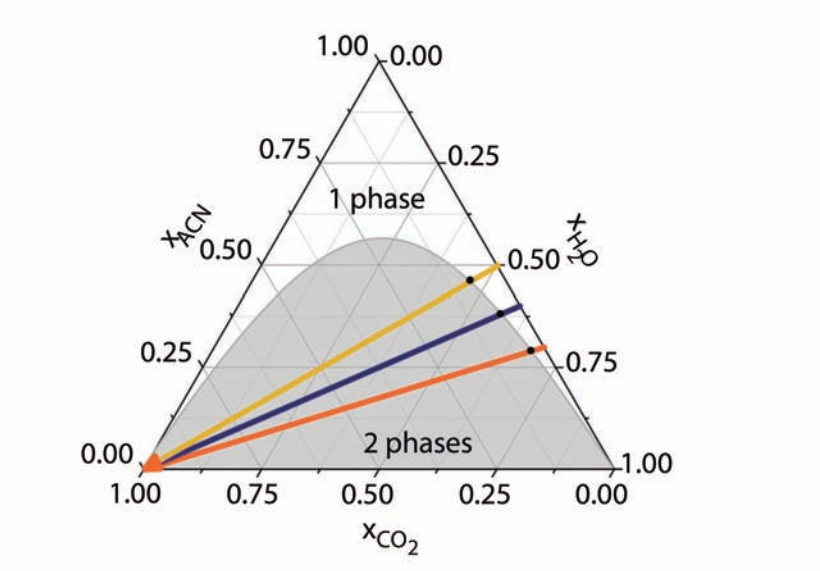

Figure 4.13: Ternary diagram of water/acetonitrile/CO_2 at 10 MPa and at 308 K. The continuous lines represents the working lines of adding CO_2 to the initial mixtures of water/acetonitrile: mixture 50/50 yellow line, mixture 60/40 dark blue line and mixture 70/30 orange line.

Table 4.4: Compositions of the ternary system water/acetonitrile/CO_2 when the single phase breaks into two liquid phases at 10 MPa and 308 K.

Water/Acetonitrile (molar relationship)[a]	x_{CO_2} [b]
50/50	0.09
60/40	0.06
70/30	0.04

[a]Water/Acetonitrile molar relationship of the initial solution,

[b]CO_2 composition where the single phase breaks into 2 liquid phases.

4.3.2 Raman spectroscopy characterization of microemulsion-like systems

The monitoring of hydrogen bond capacity of water molecules in the system water/ acetonitrile upon the addition of CO_2 and acetonitrile has also carried out. The same procedure as in the water/acetone/CO_2 system was followed, which is described in detail in Section 6.9.6 of the Experimental Part.

The R_{OH} has been calculated from the OH stretching band of water when CO_2 and acetonitrile has been added isobaric (10 MPa) and isothermally (308 K) to an initial mixture 50/50 water/acetonitrile. Figure 4.14 depicts the comparison of the evolution of the R_{OH} for both scenarios. In the acetonitrile/ water/CO_2 system the evolution of the R_{OH} when adding CO_2 to the mixture 50/50 is different as in the acetone system. In the mixtures with acetonitrile, the ratio always increases. This means that, since the first addition of CO_2, the CO_2 does not dilute the water molecules. Small additions of CO_2 make the water molecules to be closer. However, when the initial mixture 50/50 water/acetonitrile is diluted with pure acetonitrile, the addition of the latter makes the water molecules to be more diluted as the R_{OH} always decrease.

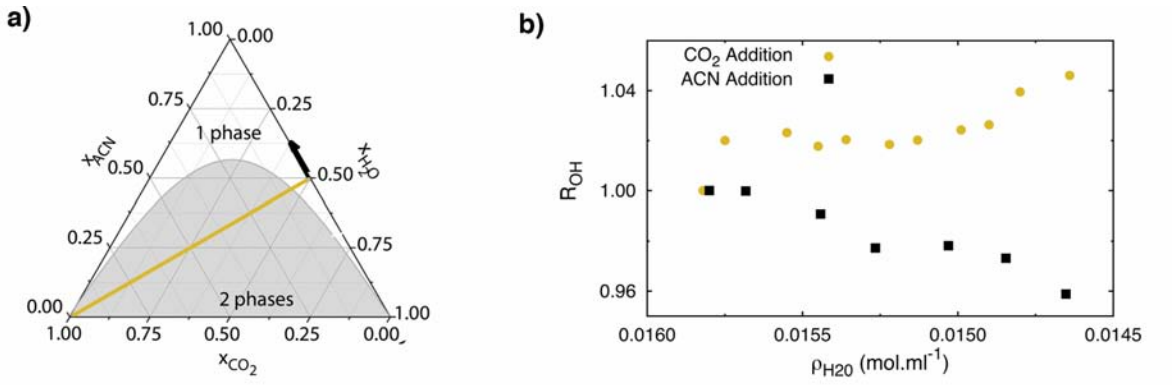

Figure 4.14: a) Composition evolution of the system upon progressive addition of acetonitrile (dark arrow) or CO_2 over the initial mixture 50/50 (yellow line) represented in a ternary diagram. b) Comparison of the evolution of the R_{OH} ratio as a function of the water density (water mols/cell volume) of the mixture 50/50 during the progressive addition of acetonitrile (black squares) and the addition of CO_2 (yellow dots) at 10 MPa and 308 K.

The evolution of the R_{OH} for the addition of CO_2 over the three different initial mixtures of water/acetonitrile: 50/50, 60/40 and 70/30 has also been assessed and the ten-

dency observed in depicted in Figure 4.15.

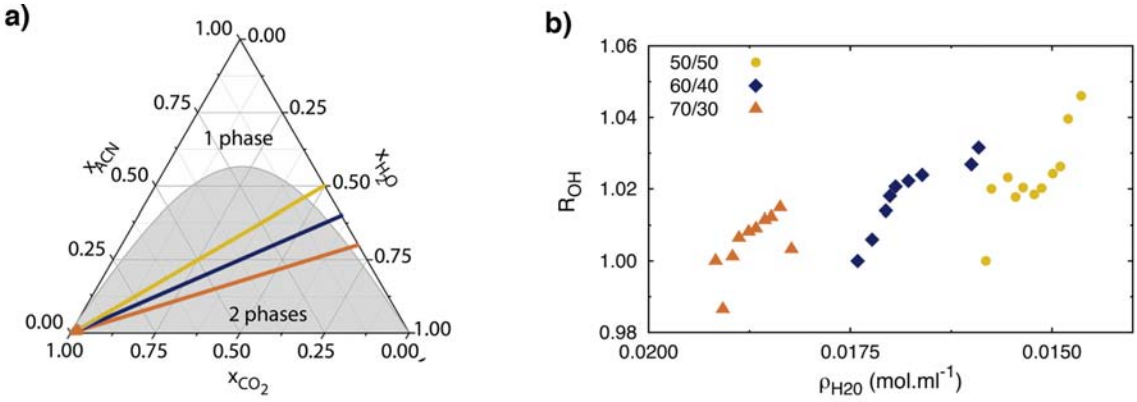

Figure 4.15: a) Composition evolution of the system upon progressive addition of CO_2 over the initial mixtures, 50/50 (yellow line), 60/40 (dark blue) and 70/30 (orange line) represented in a ternary diagram. b) Evolution of the R_{OH} ratio as a function of the water density (water mols/cell volume) of the mixtures 50/50 (yellow dots), 60/40 (dark blue diamonds) and 70/30 (orange triangles) during the progressive addition of CO_2 at 10 MPa and 308 K.

In the case of acetonitrile/water mixtures, the addition of CO_2 never increases the mean distance between water molecules as R_{OH} never decreases. Since the first addition of CO_2, the R_{OH} increases for the 3 mixtures, meaning that the water molecules tend to form clusters since the beginning of the addition of CO_2. As in the water/acetonitrile/CO_2 the miscibility between the three components is smaller than in the water/acetone/CO_2 system at the working conditions, the nanostructuring starts at smaller CO_2 concentrations. These results are in agreement with the observations ascertained from the experiments at 298 K: the shorter the miscibility region, the sooner the nanostructuring takes place.

The difference in the behavior of the evolution of the R_{OH} for the mixtures of water/acetone and water/acetonitrile upon the addition of cCO_2 at high pressure can be explained by the tendency of these organic solvents of forming hydrogen bonds with water. Acetonitrile forms fewer hydrogen bonds with water that does acetone at water-rich compositions, therefore the formation of water nanodomains in the ternary mixture of water/acetonitrile/CO_2 is easier than in the water/acetone/CO_2 system as the interaction between water and acetonitrile is not so strong as the water-acetone interaction [69]. Moreover, in polar CO_2-expanded solvents, such as a CO_2-expaned acetonitrile, signifi-

cant solvent sorting occurs and the presence of CO_2 is far more effective at inducing clustering of acetonitrile molecules than of acetone molecules [53].

4.3.3 Microemulsion-like solubilization capacity

As in the case of the acetone/water/CO_2 ternary system, the solvent power of the microemulsion-like was evaluated. The protocol followed was the same as the previous one and it is described in Section 6.9.8 of the Experimental Part. In this case, instead of using ibuprofen as a model drug, the thiadiazoline derivative NP was the compound chosen for probing the solubilization capacity of the microemulsion-like system composed of water/acetonitrile/CO_2. As described in Chapter 1, NP as ibuprofen, presents very low solubility in water.

In this case, the achievement of a single transparent phase was possible only with the initial mixture of 60/40 and working with an initial concentration of NP in acetonitrile of $2.2{\cdot}10^{-3}$ mol/mol.

4.3.4 Summary

- A ternary system with a very similar behavior at high pressure to the Water/Acetone/CO_2 system has been identified, composed of Water/Acetonitrile/CO_2.
- The phase behavior of the Water/Acetonitrile/CO_2 at 10 MPa and 308 K has been experimentally measured. The miscibility of these three components at those conditions is smaller than for the system Water/Acetonitrile/CO_2.
- The hydrogen bonding tendency of water molecules has been experimentally measured by Raman Spectroscopy. In this system, since the first addition of small quantities of CO_2, water tends to form clusters.
- The solvation capacity of the domains present at the nanoscale in the system water/ acetonitrile/ CO_2 has been tested using a poor water soluble compound, NP. It has been possible to dissolve this drug in the water-lean domains of the microemulsion-like system.

4.4 Molecular Dynamics Simulations

Molecular Dynamic (MD) simulations consist of solving numerically the equations of motion for the atoms making up the system wanted to simulate. The simulations were conducted by Dr. Jordi Faraudo from the Instituto de Ciencias de los Materiales de Barcelona, (ICMAB).

Using MD simulations, an atomistic interpretation of the previous experimental results on the microemulsion-like behavior of the water/acetone/CO_2 ternary mixture can be provided. The possibility of replacing acetone by other organic solvents has also been explored. As an example of a representative system of the microemulsion-like behavior of the mixture water/acetone/CO_2, a specific composition of the system for the mixture water/acetone 50/50 has been considered at 10 MPa and 308 K. This specific composition has been chosen in the region where Raman Spectroscopy reveals the existence of water clusters. The point in the ternary system selected has been the one with a ρ_{H20}=0.092 mol/mL. In Figure 4.16, a snapshot illustrating the simulation results is shown and in Figure 4.17 a quantitative structural analysis based on radial correlation functions is presented.

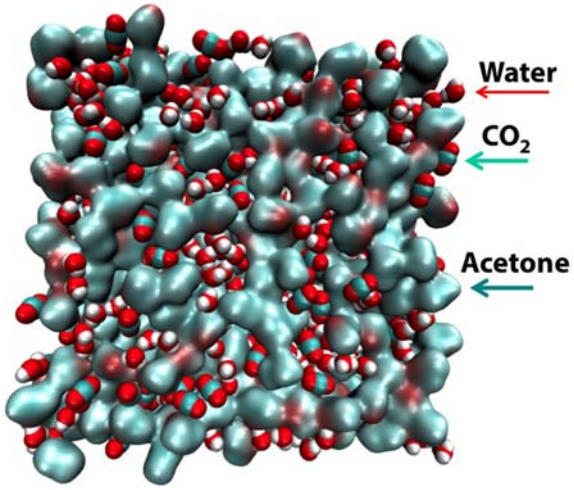

Figure 4.16: Snaphot from MD simulations of the Water/Acetone/CO_2 ternary mixture at ρ_{H20}=0.092 mol/mL, 10 MPa and 308 K. Water and CO_2 molecules are shown as spheres with Van deer Waals radius. Acetone molecules (which form a network across the system) are shown as a surface calculated using the molecular surface solver of VMD [70] with a 1.4 Å probe radius. The employed color code is red for O, white for H and cyan for C.

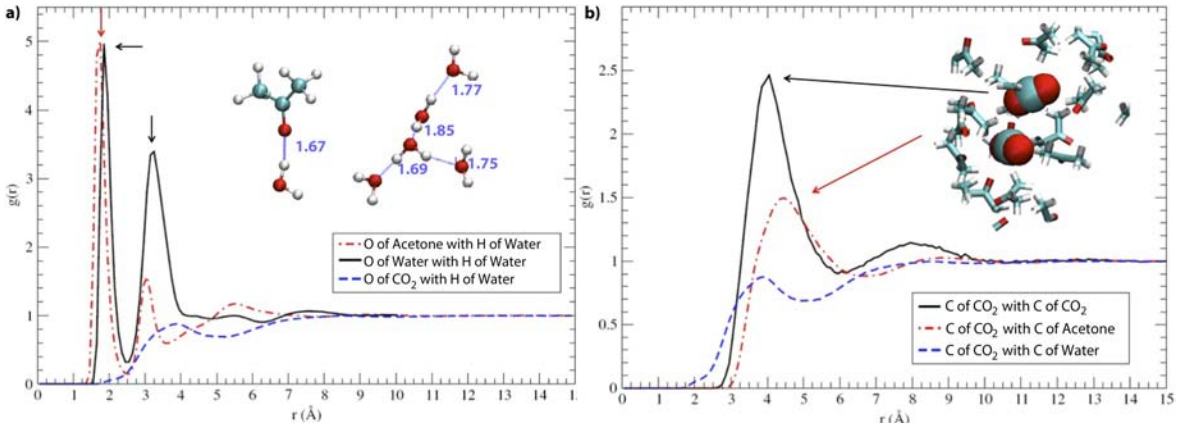

Figure 4.17: Radial distribution functions calculated from MD simulations of the ternary Water/Acetone/CO_2 mixture (10 MPa and 308K, ρ_{H20}=0.092 mol/mL, mixture 50/50) a) Correlations of water (H atom) with: O atoms from acetone (red dashed-dotted line), O atoms from water (solid black line) O atoms from CO_2 (blue dashed line). b)Correlations of C atoms from CO_2 with C atoms from CO_2 (solid black line) or C atoms from Acetone (read dashed-dotted line). CO_2-water correlations from the top panel are also reproduced here. The insets show typical molecular configurations corresponding to the peaks indicated with arrows.

The observed nanostructuration can be described as follows. There is a (possibly bicontinuous) network of acetone molecules distributed over the whole system, which contains pockets with hydrogen bonded water molecules. CO_2 molecules are distributed homogeneously across the system but avoiding contact with water rich pockets. The resulting structure can be understood by noting that acetone molecules have favorable interactions with both water and CO_2 but water and CO_2 tend to repel each other. Acetone is able to make hydrogen bonds with water through the carbonyl group, as demonstrated by the sharp peak at 1.7 Å in the acetone-water correlation function (Figure 4.17a). Acetone is also able to interact favorably with CO_2 through the apolar methyl groups, as denoted also by a clear peak in the acetone-CO_2 correlation function (Figure 4.17b). The peaks in the correlation functions also indicate that the acetone-CO_2 interaction is not as strong as the acetone-water interaction. Water molecules are found in partially ordered structures, evidenced by the presence of two sharp peaks in the correlation function (at 1.8 Å and 3.2 Å). A typical water cluster contributing to the peaks in the correlation function is also shown in Figure 4.17a. Also, water tends to be anticorrelated with (effectively repelled by)

CO_2, and the correlation function reaches the value 1 (no correlation) after distances of about 1 nm. On the other hand, the broad peaks in the CO_2 radial correlation functions shown in Figure 4.17b indicate that CO_2 molecules tend to be coordinated both with other CO_2 molecules and acetone molecules. In Figure 4.17b it is also shown a typical configuration contributing to these broad peaks in the CO_2-CO_2 and CO_2-acetone correlation functions. Typically, two or three CO_2 molecules (with C-C distance about 4 Å) are found that are surrounded by acetone molecules (with a peak at a carbon-carbon separation of 4.4 Å).

It is also instructive to compare the simulation results for the ternary water/acetone/CO_2 mixture with the results for the binary equimolar mixture acetone-water. Figure 4.18 displays the comparison of the radial correlation functions in the binary and ternary mixtures.

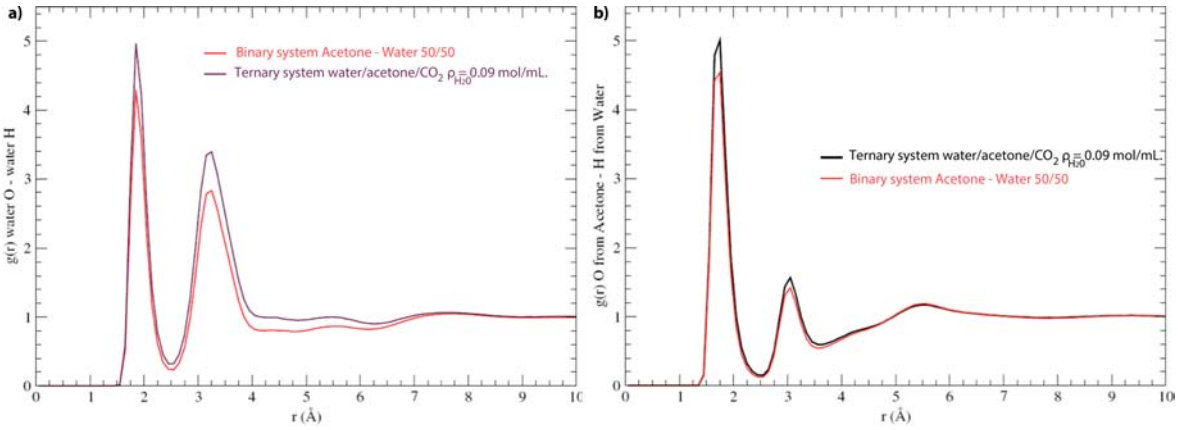

Figure 4.18: a) Comparison between the water (O)-water (H) radial distribution function obtained in presence (purple line) or absence (red line) of CO_2. The black line is calculated from the simulations of the water/acetone/CO_2 ternary mixture (10 MPa and 308 K, ρ_{H20}=0.092 mol/mL, mixture 50/50) and the red line from the simulations of the Water/acetone equimolar mixture also at 10 MPa and 308 K. b) Comparison between the radial distribution function between acetone (O atom) and water (H atom) obtained in presence (black line) or absence (red line) of CO_2. The black line is calculated from the simulations of the water/acetone/CO_2 ternary mixture (10 MPa and 308 K, ρ_{H20}=0.092 mol/mL, mixture 50/50) and the red line form the simulations of the water/acetone equimolar mixture also at 10 MPa and 308 K.

Water-water and acetone-water correlation functions show the same features found here for the ternary system, but the correlation peaks discussed previously have lower

values for the binary system. In other words, addition of CO_2 increases the estructuration of water and also increases the acetone-water interaction. The comparison between the acetone hydrogen-oxygen correlation function in the binary and ternary system are depicted in Figure 4.19. Interestingly, there is more hydrogen bonding between acetone molecules (higher peaks in the correlation functions) in the binary system. Hence, the addition of CO_2 reduces the mutual correlations between acetone molecules and increases their interaction with water.

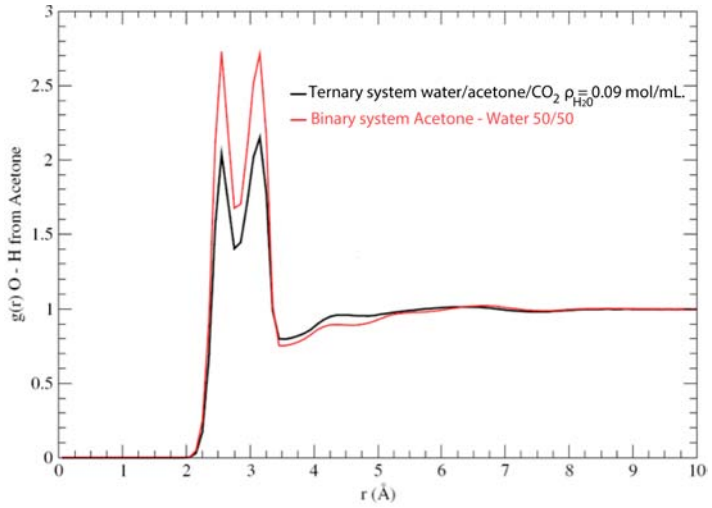

Figure 4.19: Comparison between the radial distribution function between oxygen and hydrogen atoms in acetone obtained in presence (black line) or absence (red line) of CO_2. The black line is calculated from the simulations of the water/acetone/CO_2 ternary mixture (10 MPa and 308 K, ρ_{H20}=0.092 mol/mL, mixture 50/50) and the red line from the simulations of the water/acetone equimolar mixture also at 10MPa and 308K.

The simulated structure of the system water/acetone/CO_2 is depicted in Figure 4.20. The size of water clusters has been estimated to be approximately around 2 nm. This is in agreement with the reported values of the size of the domains in surfactant-less microemulsions systems [49].

MD simulations have also been performed with the ternary system water/acetonitrile/CO_2 at 10 MPa and 308 K in order to gain more understanding of the experimental results obtained. In addition, the system ethanol/water/CO_2 has also been simulated at the same conditions of temperature and pressure. The ternary diagram of the latter is reported in the literature. In this case, the initial mixture of water/ethanol is split into two phases upon the addition of CO_2. However, the nature of the phases is different, and the system

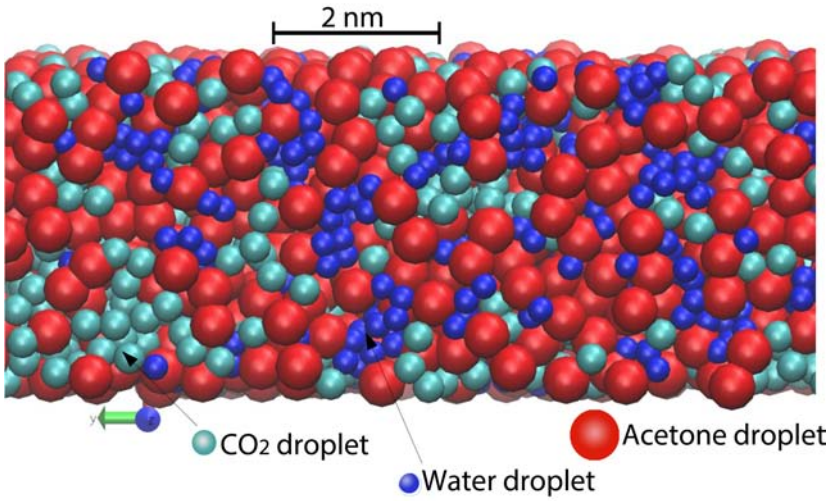

Figure 4.20: Simulated structure of the water/acetone/CO_2 system at the compositions where water forms clusters.

breaks into a water and ethanol rich dense phase and a CO_2 rich light phase. Based on this behavior, the formation of water clusters is not expected. The characterization of the water/ethanol/CO_2 by Raman Spectroscopy is not possible as the signal of OH of ethanol interferes with the OH stretching band of water and it is not possible to measure what happens to water molecules. However, it has been proven how it is not possible to dissolved ibuprofen in the ternary system water/ethanol by adding CO_2 as happened in the water/acetone/CO_2 system.

Ethanol and acetonitrile are both miscible with water but their hydrogen bonding capacity is different. For both systems, a composition of the ternary system very close to the binodal line but still in the one phase region of the ternary diagram has been chosen for carrying out the MD simulations at 10 MPa and 308 K. In Figure 4.21, the obtained radial distribution functions describing water-water, water-organic solvent and water-CO_2 correlations are shown for both systems. Comparison of the intensity of the peaks for the water-water correlations show that water is more structured in the water/acetonitrile/CO_2 mixture than in the water/acetone/CO_2 system (Figure 4.21) and in turn, these two mixtures show more water structure than the water/ethanol/CO_2 system. This strong enhancement of the water structure in the water/acetonitrile/CO_2 mixture is accompanied by a dramatic decrease in the correlation between water and acetonitrile molecules. The water hydrogen-acetonitrile nitrogen peak present at about 2 Å indicates some degree of

hydrogen bonding but the fact that the correlation function is always g(r)<1 demonstrates a global tendency of acetonitrile to anticorrelate with water. This effect is observed only in the case of acetonitrile. Ethanol-water correlations (Figure 4.21) have a similar structure (but weaker intensity) than those found between water and acetone (Figure 4.21). MD simulations have provided a theoretical support to justify the experimental Raman

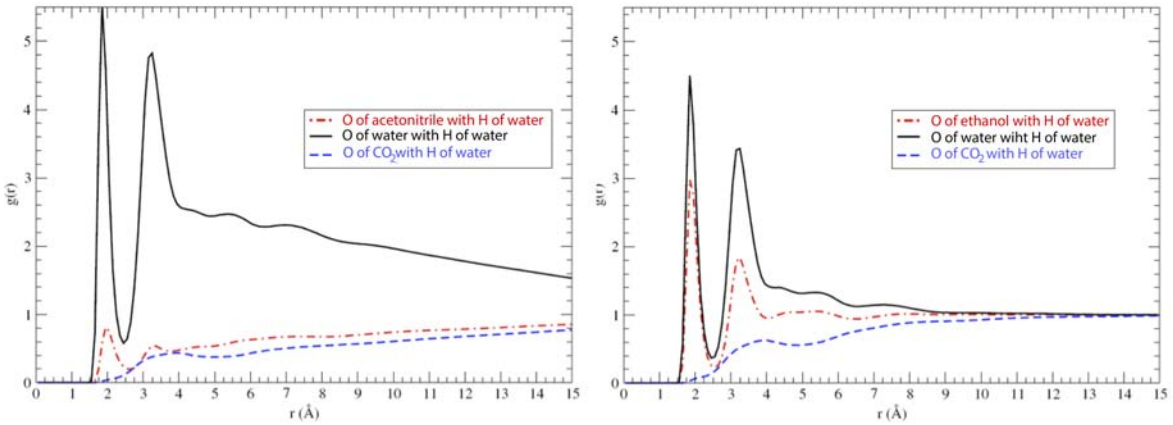

Figure 4.21: Radial distribution functions involving water molecules calculated from MD simulations of mixtures with different organic solvents. a) ternary Water/Acetonitrile/CO_2 (10 MPa and 308 K, ρ_{H20}=0.092 mol/mL, mixture 50/50). b)Water/Ethanol/CO_2 mixture (10 MPa and 308 K, x(CO2)=0.15, ρ_{H20}=0.092 mol/mL, mixture 50/50)).

measurements and the solubilization experiments performed.

4.4.1 Summary

- MD simulations strongly support the experimental results obtained by Raman Spectroscopy. MD simulations confirm the formation of water clusters upon the addition of CO_2 at 10 MPa and 308 K over an initial mixture of water/acetone 50/50.
- MD simulations have also been conducting replacing acetone by acetonitrile and ethanol. The higher structuring takes place in the acetonitrile system, then in acetone and the one with the less water structuration is the ethanol mixture. These results are in agreement with the experimental R_{OH} calculated from the OH stretching band of water by Raman Spectroscopy and by the dissolution experiments.

Bibliography

[1] C. Stubenrauch, ed., *Microemulsions: Backgrounds, New Concepts, Applications, Perspectives*. WILEY, 2009.

[2] T. Hoar and J. Schulman, "Transparent water-in-oil dispersions: The oleopathic hydro-micelle," *Nature*, vol. 152, no. 3847, pp. 102–103, 1943.

[3] P. A. Winsor, "Hydrotropy, solubilisation and related emulsification processes," *Trans. Faraday Soc.*, vol. 44, pp. 376–398, 1948.

[4] B. W. Ninham and P. L. Nostro, *Molecular Forces and Self Assembly*. Cambridge University Press, 2010.

[5] J. H. Schulman, W. Stoeckenius, and L. M. Prince, "Mechanism of formation and structure of micro emulsions by electron microscopy," *The Journal of Physical Chemistry*, vol. 63, no. 10, pp. 1677–1680, 1959.

[6] I. Danielsson and B. L. Lindman, "The definition of microemulsion," *Colloids and Surfaces*, vol. 3, no. 4, pp. 391 – 392, 1981.

[7] D. J. McClements, "Nanoemulsions versus microemulsions: Terminology, differences, and similarities," *Soft Matter*, vol. 8, no. 6, pp. 1719–1729, 2012.

[8] M. L. Klossek, *Nanostructured Liquids, Colloids and EnviEnvironment Acceptable Liquid Media*. PhD thesis, Universität Regensburg, 2013.

[9] J. L. Anderson, J. Ding, T. Welton, and D. W. Armstrong, "Characterizing ionic liquids on the basis of multiple solvation interactions," *Journal of the American Chemical Society*, vol. 124, no. 47, pp. 14247–14254, 2002.

[10] D. Langevin, "Micelles and microemulsions," *Annual Review of Physical Chemistry*, vol. 43, no. 1, pp. 341–369, 1992.

[11] L. E. Scriven, "Equilibrium bicontinuous structure," *Nature*, vol. 263, pp. 123–125, Sept. 1976.

[12] K. Shinoda and H. Kunieda, "Conditions to produce so-called microemulsions: Factors to increase the mutual solubility of oil and water by solubilizer," *Journal of Colloid and Interface Science*, vol. 42, no. 2, pp. 381 – 387, 1973.

[13] B. Lindman, K. Shinoda, U. Olsson, D. Anderson, G. Karlström, and H. Wennerström, "On the demonstration of bicontinuous structures in microemulsions," *Colloids and Surfaces*, vol. 38, no. 1, pp. 205 – 224, 1989.

[14] Y. Gao, S. Wang, L. Zheng, S. Han, X. Zhang, D. Lu, L. Yu, Y. Ji, and G. Zhang, "Microregion detection of ionic liquid microemulsions," *Journal of Colloid and Interface Science*, vol. 301, no. 2, pp. 612 – 616, 2006.

[15] C. Solans, *Microemulsions in cosmetic, Industrial Applications of Microemulsions.* Marcel Dekker, 1997.

[16] M. Lawrence and G. Rees, "Microemulsion-based media as novel drug delivery systems," *Advanced Drug Delivery Reviews*, vol. 45, no. 1, pp. 89–121, 2000.

[17] S. Wellert, M. Karg, H. Imhof, A. Steppin, H.-J. Altmann, M. Dolle, A. Richardt, B. Tiersch, J. Koetz, A. Lapp, and T. Hellweg, "Structure of biodiesel based bicontinuous microemulsions for environmentally compatible decontamination: A small angle neutron scattering and freeze fracture electron microscopy study," *Journal of Colloid and Interface Science*, vol. 325, no. 1, pp. 250 – 258, 2008.

[18] V. Dwarakanath and G. A. Pope, "Surfactant phase behavior with field degreasing solvent," *Environmental Science & Technology*, vol. 34, no. 22, pp. 4842–4848, 2000.

[19] M. Lopez-Quintela, C. Tojo, M. Blanco, L. G. Rio, and J. Leis, "Microemulsion dynamics and reactions in microemulsions," *Current Opinion in Colloid & Interface Science*, vol. 9, no. 3âĂŽÃĎÃň4, pp. 264 – 278, 2004.

[20] K. Shinoda, M. Araki, A. Sadaghiani, A. Khan, and B. Lindman, "Lecithin-based microemulsions: phase behavior and microstructure," *The Journal of Physical Chemistry*, vol. 95, no. 2, pp. 989–993, 1991.

[21] L. Do, A. Withayyapayanon, J. Harwell, and D. Sabatini, "Environmentally friendly vegetable oil microemulsions using extended surfactants and linkers," *Journal of Surfactants and Detergents*, vol. 12, no. 2, pp. 91–99, 2009.

[22] J. Eastoe, C. Yan, and A. Mohamed, "Microemulsions with co 2 as a solvent," *Current Opinion in Colloid and Interface Science*, vol. 17, no. 5, pp. 266–273, 2012.

[23] K. P. Johnston, K. L. Harrison, M. J. Clarke, S. M. Howdle, M. P. Heitz, F. V. Bright, C. Carlier, and T. W. Randolph, "Water-in-carbon dioxide microemulsions: An environment for hydrophiles including proteins," *Science*, vol. 271, no. 5249, pp. 624–626, 1996.

[24] C. Stubenrauch, T. Sottmann, R. Strey, and I. Lynch, "Comment on "gelation of microemulsions and release behaviour of sodium salicylate from gelled microemulsions" [eur. j. pharm. biopharm. 71 (2009) 297]," *European Journal of Pharmaceutics and Biopharmaceutics*, vol. 72, no. 3, p. 632, 2009.

[25] M. Sagisaka, S. Iwama, S. Hasegawa, A. Yoshizawa, A. Mohamed, S. Cummings, S. Rogers, R. Heenan, and J. Eastoe, "Super-efficient surfactant for stabilizing water-in-carbon dioxide microemulsions," *Langmuir*, vol. 27, no. 10, pp. 5772–5780, 2011.

[26] M. J. Clarke, K. L. Harrison, K. P. Johnston, and S. M. Howdle, "Water in supercritical carbon dioxide microemulsions: Spectroscopic investigation of a new environment for aqueous inorganic chemistry," *Journal of the American Chemical Society*, vol. 119, no. 27, pp. 6399–6406, 1997.

[27] S. Ray and S. Moulik, "Phase behavior, transport properties, and thermodynamics of water/aot/alkanol microemulsion systems," *Journal of Colloid And Interface Science*, vol. 173, no. 1, pp. 28–33, 1995.

[28] J. Eastoe, Z. Bayazit, S. Martel, D. C. Steytler, and R. K. Heenan, "Droplet structure in a water-in-co2 microemulsion," *Langmuir*, vol. 12, no. 6, pp. 1423–1424, 1996.

[29] J. Eastoe, C. Yan, and A. Mohamed, "Microemulsions with co2 as a solvent," *Current Opinion in Colloid & Interface Science*, vol. 17, no. 5, pp. 266–273, 2012.

[30] J. Zhang and B. Han, "Supercritical co2-continuous microemulsions and compressed co2-expanded reverse microemulsions," *The Journal of Supercritical Fluids*, vol. 47, no. 3, pp. 531–536, 2009.

[31] G. Smith, C. Donelan, and R. Barden, "Oil-continuous microemulsions composed of hexane, water, and 2-propanol," *Journal of Colloid And Interface Science*, vol. 60, no. 3, pp. 488–496, 1977.

[32] B. Keiser, D. Varie, R. Barden, and S. Holt, "Detergentless water/oil microemulsions composed of hexane, water, and 2-propanol. 2. nuclear magnetic resonance studies, effect of added nacl," *Journal of Physical Chemistry*, vol. 83, no. 10, pp. 1276–1280, 1979.

[33] N. Borys, S. Holt, and R. Barden, "Detergentless water/oil microemulsions. iii. effect of koh on phase diagram and effect of solvent composition on base hydrolysis of esters," *Journal of Colloid And Interface Science*, vol. 71, no. 3, pp. 526–532, 1979.

[34] G. Lund and S. Holt, "Detergentless water/oil microemulsions: Iv. the ternary pseudo-phase diagram for and properties of the system toluene/2-propanol/water," *Journal of the American Oil Chemists' Society*, vol. 57, no. 8, pp. 264–267, 1980.

[35] M. Zoumpanioti, H. Stamatis, V. Papadimitriou, and A. Xenakis, "Spectroscopic and catalytic studies of lipases in ternary hexane-1-propanol-water surfactantless microemulsion systems," *Colloids and Surfaces B: Biointerfaces*, vol. 47, no. 1, pp. 1–9, 2006.

[36] Y. Khmelnitsky, A. Van Hoek, C. Veeger, and A. Visser, "Detergentless microemulsions as media for enzymatic reactions. spectroscopic and ultracentrifugation studies," *Journal of Physical Chemistry*, vol. 93, no. 2, pp. 872–878, 1989.

[37] J. Drapeau, M. Verdier, D. Touraud, U. Kröckel, M. Geier, A. Rose, and W. Kunz, "Effective insect repellent formulation in both surfactantless and classical microemulsions with a long-lasting protection for human beings," *Chemistry & Biodiversity*, vol. 6, no. 6, pp. 934–947, 2009.

[38] B. Keiser and S. Holt, "Reactions in detergentless microemulsions: Incorporation of copper(ii) into meso-tetraphenylporphine ((tpp)h2) in a water/oil microemulsion," *Inorganic Chemistry*, vol. 21, no. 6, pp. 2323–2327, 1982.

[39] C. O'Connor and D. Cleverly, "Bile salt stimulated human milk lipase catalyzed ester hydrolysis in detergentless microemulsion media," *Biocatalysis and Biotransformation*, vol. 12, no. 3, pp. 193–204, 1995.

[40] M. Zoumpanioti, M. Karali, A. Xenakis, and H. Stamatis, "Lipase biocatalytic processes in surfactant free microemulsion-like ternary systems and related organogels," *Enzyme and Microbial Technology*, vol. 39, no. 4, pp. 531–539, 2006.

[41] "Green solvents-progress in science and application," *Green Chem.*, vol. 11, pp. 603–603, 2009.

[42] J. DeSimone, "Practical approaches to green solvents," *Science*, vol. 297, no. 5582, pp. 799–803, 2002.

[43] G. D. Smith, B. B. Garrett, S. L. Holt, and R. E. Barden, "The interaction of copper(ii) and n.alpha.-acyl-l-histidinol at the interface of an oil-continuous microemulsion," *The Journal of Physical Chemistry*, vol. 80, no. 15, pp. 1708–1713, 1976.

[44] B. M. Knickerbocker, C. V. Pesheck, L. E. Scriven, and H. T. Davis, "Phase behavior of alcohol-hydrocarbon-brine mixtures," *The Journal of Physical Chemistry*, vol. 83, no. 15, pp. 1984–1990, 1979.

[45] B. M. Knickerbocker, C. V. Pesheck, H. T. Davis, and L. E. Scriven, "Patterns of three-liquid-phase behavior illustrated by alcohol-hydrocarbon-water-salt mixtures," *The Journal of Physical Chemistry*, vol. 86, no. 3, pp. 393–400, 1982.

[46] J. E. Pulg, D. L. Hemker, A. Gupta, H. T. Davis, and L. E. Scriven, "Interfacial tensions and phase behavior of alcohol-hydrocarbon-water-sodium chloride systems," *The Journal of Physical Chemistry*, vol. 91, no. 5, pp. 1137–1143, 1987.

[47] J. Lara, G. Perron, and J. E. Desnoyers, "Heat capacities and volumes of the ternary system benzene-water-2-propanol," *The Journal of Physical Chemistry*, vol. 85, no. 11, pp. 1600–1605, 1981.

[48] R. Schott and A. Pfennig, "Modelling of mass-transfer induced instabilities at liquid-liquid interfaces based on molecular simulations," *Molecular Physics*, vol. 102, no. 4 PART III, pp. 331–339, 2004.

[49] M. Klossek, D. Touraud, T. Zemb, and W. Kunz, "Structure and solubility in surfactant-free microemulsions," *ChemPhysChem*, vol. 13, no. 18, pp. 4116–4119, 2012.

[50] S. Schüttl, J. Marcus, O. Diat, D. Touraud, W. Kunz, T. Zemb, and D. Horinek, "Emergence of surfactant-free micelles from ternary solutions," *Chemical Science*, vol. 5, no. 8, pp. 2949–2954, 2014.

[51] R. Wang, W. Leng, Y. Gao, and L. Yu, "Microemulsion-like aggregation behaviour of an lcst-type ionic liquid in water," *RSC Advances*, vol. 4, no. 27, pp. 14055–14062, 2014.

[52] D. Lavallee, E. Huggins, and S. Lee, "Kinetics and mechanism of the hydrolysis of chlorophyll a in ternary solvent microemulsion media," *Inorganic Chemistry*, vol. 21, no. 4, pp. 1552–1553, 1982.

[53] P. G. Jessop and B. Subramaniam, "Gas-expanded liquids," *Chemical Reviews*, vol. 107, no. 6, pp. 2666–2694, 2007.

[54] M. Wendland, H. Hasse, and G. Maurer, "Multiphase high-pressure equilibria of carbon dioxide-water-acetone," *The Journal of Supercritical Fluids*, vol. 7, no. 4, pp. 245–250, 1994.

[55] J. Elgin and J. Weinstock, "Phase equilibrium at elevated pressures in ternary systems of ethylene and water with organic liquids. salting out with a supercritical gas," *Journal of Chemical and Engineering Data*, vol. 4, no. 1, pp. 3–12, 1959.

[56] P. Traub and K. Stephan, "High-pressure phase equilibria of the system co2-water-acetone measured with a new apparatus," *Chemical Engineering Science*, vol. 45, no. 3, pp. 751–758, 1990.

[57] B. Renault, E. Cloutet, H. Cramail, T. Tassaing, and M. Besnard, "On the perturbation of the intramolecular h-bond in diols by supercritical co2: A theoretical and spectroscopic study," *Journal of Physical Chemistry A*, vol. 111, no. 20, pp. 4181–4187, 2007.

[58] T. Kawamoto, S. Ochiai, and H. Kagi, "Changes in the structure of water deduced from the pressure dependence of the raman oh frequency," *Journal of Chemical Physics*, vol. 120, no. 13, pp. 5867–5870, 2004.

[59] D. M. Carey, "Measurement of the raman spectrum of liquid water," *Journal of Chemical Physics*, vol. 108, no. 7, pp. 2669–2675, 1998.

[60] O. Knauer, M. Lang, A. Braeuer, and A. Leipertz, "Simultaneous determination of the composition and temperature gradients in the vicinity of boiling bubbles in liquid binary mixtures using one-dimensional raman measurements," *Journal of Raman Spectroscopy*, vol. 42, no. 2, pp. 195–200, 2011. cited By 9.

[61] M. Sokolova, S. Barlow, G. Bondarenko, Y. Gorbaty, and M. Poliakoff, "Comparison between ir absorption and raman scattering spectra of liquid and supercritical 1-butanol," *Journal of Physical Chemistry A*, vol. 110, no. 11, pp. 3882–3885, 2006.

[62] G. Walrafen, M. Hokmabadi, and W.-H. Yang, "Raman isosbestic points from liquid water," *The Journal of Chemical Physics*, vol. 85, no. 12, pp. 6964–6969, 1986.

[63] B. Auer and J. Skinner, "Ir and raman spectra of liquid water: Theory and interpretation," *Journal of Chemical Physics*, vol. 128, no. 22, 2008.

[64] G. E. Walrafen, M. R. Fisher, M. S. Hokmabadi, and W. Yang, "Temperature dependence of the lowâĂŽ and highâĂŽfrequency raman scattering from liquid water," *The Journal of Chemical Physics*, vol. 85, no. 12, pp. 6970–6982, 1986.

[65] J. Manrique and F. Martinez, "Solubility of ibuprofen in some ethanol + water cosolvent mixtures at several temperatures," *Latin American Journal of Pharmacy*, vol. 26, no. 3, pp. 344–354, 2007.

[66] D. Suleiman and C. A. Eckert, "Phase equilibria of alkanes in natural gas systems. 2. alkanes in ethane," *Journal of Chemical & Engineering Data*, vol. 40, no. 3, pp. 572–577, 1995.

[67] M. Munto, N. Ventosa, S. Sala, and J. Veciana, "Solubility behaviors of ibuprofen and naproxen drugs in liquid "co2-organic solvent" mixtures," *Journal of Supercritical Fluids*, vol. 47, no. 2, pp. 147–153, 2008.

[68] M. Lazzaroni, D. Bush, R. Jones, J. Hallett, C. Liotta, and C. Eckert, "High-pressure phase equilibria of some carbon dioxide-organic-water systems," *Fluid Phase Equilibria*, vol. 224, no. 1, pp. 143–154, 2004.

[69] D. Venables and C. Schmuttenmaer, "Spectroscopy and dynamics of mixtures of water with acetone, acetonitrile, and methanol," *Journal of Chemical Physics*, vol. 113, no. 24, pp. 11222–11236, 2000.

[70] W. Humphrey, A. Dalke, and K. Schulten, "Vmd: Visual molecular dynamics," *Journal of Molecular Graphics*, vol. 14, no. 1, pp. 33–38, 1996.

5

Conclusions

The work performed in the present Thesis on the use of CO_2-expanded solvents methodologies for the production of microparticulate materials, either as solids or in an aqueous suspensions, and on the study of new surfactant-less CO_2-based microemulsion-like systems has driven to the following conclusions:

- DELOS methodology has proven to be an effective method for the one-step preparation of micron sized solid particles of two poorly soluble compounds. Using ibuprofen, as a model drug of poorly water soluble compounds, it has been shown how the precipitate's final characteristics can be modulated tuning the process operational parameters.

- It has been possible to control the extremely fast one-face preferential growth of the thiadiazoline derivative NP by DELOS method. This active precipitates from conventional cooling in the form of very large needles, presenting as a consequence a cotton-like appearance. By DELOS, it has been possible to obtained micro particles of this active avoiding the cotton-like appearance.

- It has been shown the feasibility of producing stable aqueous suspensions of the thiadiazoline derivative NP and ibuprofen by DELOS-susp with the aid of surfactants with a stability larger than 2 months.
- Using DELOS-susp methodology, it has been possible to reduce more the particle size of the thiadiazoline derivative NP particles, achieving submicronparticles.
- It has been demonstrated that surfactant-free pressurized microemulsion-like systems can be formed by adding CO_2 to mixtures of water and an organic solvent, such as acetone or acetonitrile, with high mutual miscibility. The addition of CO_2 causes the rupture of the homogeneity of the initial water-organic solvent mixture and the structuration of the system at the nanoscale.
- The existence of water-rich and water-lean nanodomains in a macroscopically transparent liquid phase has been revealed by Raman spectroscopy, which has been proven to be a very useful technique to characterize the microenvironment of water molecules in these systems. These results are promising since microemulsion-like systems with compressed CO_2 are an effective way to enhance the solubility of solutes. Surfactant-free CO_2-based microemulsion-like systems enable more environmentally friendly process routes.

Based on all these conclusions, this Thesis contributes to demonstrate that CO_2-expanded solvents are very attractive eco-efficient alternative for the production of micro and submicron actives.

6

Experimental Part

6.1 Materials

NP, 4-benzyl-2-(naphtalen-1-yl)-1,2,4-thiadiazoline-3,5-dione, was supplied by Noscira S.A (Madrid, Spain). Ibuprofen ((RS)-2-(4-(2-methylpropyl)phenyl)propanoic acid) was obtained from Fagron Iberica (Barcelona, España). Poloxamer F-127, Sodium dodecyl sulfate (SDS, purity >98.5%) and Polyvinylpyrrolidone (PVP) were purchased from Sigma-Aldrich (Tres Cantos, Spain). Hydroxypropyl methylcellulose (HPMC) was supplied by Noscira, S.A (Madrid, Spain). Polysorbate 80 (Tween 80) was obtained by Fluka Analytical and Gelurice® 44/14 was purchased from Gattefosé, Saint-Priest (Lyon, Francia).

Organic solvent, HPLC grade, were obtained from Teknokroma (Sant Cugat del Vallés, Spain). The formation of micro emulsion-like systems were conducted using organic solvent reagent grade, also purchased from Teknokroma (Sant Cugat del Vallés, Spain). Carbon dioxide (purity 99.9%) was supplied by Carburos Metálicos, S.A. (Barcelona, Spain). All chemicals were used without further purification. Water was pre-treated with the Mili-Q Advantage A10 water purification system (MIlipore Ibérica, Madrid, Spain).

6.2 Solubility analysis

6.2.1 Determination of solubility in organic solvents at atmospheric pressure

Measurements at 298 K, 308 K and 313 K

Solubility of the drug studied in organic solvents at atmospheric pressure was determined according to the gravimetric method of Gracin and Rasmuson [1] which consists on the following steps: A solution containing excess solids was placed in a temperature controlled water bath and stirred for 24h. The supersaturated solution was filtered using a PTFE syringe filter (200nm) and two aliquots of 5mL of the filtered solution were taken. For each aliquot, the organic solvent was removed using a rotatory evaporator and the remaining solids were left in a vacuum chamber at room temperature overnight to ensure no residual solvent. The amount of solids was determined gravimetrically and the solubility is reported is moles of drug per mole of organic solvent based on duplicate determinations.

Measurements at low temperature

The protocol used for the determination of the solubility of the drugs at low temperature is the same described above except that instead of using a water bath a cryogenic bath is required for achieving low temperatures. For each specific temperature, a different mixture of solvent and liquid nitrogen is employed.

6.2.2 Solubility analysis in pressurized CO_2-expanded solvents

Equipment: High pressure phase Analyzer or Variable Volume Cell

Solubility measurements in CO_2-expanded solvents were performed in a home-made high pressure analyzer, which is schematized in Figure 6.1. This systems is equipped with a variable volume cell (Jergusson liquid level gauge 16T-40) placed inside a thermostatic air chamber for temperature control. The cell has two opposite borosilicate windows all along the cell height for visual observation of the cell content and changes in phase behavior. A stainless steel cylindrical solid sample holder inserted at the bottom of the cell prior to pressurization allowed the introduction of additional solids. The cell volume is

varied with the movement of a stainless steel piston that is controlled by changing the air pressure in the pneumatic system. The piston position (0-20 cm) is calibrated for the corresponding cell volume using propanol, which varied from 69.5 ml to 92.9 ml without the solid sample holder and from 66.3 ml to 89.1ml for the case when the solid sample holder is inserted into the cell. The magnetic stirrer placed at the bottom of the cell led to mixing of the solids placed in the sample holder with the cell contents.

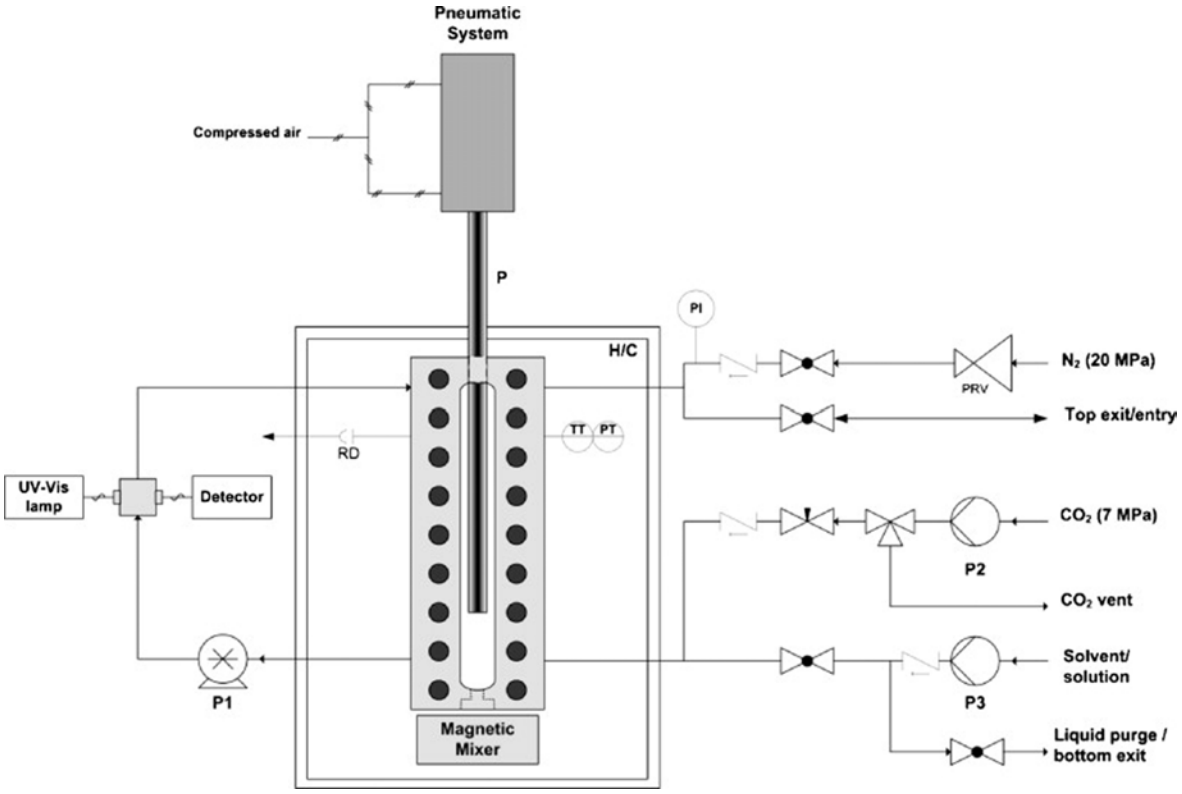

Figure 6.1: Schematic of the system with the variable volume cell, P, stainless steel piston, H/C heating/cooling air chamber, P1 recirculation pump, P2 CO_2 pump, P3 solvent/solution pump, PRV, pressure reducing vale, PI pressure indicator, TI temperature transducer, PT pressure transducer, RD rupture disc.

The system is equipped with three pumps: a recirculation pump (P1), which is a magnetically driven external gear pump (Micropumo GAH Series, Micropump, Vancuver, WA, USA) for the recirculation of the cell contents and to ensure good mixing of the mixture, a syringe pump (P2) (model 260D, Teldyne Isco Inc., Lincoln, NE, USA) to introduce compressed CO_2, and a piston pump (P3) (Jasco Inc, Easton, MD, USA) to introduce liquid solvent or solution at high pressure. The system is also equipped with pressure and tem-

perature indicators as well as safety devices, such as rupture disks.

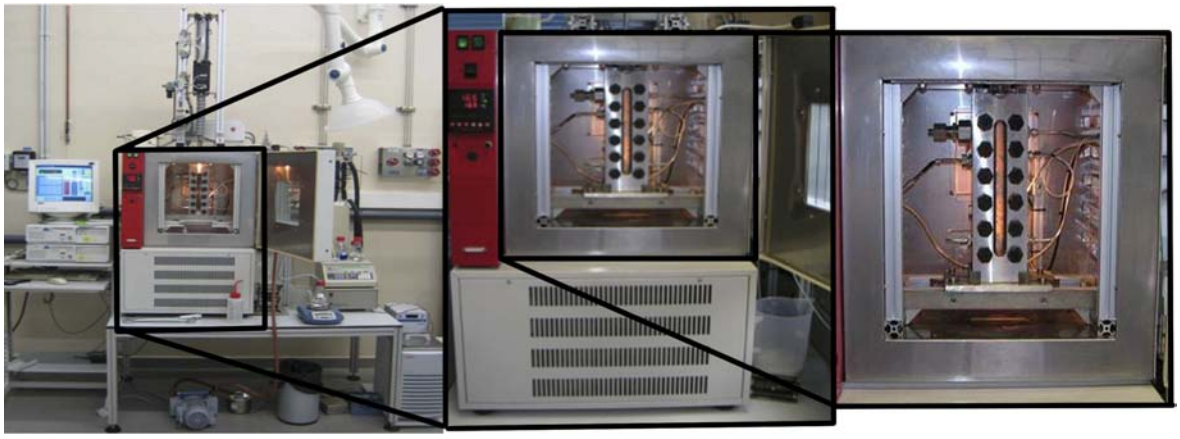

Figure 6.2: Images of the Variable Volume Cell

Experimental protocol: Vanishing point method

The phase behavior of NP in acetone, acetonitrile and in the mixtures of acetonitrile and alcohols were determined according to the Vanishing point method of Wubbols [2] at 10 MPa and at 298 K and 313 K for acetone and acetonitrile and only at 313 K for the mixtures of alcohols and acetonitrile. At those conditions, an initial mixture composition has to be selected to ensure the presence of a supersaturated solution at the beginning of each run. The vanishing point is determined when complete dissolution of the suspended crystals is achieved by adding pure organic solvent to the expanded mixture. Such solid is in equilibrium with a saturated phase of itself in a homogenous mixture between two fluids A and B. The increase of the solvating capacity of A/B binary mixture through the change of its composition provokes the progressive re-dissolution of the solute. The vanishing point method is an adequate procedure for performing solubility studies either at atmospheric pressure, where A and B are conventional solvents, or at high pressure, where A and B can be a conventional solvent and a compressed fluid.

The steps for obtaining the solubility data and the corresponding solubility curve are the ones presented below:

1. The piston is settle to its lower position that correspond to the minimum volume of the cell. If necessary, a known amount of solid is place inside the screw-on cup

located at the bottom of the cell. Vacuum is then applied by an external pump and the thermostated chamber is brought to the desired temperature.

2. Known quantities of solute, organic solvent and CO_2 are introduced into the cell to achieve the desired two phases system (a solid and a liquid phase) at the working conditions of pressure and temperature selected.

3. Once the starting biphasic point is achieved, pure organic solvent, organic solution of the solute in the organic solvent or pure CO_2 is slowly added to the cell to completely dissolve the solid and achieve a single phase again. This point corresponds to the solubility of the compound in the mixture of organic solvent/CO_2 at a specific x_W at P_W and T_Wİn some cases, the piston reached the highest position before the complete dissolution of the solute, and a new experiment need to be designed. In the latter case, the starting point of the new experiment is the final point of the previous experiment in which the maximum volume of the cell was already achieved.

4. When the vanishing point is determined, the mass balance of the components is calculated to obtained the value of the compound in the mixture of organic solvent/ CO_2.

∗ **Modeling**

Wubbolts et al. [2] developed a simple empirical model to describe the solubility of a solute in a CO_2-expanded solvent at equilibrium as function of the CO_2 concentration, (x_{CO2}) as follows:

$$C_s = C_{s(org)}(1 - x_{CO_2})^{A+Bx_{CO_2}} + C_{s(CO_2)}x_{CO_2}\,, \tag{6.1}$$

where $C_{s(org)}$ and $C_{s(CO_2)}$ represent the solute solubility in pure organic solvent and CO_2, respectively. All solubilities are reported in solute-free basis in terms of moles per mole of solvent mixture as expression indicates:

$$C_s = \frac{n_s}{n_{org} + n_{CO_2}} \tag{6.2}$$

6.3 Preparation of micro and sub microparticles using CO_2-expanded solvents

6.3.1 Preparation of micro and submicroparticles by Precipitation with a Compressed AntiSolvent, PCA

Equipment

The experimental configuration used for the PCA precipitation experiments is depicted in Figure 6.3. The configuration include a heat exchange (C1) for cooling CO_2 before it

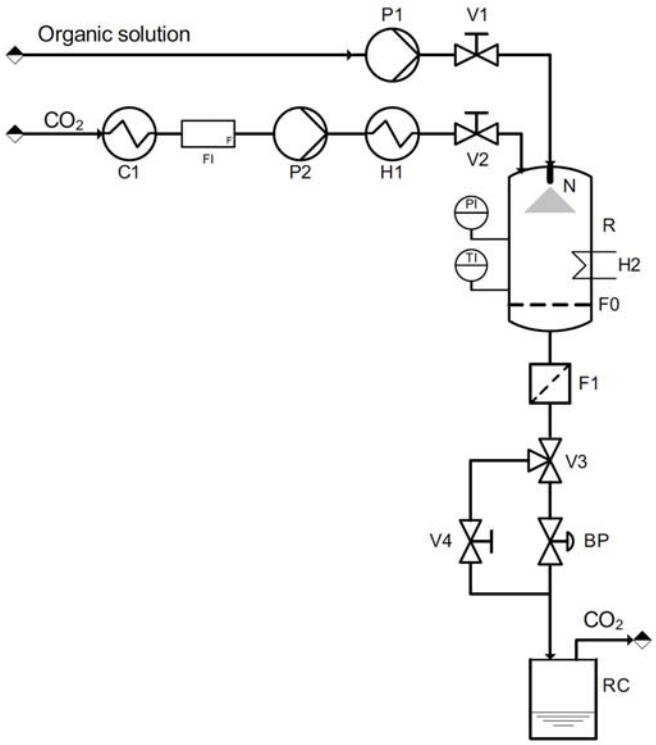

Figure 6.3: Scheme of the equipment employed in the PCA precipitation experiments.

is pumped into the precipitation vessel (R) by a Dosapro Milton Roy high pressure pump (P2). The flow of CO_2 is measured by the flowmeter F1 (Optimassmfm 7150K/01S) and it is heated by a heat exchange (H1) before it is introduce into the reactor though valve V2. The organic solution is injected through a hollow cone nozzle (N) (ϕ=100 μm, Lechlet, Metzingen, Germany) inside the precipitation vessel using (R) a HPLC pump (P1) (model PU-2080 from Jasco Inc.,Easton, US). The vessel R has an internal volume of 300mL and is

equipped with an external heating jacket (H2) which enables to control its temperature. A sintered metal fiber (F0) covered with a PTFE membrane (ϕ=0.22 μm) is place inside the autoclave in order to collected the precipitates. If the solids are not filtered by F0, they are trapped in an external filter (F1) (Headline Filters, Aylesford, UK) which comprise an internal concentric metal filter covered by a regenerated cellulose membrane (ϕ=0.22 μm). A back pressure regulator (BP) is used to control the pressure during the experiment. The depressurization valve, V4, is placed after F1. The last part of the configuration is the collector (RC) where the CO_2-expanded organic solvent is trapped. CO_2 is directed to a filter and then to the atmosphere. The system is also equipped with pressure and temperature indicators as well as safety devices, such as rupture disks.

Experimental procedure

The preparation of micro and submicronparticles by PCA was conducted using the equipment shown in Figure 6.3 and following the experimental protocol here presented. The precipitation chamber (R) is filled with CO_2 and allow to equilibrate to the operating pressure (P_W) and temperature (T_W). For achieving the desired molar fraction of CO_2 the back pressure valve (BP) is opened and CO_2 and pure organic solvent are simultaneously pumped at a flow ratio that generated the working CO_2 molar fraction (x_W) inside the vessel. After 20 minutes the steady state has been reached and injection of pure organic solvent is stopped and a certain volume of the organic solution of the compound to precipitate is sprayed though the hollow cone nozzle (N) at the same flow rate of the pure solvent, into the current of CO_2. The antisolvent effect of the compressed CO_2 over the solution provokes the precipitation of the compound as a particulate solid, which is collected in the pressurized filters F0 and F1. The removal of the possible organic solvent traces in the solid is carried out by a current of CO_2 at the same working conditions of flow, pressure and temperature during one hour. After depressurization through valve V4, dried particles are collected from the filters.

6.3.2 Preparation of micro and submicroparticles by DELOS

Equipment

- **100mL**

  The equipment used for the DELOS precipitation of ibuprofen is schematized in

Figure 6.4. The configuration comprises a 100 mL reactor. The reactor contains an external heating jacket for adjusting the desired temperature. CO_2 is introduced by a syringe pump (model 260D, ISCO Inc., Lincoln, US) trough valve V_{CO_2} to the reactor. There is a micrometric valve, $V_{CO_2 r}$ to control de flow of CO_2. After the reactor there is a filter (Gas filter) to collect any solid that could precipitate due to the antisolvent effect of CO_2. The CO_2-expaned solution is depressurized through the depressurization valve, V3. After this valves, there is the DELOS filter, which collects at atmospheric pressure the particles that precipitate by the large, abrupt and homogenous decrease in temperature that takes place in DELOS precipitations. There is a pressure indicator before the depressurization valve to ensure that the system is equilibrated at the working pressure and a temperate indicator just after valve V3 to measure the final temperature that reaches the solution. This final temperature is required for the calculation of the supersaturation during depressurization. At the end of the configuration there is a plastic bucket where the organic solvent is trapped. CO_2 is directed to a filter and to the atmosphere. The system is also equipped with pressure and temperature indicators as well as safety devices, such as rupture disks.

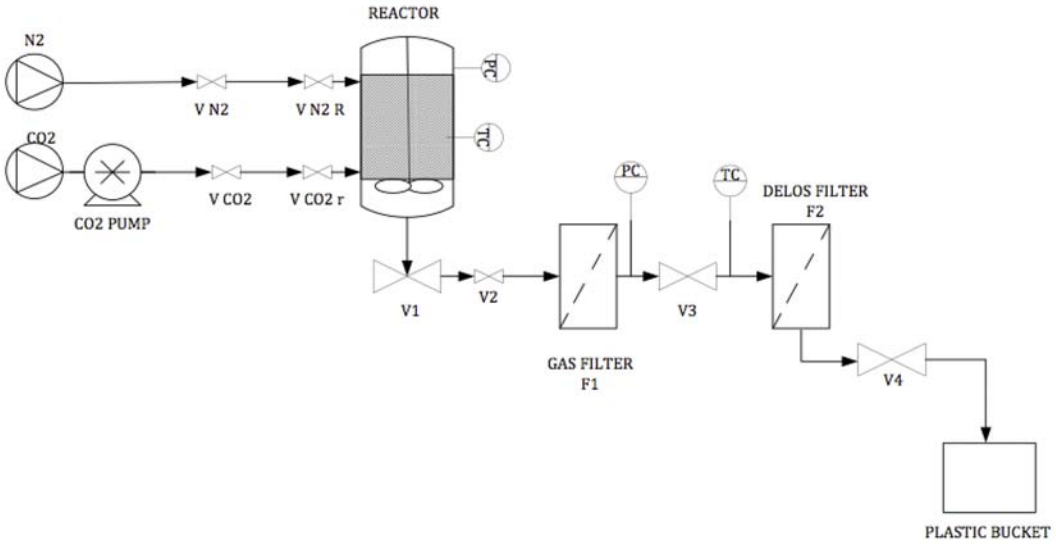

Figure 6.4: Scheme of the 100mL Plant used for the DELOS experiments.

- **300mL**

The 300mL plant used for the precipitation of NP by DELOS is shown in Figure 6.5. In this configuration, CO_2 is pumped though a high pressure pump, P1, previously cooled by a heat exchanger, S1. Before entering into the reactor, R, CO_2 is heated to the working temperature, T_W using a second heat exchanger, S2. The flow introduced through V3 is measured using a flowmeter, C. After the reactor, R, there is a valve, V4 that connects to a filter, F, which is pressurized at the working pressure, P_W in order to separate the solid that could precipitated by the antisolvent effect of the addition of CO_2. After that, there is the depressurization valve, that leads to another filter or to a systems of filters in parallel when there is a lot of solid, where the particles produced by DELOS are trapped. The end of the configuration is also a collector (RC) where the organic solvent is trapped. CO_2 is directed to a filter and then to the atmosphere.

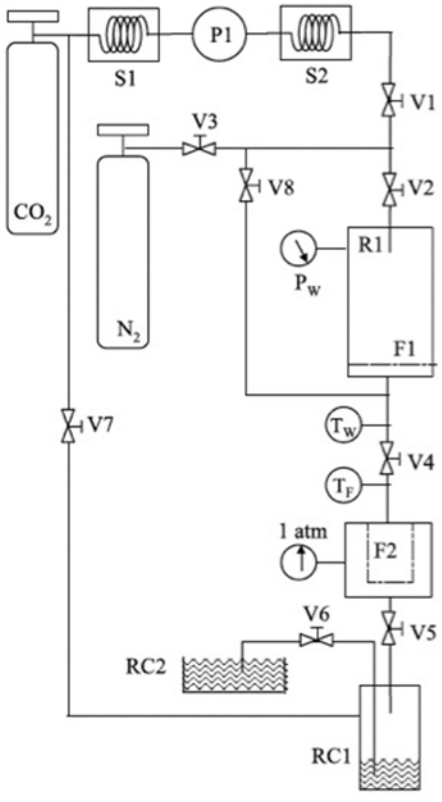

Figure 6.5: Scheme of the 300mL Plant used for the DELOS experiments.

Apart from the differences in volume of the vessel of both configuration, the de-

pressurization configuration also changed in the 300 mL plant, where the manual depressurizing valve used in the 100 mL system is substituted by an automatic one, whose flow rate can be better controlled. In the large plant, the plant is connected to a computer where a software controls and registers the operating variables.

Experimental procedure

The preparation of micro and submicronparticles of the drugs either in the 100 mL or in the 300 mL is the same and it is performed according to the following procedure: A volume of a solution of the drug in an organic solvent is introduced into the reactor, which has been previously driven to the working temperature (T_W). The volume of the solution added is calculated in order to have the desired molar fraction of CO_2 (x_W). The solution of the drug in the organic solvent is left inside the reactor for 30min stirring to ensure it reaches the working temperature. Then, the autoclave is pressurized with compressed CO_2 though valve V3 or $V_{CO_2 r}$ (300 mL or 100 mL plant respectively), producing a volumetric expanded liquid solution. The expanded mixture is left to equilibrate for at least 1hour. The Gas filter is pressurized at the working pressure. The valve that connects the reactor with the GAS filter is opened. The entry of Nitrogen is opened once the pressure of the Nitrogen flow is adjusted to the working pressure. The current of Nitrogen at P_W is used as embolus to push down the expanded solution in order to maintain constant pressure in the reactor during depressurization. In this way a homogenous depressurization is guaranteed.

Calculation of the DELOS yield

The DELOS yield is calculated weighting the mass of the particles precipitated that remains in the DELOS filter divided by the initial mass of the compound charged into the vessel:

$$DELOSYield(\%) = \frac{m_i}{m_{DELOS}}, \tag{6.3}$$

being m_1 the mass of the drug in the initial solution and m_{DELOS} the mass of the drug recovered in the DELOS filter.

6.4 Instruments, techniques and procedures used for the characterization of the micro and submicronparticles

6.4.1 Light Scattering (LS)

Equipment

The volumetric particle size distribution of the precipitates has been assessed by Light Scaterring (LS) using a particle size analyzer (Mastersizer 2000, Malvern Instruments, UK). Mastersizer 2000 uses the technique of laser diffraction to measure the size of particles. It does this by measuring the intensity of light scattered as a laser beam passes through a dispersed particulate sample. This data is then analyzed to calculate the size of the particles that created the scattering pattern. Laser diffraction measures particle size distributions by measuring the angular variation in intensity of light scattered as a laser beam passes through a dispersed particulate sample. Large particles scatter light at small angles relative to the laser beam and small particles scatter light at large angles, as illustrated in Figure 6.6 . The angular scattering intensity data is then analyzed to calculate the size of the particles responsible for creating the scattering pattern, using the Mie theory of light scattering. The Mie theory was developed to predict the way light is scattered by spherical particles and deals with the way light passes through, or is adsorbed by, the particle. Therefore, the more isotropic is the particle, the best accuracy will be obtained.

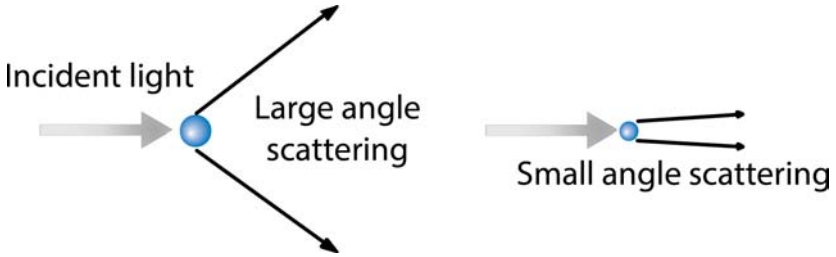

Figure 6.6: Scattering angles of different particles sizes.

The equipment gives the results as volume-equivalent sphere diameter, which is the diameter of a sphere with the same volume as the particle. The volume-equivalent sphere diameter is the unique way to describe a 3-dimensional object with one number.

Light Scattering technique is a volumetric technique, this means that measures in volume, therefore the most accurate way to present the results is as volumetric particle size

distribution. The relationship between 1 μm and 10 μm size particles is 1:1000 in the case of the volume standard even though it is 1:1 for the number standard. Thus, quite a different impression can be imparted for the particle size distribution of the same measurement target depending on which standard (volume or number) is used. A volumetric particle size distribution can be converted into a numeric one, however, as Light Scattering measures volume, the transformation entails some error. As can be seen in Figure 6.7, larger particles account for the highest volumetric percentage of the total volume of particles, and therefore shifts the distribution towards highest values.

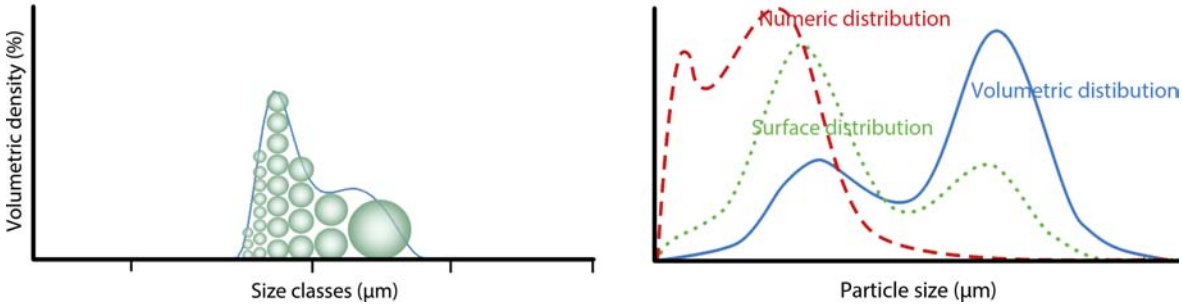

Figure 6.7: Volumetric Particle size distributions: Larger particles accounts for the larger volumetric percentage of the total volume of particles.

The optical system of Masterizer is depicted in Figure 6.8, the one of the left is the red laser source and the one of the left is the blue light source. The red laser gets bent 90° degrees with some precision folded optics, and then passes through the measurement cell, where the laser hits the particles, and particles scatter light. This scattered light is recorded in the circle plane detectors with narrow angles, as well as in the side and back detectors. In this way, it is possible to capture a wide angle range that allow to measure a wide particle size range. As particle size limits depends on the wavelength applied, an additional blue light source is included in the optical system to extend the resolution to the finest particles. The scattered light is only captured in the high angles detectors, (side and backs detectors), as no information is recorded in the focal plane detectors.

Mie theory requires knowledge of the optical properties of both the sample being measured and the dispersant medium.

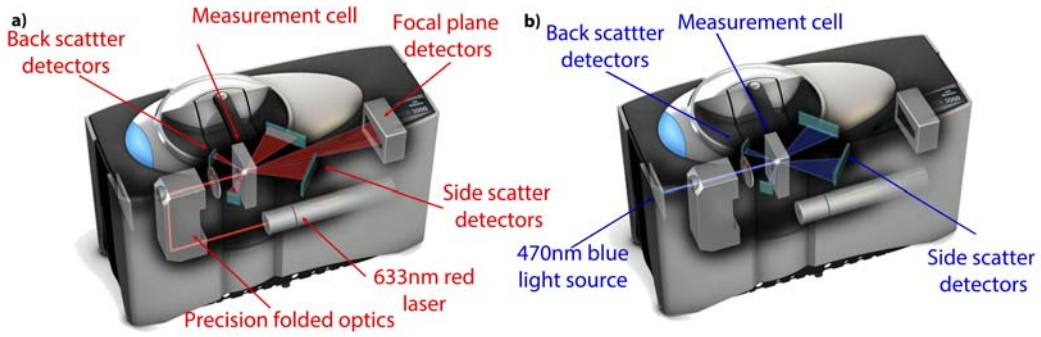

Figure 6.8: Optical system of Mastersizer, the one on the left is the red laser

Experimental Protocol

A previous treatment of the sample is required: a certain mass of each sample is suspended in a liquid dispersant medium and sonicated (Ultrasons-H, Selecta, Abrera, Spain) for achieving a homogenous suspensions of the solid in such solvent. The best dispersium media for each drug was chosen based on previous experience in *Nanomol*. The dispersium media for each drug is presented in Table 6.1 as well as the specification for the previous treatment of the sample.

Table 6.1: Operating conditions employed for the measurement of particle size distribution of micro particles by LS

Compound[a]	Dispersant medium	IR[b]	(mg/mL)[c]	Surfactant	Sonication time(s)
Ibuprofen	Ultrapure water saturated with ibuprofen	1.33	25/5	Tween80[d]	600
NP	Ultrapure water saturated with NP	1.33	25/5	-	600

[a] The refractive index used for the solids were 1.7, [b] Refractive of the dispersant medium,[c] Mass of drug per volume of dispersant.[d] 0.1% vol.

In order to have a representative measurement of particle size distribution, for each solid obtained, 3 different samples are taken and suspended in their corresponding dispersant medium. In addition, the software of Mastersizer 2000 measures 3 times each sample and gives us a result an average value. Therefore, the values presented in this

Thesis correspond to an average of 3 samples for the same solid.

The protocol for particle size distribution analysis by LS involves the cleaning for the system with pure dispersant medium, laser alienation, measuring the dispersant medium particle size as background and finally measuring the sample. The measures were characterized in volumetric distributions.

6.4.2 Scanning electron microscopy (SEM)

The surface morphology of the particulate materials was studied using a field emission scanning electron microscope (Quanta 200 FEG-ESEM, FEI, Eindhoven, The Netherlands). The samples were prepared by direct deposition of the powders onto a carbon tape placed on the surface of an aluminum stub. The samples were coated with gold for 4 minutes using a sputter coater (K550x, Emitech, Ashford, UK).

6.4.3 Morphology of particles

Size and Shape of particles were further characterized using the equipment Morphologi G3 (Malvern Instruments, UK) that use the technique of static image analysis. There are three essential stages in the measurement process:

- Sample preparation and dispersion

  This step is critical to getting good results; spatial separation of individual particles and agglomerates is the goal. The solid were prepared following the same procedure as in the Light Scattering measurement (see section 6.4.1). A drop of the suspension was sealed in between two disk holders.

- Image capture

  The instrument captures images of individual particles by scanning the sample underneath the microscope optics, while keeping the particles in focus. The Morphologi G3 can illuminate the sample from below or above, while accurately controlling the light levels.

- Data analysis

  The instrument measures a range of morphological properties for each particle.

6.4.4 X-ray microdiffraction

The crystalline degree of the prepared materials was characterized by X-ray microdiffraction using a D8 Advance X-ray diffractometer with a bidimensional detector GADDS (General Area Detector Diffraction System), (Bruker-AXS, Karlsruhe, Germany). A conventional Cu X-ray source and a 0.5nm collimator were used.θ -2θ measurements were performed from 3° to 60° in 2θ during 900 s.

6.5 Preparation of suspensions of micro particles by DELOS-susp

6.5.1 Equipment

TThis set-up comprises a 300mL reactor where CO_2 is pumped through a high pressure pump, B-1, which head is cooled by a cooling unit. Before entering the high pressure vessel, CO_2 is heated to the working temperature, T_W, using a heat exchanger (TIC). The amount of CO_2 added to the reactor through valve, V1-b, is measured by a mass flowmeter, FCO2. The vessel temperature is controlled using an external fluid heating jacket. After the vessel there is a filter (F-1) pressurized at P_W. This filter collects particles that could precipitate due to the anti-solvent effect of the addition of CO_2 when the experimental working conditions are very close to the binodal line. This filter is connected to the depressurization valve, V8, which is remotely controlled with a computer. After the depressurization valve there is a T-mixer, where the depressurized solution is co-currently mixed with the aqueous phase. During depressurization the aqueous phase is pumped at a constant flow by a peristaltic pump, B-3. The aqueous suspension is collected in a plastic bucket (T).

6.5.2 Experimental procedure

A certain volume of the solution of the drug in the organic solvent (NP in acetonitrile and ibuprofen in acetone) is placed into the reactor, once the reactor is already warmed at the working temperature. After 30 min of thermal equilibration, CO_2 is introduced to achieved the desired working pressure (P_W) and molar fraction of CO_2 (x_W.) After an hour, the CO_2-expanded solution is depressurized through a one-way automatic valve

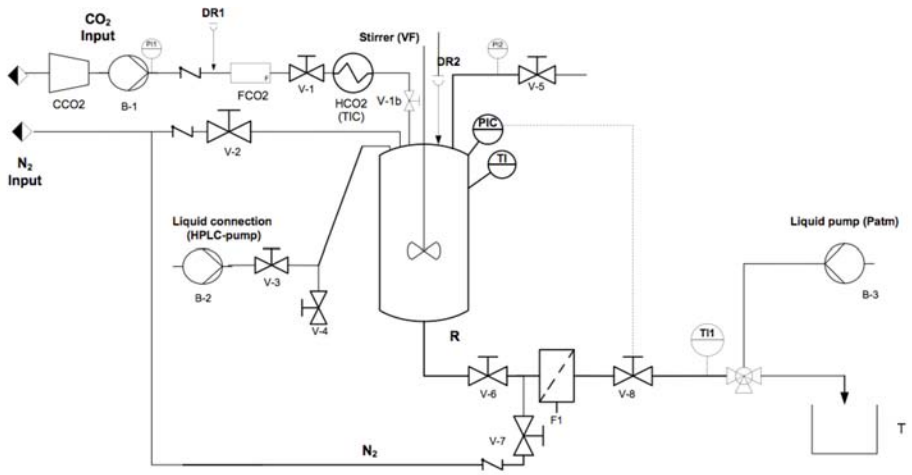

Figure 6.9: Scheme of the 300mL Plant used for the DELOS-susp experiments.

into a T mixer, to which a certain volume of water or a aqueous solution of the surfactant is being pumped. The suspension were collected in a plastic bucket.

6.6 Instruments, techniques and procedures used for the characterization of the micro suspensions

6.6.1 Light Scattering (LS)

The particle size distribution of the particles presented in the suspensions were measured by Light Scattering using the Malvern 2000 instrument. When the samples were stable enough were measured as prepared, there is, no ultrasounds were applied. In cases where the suspensions were not stable, a volume of 5mL of the suspensions were sonicated (10 min for NP and ibuprofen suspensions).

6.6.2 Turbiscan

Turbiscan technology (Multiple Light Scattering) consists in measuring the backscattering and transmission intensities versus the sample height in order to detect particle size change (coalescence, flocculation) and phase separation (sedimentation, creaming). This technique consists in sending photons (light) into the sample. These photons, after being scattered many times by objects in suspension (droplets, solid particles, gas bubbles)

emerge from the sample and are detected by the measurement device of the Turbiscan. There are two detectors: one that measure transmission for non opaque samples (0° from light source) and another one that capture the backscattering light for opaque sample (135° from the light source). Backscattering is directly related to the photon transport man free path. Thus, backscattering intensity depends on particle size and concentration. Figure 6.10 shows a picture of the configuration of Turbiscan. The detection head of Turbiscan moves up and down along the cylindrical cell. The detection head scans the entire length of the sample acquiring transition and back-scattering data each 40μm.

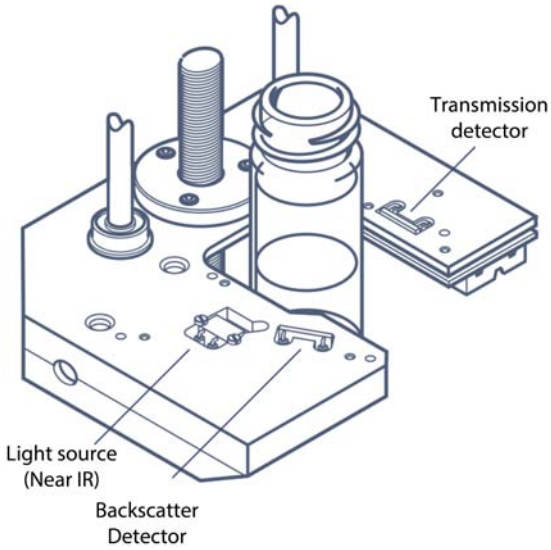

Figure 6.10: Scheme of the Turbiscan equipment.

The software of Turbiscan provides a Turbiscan Stability Index, that is a number related to the global stability of the sample. It is a quick and easy way to characterize the sample and enables to compare various formulations.

Turbiscan is used to detect at an early stage creaming or sedimentation phenomena in order to shorten the ageing test. The spectra are displayed as back scattering intensity (Y-axis) per cent relative to an external stander and on the X-axis is represented the sample height in mm. If particles tend to settle down, a progressive fall in concentration at the sample bottom occurs and this is translated into a progressive fall in backscattering a the top of the sample (Figure 6.11). Conversely, there is a progressive increase in concentration at the bottom of the sample and therefore the backscattering increases at the bottom of the sample.

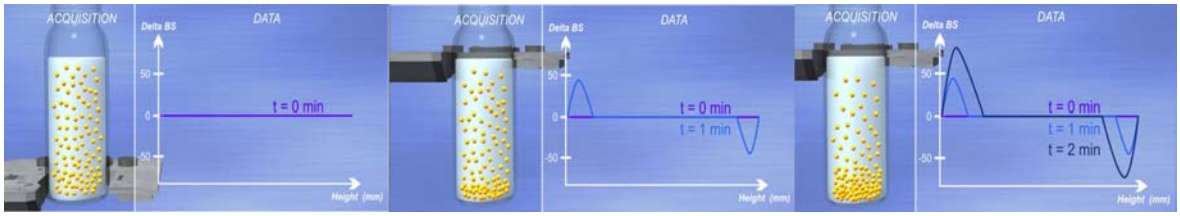

Figure 6.11: Scheme how settle down of particles is measured in Turbiscan.

The sample do not required previous treatment, however, it is very important to introduce the sample in Turbiscan just after its preparation. 20 mL of the suspension is placed inside the Turbiscan cuvettes and the measurement takes place for 8 hour.

6.6.3 Scanning probe microscopy (SEM)

For the direct observation of the particles of the suspensions, a drop of the suspensions was placed over the surface of an aluminum stub and left under vacuum for 24 hours for removal of the water and the organic solvent. The samples were coated with gold for 4 minutes using a sputter coater (K550x, Emitech, Ashford, UK).

6.7 Quantification of the excess of organic solvent in the suspensions:

Acetonitrile content by Headspace- gas chromatography - flame ionization detection (HS-GC-FID)

Acetonitrile content of suspensions after filtration/re-suspension, diafiltration or lyofilization re-constitution was analyzed by standard addition using a HP 6890 Series II gas chromatographer dotted with a flame ionization detector (Agilent Technologies, USA) and a Headspace sampler (Module 7964, Agilent Technologies, USA). 4 mL of plain and doped samples were placed in 10 mL HS vials for acetonitrile content quantification. The instrumental parameters corresponding to the Headspace module included an equilibration time of 15 min, an injection time of 0.5 min and a sampling, loop and transfer line temperature of 80, 95 and 105°C, respectively. The chromatographic column used was a DB624 (30 m x 0.32 mm x 1.8 μm i.d) from Agilent and the injection was performed in a 1:2 split mode at 275 °C. The temperature program comprised first 45 °Cduring 3 min, then

a ramp of 30 °C/min until 250 °Cand finally 2 min at that temperature. Running time was 12 min. The carrier gas was helium (46 cm/s) and the detection temperature 250 °C.

6.8 Removal of the excess of organic solvent from the suspensions

6.8.1 Filtration

Part of the as prepared suspension were filtered under vacuum thought a filter paper of pore size (0.2μm). The solid obtained after filtration was dried under vacuum for at least 48 hours. To make sure all the solvent content was removed, the solids were weighted in a high precision balance until the same weight was obtained three consecutive times.

6.8.2 Diafiltration

Diafiltration is a tangential flow filtration (TFF) method of washing or removing a permeable molecule (impurities, sats, solvents, small proteins, etc) from a solution. The equipment used is the KrossFlo® Research IIi TFF System (KE2i) and is presented in Figure 6.12. By selecting an appropriate membrane, it is possible to exchange the buffer of a solution. Tangential Flow Filtration using a hollow fiber membrane is accomplished by pumping the process solution into the inner diameter of a tubular fiber. In the case of removing the acetonitrile content of the suspensions, the pores of the membrane walls of the fiber allow the acetone and water molecules to pass through (permeate), while the particles of NP are retained in the bulk flow and continues through to the dentate (Figure 6.12). Diafiltration occurs by adding the replacement buffer, in this case, miliQ water, to the bulk flow at the same rate of permeable species.

The typical TFF system includes a pump, pressure measurement device, flow measurement device, process reservoir and hollow fiber filter module. The pump circulates the process solution from the process reservoir, through the filter and back to the process vessel at a controlled flow/shear rate. Diafiltration occurs simple by adding the diafiltration buffer to the circulation directly into the process vessel or within the recirculation loop.

In order to remove all the excess of acetontitrile in the suspensions of NP, a volume of 10mL of the suspensions were added to the sample container, then it is connected to the

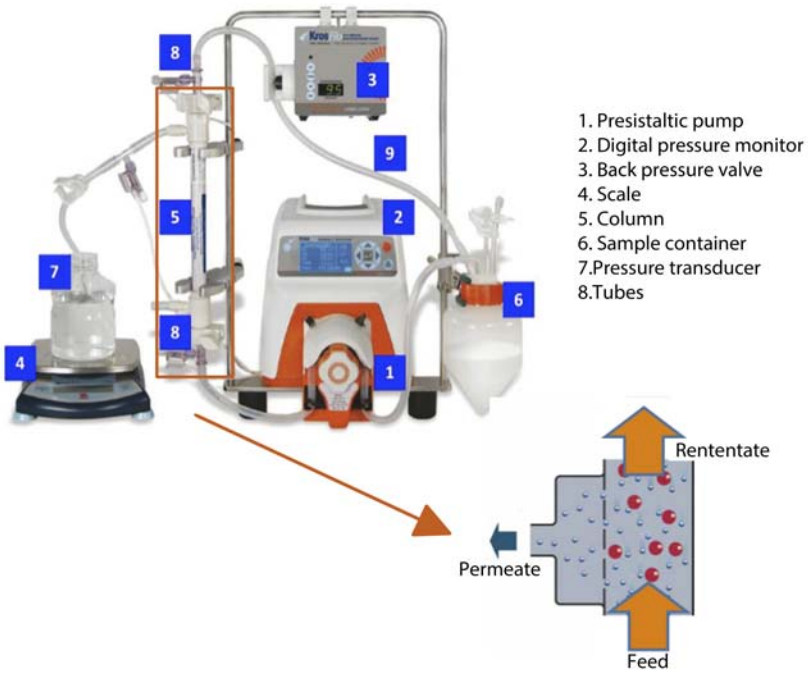

Figure 6.12: Configuration of the KrossFlo® Research IIi TFF System (KE2i).

column and the buffer reservoir. 6 cycles were required to remove the acetonitrile.

6.8.3 Liofilization

Lyophilization or freeze drying is a process in which water is removed from a product after it is frozen and placed under a vacuum, allowing the ice to change directly from solid to vapor without passing through a liquid phase. Lyophilization or freeze-drying has been done in collaboration with Telstar Company (Terrasa, Spain). The lyophlization equipment consists of a heating plate and a condenser connect to a vacuum pump. The process consists of three separate, unique, and interdependent processes:

- Freezing

  Proper freezing will ensure a good cake. The objective is to produce a frozen matrix with sufficient crystal structure to allow the sublimating material to escape. The freezing was conducted at -55°Cduring 3 hours.

- Primary drying

The pressure is reduced to a value lower its critical temperature and as a consequence there is a phase transitions from solid to gas: sublimation. Sublimation drives the unbound moisture out the product. This is usually the longest process. It was performed at -35°Cand 0.06 mBar for 33 hours.

- Secondary drying

  It is also called, desorption. In this process, the ionically bound water goes out of the material and this occurs by heating the product. It was carried out at 10°Cand lasted 4 hours.

The resulting cakes obtained after lyophilization of the suspensions were well formed and contained a residual humidity of 0.6% for the suspension with the low amount of surfactant and 0.75% for the suspension with tenfold amount of surfactant.

6.9 Formation of the microemulsions-like systems

6.9.1 Phase behavior analysis

The phase behavior analysis of the systems water/acetone/CO_2 and water/acetonitrile/CO_2 were performed in the home-made view cell, already described in previous section (section **??**).

6.9.2 Experimental procedure

A solution of water and the organic solvent is prepared at different molar relationships 50/50, 60/40 and 70/30 water/organic solvent. The solution is added to the cell once is warmed up to the working temperature (T_W) via the HPLC pump and the amount of solution is measure by difference in mass using a mass balance. The solution is added until the working pressure (P_W= 10MPa) is reached inside the cell. Prior to the addition, the cell should be completely clean and dried. In order to removed all residual air, the cell was flushed several times with CO_2.

The recirculation pump is switched on and the solution is left to equilibrate for 15 min to ensure the solution is at the working temperature. After this time, addition of CO_2 takes place working in the mode of constant flow with the ISCO pump. The flow of CO_2 is set to a low value to ensure the system has time to equilibrate and is fixed at 0.1mL/min (at

atmospheric temperature). The piston is controlled by a software and it is programmed to ensure 10MPa during the addition of CO_2. The software modifies the pneumatic pressure to let the piston move up increasing the volume to keep pressure inside the cell constant. The appearance of turbidity is considered the moment where the single liquid phase splits into 2 different liquid phases. The system is left under mixing for 30 minutes to be sure that it is the composition of phase boundary.

6.9.3 Raman characterization of the microemulsion-like systems

The Raman characterization of the microemulsion-like systems were conducted in the Applied Raman Scatterring Lab. of the SAOT center, at the Friedrich-Alexander University Erlangen-Nürnberg. The acquisition of the Raman spectra of the mixture is performed directly from the high pressure view cell with an in-house built Raman sensor (Figure 6.13)

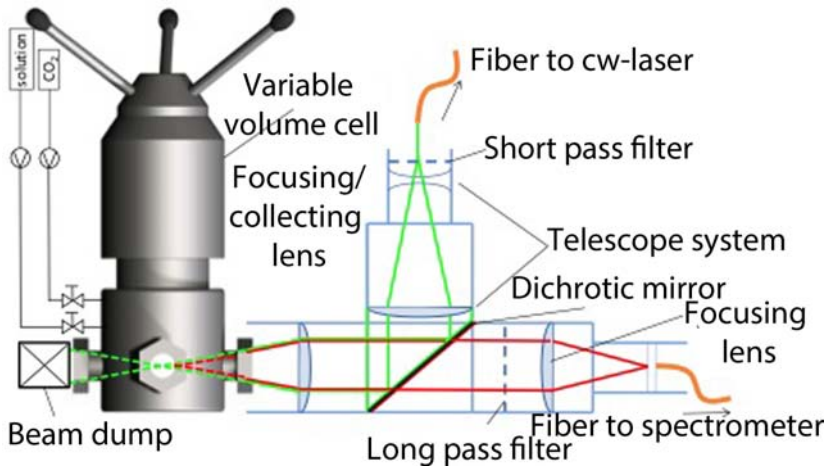

Figure 6.13: Schematic representation of the Variable Volume Cell and the in-house built Raman sensor.

6.9.4 Variable Volume Cell

A sketch of the experimental setup is shown in Figure 6.13. The optical accessible vessel is equipped with four borosilicate windows and is made of stainless steel which stands maximum pressures of 20 MPa and maximum temperatures of 393 K. The volume is adjustable between 24 mL and 56 mL by means of a moveable piston. Liquid solvents and

CO_2 are fed into the vessel using high pressure high precision syringe pumps from Teledyne ISCO. The amount of fluid pumped into the vessel is computed from the discharged volume indicated by the pumps in combination with the density of the fed fluids. Inside the vessel a magnetic stirrer agitates the fluids assuring homogeneous conditions in the one phase regime of the mixtures. For temperature control the heating jacket of the vessel was connected to a heating circulator.

6.9.5 Raman Spectrometer

The laser is a frequency doubled Nd:YVO4 continuous wave laser with a maximum power of 5 W. During the measurements the laser power was set to 250 mW since this power resulted in a sufficient signal-to-noise ratio and did not saturate the detector. The laser was guided via a glass fiber to the sensor system. At the fiber outlet a convex lens collimated the laser beam. A short pass filter blocked the wavelengths longer than 532 nm originating from light matter (SiO_2 and impurities) interactions inside the fiber. The collimated laser beam was focused into the measuring chamber with a lens of 100 mm focal length. This achromatic lens is used to collimate the backscattered Raman signals. The collimated signal is focused onto the entrance of an optical fiber bundle by means of an achromatic lens with a focal length of 200 mm. On the path to the fiber bundle the elastically scattered light is discriminated with an optical density of more than 8 at a long pass-filter and a beam-splitter. The fiber bundle is used to guide the signals to the spectrograph. The spectrograph is equipped with a grating of 600 lines mm-1 and used in connection with an charge coupled device (CCD)-detector. The chip of the detector has a dimension of 1600 x 400 pixels with a single pixel size of 16 μm x 16 μm. On the vertical axis a full vertical binning was applied and on the horizontal axis a 4 times pixel binning was used leading to 400 pixels along the spectral axis covering the wavenumber range from 300 to 3900 cm^{-1}. The quantum efficiency of the back illuminated CCD in the relevant wavelength region exceeds 0.9. In order to reduce the detector noise the readout speed was set as slow as possible to 15 kHz and the detector was cooled to 193 K. For signal evaluation a background noise spectra was taken before every measurement series and subtracted from every spectrum. Every single data point (spectra and intensity ratios) contained in the subsequent figures consists of an average of 100 individual measurements. The exposure time of a single measurement was set to 300 ms.

6.9.6 Experimental procedure

The protocol followed for the Raman characterization of the microemulsion-like systems is the following. The cell is driven to the working temperature. A certain volume of the solution composed of water and organic solvent is added to the cell until the working pressure is reached (10MPa) and is left with stirring for 15 minutes. Then, the addition of CO_2 is conducted also working at constant flow mode. In this case, the pressure is kept constant inside cell by moving manually the piston. The amount of CO_2 added to cell was 250mL/μ (at 0.8°C). After each addition, the mixture was left to homogenize for 15 min. After that time, the Raman spectra were recorded.

6.9.7 Calculation of the R_{OH}

The Raman signal contribution of water from the Raman spectrum of the ternary mixture need to be isolated and second, the OH vibration band between 3000 and 3800 cm^{-1} need to be spectrally divided in a high (non-bound water molecules) and a low wavenumber (bond water molecules) region separated from each other at the isosbestic point [3]. Following the previously made remarks the ratio of both intensities provides information regarding the development of the hydrogen bonds in the mixture.

For the reported application the deconvolution of the band's envelope is not necessary, leading to a very simple mathematical treatment of the spectra: The first step of the post processing is a baseline correction with a polynomial function of degree 4. Second step is a normalization of all spectra on the Raman-peak of acetone appearing approximately at 800 $cmcm^{-1}$ [4]. This peak is indicated as "normalization peak" in Figure 6.16 and was chosen for normalization purposes since it not spectrally interferes with neither water nor CO_2. The characteristic Raman signals of the OH-vibration, the CH-vibration and of CO_2 are exhibited. Besides the CH-peak (acetone) and the OH-band (water) the CO_2-peaks are visible in spectrum. A reliable interpretation of the OH-band Raman signal requests a purification of the OH-Raman signal from the CH-overlap. To get rid of that spectral overlap and to evaluate solely the change of the OH-band during the experiments, a spectrum of pure acetone is subtracted from every single Raman spectrum of the mixtures.

The OH-band is split into a higher wavenumber part I_{nb}, which is assigned to the non-bound water molecules, and into a smaller wavenumber part I_b, assigned to more bonded water molecules. I_b covers wavenumbers from 3050 cm^{-1} to 3450 cm-$^{-1}$, while $_{nb}$ covers

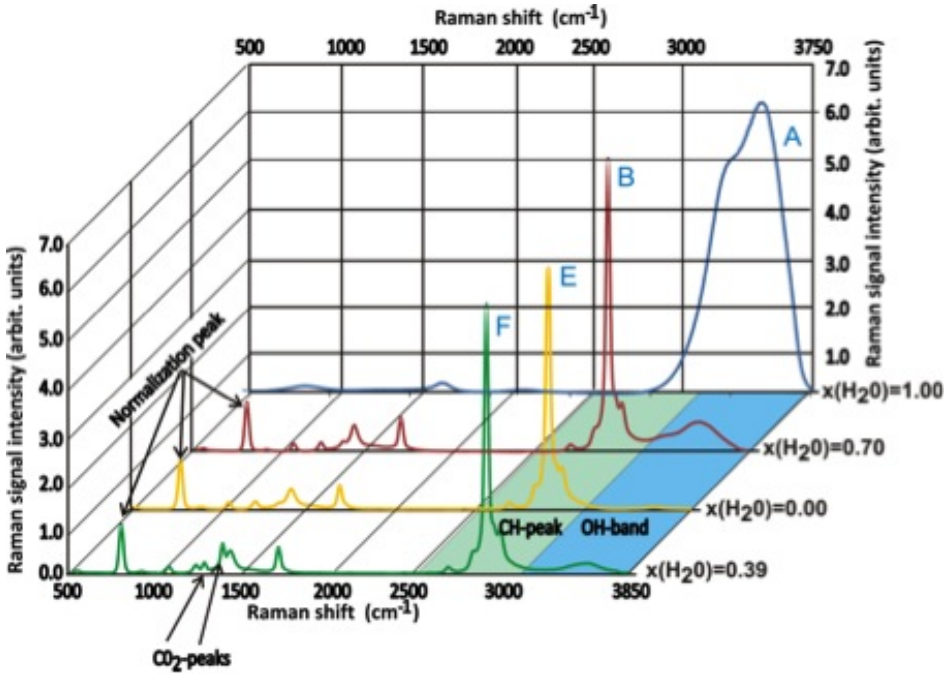

Figure 6.14: Raman spectra of different mixtures of the ternary system water/acetone/CO_2.

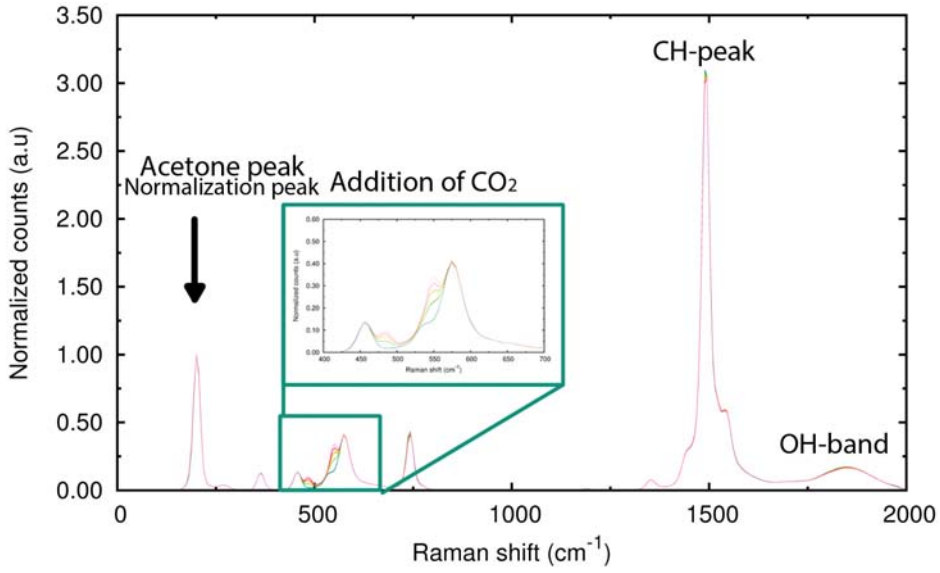

Figure 6.15: Raman spectra of different mixtures of the ternary system water/acetone/CO_2.

wavenumbers from 3450 cm^{-1} to 3850 cm^{-1}. The border between the two parts I_{nb} and I_b is set at the temperature-isosbestic point of the Raman OH stretch vibration of pure liquid water at 3450 cm^{-1} [5]. The different OH-bands indicate an increase of I_b with increasing

water mole fraction.

$$R_{OH} = \frac{I_b}{I_{nb}} \tag{6.4}$$

The R_{OH} is defined by I_b over I_{nb} and represents the development of hydrogen bonds.

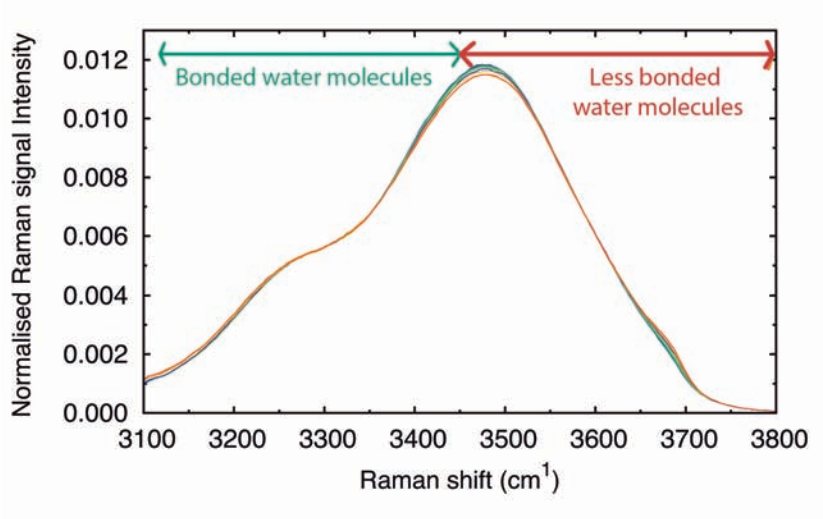

Figure 6.16: Normalised Raman spectra of the OH stretching band of water.

The higher R_{OH} is, the stronger is the development of hydrogen bonds. With increasing water molar fraction the OH Raman signal intensity ratio increases, which, indicates an amplification of the hydrogen bonds developed in the mixture.

6.9.8 Solubilization experiments of the thiadiazoline derivative NP and Ibuprofen in the microemulsion-like systems

The variable volume cell was charged initially with a solution of ibuprofen in acetone or of NP in acetonitrile. Then, water is added to the cell which provokes the precipitation of the drug due to the very poor solubility of the drug in water. The masses added to the cell of the drugs solutions and of water are already calculated in order to keep a certain relationship of water and acetone and to reach 10MPa at the beginning of the experiment. The mixture is mixed for 30 min to reach thermodynamic equilibrium. At this point, the addition of CO_2 starts. The addition is performed at a very low flow and keeping constant the pressure (10MPa) and the temperature (308K) inside the variable volume cell, therefore increasing the volume of the cell. The addition is stopped when a single transparent homogeneous phase is observed inside the cell.

6.9.9 Molecular dynamics simulations

Molecular Dynamics (MD) simulations are based on the numerical solution of the Newtonian equations of motion for all atoms of a molecular system constrained to the given thermodynamic conditions. In our simulations, water was described employing the TIP4P/2005 model, which is known to correctly reproduce the phase diagram of water both at low and high pressures [6]. This model is also the best available in reproducing the hydrogen bonding features of liquid water at all pressures. All other molecules (CO_2, acetone, acetonitrile and ethanol) were described using the CGenFF version of the CHARMM force field.

All MD simulations reported here were performed using the NAMD 2.9 software. The equations of motion were solved with a 2 fs time step. The temperature was kept constant at 308 K using the Langevin thermostat with a relaxation constant of 1 ps^{-1}. A constant pressure of 10 MPa was applied using a isotropic Nosé-Hoover-Langevin piston with standard NAMD parameters (oscillation period of 100 fs and decay time of 50 fs). Periodic boundary conditions in all directions were employed in all our simulations. Electrostatic interactions were computed using the particle mesh Ewald summation method (PME) with the standard settings in NAMD (1 Å spatial resolution and were updated each 2 time steps). Lennard-Jones interactions were truncated at 1.2 nm employing a switching function starting at 1.0 nm.

In all cases, the simulation box contained 1000 water molecules and 1000 organic solvent molecules (ethanol, acetonitrile or acetone). In the case of ternary mixtures with acetone, simulations with 353 CO_2 molecules were considered. Typical simulations have between 1.0-1.5 Œ104 atoms in a cubic box of lateral size between 50 Å and 55 Å, depending on the simulation.

In all simulations we performed an initial energy minimization followed by a short equilibration NPT simulation (typically a few ns) until the simulation box reach a stable, equilibrium size. Then, we performed 20 ns production run. Typically, only the last 10 ns of the production run were employed for data analysis. The snapshots of the simulations and the calculations of the radial distribution functions g(r) were obtained from the MD trajectories by using the Visual Molecular Dynamics (VMD) software.

Bibliography

[1] S. Gracin and Ã. C. Rasmuson, "Solubility of phenylacetic acid, p-hydroxyphenylacetic acid, p-aminophenylacetic acid, p-hydroxybenzoic acid, and ibuprofen in pure solvents," *Journal of Chemical & Engineering Data*, vol. 47, no. 6, pp. 1379–1383, 2002.

[2] F. Wubbolts, O. Bruinsma, and G. Van Rosmalen, "Measurement and modelling of the solubility of solids in mixtures of common solvents and compressed gases," *Journal of Supercritical Fluids*, vol. 32, no. 1-3, pp. 79–87, 2004.

[3] P. Geissler, "Temperature dependence of inhomogeneous broadening: On the meaning of isosbestic points," *Journal of the American Chemical Society*, vol. 127, no. 42, pp. 14930–14935, 2005.

[4] G. Dellepiane and J. Overend, "Vibrational spectra and assignment of acetone alfa, alfa, alfa acetone-d3 and acetone-d6," *Spectrochimica Acta*, vol. 22, no. 4, pp. 593–614, 1966.

[5] G. Walrafen, M. Hokmabadi, and W.-H. Yang, "Raman isosbestic points from liquid water," *The Journal of Chemical Physics*, vol. 85, no. 12, pp. 6964–6969, 1986.

[6] C. Vega and J. Abascal, "Simulating water with rigid non-polarizable models: A general perspective," *Physical Chemistry Chemical Physics*, vol. 13, no. 44, pp. 19663–19688, 2011.

A

Solubility values and solubility fitting curves

A.1 Solubility values

A.1.1 Solubility of ibuprofen in organic solvents at atmospheric pressures and low temperatures

Table A.1: Solubility values of ibuprofen in organic solvents at atmospheric pressures and low temperature

T(K)	Cs (mol/mol)			
	Ethanol	Ethyl acetate	Acetone	Acetonitrile
193	0.0042	0.0000	0.0000	0.0010
213	0.0048	0.0095	0.0148	0.0020
233	0.0099	0.0162	0.0301	0.0070
283	0.1325	0.1404	0.1656	0.0080
288	0.1712	0.1780	0.2012	0.0199
293	0.1982	0.2281	0.2490	0.0304
303	0.3175	0.3675	0.3825	0.0607
308	0.4987	0.4651	0.4633	0.1014

A.1.2 Solubility values of the thiadiazoline derivative NP in CO_2-expanded mixtures

The solubilities values that have been obtained by the Vanishing point method for achieving the solubility curve of NP in acetone/ CO_2 at 10MPa and 298K and 313K, acetonitrile/ CO_2 at 10MPa and 298K and 313K, and in the CO_2-expanded mixtures of methanol/ acetonitrile 30/70 (molar relationship) and n-butanol/acetonitrile 30/70 (molar relationship) at 10MPa and 313K are reported in Table A.2. The values of solubility in pure acetone, acetonitrile and in the mixtures of methanol/ acetonitrile and n-butanol/ acetonitrile has been obtained following the method described in Section 6.2.1.

Table A.2: Solubility values of NP in different CO_2-expanded mixtures of different compositions at P_w=10MPa and different temperatures.

Acetone			
298K		313K	
x_W	Cs (mol/mol)	x_W	Cs (mol/mol)
0.00[a]	0.007680	0.00[a]	0.0104668
0.25	0.004050	0.20	0.0067287
0.35	0.002810	0.40	0.0037382
0.52	0.001106	0.60	0.0011962
0.62	0.000740	0.80	0.0007476
0.75	0.000230	1.00	0.0000000
1.00	0.00000	-	-
Acetonitrile			
298K		313K	
x_W	Cs (mol/mol)	x_W	Cs (mol/mol)
0.00[a]	0.003940	0.00[a]	0.0104668
0.40	0.001550	0.20	0.0067287
0.50	0.001130	0.40	0.0037382
0.64	0.000717	0.60	0.0011962
0.84	0.000179	0.80	0.0007476
1.00	0.000000	1.00	0.0000000
Methanol/Acetonitrile		n-butanol/Acetonitrile	
313K		313K	
x_W	Cs (mol/mol)	x_W	Cs (mol/mol)
0.00[a]	0.00239	0.00[a]	0.00523
0.40	0.00155	0.42	0.00358
0.50	0.00119	0.50	0.00284
0.54	0.00095	0.54	0.00179
0.78	0.00035	0.90	0.00029
1.00	0.00000	1.00	0.00000

A.2 Solubility fitting curves

∗ Solubility curve of the thiadiazoline derivative NP in CO_2-expanded acetone at 298K and 10MPa

$$C_s = C_{s(org)}(1 - x_{CO_2})^{2.02+0.903*x_{CO_2}}\ , \tag{A.1}$$

∗ Solubility curve of the thiadiazoline derivative NP in CO_2-expanded acetone at 313K and 10MPa

$$C_s = C_{s(org)}(1 - x_{CO_2})^{1.93+0.33*x_{CO_2}}\ , \tag{A.2}$$

∗ Solubility curve of the thiadiazoline derivative NP in CO_2-expanded acetonitrile at 298K and 10MPa

$$C_s = C_{s(org)}(1 - x_{CO_2})^{2.01-0.44*x_{CO_2}}\ , \tag{A.3}$$

∗ Solubility curve of the thiadiazoline derivative NP in CO_2-expanded acetonitrile at 313K and 10MPa

$$C_s = C_{s(org)}(1 - x_{CO_2})^{0.77+0.68*x_{CO_2}}\ , \tag{A.4}$$

∗ Solubility curve of the thiadiazoline derivative NP in CO_2-expanded methanol/acetonitrile at 313K and 10MPa

$$C_s = C_{s(org)}(1 - x_{CO_2})^{0.417+1.22*x_{CO_2}}\ , \tag{A.5}$$

∗ Solubility curve of the thiadiazoline derivative NP in CO_2-expanded butanol/acetonitrile at 313K and 10MPa

$$C_s = C_{s(org)}(1 - x_{CO_2})^{1.34+4.75*x_{CO_2}}\ , \tag{A.6}$$

Publications

* Sala, S.; Cordoba, A.; Moreno-Calvo, E.; Elizondo, E.; Munto, M.; Rojas, P. E.; Larrayoz, M. A. A.; Ventosa, N. & Veciana, J. "Crystallization of Microparticulate Pure Polymorphs of Active Pharmaceutical Ingredients Using CO_2-Expanded Solvents." *Crystal Growth & Design, 2012, 12, 1717-1726.*

* Rojas, P.E.; Hankel, R.; Cano-Sarabia, M.; Sala, S.; Veciana, J.; Braeuer, A. & Ventosa, N. "Surfactant-free CO_2-based microemulsion-like systems." *Chemical Communications, 2014, 50, 8215-8218.*

* Rojas, P. E.,Sala, S, Elizondo, E., Veciana J.,Ventosa N. "Particle engineering with CO_2-expanded solvents: the DELOS platform". Chapter included in Advances in Organic Crystal Chemistry: Comprehensive Reviews 2015.

* Rojas,P.E., J.Shuster, R.Hankel, J.Veciana, J.Faraudo, A.Brauer, N.Ventosa, "Exploring new possibilities of CO_2-based surfactant-free microemulsion-like systems" *Langmuir, in preparation.*

* Rojas, P. E., Sala, S, Elizondo, E., Veciana J.,Ventosa N, "Preparation of suspensions of microparticles of a very poorly water soluble drug by one-step procedure using CO_2-expanded solvents" *Pharma Ress, in preparation.*